The University Of Sheffield.

An exploration of the parallel evolution of iridescent structural colour in *Heliconius* butterflies

Emma V. Curran

A thesis submitted in partial fulfilment of the requirements for the degree of Doctor of Philosophy

The University of Sheffield
Faculty of Science
Department of Animal and Plant Sciences

Submission Date

September 2018

Abstract

Understanding how selection interacts with genetic variation to produce biodiversity is a central theme in evolutionary biology. Many studies have taken advantage of the rich diversity of colouration in animals to tackle this, as colour is both ecologically relevant and a clearly visible phenotype. This has carried over into the 'omics' era, with plenty of studies addressing evolutionary questions by examining the genomics of colouration in natural populations. These studies tend to focus on discrete colour variation and pigmentation. However, most phenotypic variation is continuous, and little is known about the genetics of structural colour. *Heliconius* butterflies display warning colouration that boasts both striking diversity, alongside near-perfect convergence between mimetic species. Repeated evolution of pigment colour patterns is driven by the repeated use of a small set of genes. On the western slopes of the Andes, convergent iridescence has also evolved between the co-mimics *Heliconius erato* and *Heliconius melpomene*, which appears to vary continuously. In this thesis I (1) describe clinal variation in iridescence across hybrid zones between iridescent and non-iridescent subspecies of *H. erato* and *H. melpomene* and highlight a common selective agent (mimetic warning colouration), yet different migration-selection balance between the species. 2) I demonstrate a striking difference in levels of population structure between the co-mimics across their hybrid zones. However, in both species variation in iridescence is independent of population structure and is maintained by selection despite gene flow. (3) I describe the genetic architecture of iridescence in *Heliconius*, for the first time, using association mapping. Lack of power to estimate genetic architecture for *H. melpomene* prevented a thorough between-species comparison. However, I find potential evidence of overlapping genomic regions responsible for variation in iridescence. This thesis lays the groundwork for future research narrowing down the genetic underpinnings of iridescence in this system.

Acknowledgements

First and foremost, I would like to thank my supervisor Nicola Nadeau for her unwavering support, expertise and guidance throughout the PhD. I have had the privilege of working with her from the start of her research on iridescence, and I have learnt an enormous amount in that time. It has been quite an adventure, and not only because of those 5 weeks in the jungle.

I am also grateful to the other PhD students in the group, Mel Brien, who I've had the pleasure of being labmates with for most of my PhD, and Juan Enciso, who begun by helping us with our fieldwork in Colombia, and who is now studying in the equally exotic Sheffield. I am very fortunate to have worked on a study system with such a collaborative and adventurous spirit as the *Heliconius* community, whom I thank for interesting discussions and important butterflies. Our collaboration with Andrew Parnell and colleagues has been hugely enjoyable – thanks for guiding us biologists through the unfamiliar world of physics and for letting us play with cool machines.

This thesis has benefitted greatly from discussions at joint meetings with the Nosil, Christin and Butlin lab groups. I am grateful to Carly Lynsdale, Sean Stankowski, and Roger Butlin for their valuable comments and discussions on various chapters of this thesis. I am also grateful to Rachel Tucker for her support during lab work.

The process of carrying out a PhD can be daunting, so I feel very fortunate to have done it alongside such a brilliant group of PhD students in the department. I am grateful for their friendship and for many lost hours at Interval. I'm particularly thankful for the support of my housemates and good friends James Ord and Rob Goodsell, and also Emma Hughes and Patrick English for taking me in during the last couple of months of my PhD, and for making a stressful time an awful lot easier.

Finally, I am grateful for my family and their endless encouragement and support (be it emotional, financial, Sunday dinner related, or otherwise), and without whom none of this would have been possible.

Table of Contents

A hybrid zone in action: *Heliconius melpomene melpomene* and *Heliconius melpomene vulcanus.* Taken in Jaqué, Darién province, Panama.

1

General Introduction

Understanding the mechanisms which produce and maintain biodiversity has been the driving force of evolutionary biology since its inception. It was the evolutionary synthesis of the 1930s and 40s which bridged the gap between two previously separated fields of biology: the naturalists, who were interested in the origin of diversity, and who were proponents of Darwin's theory of evolution by natural selection (1859), and the experimental geneticists, who were interested in how genes and characters change (Mayr, 1982). The development of population genetics theory demonstrated how genetic variation and mutation was the raw material on which natural selection could act (Dobzhansky, 1937). Since then, evolutionary biology has striven to understand how natural selection interacts with genetic and demographic processes such as mutation, recombination, genetic drift, and gene flow to drive adaptation and diversification.

The progress made in genome sequencing technology in recent years, as well as the development of faster computers and analytical techniques capable of processing large quantities of genomic data, have brought about a surge of empirical studies in evolutionary genomics. Being able to acquire genomic data from many individuals allows us to use approaches such as quantitative trait locus (QTL) mapping and genome-wide association studies to detect the genetic basis of traits, and to compare genetic variation among populations to identify signatures of selection (Seehausen *et al.*, 2014). To understand the genetic basis of local adaptation, we must combine information on fitness, genotype and phenotype (Hadfield *et al.*, 2007; Barrett & Hoekstra, 2011), in line with the original vision of the evolutionary synthesis. We can now use these approaches to empirically address problems relating to adaptation and diversification. For instance, how reproductive isolation builds across the genome during speciation; how differences are maintained in the face of gene flow; how predictable evolution is on a genetic level; what the genetic architecture of adaptation is, and whether it is driven by changes at one or many genetic loci. In this thesis I hope to address some of these questions by examining a case of convergent evolution using phenotypic and genomic data from natural populations.

1.1 *Genetics of colour patterns in natural populations*

Many important insights in evolutionary biology have been made by studying colour pattern variation. Colouration is a useful trait to study, as it a clearly visible phenotype with ecological relevance. Its many functions include camouflage, sexual selection, species recognition, warning signals to predators, mimicry and thermoregulation (Roulin, 2004; Protas & Patel, 2008). Colour patterns may also evolve neutrally through genetic drift, or through selection on a correlated traits (Gould & Lewontin, 1979).

The maintenance of colour polymorphisms of the shells of snails in the genus *Cepaea*, is an early example of an evolutionary problem which was tackled by applying both ecological and genetic approaches. Genetic crosses revealed how different aspects of shell pattern variation were explained by tightly linked loci, or a supergene. This work was important in demonstrating how natural selection can maintain variation (Cain & Sheppard, 1954; Jones *et al.*, 1977).

Work in model systems with well-developed resources for genetic analysis, the fly *Drosophila* and mouse *Mus musculus*, revealed a suite of genes involved in pigmentation pathways (Wittkopp *et al.*, 2003; Hoekstra *et al.*, 2006), paving the way for candidate gene studies in non-model organisms (Protas & Patel, 2008). Such studies revealed the conserved role of the *melanocortin-1 receptor* (*MC1R*) in pigmentation across vertebrates (Hoekstra, 2006). Changes in the coding region of *MC1R* is responsible for colour pattern variation in mammals including pocket mice (Hoekstra & Nachman, 2003), jaguars, jaguarundi (Eizirik *et al.*, 2003) and woolly mammoths (Römpler *et al.*, 2006), birds including bananaquits (Theron *et al.*, 2001), lesser snow geese and arctic skua (Mundy *et al.*, 2004), as well as squamate reptiles (Rosenblum *et al.*, 2004) and cavefish (Mundy, 2009).

Candidate gene approaches are, however, biased by nature, as they can only follow up on genes known to be involved in pigmentation in model organisms. With the arrival of population genomics approaches, it is now possible to investigate the genetic basis of colour pattern variation in natural populations in wide variety of organisms with no prior knowledge of the genes which may be involved. This provides a less biased perspective on the genetic basis of colouration in

more evolutionary scenarios, and across a wider range of ecological settings. San-Jose and Roulin (2017) provide a comprehensive review of studies focusing on genomics of colouration in natural populations. They highlight how many current studies focus heavily on pigmentation, and colour which is determined by large effect loci, and that there is a lack of studies focusing on structural colour, and continuous colour variation. In my thesis I hope to address these two understudied themes, so I introduce them in greater detail below.

1.1.1 *Structural colouration*

Some of the most spectacular colours in nature are not produced by pigments, however, but instead from physical nanoscale features, the precise arrangement of which allow the selective reflection of specific wavelengths of light (Srinivasarao, 1999). Reflective structures may act alone, or in concert with pigments to enhance their colour (Vukusic *et al.*, 2000), and they are found in bird feathers, butterfly and fish scales, beetle elytra, and even some plant species. A wide variety of types of structures can produce colour. Iridescence, which is angle dependent structural colour, is famously displayed in the magnificent plumage of male peacocks (*Pavo cristatus*). In peacocks, iridescence is produced by a regular lattice arrangement of melanosomes embedded within the feather keratin (Figure 1.1 A, D; Zi *et al.*, 2003). In the butterfly *Morpho rhetenor*, ridges on the wing scales are composed of alternating layers of chitin and air which are highly periodic, and the spacing of the layers are proportional to blue wavelengths, and as a result can reflect nearly 75% of blue light (Figure 1.1 B, E; Vukusic *et al.*, 1999; Burg & Parnell, 2018). Not all structural colour is iridescent, however. The bright whiteness of *Cyphochilus* spp. beetles is produced by the aperiodic internal structure of scales which scatters all visible wavelengths of light (Figure 1.1 C, F; Vukusic *et al.*, 2007).

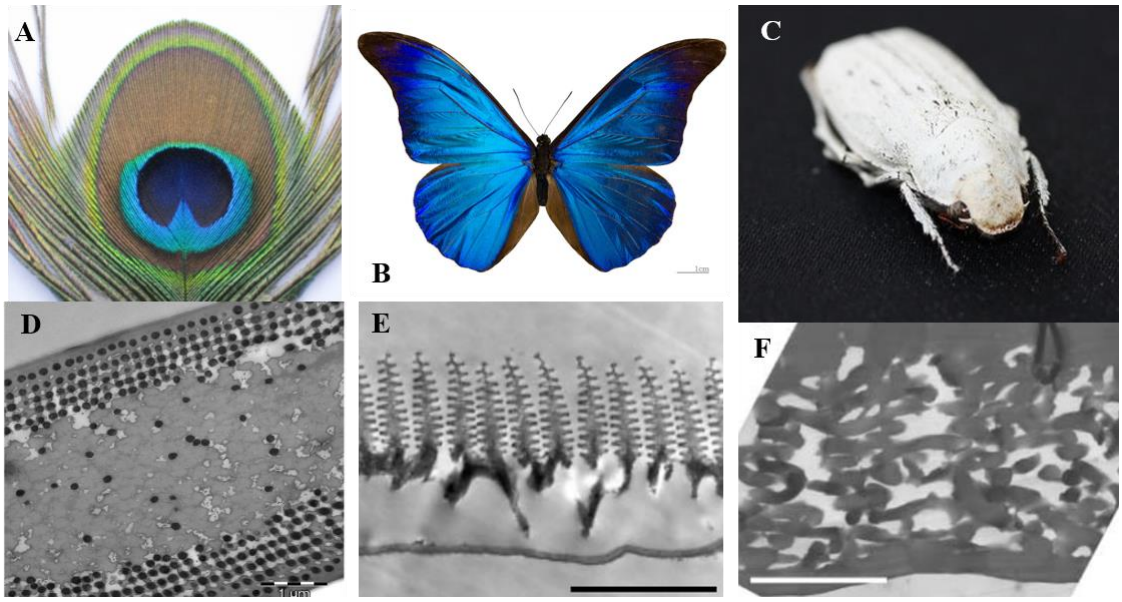

Figure 1.1 – Different structures responsible for structural colour in animals. (**A)** Male peacock (*Pavo cristatus*) feather (photograph from Medina *et al.*, 2015) (**B**) *Morpho rhetenor* (credit: Didier Descouens) (**C**) *Cyphochilus* sp. (photograph from Wilts *et al.*, 2018). (**D)** Transmission electron microscope (TEM) image of the lattice of photonic-crystal structures in the barbule of a male peacock feather. Scale bar is 1 μm (image from from Medina *et al.*, 2015) (**E**) TEM image of the cross-section of a *Morpho rhetenor* scale, showing the layers formed by the scale ridges. Scale bar is 3 μm (image from Vukusic *et al.*, 1999). (**F**) TEM image of a white scale from the elytra of a *Cyphochilus* beetle. The disordered internal structure of the scale is shown. Scale bar is 3 μm (image from Vukusic *et al.*, 2007).

As is the case with pigmentation, structural colour has been shown to have a wide range of ecological functions. There is evidence of blue structural colour being used for species recognition in lycaenid butterflies (Bálint *et al.*, 2012). Its role in mating systems has been demonstrated in *Heliconius* butterflies, where male *Heliconius cydno* were more likely to approach females reflecting polarized light, an optical phenomenon associated with iridescence (Sweeney *et al.*, 2003). Ultraviolet (UV) structural colour appears to act as a condition-dependent signal in *Colias* butterflies (Kemp *et al.*, 2006) and blue tits (Keyser & Hill, 1999), with blue tits showing a preference for UV reflecting partners (Hunt *et al.*, 1999). Structural colour has also be shown to play a role in thermal tolerance in the tiger beetle *Neocicindela perhispida* (Hadley *et al.*, 1992), and as a signal of toxicity in the hibiscus harlequin bug *Tectocoris diophthalmus* (Fabricant *et al.*,

2014).

The optical properties of structural colour may provide advantages over pigment colour when signalling in certain situations. Iridescence reflects highly saturated colour and produces directional flashes, allowing visual signals to be detected from greater distances. *Morpho* butterflies are a shining example of this (Vukusic *et al.*, 1999). The famous naturalist Henry Walter Bates claimed to have witnessed *Morpho* from 'a quarter of a mile off' (Bates, 1864), and they can be seen from low-flying aircraft (Silberglied, 1984). Iridescent visual signals can also be enhanced by polarised reflectance, and this is thought to be adaptive in nymphalid butterflies that live in forests with uneven light environments (Douglas *et al.*, 2007). High reflectance can also amplify floral signals to bees (Moyroud *et al.*, 2017), and enhance predator learning of structural aposematic colouration (Waldron *et al.*, 2017).

Despite a growing body of research surrounding the physical structures responsible for structural colouration (reviewed in Burg & Parnell 2018) and the functional roles it plays in nature (reviewed in Doucet & Meadows 2009), almost nothing is known of its genetic basis (but see Zhang *et al*. 2017).

1.1.2 *Continuous colour variation*

There has been considerable success working with discrete colour and pattern traits which generally have a simple genetic basis composed of large effect loci that are straightforward to detect. This is unlikely to be representative of the majority of colour pattern variation, however, as most phenotypic variation is likely to be continuous, with a more polygenic genetic basis (Rockman, 2011; San-Jose & Roulin, 2017). Prior to the surge in availability of empirical genomic data, much of the theoretical work surrounding the genetic basis of adaptation posited that evolution largely proceeds gradually via many genetic changes of small effect (Orr, 2005). Fisher (1930) reasoned in his geometric model of adaptation, that mutations with large, widespread effect are more likely to have deleterious outcomes for certain traits, therefore mutations with a smaller effect are more likely to have a net benefit, nudging a trait in the direction

of its phenotypic optimum. More recent theory suggests that the size distribution of mutations will normally be exponential, with a few mutations of large effect and many of small effect and that they will generally accrue in that order, with diminishing returns (Orr, 1998, 2005). This is partly because large effect mutations are less likely to be lost by drift and they can allow populations to jump across valleys, to new adaptive peaks. It is also now more widely acknowledged that genetic architecture itself can evolve. So even if many small-effect loci initially contribute to adaptation, if populations are under selection towards different optima, but still experience ongoing gene flow, this tends to result in a genetic architecture of fewer divergent alleles, which have larger effects and are more tightly linked (Griswold, 2006; Yeaman & Whitlock, 2011).

If quantitative traits with continuous variation are controlled by many loci, it can be difficult to get enough statistical power to detect the causative loci using genetic mapping techniques, as each locus has a small phenotypic effect size, and causal variants may occur at low frequencies (Slate, 2005; MacKay *et al.*, 2009; Rockman, 2011). In addition, as phenotypic differences in polygenic traits may be produced by only small changes in allele frequency at individual loci, these may be indiscernible from the background levels of genetic differentiation, for example in genome scans to detect loci under divergent selection (Le Corre & Kremer, 2012). However, it should be noted that in some cases a relatively small number of loci with large phenotypic effects can explain most of the variation in apparently quantitative traits (Liu *et al.*, 2009; Johnston *et al.*, 2011). The increasing use of whole genome resequencing data increases the efficiency of GWAS, as, in theory, genetic markers should represent the entire genome, so there is no reliance on linkage disequilibrium between causative and typed markers, which can be very low for standing genetic variation in large populations. This kind of approach has been applied in *Drosophila melanogaster* to reveal the genetic architecture of continuous variation in pigmentation (Dembeck *et al.*, 2015), although it can still be challenging to obtain enough statistical power to detect loci with smaller effects on phenotype (Kardos *et al.*, 2016).

1.2 *Repeated evolution*

Understanding the ecological and genetic processes underlying diversity in traits such as colouration can tell us about the processes underlying local adaptation and even speciation, but what can we learn from occasions where extremely similar phenotypes evolve multiple times? Distantly related species often adopt very similar evolutionary strategies to deal with environmental problems. Traditionally, such occurrences of convergent phenotypic evolution were presented as evidence of the remarkable consistency with which natural selection could fit organisms to their environments (Conway Morris, 2003). Yet the striking similarity that can often be seen between distantly related taxa may also be indicative of some internal genetic or developmental constraints, limiting the amount of possible phenotypic outcomes, thus increasing the likelihood of convergent evolution (Wake, 1991; Losos, 2011). It is emerging that similar traits in distinct taxa often evolve via changes in the same genes, suggesting that evolution may have a tendency to proceed via the path of least genetic resistance (Martin & Orgogozo, 2013). While this pattern of gene reuse underlying phenotypic convergence is increasingly well-documented (e.g. Protas *et al.*, 2006; Chan *et al.*, 2010; Colombo *et al.*, 2013), there are also a growing number of examples where highly similar phenotypic endpoints have been reached in independent populations via different genetic pathways (e.g. Fox *et al.*, 2009; Meyer *et al.*, 2013; Thurber *et al.*, 2013).

In the literature, there seems to be some dispute surrounding the terminology of repeated evolution. Examples are often divided into cases of parallel evolution, whereby the independent evolution of highly similar phenotypes occurs in separate taxa from closely related, or identical ancestral stock, and convergent evolution, whereby the phenotypically converging taxa have a more distant common ancestor (Arendt & Reznick, 2008; Conte *et al.*, 2012). It is thought that cases of parallel evolution are more likely to have a similar genetic basis than convergent evolution, and probability estimates support this (Conte *et al.* 2012). However, these definitions probably simply represent two ends of a continuum, rather than two discrete categories, and so I use the terms parallel and convergent evolution interchangeably in this thesis. It might be rather more important to be explicit about the level of convergence being discussed, for instance

convergent evolution at the functional, phenotypic, genetic, or mutational level. Additionally, when discussing convergent genetic evolution, it is useful to identify the nature of the alleles involved, as it can occur via three separate routes: via multiple independent mutations, via selection on shared ancestral standing variation, or via gene flow between populations (Stern, 2013; Lee & Coop, 2018).

There are numerous factors which may affect the extent to which convergent phenotypic evolution is also convergent on the genetic level. Genetic biases may reduce the number of potential genetic pathways to phenotypic change. High levels of pleiotropy in a genome increases the likelihood of widespread deleterious effects if mutations arise in the coding regions of pleiotropic genes, genetic changes might be restricted to particular *cis*-regulatory regions (Prud'homme *et al.,* 2007; Christin *et al.,* 2010). Physical properties of the genome may predispose certain genomic regions to higher than average mutation rates (Martin & Orgogozo, 2013), If such a region influences an adaptive phenotype, it may facilitate independent evolutionary events which are convergent at both the phenotypic and genotypic level. An example of this is in threespine stickleback fish (*Gasterosteus aculeatus*), where different populations have undergone independent losses of a skeletal pelvic structure owing to *cis*-regulatory mutations of the *Pituitary homeobox transcription factor 1* (*Pitx1*) gene, which is thought to be located within a particularly fragile genomic region (Chan *et al.,* 2010). The genetic architecture of trait might also affect the probability of gene reuse during phenotypic convergence. Highly polygenic phenotypes might be achieved through many alternative genetic pathways, since there are many different locations at which genetic changes could alter that phenotype (reviewed in Gompel & Prud'homme, 2009). Polygenic traits are more prone to evolutionary contingencies, such as the sequence in which mutations emerge (Conte *et al.* 2012). However, evidence suggests the number of potential mutational pathways available to selection may be limited (Weinreich *et al.,* 2006). Most studies exploring the genetic basis of convergent evolution tend to focus on traits with a simple genetic basis. As the genetic architecture may itself influence the likelihood of gene reuse, more studies looking at the genetic basis of convergent quantitative traits, with more complex genetic architectures, are needed.

1.3 *The Heliconius butterflies*

The study of *Heliconius* butterflies over the past 150 years has provided a substantial contribution to our understanding of evolutionary processes. *Heliconius* is a Neotropical genus consisting of 48 species, which belongs to the tribe Heliconiini (Nymphalidae: Heliconiinae) and is thought to have arisen 10.5–13.4 Ma (Kozak *et al.*, 2015; Merrill *et al.*, 2015). *Heliconius* butterflies have bright wing patterns of reds, yellows and white which contrast sharply against a black background, which they boldly display during slow and deliberate flight. These patterns serve as a warning signal to predators, advertising their distastefulness. However, it is the diversification of these colour patterns within and between species within the genus, as well as extensive mimicry between species, which has captured the interest of evolutionary biologists for several decades. Indeed, it was observations of the repeated emergence of similar colour patterns among *Heliconius* and other Neotropical genera that led the famous naturalist Henry Walter Bates to establish mimicry theory (1862).

Since then, observations and experiments in the field have demonstrated the role of Müllerian mimicry (i.e. mimicry between unpalatable species; Müller, 1879) in *Heliconius* (Kapan, 2001). Work on hybrid zones between parapatric colour pattern races of the same species has demonstrated that strong selection acts to remove hybrid phenotypes, as predators are more likely to attack novel colour morphs (Mallet & Barton, 1989; Langham, 2004). Colouration in *Heliconius* has also been shown to play a role in the maintenance of species barriers between recently diverged sister species, with each species preferring their own colour pattern during mate choice (Merrill *et al.*, 2012, 2014).

Once *Heliconius* research entered the ‘genomic era’, it became possible to identify the genes responsible for colour pattern variation. It has been found that a genetic ‘toolkit’ of up to 5 genes in some species, is used to produce colour variation, with each gene controlling a different pattern element. These include *cortex*, which controls yellow and white patterns (Joron *et al.*, 2006; Nadeau *et al.*, 2016); *optix*, which controls red patterns (Reed *et al.*, 2011); and *WntA*, which controls the size and shape of pattern elements (Martin *et al.*, 2012). Two other loci are also

known to affect wing patterning in *Heliconius*, the *K* locus, which controls a switch between white and yellow in *H. cydno* and *H. melpomene* (Kronforst *et al.*, 2006), and a locus on chromosome 13, which controls the shape of the forewing band in *H. erato* and *H. melpomene* (Nadeau *et al.*, 2014). While use of these loci is highly conserved across *Heliconius*, novel genetic architectures of colour and pattern loci have evolved. For instance, there is evidence that *H. melpomene* utilises all 5 of the loci described above (reviewed in Nadeau, 2016), whereas in *Heliconius numata*, the vast majority of colour pattern variation is controlled by a single supergene locus which maps to the same region as cortex (Joron *et al.*, 2011), with the other four loci having minor effects on phenotype (Jones *et al.*, 2012). In *Heliconius* it appears that both convergence and divergence in wing colour pattern can be achieved by the repeated use of the same genetic loci. In addition, it has been shown that mimicry has been facilitated on multiple occasions through adaptive introgression of colour patterns between species (Pardo-Diaz *et al.*, 2012; The Heliconius Genome Consortium, 2012; Enciso-Romero *et al.*, 2017).

Whilst we now have a good understanding of the genetic basis of pigment colour in *Heliconius*, and the evolutionary dynamics maintaining both the diversity and convergence among the patterns which they make up, we know very little about structural colour in the genus. As with pigmentary colours in *Heliconius*, iridescent structural colour is also mimetic between species (Thurman & Seymoure, 2016), and plays a role in mate choice (Sweeney *et al.*, 2003). In *Heliconius*, there are two main ways in which structural colour is produced. First, by the overlapping of lamellae which form ridges that run the length of the scale surface, termed 'ridge reflectors'. The extent to which the lamellae overlap to form multi-layered ridge reflectors, and how densely packed the ridges are, determine the extent of iridescence (Fig 1.1 B, C; Parnell *et al.*, 2018). Second, in *H. doris*, blue structural colour is produced by the thin film structure of the lower lamina of cover scales. In the green form of *H. doris*, this structure interacts with short-wavelength absorbing (yellow) pigments to produce green (Wilts *et al.*, 2017). In this thesis I focus on iridescent colour produced by ridge reflectors.

Ridge reflectors appear to have several origins in *Heliconius* (Figure 1.1A). There is a clade in which all members display iridescence, which includes *H. antiochus, H. leuchadia, H. sara, H.*

hewitsoni, *H. sapho, H. congener and H. eleuchia*. The oldest origin of iridescence in *Heliconius* was likely in the common ancestor of this clade 2–5 million years ago (Kozak *et al.*, 2015; Parnell *et al.*, 2018). More recently, iridescence appears to have evolved in *H. cydno*, likely so it can form effective mimicry rings with *H. sapho* and *H. eleuchia.* It has evolved even more recently in *H. erato* and *H. melpomene*, which both lack iridescence in most of their range, except for on the western slopes of the Andes in Colombia and Ecuador.

In this thesis I explore the evolution of iridescence in the co-mimics *H. erato* and *H. melpomene*, with respect to two interesting features of *Heliconius* biology – the hybrid zones between conspecific colour pattern races, and the convergence of wing colour patterns between co-mimics. Below, I summarize the aims of each of the chapters in this thesis, and the methods used to tackle them.

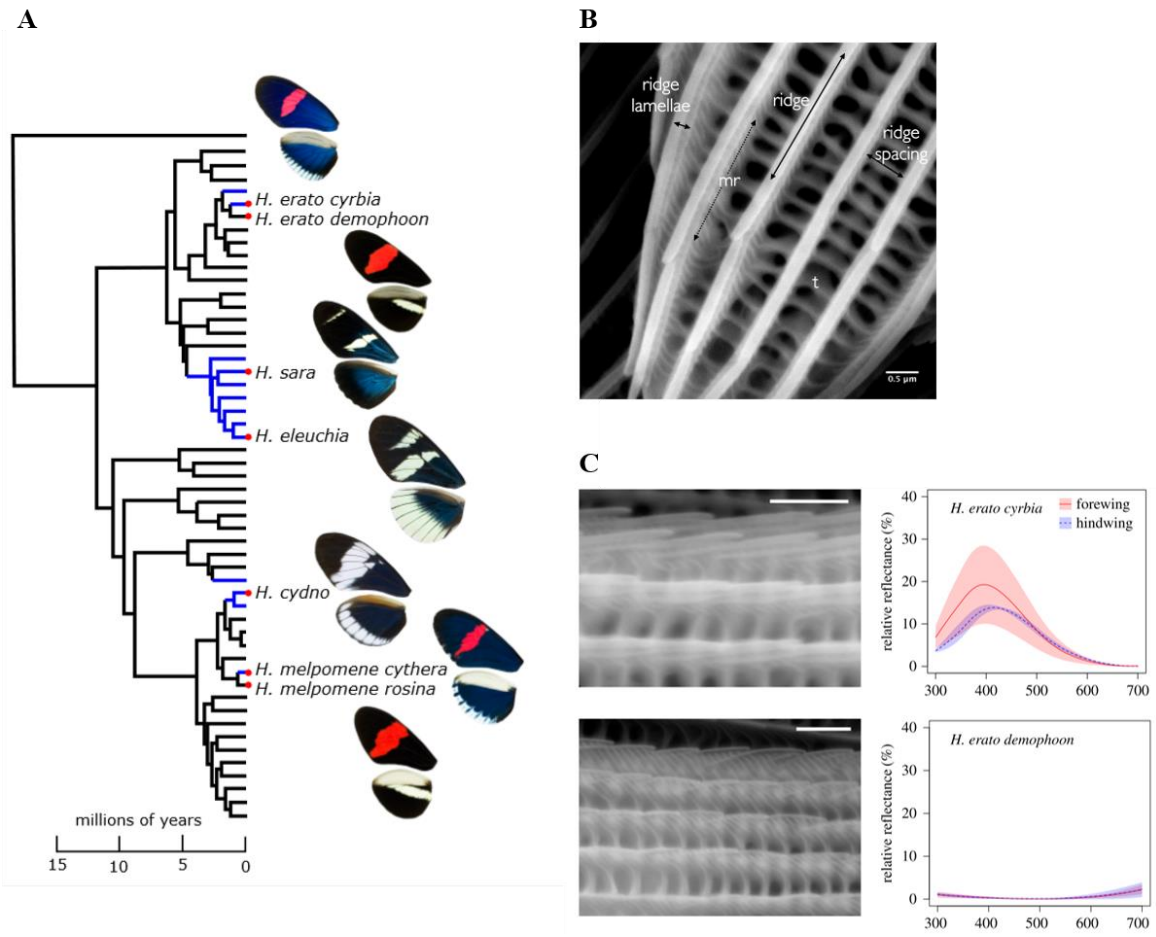

Figure 1.2 – The origins and structure of ridge reflectors in *Heliconius*, all figures are from Parnell et al. (2018). (**A**) Phylogenetic distribution of iridescence produced by ridge reflectors across *Heliconius.* Blue branches indicate the presence of iridescence. (**B**) The general structures of a *Heliconius* scale demonstrated on the tip of a *H. eleuchia* scale. Ridges run the length of the scale and are composed of overlapping ridge lamellae. Micro ribs (mr) are indented striations on the walls of the ridges. The trabeculae (t) connect these structures to the lower lamina. (**C**) Scanning electron micrographs (bars are 1 µm) of wing scales of the iridescent *H. erato cyrbia* (upper) and the non-iridescent *H. erato demophoon* (lower) and their corresponding reflectance spectra. Reflectance spectra are taken from the angle of maximum reflectance. The mean (lines) and standard deviation (shaded area) of measurements from the forewing (red) and hindwing (blue) of four individuals from each subspecies are shown. Flatter ridge lamellae with greater overlap result in reflection of blue wavelengths in *H. erato cyrbia.*

1.4 *Outline of thesis chapters*

Each of the chapters in this thesis uses data from wild caught *Heliconius erato* and *Heliconius melpomene* individuals, collected from sites in Panama, Colombia, and Ecuador. Samples we collected were supplemented by the collections of other groups, who are acknowledged below.

In Chapter 2 I describe variation in iridescence across parallel hybrid zones in the co-mimics *Heliconius erato* and *Heliconius melpomene* and compare the selection pressures acting on iridescence between species. Using colour measurements from photographs of samples, I reconstruct clines in iridescence for each species. I then compare the position of the iridescence clines to clines in a pigment colour pattern which also varies across the hybrid zones, and which has a known genetic basis, to make estimates of the strength of selection acting on colour traits. I then discuss the selection pressures acting on colour traits within and between species, based on the shape and position of colour pattern clines relative to one another.

In Chapter 3, I aim to determine the extent of population genetic structure across the hybrid zones in each species. I ask whether differentiation in iridescence, a quantitative trait, varies independently of genome-wide differentiation across the hybrid zone, and whether it is maintained by selection. Using reference aligned sequence data from individuals sampled across the hybrid zone in each species, I apply population genomic approaches to describe the levels of genetic structure present in each species. I then use geographic cline analysis to compare the average genetic structure across the hybrid zones to the iridescence clines in each species. I also discuss the different scenarios which might have led to the formation of each hybrid zone. For instance, whether divergence between iridescent and non-iridescent colouration occurred in the presence of gene flow, or whether differences arose in allopatry, followed by secondary contact.

In Chapter 4, I aim to estimate the genetic architecture of iridescence in *H. erato* and *H. melpomene* and identify potential candidate loci involved in controlling variation in iridescence, which are also under divergent selection. I then ask whether there is evidence of iridescence evolving via a similar or distinct genetic route in each species. To do this I use two approaches, firstly I use genome-wide association studies (GWAS) to identify variants associated with

iridescence. I then use a top-down approach to look for loci under selection using EigenGWAS, which looks for variants associated with population structure. I then compare the findings between the co-mimics.

Finally, in Chapter 5, I finish with a discussion of the overall findings in this thesis and I suggest future directions for further research building from this work.

1.5 *A note on contributions made to this thesis*

The analyses carried out in this thesis wouldn't have been possible were it not for the collaborative spirit of the *Heliconius* research community. Acquiring samples from the regions we were interested in is challenging, and we would not have had the necessary data without the help of other groups.

Our own fieldwork in Colombia was organised by Carolina Pardo-Diaz, Camilo Salazar and Mauricio Linares, who have valuable experience and knowledge of collecting butterflies in the region. During two field trips to Colombia, we were also assisted in collecting by Juan Enciso, Melanie Brien, Carlos Arias and Juan Camilo Dumar.

Our samples were supplemented from the collections of other groups who had also sampled in regions of interest to us. We were generously supplied additional samples from Chris Jiggins, Tim Thurman, W. Owen McMillan, Camilo Salazar, Richard Merrill and Stephen Montgomery.

Unless otherwise stated, all data collection and analyses were carried out by myself.

Roger Butlin and Sean Stankowski provided important advice and discussion regarding the analyses in chapters 2 and 3.

Victor Soria-Carrasco provided assistance and advice for processing raw sequence reads and calling variants. These datasets were used in chapters 3 and 4.

1.6 *Appendices*

At the end of this thesis, I include a submitted manuscript and a published paper as appendices. I include these studies, on which I am a co-author, as they provide relevant context to the thesis, which I describe below.

The first appendix is a manuscript which, at the time of writing, is under review at the journal Interface Focus. In this study, crosses were carried out between iridescent and non-iridescent races of *Heliconius erato*. Phenotypic variation was measured in the resulting F2 generation, revealing that iridescence is a quantitative trait controlled by multiple genes, and that it is sex-linked. It is also found that the spacing between scale ridges, which affects the intensity of iridescence, also varies quantitatively in the F2 generation. This research is relevant to the themes of this thesis, as it investigates the genetic architecture of iridescence in *H. erato* and lends support to my findings, as well as providing extra information about the role of loci on the sex chromosome which likely affect iridescence. I contributed to this study by devising the protocol to photograph samples and measure the blue content of photographs. I also assisted with performing the crosses and taking the small angle X-ray scattering (SAXS) measurements used to quantify ridge spacing.

The second appendix is a paper published in the journal Interface. In this study, the nanostructures responsible for producing iridescence in *Heliconius* are described. This work is very significant to the research in this thesis, as it allowed us to understand the phenotype which inspired this project. I contributed by assisting with taking SAXS measurements used to described scale structures.

2

Clines in iridescent structural colour in the Müllerian mimics *Heliconius erato* and *Heliconius melpomene*

2.1 *Summary*

Studying variation in animal colouration in wild populations has provided important examples of how natural selection acts on adaptive mechanisms. To date, much of this work has focused on colouration produced by chemical pigments, yet some of the most vivid colours in nature are structural, produced by the interaction of light with physical nanoscale features. Structural colours can be difficult to quantify, and so natural variation in them has rarely been studied. Here, we examine variation in iridescent structural colour in the butterflies *Heliconius erato* and *Heliconius melpomene*, Müllerian co-mimics which have been extensive studied owing to their geographic variation in pigment warning colour patterns. Populations on the west coast of Ecuador and Colombia display vivid iridescent blue. We quantify variation in iridescence using digital photography and use geographic cline analysis to model clinal variation in both iridescence and pigmentary colour across parallel hybrid zones over the border of Colombia and Panama, between iridescent and non-iridescent races of both species. We find evidence that iridescence is under divergent selection, and that it functions as part of the warning signal. The iridescence cline is much wider in *H. melpomene,* suggesting that either the strength of selection is weaker on iridescence, the rate of dispersal is greater, or quite likely a combination of the two. In addition, we find evidence of a second pair of clines in iridescence across the border of Colombia and Ecuador, between two iridescent races of each species. We have, for the first time, quantified variation in iridescence in natural populations in *Heliconius* butterflies, a model system in evolution, laying the foundation for a holistic understanding of colour pattern variation in this group.

2.2 *Introduction*

Studies of animal colouration have been crucial in the progress of evolutionary biology. The case of industrial melanism in *Biston betularia*, the peppered moth, was one of the first observations of natural selection in action in a wild population (Kettlewell, 1955), and studies of mimicry in butterflies pioneered the field of ecological genetics in the 1950s-'70s, and were among the first to consider the genetic basis of adaptation in natural populations (Clarke & Sheppard, 1962, 1972; Ford, 1977). Now, in the genomic era, research based on animal colouration is giving us insight into how new adaptations, and even species evolve (e.g. Soria-Carrasco *et al*. 2014; Küpper *et al*. 2015; Marques *et al*. 2017).

The clear adaptive functions of colour, such as in crypsis (e.g. stick insects, Sandoval 1994; mice, Nachman *et al*. 2003), aposematism (e.g. poison dart frogs, Santos *et al*. 2003; wood tiger moths, Nokelainen *et al*. 2012) and mate choice (e.g. guppies, Endler 1983; cichlids, Seehausen *et al*. 2008), and the ease with which it can be measured, make it an attractive subject of research for evolutionary biologists. Most studies to date have focused on colour produced through the selective absorption of certain wavelengths of light by pigments (San-Jose & Roulin 2017). Alternatively, colours can also be produced by nanoscale structures which interfere with visible light, often combining with pigments to produce some of the brightest and most striking colours in nature (Shawkey *et al.*, 2009; Shawkey & Alba, 2017). Iridescence, which is angle-dependent structural colour, has unique optical properties that can enhance visual signals. Polarisation is thought to improve visual communication in iridescent nymphalid butterflies in the complex light environments of forests (Douglas *et al.*, 2007), and high reflectivity has been shown to hasten avoidance learning in predators of aposematic prey (Waldron *et al.*, 2017). Whilst there is a reasonably good understanding of iridescence from a functional perspective (Doucet & Meadows, 2009), almost nothing is known about its genetic control (but see Zhang *et al*. 2017).

The *Heliconius* butterflies of South and Central America have been extensively studied, owing to their extraordinary geographic variation in colour patterns within species, and remarkable convergence between certain co-occurring species. They are an example of Müllerian

mimicry; whereby shared warning colouration confers shared protection against predators (Brown, 1981; Kapan, 2001). *Heliconius erato* and *Heliconius melpomene* are classic examples of Müllerian co-mimics. Their warning colours are largely made up of discrete pattern elements produced by pigments, and we now have a good understanding of the 'genetic tool-kit' of 5 genes which control the majority of this pattern variation (reviewed in Nadeau 2016). West of the Andes, however, in Colombia and Ecuador, iridescent blue is also present on their wings. This appears to have evolved independently in each species (Parnell *et al.*, 2018), however the selection pressures and genetic architecture controlling variation in the trait are currently unknown. Mimetic, iridescent races of *H. erato* and *H. melpomene* form parallel hybrid zones with conspecific non-iridescent races (Mallet, 1986), and while variation in iridescence has been reported as appearing quantitative, this has not been explicitly measured in the past. However, evidence shows that iridescence has physical properties which could produce quantitative variation. In *Heliconius*, the colour and intensity of iridescence can evolve and be modified through quantitative variation in wing scale ultrastructure, via small changes in the shape and density of iridescence-producing scale ridges (Parnell *et al.*, 2018), and outside of *Heliconius*, artificial selection experiments have been able to gradually produce violet structural colour from standing variation in brown populations of the butterfly *Bicyclus anynana* (Wasik *et al.*, 2014). Quantitative traits show continuous variation, and are expected to have complex genetic architectures consisting of many loci each with a small effect on phenotypic variation (MacKay *et al.*, 2009). As a result it can be difficult to gain enough statistical power to detect such loci in mapping studies (Barton & Keightley, 2002; Rockman, 2011). This means that studying the evolution of continuous traits can be challenging when analyses focus on their genetic basis.

Here, we can take advantage of the phenotypic variation occurring across the hybrid zones between iridescent and non-iridescent races of the co-mimics *H. erato* and *H. melpomene* to compare the selection regimes acting on iridescence between species. Hybrid zones are regions where two genetically distinct populations come into contact and interbreed, resulting in clinal variation in allele frequencies and quantitative traits across the hybrid zone. Clines can be maintained by divergent selection along an environmental gradient (Endler, 1977), or by a balance

between migration between the differentiated populations, and selection against unfit hybrid offspring, also known as the tension zone model (Barton & Hewitt, 1985). Since *Heliconius* species are often composed of many adjacent colour pattern races connected by hybrid zones (Mallet, 1993; Rosser *et al.*, 2012), studying these hybrid zones has provided much insight into the evolution of warning colouration in the genus. The width, or steepness of a cline can be informative about the strength of selection acting on that trait. Narrow clines can indicate strong selection against hybrids, whereas wider clines suggest weaker selection or greater migration rates between parental populations (Barton & Hewitt, 1985). Narrow clines in *H. erato* reveal that strong positive frequency-dependent selection maintains hybrid zones in Peru (Mallet & Barton, 1989). The positions of clines relative to one another also provides insight into how selection is acting. The centre of a cline indicates the point at which the direction of divergent selection changes, therefore if the centres of clines in different traits coincide, they may be controlled by the same source of selection (Barton & Hewitt, 1985), however if they become displaced, this suggests they are being controlled by separate selective regimes (Baldassarre *et al.*, 2014). It has been discovered that different colour pattern clines within a single *Heliconius* species can become uncoupled due to the joint effects of differences in dominance, dispersal, and strength of selection (Salazar, 2012). If many clines coincide and are "stepped", that is they are steeper than expected at the centre, and are flanked by shallow tails, this suggests that the loci are in linkage disequilibrium (though not necessarily physically linked), with the strength of direct selection on each individual locus being outweighed by the indirect selection acting on all loci in linkage disequilibrium (Kruuk *et al.*, 1999). A cline with a stepped shape may therefore be reflecting strong selection at many loci across the genome, rather than solely on the trait in question (Szymura & Barton, 1991).

Until now, work on *Heliconius* hybrid zones has only focused on discrete pigmentary colouration with a simple genetic basis. Here we use cline theory to look at the selection regimes acting on quantitative iridescent structural colour in *H. erato* and *H. melpomene* and compare this to the clines seen in a trait controlled by a single genetic locus, the yellow bar on the hindwing. The yellow bar is one of the colour pattern elements that have been well studied in the past and

has been shown to function as a warning signal to predators (Mallet, 1986; Blum, 2002). We predict that if iridescence is under the same selection regime as the yellow bar, and is part of the warning signal, we would expect the cline centres of these traits to coincide. We also predict that if iridescence is evolving convergently, due to Müllerian mimicry, the iridescence clines should also coincide between species. This study is the first description of geographic variation in iridescence in *Heliconius*, and it lays the foundation for future research to take advantage of the genetic and phenotypic variation found across the hybrid zone and begin to uncover the genetic architecture of iridescence.

2.3 *Materials and Methods*

2.3.1 *Collection of butterfly samples*

Wild *Heliconius melpomene* and *Heliconius erato* individuals were collected with hand nets from several sites along the Pacific coast of Colombia and Panama during 2015 and 2016 (Figure 2.1, Table 2.1). Wings were removed from individuals and stored inside envelopes. Bodies were preserved in NaCl saturated 20% dimethyl sulfoxide (DMSO) 0.25M EDTA for future genetic analysis. 353 *H. erato* and 53 *H. melpomene* individuals were collected in total. Samples collected on our field trips are housed in the University of Sheffield. Samples were also acquired from collections housed in the University of Cambridge, Universidad del Rosario, and the Smithsonian Tropical Research Institute (STRI), which were collected between 2003 and 2015 (Figure 2.1, Table 2.1). In total, 682 *H. erato* and 184 *H. melpomene* were included in the analysis.

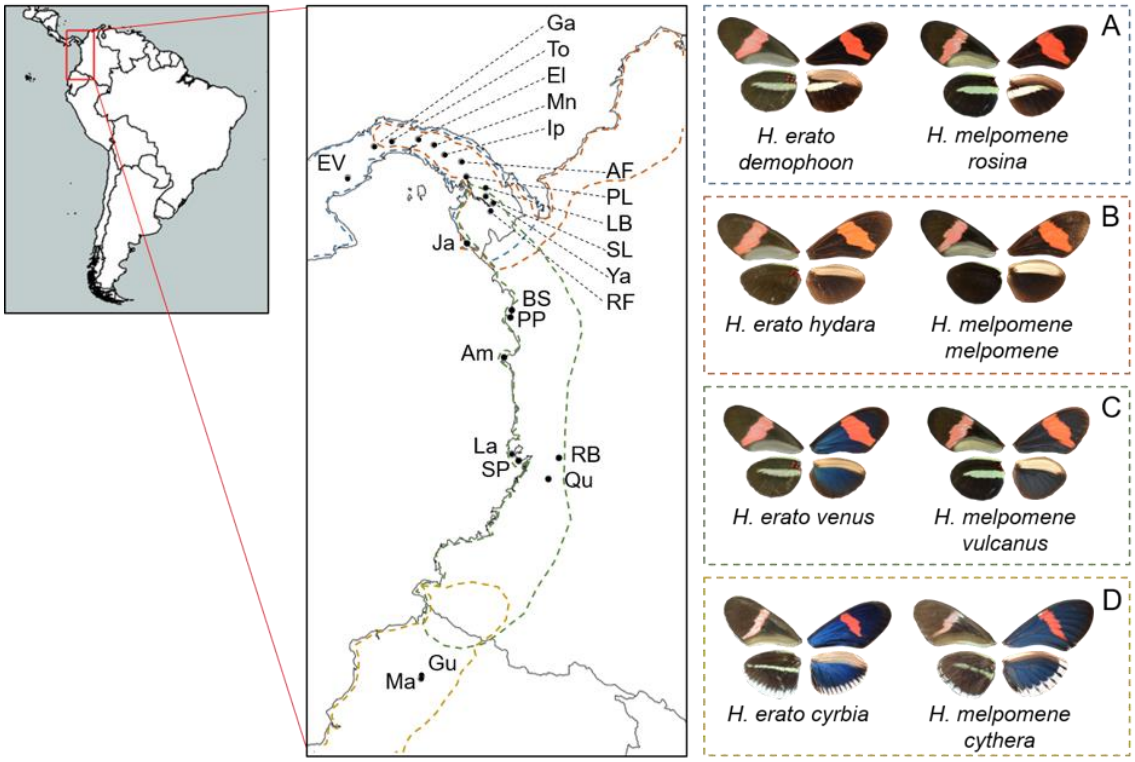

Figure 2.1 – Sampled populations in Colombia, Panama and Ecuador (black points). Sites are labelled with abbreviations, for further information about these sites and collections, see Table 2. Photographs show the phenotypes of mimetic races of *H. erato* and *H. melpomene* from (**A**) Central America, (**B**) North Colombia, (**C**) Western Colombia, and (**D**) Western Ecuador. For each pictured phenotype, the wings on the left-hand side show the ventral wing pattern, and the wings on the right-hand side show the dorsal wing pattern. Approximate ranges for the mimetic race pairs are outlined with dashed lines (Rosser *et al.*, 2012).

Table 2.1 – Number of *H. erato* and *H. melpomene* individuals from each sampling location. Abbreviation of site name in brackets. The institutions housing the collections (the University of Sheffield, the University of Cambridge, Universidad del Rosario, and the Smithsonian Tropical Research Institute) are also recorded.

Locality (Site, Province, Country)		Lat., Lon.	*Heliconius erato*	*Heliconius melpomene*	Collection housed in	Year(s) collected
(Ma)	Mashpi, Pichincha, Ecuador	0.17533, -78.90752	25	21	Sheffield	2014, 2015
(Gu)	Guayllabamba, Pichincha, Ecuador	0.22022, -78.88961	7	6	Sheffield	2014
(Qu)	El Queremal, Valle del Cauca, Colombia	3.53199, -76.75461	43	9	Sheffield	2015
(RB)	Río Bravo, Valle del Cauca, Colombia	3.88274, -76.57716	0	11	Sheffield	2015
(SP)	San Pedro, Valle del Cauca, Colombia	3.83691, -77.25734	41	0	Sheffield	2015
(La)	Ladrilleros, Valle del Cauca, Colombia	3.939444, -77.36889	23	3	Rosario	2003, 2004, 2007, 2008, 2010, 2012
(Am)	Amargal, Chocó, Colombia	5.57187, -77.50211	68	5	Sheffield	2015
(PP)	Playa Parra, Chocó, Colombia	6.24066, -77.39544	18	0	Sheffield	2016
(BS)	Bahía Solano, Chocó, Colombia	6.38765, -77.38557	73	17	Sheffield	2016
(Ja)	Jaqué, Darién, Panama	7.48767, -78.12733	110	11	Sheffield	2015
(RF)	Rancho Frío, Darién, Panama	8.01974, -77.73252	19	1	Cambridge	2011

Table 2.1 – continued

Locality (Site, Province, Country)		Lat., Lon.	*Heliconius erato*	*Heliconius melpomene*	Collection owner	Year collected
(Ya)	Yaviza, Darién, Panama	8.15602, -77.69308	40	1	Cambridge	2011
(SL)	Santa Librada, Darién, Panama	8.27971, -77.80982	19	23	Cambridge	2011
(LB)	Puerto Lajas Blancas, Darién, Panama	8.39141, -77.84473	1	2	Cambridge	2011
(PL)	Puerto Lara, Darién, Panama	8.61355, -78.13982	58	28	Cambridge	2011
(AF)	Agua Fría, Darién, Panama	8.858867, -78.22508	18	8	STRI	2015
(Ip)	Ipeti, Panama, Panama	8.972917, -78.5106	16	17	STRI	2015
(Ma)	Mangowichi, Panama, Panama	9.137667, -78.68952	35	12	STRI	2015
(El)	El llano, Panama, Panama	9.237533, -78.95347	30	1	STRI	2015
(To)	Tocumen, Panama, Panama	9.200417, -79.39525	20	3	STRI	2015
(Ga)	Gamboa, Colón, Panama	9.11605, -79.69837	7	0	STRI	2015
(EV)	El Valle, Coclé, Panama	8.593233, -80.14108	11	5	STRI	2015

2.3.2 *Phenotypic measurements*

Digital images of butterfly wings were recorded using a Nikon D7000 DSLR camera fitted with an AF-S DX Micro NIKKOR 40 mm f/2.8G lens (Nikon UK Ltd., Surrey, UK), mounted on an adjustable platform. Standardised lighting conditions were achieved using two external natural daylight fluorescent lights, mounted to illuminate at 45 degrees from incident, to maximise brightness of observed iridescent colour. Photographs were taken with a shutter speed of 1/60 sec and an aperture of f/10. Each sample was photographed with an X-Rite colorchecker passport (X-Rite, Inc., MI, USA) in shot. The Nikon raw (.NEF) image files were converted to standard raw files (.DNG) using Adobe DNG converter (Adobe Systems Inc., USA). The RGB channels in the images were then linearized using the neutral grey scale on the X-Rite colorchecker passport and the GNU Image Manipulation Program, version 2.8. Images were saved as TIFF files to reduce the loss of information from compression.

The mean RGB values of a region on the right forewing and a region on the right hindwing were measured (Figure 2.2). If the wings on the right-hand side showed damage, wings on the left-hand side were used. These regions were defined by wing venation, to allow consistency between samples. Wing regions were selected using the polygon selection tool in ImageJ, version 1.50b (Abràmoff *et al.*, 2004), and the mean RGB scores in these wing regions were measured using the Color Histogram plugin. The blue colour appears faded, likely due to wear, on the oldest and most damaged individuals. These were therefore excluded prior to phenotypic measurement, leaving 561 *H. erato* and 167 *H. melpomene* individuals.

Figure 2.2 – The wing regions highlighted were used to gather mean RGB scores for each individual.

To test how large the error in RGB measurements was compared with real variation between individuals, a test for repeatability outlined in Whitlock and Schluter (2009) was carried out. 26 individuals were photographed a second time under the same conditions on a different day, and a second set of RGB measurements were taken. These individuals were selected from regions in which varying levels of iridescence are seen (20 individuals from Valle del Cauca, Colombia, and 6 individuals from Daríen, Panama). Variance among individuals was calculated by taking the difference between the group mean square and the error mean square, and dividing it by the number of replicates. These components of variance were extracted from a linear regression in R version 3.2.3 (R Development Core Team 2015). The fraction of total variance that is due to true differences between individuals was then calculated by dividing the variance among individuals by itself plus the variance within individuals (the error mean square).

A measure of iridescence was determined for each individual by taking the mean blue channel value (B) and the mean red channel value (R) for both wing regions and calculating:

Eq1. $$BR = (B-R)/(B+R)$$

This gives a standardised score of how blue an individual is, with BR = 1 being the bluest, and BR = -1 being the most red.

Due to a lack of sampling sites across the Ecuadorian-Colombian border, where the *H. erato venus/H. erato cyrbia* and *H. melpomene vulcanus/H. melpomene cythera* hybrid zones lie, the Ecuadorian individuals were excluded from the full hybrid zone analysis below. Instead, we carried out Welch's two-sample t-tests for each species to compare BR scores between the most southerly Colombian populations and the Ecuadorian population. A significant difference in iridescence would indicate the presence of a second iridescence cline across the more southern hybrid zone.

2.3.3 *Estimation of 'yellow bar' allele frequencies*

Allele frequencies for the yellow hindwing bar were estimated based on phenotype for both species. This was done for all sampling sites in Colombia and Panama with five or more individuals. The 'yellow bar' phenotype was scored categorically, according to Mallet (1986), who showed that this phenotype segregates in the same way for both *Heliconius erato* and *H. melpomene.* Individuals of both species lacking a yellow bar entirely were assigned to category 1, the North Colombian phenotype (Figure 2.1 B). Individuals with the "shadow bar" phenotype, where the outline of the bar can be seen on the underside of the hindwing without any yellow pigment, and without a bar on the upper side of the hindwing, were assigned to category 2, the "heterozygote" phenotype. Individuals with a yellow bar present on the underside of the hindwing only were assigned to category 3, the West Colombian phenotype (Figure 2.1 C). Individuals with a yellow bar on both sides of the hindwing were assigned to category 4, the Central American phenotype (Figure 2.1 A). Variation in the yellow bar across this hybrid zone is controlled by three alleles: the North Colombian yellow bar allele (Y), the West Colombian yellow bar allele (y_{wc}) and the Central American yellow bar allele (y_{ca}). The genotype of the North Colombian phenotype is YY, the genotype of the West Colombian phenotype is $y_{wc}y_{ca}$ or $y_{wc}y_{wc}$, the genotype of the Central American phenotype is $y_{ca}y_{ca}$. Whilst Y is effectively dominant, Yy_{wc} and Yy_{ca} individuals both have the category 2 "shadow bar" phenotype. We calculated the allele

frequencies at each locality for each species using the Hardy-Weinberg equation for three alleles, based on the observed frequencies of the four genotypic categories:

$$p^2 + 2pq + q^2 + 2pr + 2qr + r^2 = 1$$

and

$$p + q + r = 1$$

where p, q and r are the allele frequencies and p^2 was the observed frequency of the North Colombian phenotype (YY) and q^2 was the observed frequency of the Central American phenotype ($y_{ca}y_{ca}$), allowing me to solve for r, the frequency of the West Colombian allele.

We are primarily interested in the frequency of the West Colombian allele (y_{wc}) as it is the West Colombian population that has the iridescent blue colour and therefore we may expect some concordance and coincidence in the clines of the two traits if they are subject to the same selective pressures. The yellow bar allele for the Ecuadorian samples is recorded as y_{ec}, as the iridescent Ecuadorian races, *H. erato cyrbia* and *H. melpomene cythera* (Figure 2.1 D) are phenotypically distinct, with the presence of a white wing margin that is controlled by a fourth allele at this locus (Joron *et al.*, 2006). They form a second hybrid zone near the Colombian-Ecuadorian border with *H. erato venus* and *H. melpomene vulcanus* (Figure 2.1 C), however it is difficult to access this region for sampling, preventing us from carrying out full geographic cline analysis on this hybrid zone.

2.3.4 *Geographic cline analysis*

We modelled the changes in frequency of the West Colombian yellow bar allele (y_{wc}) and level of iridescence (BR) in *Heliconius erato* and *Heliconius melpomene* along the transect by fitting a number of equilibrium geographic cline models (Szymura & Barton, 1986, 1991; Gay *et al.*, 2008) using the Metropolis-Hastings Markov chain Monte Carlo algorithm

(Metropolis *et al.*, 1953; Hastings, 1970), all carried out in the R package HZAR (Derryberry *et al.*, 2013).

For these analyses, the blue score of these individuals were rescaled between 0 and 1. This was done by taking the blue score (BR value from eq1) of each individual, minus the lowest blue score recorded for the species, divided by the maximum blue score minus the minimum blue score. Ecuadorian populations were excluded, as were sampling sites with less than five individuals, leaving 529 *H. erato* and 126 *H. melpomene*.

For each trait, we compared the fit of fifteen models, to determine the parameters which best describe cline shape. These models represented different combinations of five exponential decay curve (tail) fitting options (no tails fitted; left tail only; right tail only; both tails; mirrored tails), and three methods of fitting allele frequencies at the cline ends (pMin, pMax) for the yellow bar (fixed to pMin = 0 and pMax = 1; observed values; estimated values). For the iridescence cline, the trait means and variances at the cline ends were either estimated within the model, or fixed to the observed value at the first and last locality. The Metropolis-Hastings algorithm was run with a chain length of 100,000 and a burn-in of 10%, with a randomly selected seed.

Model selection was carried out using Akaike information criterion score corrected for small sample size (AICc). The model with the lowest AICc score was selected as the best fitting model.

We extracted the maximum-likelihood cline for each trait, which provided us with estimates of the geographical cline centre, the width of the cline (1/maximum slope) and, depending on the model implemented, pMin and pMax; the starting positions of the tails (δ, left and/or right), as the distance from the centre of the cline; and the slopes of the tails (τ, left and/or right). For each parameter, we also extracted the range of values within two log-likelihood units of the maximum-likelihood estimate.

We tested whether the clines for iridescence and the yellow bar allele were coincident, i.e. whether the cline centres were the same, and whether they were concordant, i.e. whether the cline widths were the same. To do this within species, we first modelled the iridescence cline in

each species allowing the centre and width to be unconstrained. We then fixed the cline centre to be equal to the centre of maximum likelihood yellow bar allele frequency cline for each species. Finally, the cline width was fixed to be equal to the width of the best fitting yellow bar allele frequency cline for each species. This was then repeated reciprocally, by fixing the centre and width of the best fitting yellow bar cline to be the same as the best estimates of the corresponding values for the iridescence cline.

Similarly, to test for coincidence and concordance of the iridescence clines between the two species, we modelled the iridescence cline in *H. erato* three times, once allowing the cline centre and width to be unconstrained, once fixing the centre to be equal to the centre of the best fitting iridescence cline in *H. melpomene*, and once fixing the widths to be equal to the width of the best fitting iridescence cline in *H. melpomene.* Again, this was repeated reciprocally, by fixing the centre and width of the best fitting iridescence cline in *H. melpomene* to be the same as the best estimates of the corresponding values for the iridescence cline in *H. erato*.

In each test, if the centre constrained model had an AICc score more than two points lower than the unconstrained model, the clines were considered coincident, and if the width constrained model had an AICc score more than two points lower than the unconstrained model, the clines were considered concordant.

2.3.5 *Estimating strength of selection*

To estimate the strength of selection acting on y_{wc} in each species, the following equation was used from Barton and Gale (1993):

$$s^* = (1.782\sigma/\omega)^2$$

Where s^* is the difference in mean fitness between populations at the edge of the cline, and populations at the centre. This demonstrates the total selection acting on the locus/loci which contribute to the phenotype. This is the total selection required to maintain a cline of width (ω), given the dispersal distance per generation (σ). I used the maximum likelihood estimate of cline

width for y_{wc} from the geographic cline analyses. I also estimated *s** for the two log-likelihood support limits of cline width. Dispersal estimates were taken from Mallet *et al*. (1990) and Blum (2002).

2.4 *Results*

2.4.1 *Phenotypic variation*

Strong phenotypic variation was observed across our range of sampling sites, with several major differences being apparent between the co-mimetic species pair, *H. erato* and *H. melpomene* (Figure 2.3). The Ecuadorian yellow bar allele (y_{ec}) was fixed in all Ecuadorian sampling sites, and the West Colombian yellow bar allele (y_{wc}) was fixed in all Colombian sampling sites, apart from at some of the northernmost Colombian sampling sites near Bahía Solano (Figure 2.3 A, B). In *H. melpomene*, the frequency of y_{wc} gradually decreases, and persists at comparable frequencies to the North Colombian yellow bar allele (Y) for ~200 km, before the Central American yellow bar allele (y_{ca}) becomes predominant (Figure 2.3 A). In contrast, in *H. erato* Y becomes the predominant allele, rather than persisting alongside y_{wc}, and towards the end of the transect, y_{ca} becomes the predominant allele (Figure 2.3 B).

In both species the blue score, which was used as a proxy for the level of iridescence, decreases across the transect (Figure 2.3 C, D). The colour measurements used to calculate the blue score were highly repeatable (Table 2.2). The distribution of these values is bimodal in the two species (Figure 2.4). The bluest *H. melpomene* individuals have much lower blue scores than the bluest *H. erato* (Figure 2.4), which is expected, as *H. melpomene* display less vivid iridescence. A significant difference in the blue score between the Ecuadorian and the southernmost Colombian populations of *H. erato* (t (38.5), $p = 0.022$; figure 2.5 A) indicates that a second iridescence cline exists across the *H. erato venus/H. erato cyrbia* hybrid zone. A significant difference in blue score can also be seen between the Ecuadorian and the southernmost Colombian populations of *H. melpomene* (t (10.1), $p = 0.009$; figure 2.5 B), indicating that a second iridescence cline also exists across the *H. melpomene vulcanus/H. melpomene cythera*

hybrid zone. The lack of sampling between Ecuador and Colombia means that we cannot infer how iridescence or the yellow bar alleles change across this region, therefore all subsequent analyses focus on the transect through Colombia and Panama.

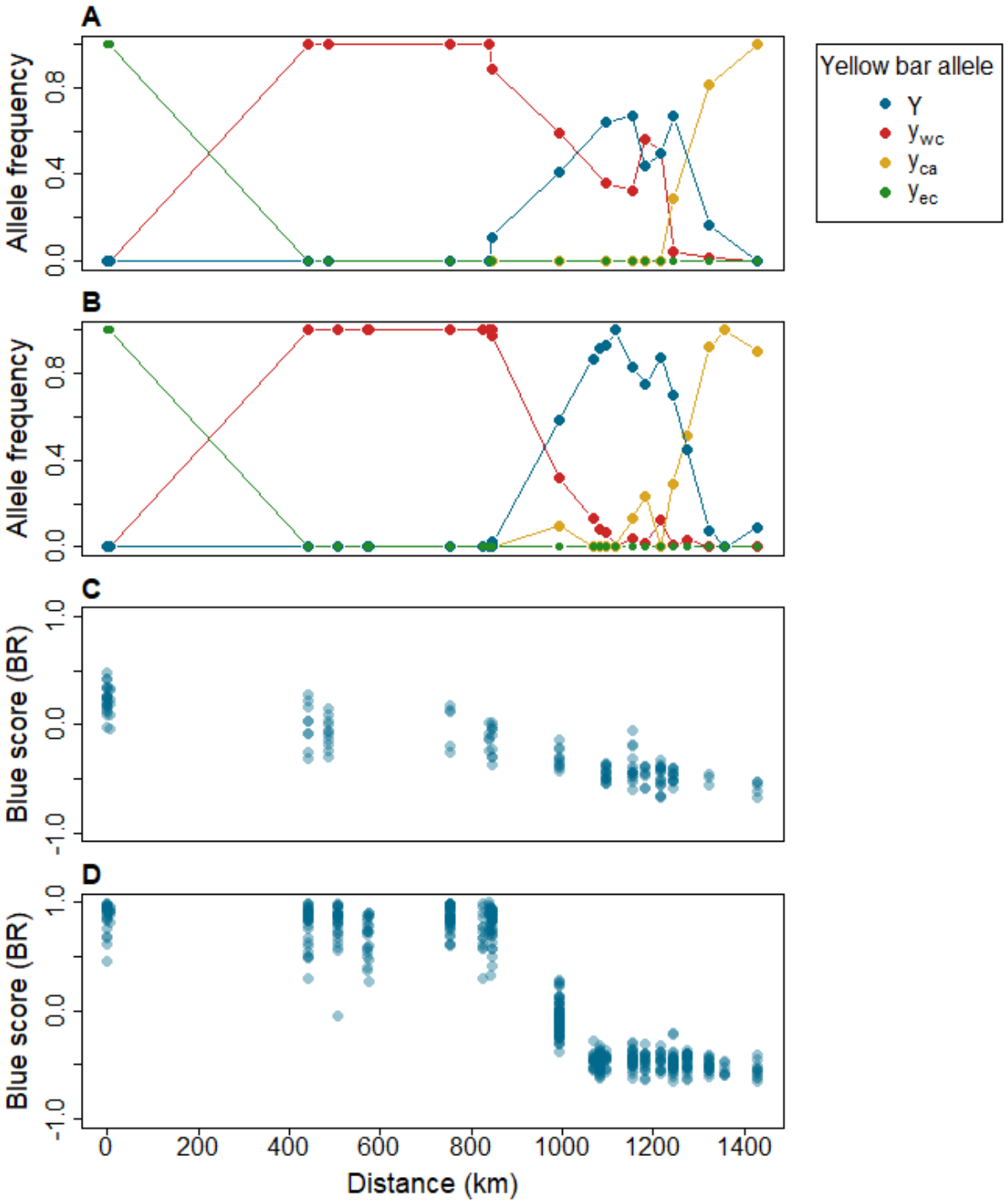

Figure 2.3 – Variation in wing pattern phenotypes across the transect, from 0 km at Mashpi, Ecuador, to 1429.18 km at El Valle, Panama. (**A, B**) Frequency of the North Colombian (Y), West Colombian (y_{wc}), Central American (y_{ca}), and Ecuadorian (y_{ec}) yellow bar allele at each site with

5 or more samples for (**A**) *H. melpomene* and (**B**) *H. erato*. (**C, D**) Blue score (BR) values of each individual for (**C**) *H. melpomene* and (**D**) *H. erato*.

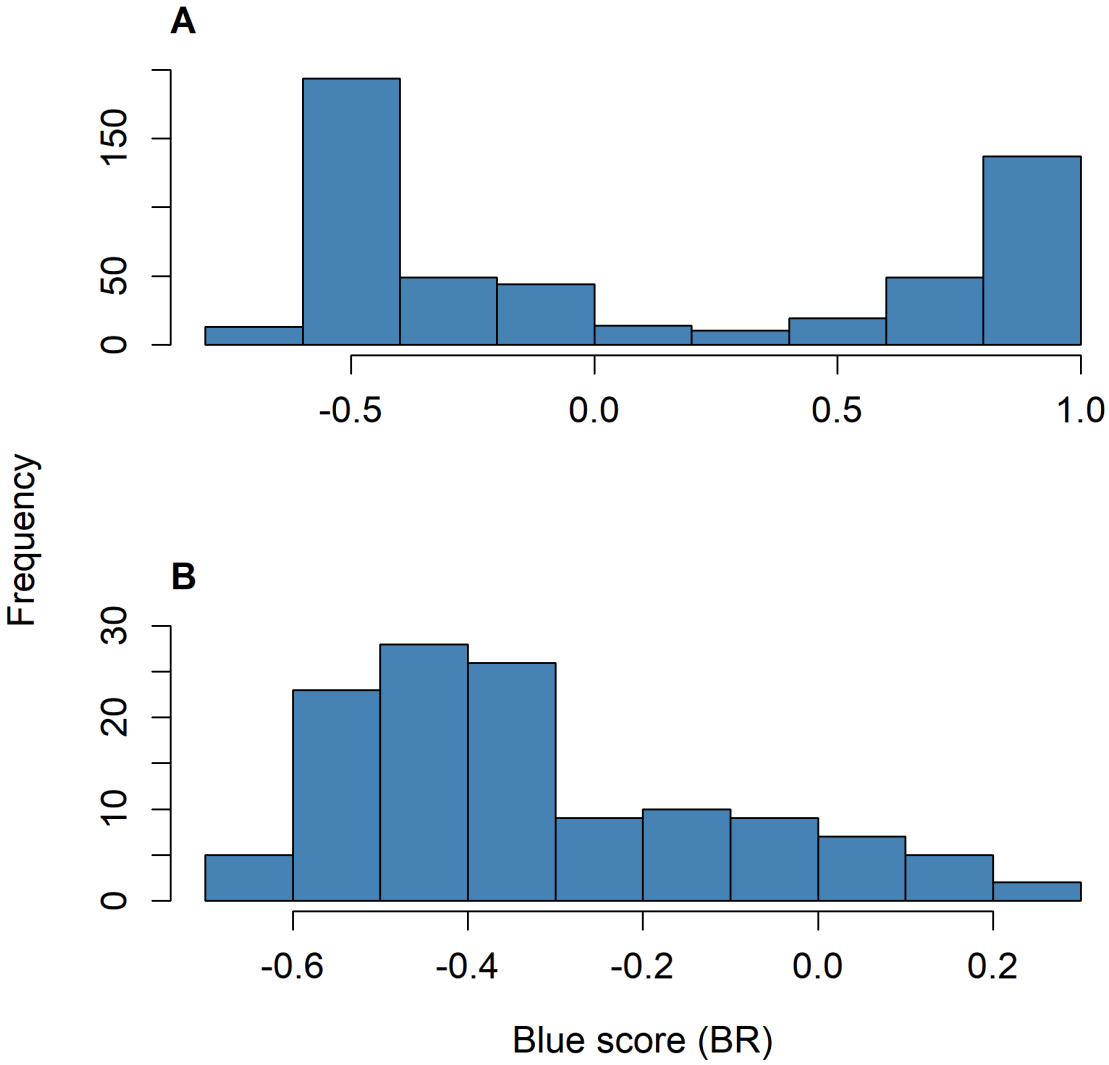

Figure 2.4 – Histograms showing the distribution of blue scores for (**A**) *H. erato* and (**B**) *H. melpomene* individuals from Colombia and Panama.

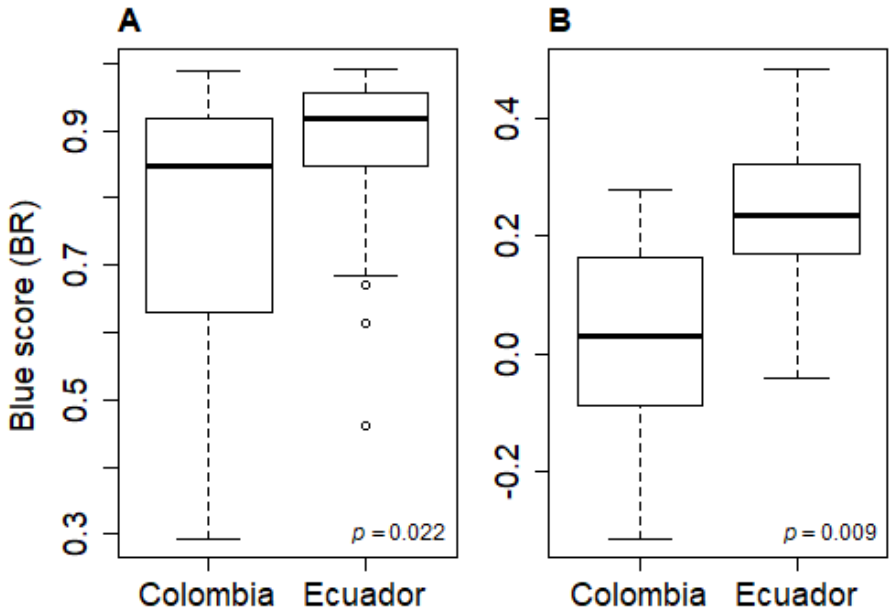

Figure 2.5 – Comparison between levels of iridescence in the southern-most Colombian population and the Ecuadorian populations of **(A)** *H. erato* and **(B)** *H. melpomene*.

Table 2.2 – The repeatability of measurements of mean red and blue colour channels from defined wing regions from digital photographs.

Measurement	Df	Mean square groups	Mean square error	F value	P	Repeatability
Wing region 1, blue mean	25, 26	1298.8	9.3	139.3	<0.001	0.986
Wing region 2, blue mean	25, 26	1763.6	23.8	74.13	<0.001	0.973
Wing region 1, red mean	25, 26	310.59	2.05	151.7	<0.001	0.987
Wing region 2, red mean	25, 26	396.6	2.3	171.3	<0.001	0.988

2.4.2 *Geographic cline analysis*

To compare the selection regime acting on iridescence and the yellow bar in *H. erato* and *H. melpomene*, clines were modelled on variation in the blue score (BR), and the frequency of the y_{wc} allele. For *H. erato*, the best cline model for the blue score fitted a right tail to the cline at the Panamanian end of the transect, and estimated the cline to be 86.66 (16.84 – 147.54) km wide, with the cline centre at 544.67 (534.47 – 555.79) km along the transect (Table 2.3, Figure 2.6 A). For the y_{wc} allele frequency cline in *H. erato*, the best model also fitted a right tail, and estimated the cline to be 99.17 (10.68 – 148.40) km wide, with the centre being 536.63 (427.82 – 548.23) km along the transect (Table 2.3, Figure 2.6 A).

In *H. melpomene*, the best fitting model for the blue score did not include tails at either end of the cline, and used the observed mean and variance at either end. It estimated the cline to be 574.26 (442.04 – 728.80) km wide, with the cline centre being 541.47 (495.39 – 585.69) km along the transect. For y_{wc} in *H. melpomene*, the best fitting cline model also did not include tails, and fixed pMin and pMax to the observed allele frequencies at the ends of the cline. It estimated the cline to be 452.47 (303.85 – 714.66) km wide, with the cline centre being 649.14 (593.89 – 695.66) km along the transect (Table 2.3, Figure 2.6 B).

In *H.* erato, the iridescence and yellow bar clines are both coincident and concordant (Table 2.4). The two log-likelihood support limits of the cline centre and width estimates for blue score and y_{wc} overlap in *H. erato* (Table 2.3). When comparing an unconstrained maximum likelihood cline for blue score, to models where its centre and width were constrained to be the same as that of the y_{wc} allele frequency cline, the width constrained models had the lowest AICc score of -1279.16. However, neither the unconstrained model (ΔAICc 1.99), nor the centre constrained model (ΔAICc 1.74) had a worse fit, suggesting that the clines of these two traits are both coincident and concordant. When this same test was repeated reciprocally, by fixing the parameters of the maximum likelihood allele frequency cline model for y_{wc} to be equal to the corresponding values of the blue score cline, similar results were found. The width constrained

model had the lowest AICc score (21.46), and neither the centre constrained model (ΔAICc 1.42), nor the unconstrained model (ΔAICc 1.75) were worse fits.

For *H. melpomene*, the iridescence and yellow bar clines are concordant, but not coincident (Table 2.4). The two log-likelihood support limits of the cline centre estimates for blue score and y_{wc} do not overlap, whereas the support limits for the cline widths of the traits do overlap (Table 2.3). When comparing an unconstrained maximum likelihood cline for blue score, to models where its centre and width were constrained to be the same as that of the y_{wc} allele frequency cline, an unconstrained model had the lowest AICc score of -185.18. The width constrained model was not a worse fit than the unconstrained model (ΔAICc 0.98), however the centre constrained model was a worse fit (ΔAICc 26.96), suggesting that the clines of these two traits are concordant, but not coincident. When this test was repeated reciprocally, by fixing the parameters of the maximum likelihood allele frequency cline model for y_{wc} to be equal to the corresponding values of the blue score cline, the results supported this finding. The width constrained model had the lowest AICc score of 18.65, the centre constrained model was a worse fit (ΔAICc 10.23), and the unconstrained model was not a worse fit (ΔAICc 0.92).

The iridescence clines were coincident between species, but the cline in *H. melpomene* is much wider (Table 2.5). The two log-likelihood support limits of the cline centre estimates for blue score overlaps between *H. erato* and *H. melpomene*, whereas the two log-likelihood support limits for the cline widths do not overlap (Table 2.3). When comparing an unconstrained maximum likelihood cline for blue score in *H. erato*, to models where its centre and width were constrained to be the same as that of the maximum likelihood blue score cline in *H. melpomene*, the centre constrained model had the lowest AICc score of -1279.06. The unconstrained model was not a worse fit (ΔAICc 1.92), but the width constrained model was a much worse fit (ΔAICc 559.72). When tested the other way, by fixing the parameters of the maximum likelihood blue score cline for *H. melpomene* to be equal to the corresponding values of the blue score cline for *H. erato*, supporting results were found. The centre constrained cline had the lowest AICc score of -187.30, the unconstrained cline was a marginally worse fit (ΔAICc 2.1), and the width constrained model had a far worse fit (ΔAICc 114.45).

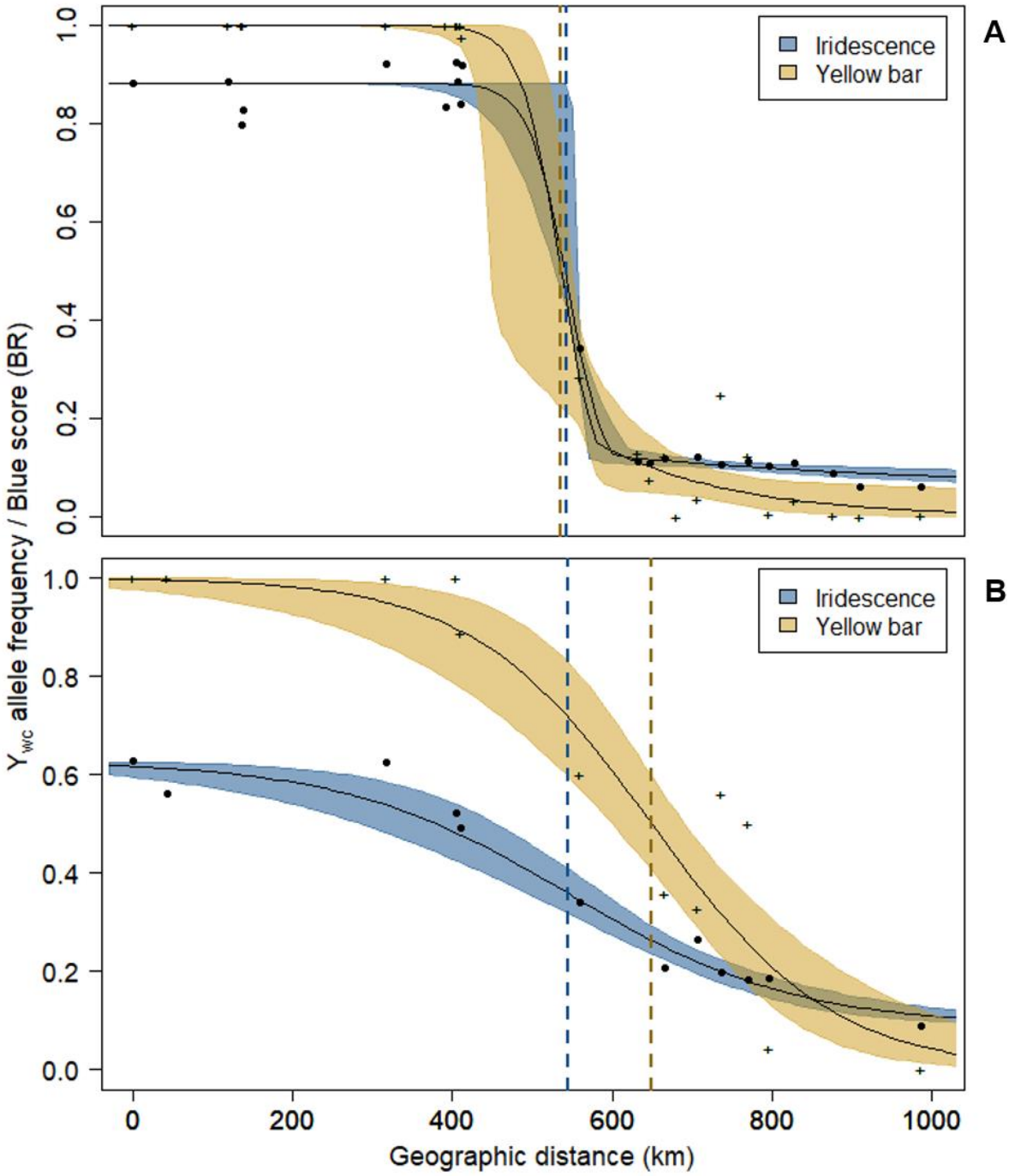

Figure 2.6 – The best fitting geographic clines of iridescence and the West Colombian yellow bar (y_{wc}) allele frequency across a transect of sampling sites (points) for (**A**) *Heliconius erato* and (**B**) *Heliconius melpomene*, over the associated 95% credible cline region (coloured regions). The transect begins (at 0 km) in the Cauca Valley region of Colombia. Vertical dashed lines show the cline centre for each trait.

Table 2.3 – Maximum likelihood estimates of parameters from the best fitting cline models describing variation in iridescence and yellow bar allele frequency across hybrid zones in *Heliconius erato* and *H. melpomene.*

Species	Trait	Best model	Centre (km)	Width (km)	pMin	pMax	δ_R	τ_R
Heliconius erato	Iridescence (BR)	Right tail, fixed mean/variance at cline ends	544.67 (534.47 – 555.79)	86.66 (16.84 – 147.54)	N/A	N/A	52.84 (10.04 – 96.51)	0.06 (0.009 – 0.13)
Heliconius erato	Yellow bar (y_{wc} allele frequency)	Right tail, fixed pMin and pMax	536.63 (427.82 – 548.23)	99.17 (10.68 – 148.40)	0	1	43.23 (0.008 – 85.01)	0.18 (0.008 – 0.64)
Heliconius melpomene	Iridescence (BR)	No tails, fixed mean/variance at cline ends	541.47 (495.39 – 585.69)	574.26 (442.04 – 728.80)	N/A	N/A	N/A	N/A
Heliconius melpomene	Yellow bar (y_{wc} allele frequency)	No tails, fixed pMin and pMax	649.14 (593.89 – 695.66)	452.47 (303.85 – 714.66)	0	1	N/A	N/A

Two log-likelihood support limits are shown in brackets. Width is 1/maximum slope; pMin is the minimum allele frequency at the right end of the cline; pMax is the maximum allele frequency at the left end of the cline; δ_R is the distance from the cline centre at which the right tail begins. T_R is the slope of the right tail.

Table 2.4 – Comparison of iridescence and yellow bar clines within species. Comparisons labelled A are the blue score maximum likelihood cline models with centres and widths constrained to be equal to the corresponding values of the y_{wc} allele frequency cline. Comparisons labelled B are the maximum likelihood allele frequency cline of y_{wc} with centres and widths constrained to be equal to the corresponding values of the blue score cline.

Species	Comparison	Model	Centre (km)	Width (km)	Log-likelihood	AICc	ΔAICc
Heliconius erato	A	No constraints	545.43 (534.34 – 554.66)	83.81 (23.54 – 148.99)	643.64	-1277.17	1.99
	A	Width constrained	542.73 (540.65 – 545.12)	99.17 (fixed)	643.62	-1279.16	0
	A	Centre constrained	536.63 (fixed)	134.22 (118.70 – 152.03)	642.75	-1277.42	1.74
	B	No constraints	536.15 (438.32 – 547.75)	99.35 (26.6 – 147.50)	-7.57	23.21	1.75
	B	Width constrained	538.19 (479.34 – 548.08)	86.66 (fixed)	-7.71	21.46	0
	B	Centre constrained	544.67 (fixed)	78.20 (51.30 – 135.43)	-8.42	22.88	1.42

Heliconius melpomene	A	No constraints	545.42 (496.48 – 584.79)	568.29 (442.85 – 725.69)	95.69	-185.18	0
	A	Width constrained	572.50 (544.62 – 598.94)	452.47 (fixed)	94.15	-184.20	0.98
	A	Centre constrained	649.14 (fixed)	342.07 (271.62 – 451.27)	81.16	-158.22	26.96
	B	No constraints	648.61 (593.61 – 695.77)	460.33 (304.06 – 714.72)	-6.70	19.57	0.92
	B	Width constrained	641.18 (584.42 – 698.52)	574.26 (fixed)	-7.28	18.65	0
	B	Centre constrained	541.47 (fixed)	710.07 (515.12 – 1065.58)	-12.40	28.88	10.23

Table 2.5 – Comparison of iridescence clines between species. Comparisons labelled A are the *H. erato* blue score maximum likelihood cline models with centres and widths constrained to be equal to the corresponding values of the *H. melpomene* blue score cline. Comparisons labelled B are the *H. melpomene* blue score maximum likelihood cline models with centres and widths constrained to be equal to the corresponding values of the *H. erato* blue score cline.

Comparison	Model	Centre (km)	Width (km)	Log-likelihood	AICc	ΔAICc
A	No constraints	543.87 (534.43 – 555.15)	92.56 (22.19 – 147.98)	643.63	-1277.14	1.92
A	Width constrained	512.31 (501.13 – 522.94)	574.26 (fixed)	362.21	-716.34	559.72
A	Centre constrained	541.47 (fixed)	106.96 (94.56 – 124.38)	643.57	-1279.06	0
B	No constraints	543.03 (496.39 – 584.46)	566.81 (439.77 – 728.28)	95.70	-185.20	2.1
B	Width constrained	685.33 (670.49 – 698.96)	86.66 (fixed)	38.48	-72.85	114.45
B	Centre constrained	544.67 (fixed)	564.48 (477.84 – 679.18)	95.70	-187.30	0

2.4.3 *Estimating strength of selection*

We estimated a coefficient for the difference in mean fitness (s^*) across the hybrid zone in both species (Table 2.6), using the maximum likelihood estimates, and two log-likelihood support limits of cline width for y_{wc} (Table 2.3). Mallet *et al*. (1990) gives comparable dispersal estimates for both species of 3.7 km for *H. melpomene* and 2.6 km for *H. erato*. Using these dispersal estimates gives s^* of 0.000212 for *H. melpomene* and 0.00218 for *H. erato*. Blum (2002) suggests that dispersal is actually much higher at 10 km for *H. erato*, in which case s^* is estimated to increase to 0.0323. A comparable estimate of dispersal is not given for *H melpomene*, but based on Mallet *et al*.'s estimate of it being 1.4 times higher than *H. erato*, dispersal in *H. melpomene* could be 14 km, which would estimate s^* as 0.00304.

Table 2.6 – Estimates of the selection coefficient s^* for y_{wc} for varying estimates of dispersal (σ). Estimates of s^* for the two log-likelihood support limits are in brackets. The width of the yellow bar and iridescence clines are not significantly different; therefore, these estimates also apply to the difference in mean fitness due to variation in iridescence.

Species	s^* ($\sigma = 2.6$)	s^* ($\sigma = 3.7$)	s^* ($\sigma = 10$)
H. erato	0.00218 (0.000975 – 0.188)	--	0.0323 (0.0144 – 2.784)
H. melpomene	--	0.000212 (8.51×10^{-5} – 0.000471)	--

2.5 *Discussion*

This is the first time that variation in iridescent structural colour in *Heliconius* has been studied, largely due to the challenges of measuring it. The use of digital photography is an effective method with high repeatability and has allowed us to quantify variation in iridescence across natural populations, and model how it changes with geography. In both *Heliconius erato* and its Müllerian co-mimic *Heliconius melpomene*, we have identified two clines in iridescence. One near the border of Panama and Colombia, across hybrid zones between iridescent and non-iridescent races, and one near the border of Ecuador and Colombia, across hybrid zones between different iridescent races. This suggests that iridescence is under divergent selection. As it was not possible for us to carry out enough sampling to measure the Ecuadorian clines, here we focus on the Panamanian clines.

Our main findings are that iridescence clines are coincident, but not concordant between species, suggesting that they share a common selective agent: selection against hybrid colour phenotypes which are less effective at deterring predators. This also suggests that the convergent evolution of iridescence in these species is due to Müllerian mimicry. The iridescence cline is significantly wider in *H. melpomene*, suggesting weaker selection on iridescence. This may be due to imperfect mimicry between the species, possibly due to developmental constraints preventing *H. melpomene* from producing as vivid iridescence as its co-mimic. We also find that while the iridescence and yellow bar clines are coincident in *H. erato*, which is to be expected if they both selected to function as part of the warning signal, the clines in the same traits have become uncoupled in *H. melpomene.*

We found evidence for shared cline centres and widths between the iridescence and West Colombian yellow bar (y_{wc}) clines in *H. erato*. This would be expected if both traits were subject to similar sources, and strength of selection (Barton & Hewitt, 1985). When clines are formed due to the balancing forces of dispersal between locally adapted parental populations and selection against hybrid offspring, the centre of the cline represents the location where the direction of divergent selection changes (Endler, 1977). Local warning colour patterns in *Heliconius* are

maintained by predator mediated positive frequency dependent selection, and so rarer hybrid colour morphs experience increased predation (Benson, 1972; Mallet & Barton, 1989; Langham, 2004; Dell'aglio *et al.*, 2016), therefore the centre of colour pattern clines across hybrid zones of conspecific *Heliconius* colour pattern races represent the location where the most frequent, and therefore effective, warning colour pattern shifts to that of a neighbouring colour pattern race. The coincidence of the cline centres for iridescence and the y_{wc} allele suggests that iridescence is also under the same divergent selection as the yellow bar phenotype. As it is known that pigment colouration in *Heliconius* functions as a signal of distastefulness to predators (Mallet & Barton, 1989; Kapan, 2001; Dell'aglio *et al.*, 2016), we can't reject the hypothesis that iridescence also functions as a warning signal. The cline widths were not significantly different from one another, suggesting that the strength of selection acting on both these traits is also similar. If the genes controlling iridescence and the yellow bar were physically linked, then we would also expect to see the cline centres of the two traits coincide. This does not appear to be the case, however, as crosses between iridescent and non-iridescent races of *H. erato* (*H. erato cyrbia*, and *H. erato demophoon*, respectively) show that iridescence and the yellow bar appear to segregate independently of one another (Brien, submitted, Appendix 1). It is also possible that the coincidence and concordance of the clines is a result of secondary contact between the iridescent and non-iridescent races, and that they represent an abrupt discontinuity between genetically differentiated populations (Barton, 1983). When several traits under selection change simultaneously across a contact zone, the linkage disequilibrium between them can produce a sharp step at the cline centres (Szymura & Barton, 1986). Since there is a right tail in both iridescence and the yellow bar clines, there is a possibility that the clines are both stepped, but we were unable to fit the left tail here due to uneven sampling of the hybrid zone. Alternatively, the right tails may reflect genuine asymmetry, due to hybrid zone movement or asymmetric selection favouring the North Colombian yellow bar alleles and non-iridescent alleles across the hybrid zone into western Colombia.

A different selection regime appears to be affecting colour pattern in *H. melpomene*. The centre of the y_{wc} allele frequency cline for this species is located significantly further north than

the cline centre for iridescence. This would suggest that the two colour pattern traits are influenced by different drivers of divergent selection. The centre of the iridescence cline in *H. melpomene* does, however, significantly overlap with the iridescence cline in *H. erato*. This suggests that iridescence shares a common source of selection in the two species, and the close coincidence of colour pattern clines in separate species suggests a role for Müllerian mimcry in the evolution of iridescence. It is also possible that the hybrid zones in both species also coincide with population density troughs, which can trap clines and prevent them from moving (Barton, 1979; Barton & Turelli, 2011). It has been suggested that concordant *H. erato* and *H. melpomene* hybrid zones in Peru are spatially stable due to a population density trough caused by a rainfall peak at the edge of the Amazon basin (Rosser *et al.*, 2014).

The uncoupling of the iridescence and y_{wc} allele frequency clines in *H. melpomene* may be a result of dominance drive. If a trait with a dominant and a recessive allele is under positive frequency-dependent selection, even if both alleles have equal fitness, the dominant allele will tend to increase in area relative to the recessive allele (Mallet, 1986). Mallet (1986) predicted that the cline which has formed between the Central American yellow bar allele (y_{ca}) and the North Colombian yellow bar allele (Y) could shift position due to dominance drive, as the location of the hybrid zone is not determined by selection caused by environmental features, and Y is dominant to y_{ca}. The y_{wc} allele is recessive with respect to the Y allele, but dominant with respect to the y_{ca} allele. Since *H. melpomene* generally disperses further per generation than *H. erato* (Mallet *et al.*, 1990; Nadeau *et al.*, 2014), the y_{wc} allele could spread unnoticed as a recessive allele through the Y dominant region, and to re-emerge where the y_{ca} allele begins to become prevalent. As y_{wc} is dominant with respect to y_{ca}, this could cause the y_{wc} allele frequency cline to move north due to dominance drive. Lower dispersal per generation, and stronger selection, could explain why cline uncoupling by dominance drive is not seen in *H. erato*.

An alternative explanation is that the y_{wc} allele frequency cline has become uncoupled due to weaker selection acting on colour patterns in this species. Selection coefficient estimations show that selection on the y_{wc} allele could be approximately ten times weaker in *H. melpomene* than in *H. erato.* Since the widths of the iridescence clines are not significantly different from the widths

of the y_{wc} allele frequency clines in both species, this suggests that weaker selection is also acting on iridescence in *H. melpomene*.

Whilst the wider colour pattern clines in *H. melpomene* could indicate weaker selection, it might also be evidence of greater levels of gene flow, or both. *H. melpomene* is generally thought to have a higher per generation dispersal rate. Estimates based on cline width and linkage disequilibrium across a hybrid zone have calculated a dispersal rate of 3.7 km for *H. melpomene*, and 2.6 km for *H. erato* (Mallet *et al.*, 1990). While there are dispersal rate estimates of up to 10 km for *H. erato* (Blum, 2002), evidence from population genetics supports that *H. melpomene* disperses further, as *H. erato* shows higher genome-wide F_{ST} estimates across hybrid zones than its co-mimic (Nadeau *et al.*, 2014). Other studies on parallel hybrid zones between neighbouring colour pattern races in this species pair show that *H. melpomene* tend to have wider clines than *H. erato*, but do not show as extreme a disparity in cline widths as is seen in the present study. A study in Peru found clines in colour pattern loci ranging from 8.5 – 10.2 km wide in *H. erato*, and from 11.7 – 13.4 km wide in *H. melpomene* (Mallet *et al.*, 1990). Another study in Ecuador found clines in two colour pattern loci to be 8.9 and 22.6 km wide in *H. erato*, and in 15.7 and 31.7 km wide in *H. melpomene* (Salazar, 2012). The two log-likelihood support limits for iridescence and y_{wc} cline width overlap with these other cline width estimates in *H. erato*, whereas in *H. melpomene*, the clines we model are clearly much wider. Our estimates reveal much lower selection coefficients for y_{wc} in *H. melpomene*, compared to *H. erato*, when using the dispersal estimates of Mallet *et al*. (1990). The *H. melpomene* cline is approximately 4.6 times wider than that of *H. erato*. Therefore, if the strength of selection were the same between species then *H. melpomene* dispersal would have to be 4.6 times higher, which perhaps seems unlikely. It therefore seems most likely that the difference in the width of iridescence and y_{wc} clines between the two species is caused by a less extreme reduction in fitness in the centre of the clines for *H. melpomene*, compared to *H. erato*. Given that the cline widths for iridescence are not significantly different from the y_{wc} cline widths within species, it is likely that a similar disparity exists between the co-mimics regarding the strength of selection on iridescence. *H. melpomene* displays less vivid iridescence than its co-mimic, and the reflectance spectra of iridescent *H. erato* and *H. melpomene*

can be clearly discriminated by the avian visual system (Parnell *et al.*, 2018). There is also evidence that highly reflective warning colours can enhance avoidance learning in avian predators (Waldron *et al.*, 2017). This could mean that the brighter iridescence in *H. erato* serves as a more efficient warning signal, leading to stronger selection on structural colour in this species relative to *H. melpomene*. Imperfect mimicry is likely a by-product of developmental constraints limiting the evolutionary potential of *H. melpomene* to modify the scale ultrastructures required to produce as vivid an iridescent colour as *H. erato* (Parnell *et al.*, 2018). Since the clines in iridescence in both species are relatively wide compared to dispersal distance per generation, and because the estimates of *s** are very low, it would be useful to compare the phenotypic clines to the average genetic clines across the hybrid zones, to test the possibility that the clines in iridescence are neutral.

It is also necessary to consider how the genetic architecture of a trait can influence cline width. Iridescence is a quantitative trait, showing continuous variation. In general, it is thought that several loci are required to produce continuous variation. A classic example of this is human height, which is thought to be influenced by ~180 separate loci (Lango Allen *et al.*, 2010). When considering a multilocus cline, if selection is strong and linkage disequilibrium among loci is high, all the loci involved tend to behave as a single locus, whereas if selection is sufficiently weak, and linkage between loci is sufficiently loose, each locus involved in the trait is effectively independent, reducing the steepness of the cline (Kruuk *et al.*, 1999). It is also possible, as is the case with human height, that environmental variation can contribute to the production of continuous variation. Age and wear on the wings introduce measurement error which increases phenotypic variance, therefore it is possible for relatively few loci to produce apparently continuous variation. Since iridescence clines in both species are the same width as the yellow bar clines, it appears that the iridescence cline is not behaving in a way that would indicate a genetic architecture of many independent loci. Whether this is due to a sufficient build-up of LD between multiple loci, or because iridescence is controlled by a small number of loci, is difficult to tell from phenotypic analysis alone.

Finally, it is worth noting that while measuring iridescence from digital photographs has proved to be an efficient and repeatable method which has allowed us to effectively reconstruct geographic clines, it certainly does not capture all the variation in the visual properties of iridescence. Iridescent colour changes depending upon the angle with which it is viewed, and iridescence in *Heliconius* is known to reflect into the UV (Parnell *et al.*, 2018). Our photographs are only taken from a single angle, and the camera we used can only detect colour in the visible spectrum. Other methods of quantification, such as reflectance spectroscopy, or measuring the physical scale structures which produce iridescence may provide more information about variation in iridescence. In addition, the blue score used in this study only uses the blue and red colour channels, not green, therefore it doesn't quantify the whole colour-space. Any future work on iridescence clines may benefit from considering these other aspects of variation.

2.6 *Conclusions*

Here we use geographic cline analysis to compare the selective regimes of convergent iridescent blue phenotypes in the Müllerian mimics *Heliconius erato* and *Heliconius melpomene* across parallel hybrid zones. In *H. erato* a cline in iridescent colour is coincident with a cline in a colour pattern known to function as a warning of distastefulness to predators. This suggests that iridescence is under the same selection pressure, also playing a role in the warning colour pattern. This is also supported by the finding that iridescence clines are coincident between species, suggesting a change in the direction of selection in the same geographic location in both species. However the iridescence cline is significantly wider in *H. melpomene.* It seems unlikely that this difference can be accounted for by the greater dispersal distances of *H. melpomene* alone, and is more likely a result of weaker selection acting on iridescence in this species, perhaps driven by developmental constraints in the ability of *H. melpomene* to produce the scale structures required to mimic the vivid iridescent blue of certain *H. erato* races. A more polygenic genetic architecture of iridescence in *H. melpomene* could also produce wider clines. Determining the genetic architecture of iridescence in each species would allow us to disentangle these potential

explanations. This is the first investigation into the selection pressures shaping the evolution of iridescence in natural populations of *Heliconius* butterflies. The hybrid zones described in this study provide an ideal setting to study both the genetic basis of iridescence, of which almost nothing is known in animals or plants, as well as the role that quantitative traits play in local adaptation.

3

Quantitative trait divergence is independent of genetic structure across parallel hybrid zones in *Heliconius erato* and *Heliconius melpomene*

3.1 *Summary*

Hybrid zones provide an important insight into how local adaptation proceeds. It has been found that phenotypic differentiation across hybrid zones can be maintained by divergent selection at the underlying loci, despite gene flow across the rest of the genome. This has been demonstrated in traits which show discrete variation and are controlled by few major effect loci. However, divergence in quantitative traits may require divergence at multiple loci, which may lead to greater overall genetic structure. We investigate whether this occurs in the *Heliconius* butterflies of south and central America, where parapatric races with divergent warning colouration come into contact and form hybrid zones. West of the Andes, in Ecuador and Colombia, the Müllerian mimics *Heliconius erato* and *H. melpomene* display quantitative variation in iridescent structural colour. Here, we ask whether divergence in a continuously variable trait is maintained by divergent selection despite high levels of gene flow, or whether strong genetic structure is present. We investigate the population genetic structure of parallel hybrid zones between iridescent and non-iridescent colour pattern races of the co-mimics, using population genomic data from individuals across transects traversing the hybrid zones. We find that *H. erato* shows clear genetic structure across hybrid zones, whereas *H. melpomene* shows very weak structure. In both species, clines in iridescence are uncoupled from genetic structure. This suggests that, much like discrete traits controlled by major effect loci, divergent selection is sufficient to maintain phenotypic differentiation in locally adapted quantitative traits across hybrid zones, despite gene flow. We tentatively suggest that the differences between species are due to alternative population histories, with iridescence diverging in sympatry between races in *H. melpomene*, and in allopatry in *H. erato*, followed by secondary contact.

3.2 *Introduction*

The study of hybrid zones, where genetically differentiated populations are in contact and interbreed, has provided considerable insight into the evolutionary processes shaping taxonomic boundaries. Hybrid zones can be formed in a continuously distributed population, where different alleles are favoured at either end of an ecological gradient, a process known as primary intergradation (Endler, 1977). Alternatively, they can be formed when previously isolated populations, which have become genetically differentiated in allopatry, come into contact, in what is known as a secondary contact hybrid zone (Endler, 1977). Both scenarios can result in clinal variation in quantitative traits and allele frequencies across the hybrid zone. When populations diverge in allopatry and come into secondary contact, several scenarios might occur. Gene flow between previously isolated populations may swamp any adaptive divergence or genetic differentiation which may have accrued in allopatry, homogenising the populations (Abbott *et al.*, 2013), or resulting in the collapse of the diverged taxa into a hybrid swarm (e.g. Taylor *et al*. 2006). Alternatively, independent lineages may emerge following secondary contact, through hybrid speciation (e.g. Ungerer *et al*. 1998; Gompert *et al*. 2006; Stemshorn *et al.* 2011). Divergence in allopatry may have progressed to the point where the two taxa have become entirely reproductively isolated (Coyne & Orr, 2004). Finally, a 'tension zone' may form, where a balance is maintained between gene flow between the parental populations, and selection against their hybrid offspring (Barton & Hewitt, 1985). In this model, the taxonomic boundary between populations is semipermeable, whereby some alleles may pass freely via gene flow between populations, whereas those which are selected against in the adjacent population will not. This can produce a heterogenous landscape of introgression across the genome.

It was previously thought that widespread genomic divergence was required to maintain adaptive differentiation between taxa, however it is now understood that barriers to gene flow need only consist of differences at individual genetic loci (Wu, 2001). Differentiation in phenotypes which show abrupt, discrete variation across hybrid zones can be maintained by strong divergent selection at genomic regions controlling those traits, despite high levels of gene flow and introgression across the rest of the genome. This has been demonstrated in crows

(Poelstra *et al.*, 2014), *Heliconius* butterflies (Nadeau *et al.*, 2014), and warblers (Toews *et al.*, 2016). In contrast, studies which examine clines in quantitative traits that are under divergent selection across hybrid zones, often find that they are accompanied by stepped clines in genetic markers, indicating indirect selection on many different loci across the genome and genetic structure across the hybrid zone, despite some gene flow [e.g. *Larus* gulls (Gay *et al.*, 2008) and *Bombina* toads (Szymura & Barton, 1986)], although divergent selection has also been shown to act on quantitative traits across hybrid zones without population structure [e.g. floral traits in *Ipomopsis* (Milano *et al.*, 2016)]. Quantitative traits tend to have a more complex, polygenic genetic architecture (e.g. human height, Lango Allen *et al*. 2010). Polygenic local adaptation may only require small allele frequency changes, but can also involve greater levels of covariance between loci (Le Corre & Kremer, 2012). The combined action of divergent selection and the build-up of statistical associations between loci can reduce effective migration rates across the genome (Flaxman *et al.*, 2014), therefore an increased level of overall genome-wide differentiation, and population level genetic structure may be expected across hybrid zones over which continuous phenotypic variation is maintained.

We address this in the *Heliconius* butterflies of South and Central America. *Heliconius erato* and *Heliconius melpomene* are Müllerian mimics with bright aposematic wing colour patterns. Where they co-occur, they converge on almost identical wing colour patterns to share the cost of educating predators of their distastefulness. Both species consist of many parapatric colour pattern races connected by hybrid zones. When conspecifics of different races hybridise, their offspring can display novel colour patterns, unlike either parental race. Since predators learn to avoid warning colour patterns, rare phenotypes are at a disadvantage, resulting in positive frequency dependent selection on colour patterns (Mallet & Barton, 1989; Langham, 2004), and maintenance of stable hybrid zones (Mallet, 1986). The diverse colour pattern variation seen in the *Heliconius* genus has been extensively studied, and the vast majority of this variation is determined by a small genetic 'tool kit' of around five major effect loci (Kronforst *et al.*, 2006; Baxter *et al.*, 2009; Reed *et al.*, 2011; Martin *et al.*, 2012; Nadeau, 2016; Nadeau *et al.*, 2016). Generally, it has been found that there are very low levels of genetic differentiation throughout

most of the genome across hybrid zones between parapatric colour races, with a few scattered peaks of divergence, the majority of which correspond to loci controlling colour pattern differences (Nadeau *et al.*, 2012, 2014; Martin *et al.*, 2013; Supple *et al.*, 2013). These examples have helped to demonstrate how discrete differences can be maintained by strong selection in the face of gene flow. However, there are also neighbouring races of *H. erato* and *H. melpomene* which show continuous phenotypic variation across hybrid zones. Close to the border of Panama and Colombia, there are parallel hybrid zones between conspecific races of *H. erato* and *H. melpomene*, across which continuous variation in structural colour is shown. *H. erato venus* and *H. melpomene vulcanus* from Colombia both display blue iridescence, and they hybridize with non-iridescent conspecific races from Northern Colombia and Panama. This provides an opportunity to determine whether this continuous phenotypic divergence is accompanied by genetic structure across the hybrid zone, or whether differentiation is simply maintained by selection in the face of gene flow, as is seen with discrete colour variation in these species.

In this study, we use reference aligned sequence data from individuals sampled across the hybrid zone in each species to determine (i) the extent of genetic structure across the hybrid zone in each species, (ii) whether iridescence varies independently of genetic structure across the hybrid zone, and (iii) whether it is likely that quantitative trait divergence occurred in the presence of gene flow, via primary intergradation, or whether differences arose in allopatry, followed by secondary contact. To do this we used population genomic techniques to characterise genetic structure, and geographic cline analysis to compare variation in genetic structure with variation in iridescence.

3.3 *Materials and Methods*

3.3.1 *Butterfly specimens*

We photographed the wings of 518 *H. erato* and 124 *H. melpomene* individuals which had been collected from wild populations in Ecuador, Colombia and Panama, and phenotyped them to assess their level of iridescence. Collection of the samples is described in Chapter 2, section 2.2.1, and phenotyping protocols are described in Chapter 2, section 2.2.2. Of these samples, we selected a subset of individuals, from localities across the range, to include in genetic analysis (Table 3.1).

Table 3.1 – Summary of the number of individuals from each species that were sequenced from each locality. The number of individuals selected for each type of sequencing is also indicated (RAD-seq: Restriction site associated DNA sequencing; WGS: Whole genome re-sequencing)

		Heliconius melpomene		*Heliconius erato*
Locality	Lat., Lon.	RAD-seq	WGS	RAD-seq
Balsas, El Oro, Ecuador	-3.771738,-79.827451	2	0	10
Mashpi, Pichincha, Ecuador	0.17533, -78.90752	5	9	22
Valle del Cauca, Colombia	3.53199, -76.75461	1	10	63
Amargal, Choco, Colombia	5.57187, -77.50211	1	4	39
Bahia Solano, Choco, Colombia	6.38765, -77.38557	10	0	48
Jaque, Darien, Panama	7.48767, -78.12733	1	10	68
Darien Road, Darien, Panama	8.61355, -78.13982	1	12	49

3.3.2 *Sequencing data*

We used two approaches to generate genomic data. Restriction associated DNA (RAD) sequencing was carried out on 299 *H. erato* and 21 *H. melpomene* individuals, and whole genome re-sequencing was carried out on 45 *H. melpomene*, from sites in Panama, Colombia and Ecuador (Table 3.1). Genomic DNA was extracted from each individual using DNeasy Blood and Tissue Kits (Qiagen). Library preparation and sequencing was carried out by Edinburgh Genomics (University of Edinburgh).

Single-digest RAD libraries were prepared using *Pst1* as the restriction enzyme for 320 individuals, including 267 *H. erato* individuals from a transect across the hybrid zone in Panama and Colombia. Individuals were barcoded with sequences of eight base pairs in length and were pooled into 14 multiplexed libraries. Libraries were sequenced across four lanes in total of the Illumina HiSeq 2500 platform (v4 chemistry), generating 125 base paired-end reads. In total, we obtained 1,470,287,706 DNA sequence reads for *H. erato*. We separated the pooled paired-end reads for each individual using the RADpools program in the RADtools package version 1.2.4 (Baxter *et al.*, 2011), using the option to allow one mismatch in the barcode. Two *H. erato* individuals was discarded due to low read count (<100,000 reads), leaving a total of 265 *H. erato* individuals to be included in the analysis.

TruSeq Nano, gel free libraries were prepared from the genomic DNA samples of 45 *H. melpomene* individuals, including 36 individuals from a transect across the hybrid zone in Panama and Colombia. Libraries were sequenced across five lanes of the Illumina HiSeq 2500 platform (v4 chemistry), generating 125 base paired-end reads. Sequencing was repeated for all individuals across two lanes to increase depth of coverage. In total, we obtained 1,416,796,324 DNA sequence reads for *H. melpomene*.

We checked the quality of all the raw sequencing reads using FastQC (v 0.11.5) and removed any remaining adapters using Trim Galore (v 0.4.1). We aligned the sequence data of all individuals, both RAD sequenced and WGS, to their corresponding reference genomes, either *Heliconius melpomene* version 2 (Davey *et al.*, 2016) or *Heliconius erato* (Van Belleghem *et al.*, 2017) obtained from lepbase (Challis *et al.*, 2016), using bowtie2 (v 2.3.2), using the local

alignment option, and the very-sensitive preset parameters options to improve accuracy of the alignment. We used samtools (v 1.3.1) to sort and index the resulting BAM alignment files. We removed any duplicates which may have arisen during library preparation using the MarkDuplicates program in Picard tools (v 1.92).

3.3.3 *Population structure*

To compare the population structure of *H. erato* with *H. melpomene* across the hybrid zones of interest, we estimated the ancestry of each individual using ADMIXTURE (Alexander *et al.,* 2009), a model-based program which estimates ancestry of unrelated individuals from multilocus single nucleotide polymorphism (SNP) datasets using a maximum likelihood approach. To generate SNP datasets from the 265 RAD sequenced *H. erato* and the 36 whole genome re-sequenced *H. melpomene* from across the hybrid zone transect, we used samtools mpileup (v 1.5) to compute genotype likelihoods and bcftools (v 1.5) for variant calling. This was carried out separately for each species. For a site to be a variant, the probability that it was homozygous for the reference allele across all samples was required to be less than 0.05. Sites were assumed to be biallelic, and insertions and deletions were ignored. For *H. melpomene* we identified 30,027,707 single nucleotide polymorphisms (SNPs), and for *H. erato* we identified 5,088,449 SNPs. These SNP datasets were then filtered to remove SNPs at sites with a phred quality score lower than 30, SNPs at sites which lacked sequence data in 50% or more of the individuals, and SNPs with a minor allele frequency lower than 0.05. Private variants were also removed. This reduced the initial number of called SNPs down to 17,847,578 SNPs in *H. melpomene* and 217,402 SNPs in *H. erato*. For each species, ADMIXTURE (Alexander *et al.*, 2009) was run for a range of assumed genetic clusters (K = 1 to 7), with 10 replicates for each value of K. The optimal value of K was selected using ADMIXTURE's cross-validation procedure, where the K value with the lowest cross-validation error was selected as the best number of genetic clusters to describe the population structure.

We also carried out a principal components analysis to further our investigation of population structure. We used the software PCAngsd (Meisner & Albrechtsen, 2018), which estimates a covariance matrix based on genotype likelihoods for low depth sequence data. We then used eigenvector decomposition to retrieve the principal components of genetic structure. We used the program ANGSD (Korneliussen *et al.*, 2014) to estimate genotype likelihoods, i.e. the marginal probability of the sequencing data given a genotype in a particular individual at a particular site, from the alignment files for each species. We only included sites which had sequence data present in more than 50% of individuals, and which had a minimum mapping quality and base quality score of 20. A likelihood ratio test (*P*-value < 10^{-6}) determined whether sites were variable. This resulted in an estimated 100,538 variable sites for *H. erato* and 15,684,967 variable sites for *H. melpomene*.

3.3.4 *Population differentiation*

To test the extent of genetic differentiation between the iridescence and non-iridescent races, we first measured F_{ST} between all the individuals from the iridescent populations south of the hybrid zone, and all the non-iridescent individuals north of the hybrid zone. Individuals from Jaqué, our sampling site in the hybrid zone, were excluded. Two SNP datasets were generated, one for each species, using samtools mpileup and bcftools (v 1.5), following the same protocol described above, in section 3.2.3, but excluding all individuals collected from the hybrid zone site Jaqué. After filtering, the SNP datasets consisted of 194,839 SNPs for *H. erato* and 17,855,113 SNPs for *H. melpomene*. The SNP datasets were output as variant calling files (VCF). VCFs were converted to genotype likelihood files (Soria-Carrasco 2018), which were used to infer allele frequencies by maximum likelihood, using the iterative soft expectation-maximization algorithm (EM) (Li, 2011) implemented in the program estpEM as used by Soria-Carrasco et al. (2014) and provided by the authors. In each species, genetic differentiation between the two populations was calculated using F_{ST}. Specifically, Hudson's F_{ST} estimator was used (Hudson *et al.*, 1992):

$$F_{ST}^{Hudson} = 1 - \frac{Hw}{Hb} = \frac{p_1(1-p_1) + p_2(1-p_2)}{p_1(1-p_2) + p_2(1-p_1)}$$

Where *Hw* is the within-population heterozygosity, *Hb* is the between-population heterozygosity, and p_1 and p_2 represent the allele frequencies in each population. This was calculated in R for every SNP. Average genome-wide F_{ST} was calculated as a "ratio of averages", by averaging the variance components, *Hw* and *Hb*, separately, as recommended by Bhatia *et al*. (2013).

Since the populations in this study are spread across a large geographic area, it is important to distinguish whether any genetic differentiation is a result of isolation caused by barriers to gene flow, or whether these patterns are simply driven by isolation by distance. To test this, we first estimated average genome-wide F_{ST}, as described above, between all pairs of populations. This was done separately for each species. We then tested for a correlation between the resulting matrices of pairwise F_{ST} and matrices of pairwise geographic distances between the sites using a Mantel test implemented in the R package *ecodist*. If a significant correlation was found, this would suggest isolation by distance is playing a role in the generation of genetic differentiation.

3.3.5 *Cline analysis*

If variation in iridescence across the hybrid zone in *H. erato* and *H. melpomene* is simply the result of neutral diffusion of alleles following secondary contact, we would expect the phenotypic variation to covary with genetic structure across the hybrid zone. If iridescence is under divergent selection, we would expect genes which contribute to this trait to introgress less between the iridescent and non-iridescent populations than neutral alleles, therefore we would expect the iridescence cline to be narrower than a cline in average ancestry (e.g. Scordato et al. 2017). To test this, we compared the shape and position of clines in iridescence with clines in genetic structure across the hybrid zones.

To fit a cline in genetic structure, we took the individual ancestry estimates when two genetic clusters were assumed ($K = 2$) using the ADMIXTURE software and averaged the results across individuals at each sampling location, generating a mean and variance in admixture

proportion for each site across the hybrid zone in each species. We then fitted geographic cline models to variation in the mean admixture proportion of populations by treating it as an allele frequency using the R package Hybrid zone analysis in R (Derryberry *et al.*, 2013). We fit molecular cline models using the Metropolis-Hastings Markov chain Monte Carlo algorithm (Metropolis *et al.*, 1953; Hastings, 1970) to variation in the admixture proportions across the hybrid zone in each species. We fit ten cline models for each species, which varied in five exponential decay curve (tail) fitting options (no tails fitted; left tail only; right tail only; both tails fitted; mirrored tails), and whether the cline ends were fixed to the observed trait mean and variance at the first and last locality, or whether they were estimated. The best fitting model was selected using Akaike information criterion score corrected for small sample size (AICc). The lowest AICc score indicated the best fitting model. We obtained estimates for the geographical cline centre (in km along the transect) and the cline width (1/maximum slope) by extracting the maximum-likelihood cline from the best-fitting model. We also extracted the range of cline centre and width values within two log-likelihood units of the maximum-likelihood estimate.

To test whether clines in iridescence varied independently of clines in admixture proportions, we tested whether they were coincident (i.e. their centres are in the same position) or concordant (i.e. the same width). We ran the maximum likelihood model for the admixture proportion cline in each species three more times, once with the cline centre fixed to be the same as that of the iridescence cline (as modelled in Chapter 2), once with the cline width fixed to be the same as that of the iridescence cline, and once with the cline centre and width unconstrained. If the centre or width constrained model had an AICc score lower, or within two points of the unconstrained model, the clines were considered coincident or concordant, respectively. To confirm these results, we repeated this test reciprocally, by running the maximum likelihood iridescence cline three more times, this time constraining its parameters to be the same as the admixture proportion cline.

3.4 *Results*

3.4.1 *Population Structure*

Using the SNP datasets generated from the reference aligned sequence data, we estimated ancestries for *H. erato* and *H. melpomene* individuals across the hybrid zone, based on varying numbers of genetic clusters using ADMIXTURE. This revealed contrasting patterns of population structure between the co-mimics. The best supported number of genetic clusters in *H. erato* was two, with a "Panama-like" genetic background, and a "Colombia-like" genetic background (Figure 3.1B), with individuals of consistently mixed ancestry found in Jaqué, the sampling site in the hybrid zone. Some introgression from Panamanian *H. erato* populations could also be detected in northern Colombian populations. A single genetic cluster was the best supported model of ancestry for *H. melpomene*, suggesting very little population structure across the hybrid zone for this species. When $K = 2$ in *H. melpomene*, the individuals from the hybrid zone do not show an intermediate ancestry between Panamanian and Colombian populations (Figure 3.1E), as is seen in *H. erato.*

PCA was carried out using the software PCAngsd, based on the genotype likelihoods generated in the software ANGSD. PCA results support the ancestry results, with three clear clusters separated along a single axis for *H. erato*, representing the Colombian populations, the Panamanian populations, and individuals from the hybrid zone (Figure 3.1C). PC1, the first eigenvector, explains 12.3% of genetic variation in *H. erato*, with all subsequent eigenvectors explaining less than 0.5% of genetic variation each (Figure 3.1D). In *H. melpomene*, PC1 explains 6.65% of genetic variation, and this roughly matches geography, separating Colombian from Panamanian individuals, however hybrid zone individuals do not cluster in between Panamanian and Colombian populations (Figure 3.1F), consistent with ADMIXTURE results which show that hybrid zone individuals do not have hybrid ancestry. The first eigenvector also explains proportionally less of the total genetic variation in *H. melpomene* (Figure 3.1G) than is seen in *H. erato* (Figure 3.1D), suggesting less overall population structure in *H. melpomene.*

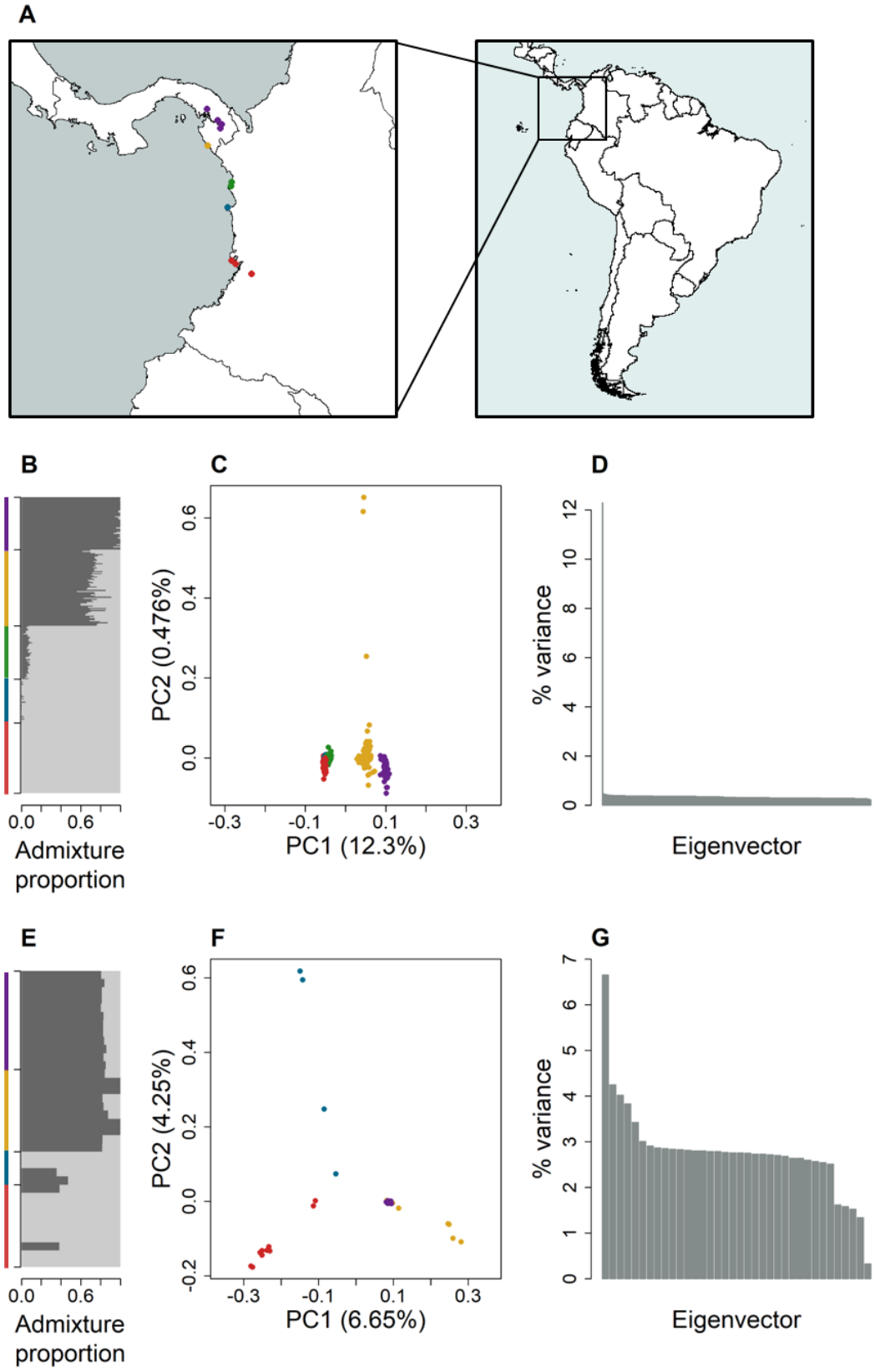

Figure 3.1 – Population structure across the hybrid zones in *H. erato* and in *H. melpomene*. (**A**) Sampling locations across the hybrid zone. (**B, E**) ADMIXTURE analysis, with k = 2. Each horizontal bar represents an individual, and the colour of bar represents the estimated proportion of ancestry which derives from population 1 (dark grey) or population 2 (light grey). Vertical bars

indicate the population of origin, colours match those on the map. (**C, F**) Principal components analysis. Colour of points indicates the population of origin, colours match those on the map. (**D, G**) Percent of genetic variance explained by each eigenvector from the principal components analysis.

3.4.2 *Genomic differentiation and isolation by distance*

Using SNPs from reference-aligned sequence data from either side of the hybrid zone, excluding the population from within the hybrid zone, genome-wide average Hudson's F_{ST} was estimated for each species, using the ratio of averages approach. This revealed that genome-wide divergence is greater across the hybrid zone in *H. erato*, with an average F_{ST} of 0.188 (Figure 3.2A), compared to *H. melpomene*, which shows an average genome-wide F_{ST} of 0.0739 (Figure 3.2B).

There is a significant and positive relationship between pairwise geographic distance and pairwise average F_{ST} among sampling locations in *H. erato* (Mantel test: r = 0.644, p = 0.02; Figure 3.3 A), showing that populations further apart have significantly higher F_{ST}, which is consistent with isolation by distance. However, F_{ST} is consistently higher in between race pairwise comparisons compared to within race comparisons (Figure 3.3A). This suggests that large geographic distances alone are insufficient in explaining elevated F_{ST} between iridescent and non-iridescent populations of *H. erato*, and that there may be, or may have been, an additional barrier to gene flow. In contrast, there is not a significant relationship between geographic and genetic distance in *H. melpomene* (Mantel test: r = 0.121, p = 0.238; Figure 3.3 B).

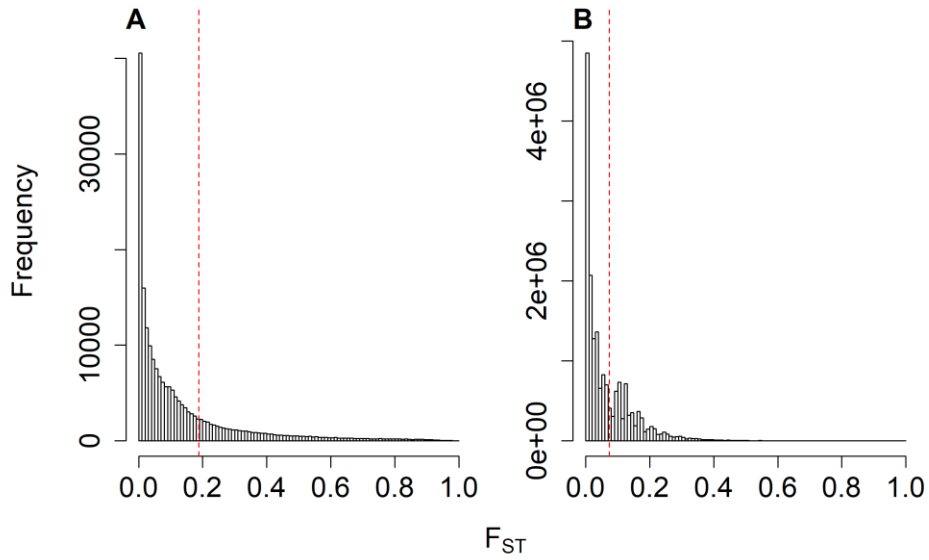

Figure 3.2 – The distribution of Hudson's F_{ST} for (**A**) 194,839 SNPs in *H. erato*, and (**B**) 17,855,113 SNPs in *H. melpomene*. Vertical red dashed lines indicate the genome-wide average F_{ST}, calculated as a ratio of averages.

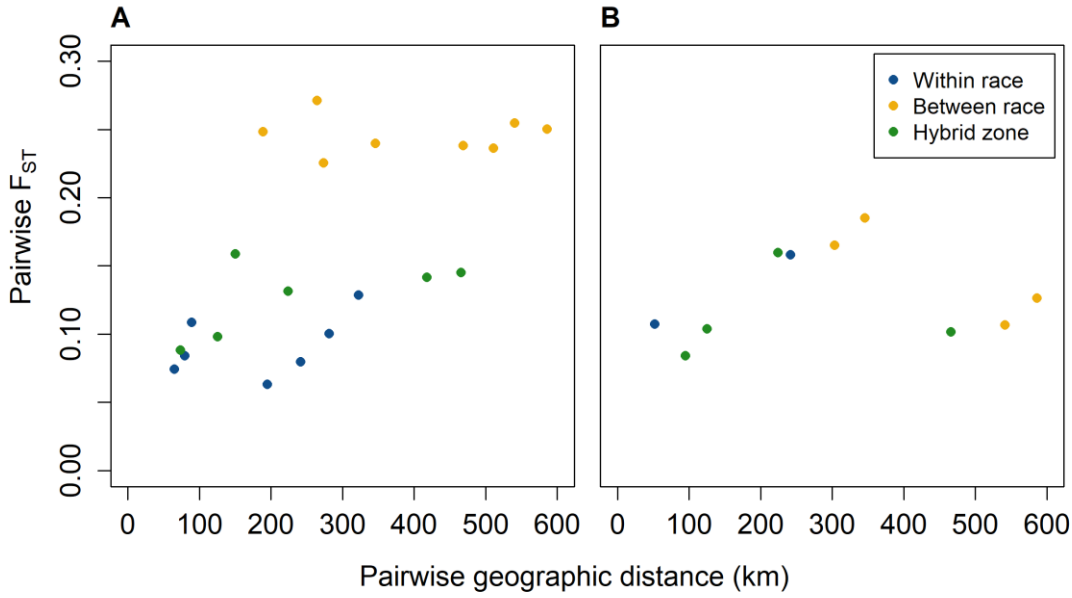

Figure 3.3 – Relationship between geographic distance and genetic distance (genome-wide average F_{ST}) between sampling sites in (**A**) *H. erato* and (**B**) *H. melpomene*. Pairwise comparisons are colour-coded to indicate comparisons between populations of the same colour pattern race (blue), between populations of different colour pattern races (yellow), and comparisons where one population is from the hybrid zone (green).

3.4.3 *Cline analysis*

To test whether variation in iridescence was independent from genetic structure across the hybrid zone, we fitted cline models to variation in the mean admixture proportions of populations across the transect and compared cline shape and position to that of the maximum likelihood cline for iridescence, estimated in Chapter 2. This was carried out for each species.

In *H. erato*, the admixture and iridescence clines were neither coincident nor concordant. For this species, the best fitting admixture proportion cline had no tails, and fixed *pMin* and *pMax* to the observed proportions at the right, and left ends of the cline, respectively (Table 3.2). The cline was estimated to be 155.51 (116.23 – 206.30) km wide, centred 516.22 (495.08 – 534.94) km along the transect. When the unconstrained maximum likelihood admixture proportion cline was compared to models where its centre and width were constrained to be the same as that of the maximum likelihood iridescence cline, the unconstrained model was the best fit, with the lowest AICc score of 9.44. The centre constrained model had a worse fit (ΔAICc 3.33; Table 3.3), suggesting that the admixture proportion and iridescence clines are not coincident in *H. erato* (Figure 3.5 A). Despite this, the confidence intervals of the cline centres do narrowly overlap, perhaps due to their proximity. The width constrained model was also a worse fit than the unconstrained model (ΔAICc 2.84; Table 3.3), with the admixture proportion cline being wider than the iridescence cline (Figure 3.5 A). Tests for cline concordance and coincidence were repeated reciprocally, by fixing the maximum likelihood iridescence cline model to have parameters equal to that of the admixture proportion cline model (Table 3.3), and the tests supported the results above, with the centre constrained iridescence cline (ΔAICc 53.98; Table 3.3), and the width constrained iridescence cline (ΔAICc 3.89; Table 3.3) having a significantly worse fits than the unconstrained model, suggesting that the iridescence cline is independent from the genetic structure seen across the hybrid zone in *H. erato.*

In *H. melpomene*, the best fitting admixture proportion cline did not fit any tails and fit an estimated *pMin* and *pMax* at the right and left ends of the cline (Table 3.2). The cline was estimated to be 11.64 (0.04 – 817.27) km wide, centred 322.04 (200.00 – 557.51) km along the

transect. The wide confidence intervals reflect that there was little power to fit a cline in admixture proportion in *H. melpomene*, likely because the population structure analysis carried out in ADMIXTURE only supported the presence of a single genetic cluster and did not distinguish between colour pattern races. When the unconstrained maximum likelihood admixture proportion cline was compared to models where its centre and width were constrained to be the same as that of the maximum likelihood iridescence cline, the centre constrained model was the best fit, with the lowest AICc score of 7.83. The unconstrained model was a marginally worse fit (ΔAICc 2.15; Table 3.3), and the width constrained model was not a worse fit (ΔAICc 1.23; Table 3.3). A reciprocal test that constrained the iridescence cline centre to be the same as the admixture proportion cline centre did not support this set of results, with the width constrained cline having the lowest AICc score of -146.75. The unconstrained cline was not a worse fit (ΔAICc 0.03; Table 3.3), and the centre constrained cline was a worse fit (ΔAICc 12.79; Table 3.3). The discrepancy between the two sets of cline comparisons is likely due to the poor support for clinal variation in admixture proportions in *H. melpomene.* Population genetic structure across this hybrid zone is not well described by a sigmoidal curve, however variation in iridescence is (Figure 3.5 B), suggesting that variation in iridescent structural colour is independent of genetic structure across the hybrid zone in *H. melpomene*.

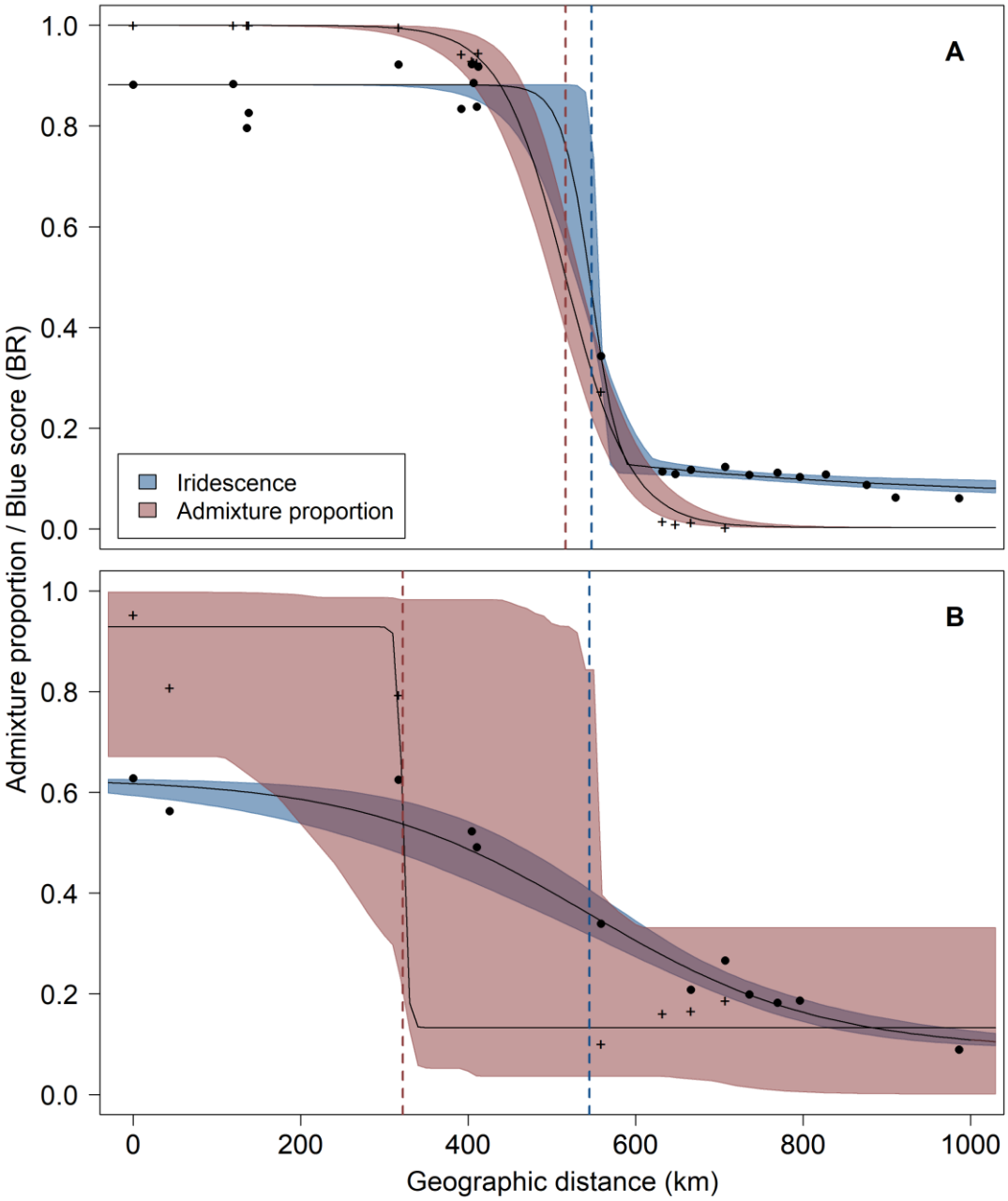

Figure 3.5 – Clinal variation in admixture proportion and iridescence across hybrid zones in (**A**) *H. erato* and (**B**) *H. melpomene*. Lines are maximum likelihood clines fitted to either the mean admixture proportions of populations (marked by crosses) or the mean iridescence score of populations (marked by filled circles) across the transect, over the associated 95% credible cline region (coloured regions). The transect begins (at 0 km) in the Cauca Valley region of Colombia. Vertical dashed lines show the cline centres.

Table 3.2 – Maximum likelihood estimates of parameters from the best fitting cline models describing variation in admixture proportions across hybrid zones in *Heliconius erato* and *H. melpomene.* Iridescence clines estimated in chapter 2 are included.

Species	Cline	Best model	Centre (km)	Width (km)	*pMin*	*pMax*
Heliconius erato	Admixture proportion	No tails, fixed pMin and pMax	516.22 (495.08 – 534.94)	155.51 (116.23 – 206.30)	0.003 (fixed)	0.999 (fixed)
Heliconius erato	Iridescence (BR)	Right tail, fixed mean/variance at cline ends	544.67 (534.47 – 555.79)	86.66 (16.84 – 147.54)	N/A	N/A
Heliconius melpomene	Admixture proportion	No tails, pMin and pMax estimated	322.04 (200.00 – 557.51)	11.64 (0.04 – 817.27)	0.13 (0.0004 – 0.311)	0.93 (0.672 – 0.999)
Heliconius melpomene	Iridescence (BR)	No tails, fixed mean/variance at cline ends	541.47 (495.39 – 585.69)	574.26 (442.04 – 728.80)	N/A	N/A

Two log-likelihood support limits are shown in brackets. Width is 1/maximum slope; *pMin* is the minimum proportion at the right end of the cline; *pMax* is the maximum proportion at the left end of the cline.

Table 3.3 – Comparison of iridescence and admixture proportion clines within species. Comparisons labelled A are the maximum likelihood admixture proportion cline with centres and widths constrained to be equal to the corresponding values of the iridescence cline. Comparisons labelled B are the iridescence maximum likelihood cline models with centres and widths constrained to be equal to the corresponding values of the admixture proportion cline.

Species	Comparison	Model	Centre (km)	Width (km)	Log-likelihood	AICc	ΔAICc
Heliconius erato	A	No constraints	516.73 (496.24 – 535.59)	154.53 (106.98 – 202.74)	-0.64	9.44	0
	A	Width constrained	537.49 (523.13 – 548.68)	86.66 (fixed)	-3.10	12.28	2.84
	A	Centre constrained	544.67 (fixed)	57.74 (34.86 – 159.61)	-3.34	12.77	3.33
	B	No constraints	548.37 (534.98 – 557.49)	64.60 (7.68 – 144.77)	541.38	-1072.62	0
	B	Width constrained	534.34 (530.98 – 537.55)	154.53 (fixed)	538.41	-1068.73	3.89
	B	Centre constrained	516.73 (fixed)	191.76 (176.95 – 207.22)	513.37	-1018.64	53.98

Heliconius melpomene	A	No constraints	332.70 (197.69 – 549.75)	39.65 (0.44 – 860.34)	-0.34	9.98	2.15
	A	Width constrained	366.41 (147.13 – 538.59)	557.23 (fixed)	-1.16	9.06	1.23
	A	Centre constrained	544.79 (fixed)	3.79 (0.01 – 86.26)	-0.54	7.83	0
	B	No constraints	434.93 (390.68 – 494.96)	197.08 (2.71 – 312.62)	76.46	-146.72	0.03
	B	Width constrained	410.52 (407.52 – 415.79)	11.64 (fixed)	75.43	-146.75	0
	B	Centre constrained	322.04 (fixed)	354.58 (172.80 – 552.43)	69.03	-133.96	12.79

3.5 *Discussion*

Here we investigate the genetic structure and history of two parallel hybrid zones between different colour pattern races of the Müllerian mimics *Heliconius erato* and *Heliconius melpomene*, across which both species display continuous phenotypic variation in iridescent structural colour. We find that the shape and position of iridescence clines are independent of genetic structure across hybrid zones, and that quantitative trait variation appears to be maintained by divergent selection in the face of gene flow. We also find some evidence of alternate histories of hybrid zone formation between the two co-mimics.

Generally, we found there to be a greater level of population structure in *H. erato* compared to *H. melpomene.* In *H. erato*, there is evidence of two main genetic clusters, one representing the non-iridescent populations from Panama, the other representing the iridescent Colombian populations. Individuals from the hybrid zone are consistently of mixed ancestry, which indicates admixture between the two genetic clusters. This could be indicative of a period where the two ancestral groups were isolated from one another, followed by secondary contact and subsequent gene flow. This is different to the situation seen in Peruvian and Ecuadorian hybrid zones between different colour pattern races of *H. erato*, where similar population structure analysis revealed a single genetic cluster across the hybrid zone in both cases, indicating that the hybrid zones formed via primary intergradation, or very ancient secondary contact (Nadeau *et al.*, 2014).

Less population-level genetic structure is evident across the *H. melpomene* hybrid zone. The ADMIXTURE analysis did not support more than a single ancestral genetic cluster for this species, although the PCA does show that some of the genetic variation follows geography. Interestingly, there are clear phenotypic intermediates in the hybrid zone, which show intermediate levels of iridescence, but none of these individuals is of mixed ancestry. A primary intergradation scenario might explain this pattern, perhaps driven by local positive frequency dependent selection on colour patterns, and pressure to mimic local *H. erato* races. However, periods of allopatry cannot be ruled out, if subsequent gene flow was sufficient to erase traces of any genetic differentiation which occurred during isolation.

Regardless of pairwise geographic distances between *H. erato* populations, pairwise genetic differentiation (F_{ST}) was higher between populations from different colour pattern races, than within them. This indicates past or present barriers to gene flow between iridescent and non-iridescent populations and does not support a scenario where differentiation between the two genetic clusters identified by ADMIXTURE arose simply because of isolation by distance. The reduction in gene flow could be a result of strong selection against hybrid offspring, although a lack of a step in the admixture proportion cline argues against this (Szymura & Barton, 1991). Alternatively, it could be a signature of secondary contact following a period of allopatry (eg. Stankowski *et al*. 2015), or a combination of the two. In *H. melpomene*, there is no significant correlation between geographic and genetic distance, suggesting there is no isolation by distance, however this might also be a result of too few population comparisons in the distance matrices. Although we do see some weak geographic structure in the PCA, this is consistent with other studies which demonstrate lower levels of population structure in *H. melpomene* compared to *H. erato* (Nadeau *et al.*, 2014), likely because of its greater dispersal distance (Mallet *et al.*, 1990). It is also possible that the reduced number of sampling sites and individuals we have for *H. melpomene* means that we lack the power to detect an association between matrices of pairwise geographic and genetic distance.

While there may be evidence of secondary contact in *H. erato*, there is some support that iridescence varies independently of genetic structure. The centre of the iridescence cline is uncoupled from the admixture proportion cline, however they are situated close to one another. It is possible that the absence of gene flow from the non-iridescent populations to the north during historical bouts of isolation aided the evolution of iridescence, a quantitative trait, but after secondary contact the cline shifted, as it is not dependent on environmental features. Clines in morphological traits can become uncoupled from background genetic clines when direct natural (Vines *et al.*, 2016), or sexual (Baldassarre *et al.*, 2014) selection outweighs the effects of indirect selection from other loci in linkage disequilibrium (LD). Spatial variation in quantitative traits can also be non-adaptive, arising via purely stochastic processes (Storz, 2002), however the iridescence cline is significantly narrower than the admixture proportion cline. This demonstrates

a reduced exchange of alleles at loci controlling iridescence, likely due to selection against individuals with intermediate phenotypes. This is evidence that the iridescence cline isn't simply the result of neutral diffusion of alleles following secondary contact. The wider cline in admixture proportion may represent genome wide selection against hybrids, albeit weaker than selection on iridescence. Alternatively, it could represent genome-wide divergence collapsing following secondary contact, although this would require contact to have occurred relatively recently.

In *H. melpomene*, the centres and widths of the iridescence and admixture proportion clines were not significantly different from one another. This result is likely due to the poor fit of a sigmoidal cline to variation in admixture proportions across the hybrid zone, rather than a close relationship between clines in iridescence and genetic structure. However, there is a sharp step in admixture proportions separating the west Colombian populations from the hybrid zone and Panamanian populations, indicating a degree of spatial coupling in population genetic structure and variation in iridescence. However, the ADMIXTURE cross-validation procedure revealed the best supported number of genetic clusters across the *H. melpomene* hybrid zone to be one, so forcing *K* to equal two for this analysis may not portray a realistic picture of genetic structure across the transect for this species.

Overall, divergence in structural colour, a continuously variable trait, appears to be independent of genetic structure. This is particularly pronounced in *H. melpomene*, which shows very little genetic structure across the hybrid zone, but also has a very wide iridescence cline (Chapter 2), suggesting that selection is weak. There is a strong pattern of population structure across the *H. erato* hybrid zone, but some evidence that iridescence varies independently of it. Quantitative trait divergence may require a more complex pattern of genetic differentiation than traits with a Mendelian pattern of inheritance, so a reduction in gene flow could have facilitated the evolution of iridescence, which is more vivid in *H. erato* (Parnell *et al.*, 2018). Nevertheless, our results support assertions that continuous variation in quantitative traits can be maintained by divergent selection in the face of gene flow across hybrid zones.

A next step in confirming this would be to fit many clines in putatively neutral markers across the hybrid zones. Comparing clines of neutral markers to clines in phenotypic traits allows the estimation of levels of selection (Brumfield *et al.*, 2001; Gay *et al.*, 2008). It also gives an indication of the extent to which indirect selection is acting across the genome, as when many loci are under strong divergent selection, LD can build between loci under selection and neutral loci, resulting in sharp, stepped clines at loci not under direct selection, resulting in a strong, genome-wide, barrier to introgression (Szymura & Barton, 1991). If this is not occurring, alleles at neutral loci should pass freely across the hybrid zone. A recent study by Westram *et al*. (2018) combined cline reconstruction, of a genome-wide SNP set, with simulations to distinguish between neutral and non-neutral clines. They demonstrated that such approaches provide more information than genome scan approaches, as they not only allow the detection of different forms of selection, but they incorporate spatial data and reveal genome-wide patterns of LD.

Based on current evidence, it is difficult to say which historical events may have resulted in past episodes of population subdivision across the hybrid zones in the present study. The origin of iridescence in *H. erato* and *H. melpomene* on the western slopes of the Andes, is thought to be very recent (~100,000 years ago or less; Parnell *et al*. 2018; Kozak *et al*. 2015). Indeed, diversity in the *Heliconius* genus is very rich in the foothills of the Andes and the adjacent Amazon basin in Colombia, Ecuador and Peru, as a large proportion of colour pattern races and recently evolved species are found here (Rosser *et al.*, 2012). It has been suggested that the rise of the Andes is responsible for this diversity, as it coincides with a steady increase in diversification rates in *Heliconius* from the mid-Miocene, although this correlation is weak (Kozak *et al.*, 2015; Merrill *et al.*, 2015). Climatic features can affect distributions of *Heliconius*, and the position of hybrid zones closely correlates with local rainfall peaks (Rosser *et al.*, 2014), therefore it is possible that historical changes in local climate could have affected past species distributions.

We cannot rule out periods of primary divergence for *H. erato*, and periods of allopatry in *H. melpomene*, as it is difficult to distinguish between primary intergradation and ancient secondary contact. It is perhaps inappropriate to attempt to strictly categorise a hybrid zone as either primary or secondary, since populations can have complicated histories of expansion and

contraction, with hybrid zones developing through multiple episodes of isolation and contact (Gompert *et al.*, 2017). Endler (1977) highlighted the challenges of this, stating "unless we observe a zone of intergradation within a few hundred generations of secondary contact, it will be impossible to distinguish secondary intergradation from primary intergradation". Demographic modelling approaches may, however, shed light on which scenario was of greater importance during the formation of the hybrid zones studied here (e.g. Filatov *et al*. 2016), and should be considered in future work on this system.

3.6 *Conclusions*

We provide evidence that variation in quantitative traits can be maintained across hybrid zones by divergent selection in the face of gene flow. This has been well documented in traits which show discrete variation, but less so in traits which show continuous variation across hybrid zones, such as iridescence in the co-mimics, *Heliconius erato* and *Heliconius melpomene*. We also find evidence of different histories of hybrid zone formation between the two species. Patterns of population structure and elevated F_{ST} between colour pattern races suggest the *H. erato* hybrid zone formed through secondary contact, whereas a lack of these population genomic signatures in *H. melpomene* suggest that either primary intergradation played a more important role in the formation of the iridescence cline for this species, or that population structure has been eroded in this species, either because of more ancient secondary contact, or higher dispersal. Despite the difficulty in distinguishing between these scenarios, we find that iridescence cline centres have different locations to clines in average ancestry in both species, suggesting that genetic structure across hybrid zones is not required to maintain differences in traits which vary continuously, despite the prediction that they will have more complex genetic architectures than traits which show discrete variation. Since the iridescence cline is independent of the cline in population-level genetic structure, the hybrid zone could be useful for association mapping of iridescence. This will provide novel insight into the genetic control of structural colour, of which almost nothing is currently known.

4

Genome-wide association mapping of convergent iridescent structural colour using natural hybrid zones in *Heliconius erato* and *Heliconius melpomene*

4.1 *Summary*

The convergent evolution of phenotypes in divergent lineages can occur by repeated use of the same genes, or by changes at different genes. Gene reuse may reflect genetic biases. If evolution tends to follow the path of least genetic resistance, evolution may be predictable to an extent. Gene reuse appears to be common, however most studies tend to focus on traits that show discrete variation and are controlled by one, or a small number of large effect loci. Here we address this issue in a quantitative trait, iridescent structural colour, which is mimetic between *Heliconius erato* and *Heliconius melpomene*. We use single and multi-locus genome-wide association studies (GWAS) to describe the genetic architecture of iridescence, and use a bottom-up GWAS-based approach to look for genetic variants associated with population structure that are likely to be under selection. This allowed us to identify candidate SNPs which were potentially both under divergent selection and associated with iridescence. We find that iridescence in *H. erato* is likely controlled by multiple genes, although it is unlikely to be highly polygenic. We also identify some candidate SNPs that appear to be under divergent selection and are associated with iridescence. In *H. melpomene*, there were no SNPs which surpassed our confidence thresholds in either GWAS of iridescence, likely due to lack of power as a result of small sample size. As a result, we could not determine whether iridescence evolved using the same genes in each species. This is the first description of the genetic architecture of structural colour in *Heliconius* butterflies. In contrast with pigment colour and pattern elements in the genus, each of which are controlled by a single locus, iridescence appears to be controlled by multiple genes.

4.2 *Introduction*

There are many instances in nature where the same phenotypic solution has been repeatedly used to solve the same environmental problem. Referred to as convergent evolution, it has often been used as convincing proof of the role of natural selection (Schluter & Nagel, 1995). However, the extent to which repeated phenotypic evolution relies on repeated use of the same genes can tell us about constraints on evolution. For instance, certain genes may be 'hotspots' of repeated evolution due to high mutation rates, few pleiotropic constraints, and large effect sizes (Conte *et al.*, 2012; Linnen *et al.*, 2013; Martin & Orgogozo, 2013). Genes can be repeatedly used during phenotypic evolution via several distinct modes. It can occur as a result of selection acting on common standing genetic variation in different populations (e.g. Colosimo *et al.* 2005), due to introgression of adaptive loci between lineages (e.g. Song *et al.* 2011), or through multiple independent mutations at the same gene (e.g. Zhen *et al.* 2012).

Despite genomic data being increasingly feasible to generate, identifying the genes involved in local adaptation remains a challenge. There have been numerous studies which have successfully identified large effect genes which underlie discrete trait variation and major phenotypic shifts in natural populations, such as genes controlling colour patterns in mice (Manceau *et al.*, 2011), and mimicry in *Papilio* butterflies (Kunte *et al.*, 2014). There are also a growing number of examples of large effect genes being reused during repeated adaptation to similar environments, such as in the repeated pelvic reduction in threespine stickleback (Chan *et al.*, 2010), and with the gene *Mc1r*, which has been repeatedly implicated in melanic pigmentation in several mammalian and avian species (Nachman *et al.*, 2003; Mundy, 2005; Hoekstra *et al.*, 2006).

In contrast, there also several examples of nonconvergence at the molecular level during the evolution of convergent traits, such as in weedy rice adaptation to agricultural environments (Thurber *et al.*, 2013), and in the parallel evolution of benthic and limnetic ecomorphs (Elmer *et al.*, 2014), and visual systems (Härer *et al.*, 2018) in cichlids.

Some general trends have emerged, and it seems as if the repeated use of genes is relatively common, however the probability of gene reuse declines with increased phylogenetic distance (Conte *et al.*, 2012). It is unknown whether convergent traits are more prone to evolve via the same genetic route if they display discrete variation and are controlled by single, large-effect genes, since there are few studies to date focusing on the convergent evolution of quantitative traits with a more complex genetic basis. Traits controlled by many genes have more targets of selection, and therefore may be more prone to evolutionary contingencies, such as the order in which mutations occur (Gompel & Prud'homme, 2009; Conte *et al.*, 2012), however there is also evidence that the number of alternative mutational pathways to fitter phenotypes which are accessible to selection may be limited (Weinreich *et al.*, 2006). Mapping the genetic basis of quantitative traits controlled by many genes is a challenging task. Until recently, empirical studies uncovering the genetic basis of adaptation focused on traits with a genetic architecture of one or a small number of loci of large effect, as these are the most readily discoverable, however they might not be representative of the way in which evolution normally proceeds (Rockman, 2011). Some have argued that evolutionary change is most likely to occur largely through many changes of small effect (Fisher, 1919; Charlesworth *et al.*, 1982), while other theory suggests that certain situations, such as adaptation towards a fixed optimum, may result in an exponential distribution of effect sizes of adaptive substitutions, with a few large effect, and many small effect substitutions (Orr, 1998). Alternatively, when faced with certain selection-migration dynamics, genetic architecture itself might evolve towards fewer, more tightly linked loci of larger effect (Yeaman & Whitlock, 2011).

Studies which integrate top-down, phenotype-focused analyses such as genome-wide association studies (GWAS), with bottom-up genome scans, focused on identifying loci under selection regardless of phenotype, are able to identify candidate loci for phenotypes, while also assessing whether they are under divergent selection between populations (Berg & Coop, 2014). Recently, this approach has revealed loci underlying adaptive divergence in quantitative and complex traits (Chaves *et al.*, 2016; Bosse *et al.*, 2017; Brennan *et al.*, 2018).

The *Heliconius* butterflies of South and Central America provide an excellent system in which to investigate the genetic basis of convergent traits (Merrill *et al.*, 2015). They are toxic species, which display bright wing colour patterns serving as warning signals to predators (Jiggins, 2008). Certain species form Müllerian mimicry rings to share the cost of educating predators of their aposematism, resulting in close convergence of colour patterns between distantly related species, and strong selection against non-mimetic patterns (Mallet & Barton, 1989; Kapan, 2001). Much of the colour pattern variation in *Heliconius* is composed of pigmentary colouration, which is controlled by a 'genetic toolkit' of five genes, which have been repeatedly implicated in colour pattern in the genus (Nadeau, 2016). One of these is *cortex*, a major locus which is responsible for convergent yellow and white colour patterns in the co-mimics *Heliconius erato* and *Heliconius melpomene* (Joron *et al.*, 2006; Nadeau *et al.*, 2016), and is in the same region as a 'supergene' locus in *Heliconius numata* which incorporates two chromosomal inversions and controls the majority of colour pattern variation in the species (Joron *et al.*, 2011). Its role in wing patterning in other lepidopteran species shows it has been repeatedly targeted by natural selection (Beldade *et al.*, 2009; Van't Hof *et al.*, 2011; Ito *et al.*, 2016). Another major wing patterning locus in *Heliconius* is *optix*, which controls convergent red patterns in *H. erato* and *H. melpomene* (Reed *et al.*, 2011), and has also been co-opted in the diversification of wing colouration in multiple other nymphalid genera (Martin *et al.*, 2014; Zhang *et al.*, 2017). The gene *WntA* is consistently used to control the size and shape of colour patterns across the *Heliconius* genus (Martin *et al.*, 2012). Repeated evolution at regulatory modules (Reed *et al.*, 2011; Martin *et al.*, 2012; Nadeau *et al.*, 2016; Van Belleghem *et al.*, 2017), as well as adaptive introgression of colour pattern loci between closely related *Heliconius* species (Pardo-Diaz *et al.*, 2012; The Heliconius Genome Consortium, 2012; Enciso-Romero *et al.*, 2017), has been important in driving convergence and mimicry in the genus.

While gene reuse appears to be common during the convergent evolution of pigmentary colouration, this has not been explored in iridescent structural colouration. Iridescence appears to have evolved independently up to five times in *Heliconius* (Parnell *et al.*, 2018), and the physical structures which produce iridescence have only recently been described in the genus (Wilts *et al.*,

2017; Parnell *et al.*, 2018), yet its genetic basis remains unknown. Close to the border of Panama and Colombia, the co-mimics *H. erato* and *H, melpomene* form intra-specific hybrid zones between iridescent and non-iridescent colour pattern races (see Chapters 2 and 3). Whereas pigmentary pattern elements in *Heliconius* show discrete variation, iridescence appears to vary continuously (see Chapter 2). Here, we take advantage of phenotypic variation and genetic admixture across these hybrid zones to estimate the genetic basis of iridescence using genome-wide association studies (GWAS). We combine this approach with a bottom-up method to look for loci under putative divergent selection, using a recent method EigenGWAS (Chen *et al.*, 2016), allowing us to identify candidate SNPs which are both associated with iridescence and local adaptation.

4.3 *Materials and Methods*

4.3.1 *Butterfly specimens and phenotyping*

The *Heliconius erato* and *Heliconius melpomene* specimens used in this study include samples we collected from wild populations in Ecuador, Colombia and Panama, alongside samples acquired from other institutions, as described in Chapter 2, section 2.2.1. The wings of specimens were photographed, and RGB colour channel values were extracted so that a blue score (BR) could be calculated, to be used as a proxy for the level of iridescence, as described in Chapter 2, section 2.2.2. Variation in the 'yellow bar' phenotype on the hindwing of each individual was also recorded from photographs, as described in Chapter 2, section 2.2.3. For the purposes of genome-wide association mapping, the yellow bar was then scored as a binary trait, based on whether it was present (1) or absent (0) on the ventral surface of the hindwing.

4.3.2 *Sequencing data*

A subset of individuals from localities spanning the range of clines in iridescence in both species were selected to obtain sequence data. Restriction-site associated DNA (RAD) sequencing was carried out on 299 *H. erato* individuals (two of which were discarded due to low read count) and 21 *H. melpomene*, and whole genome re-sequencing was carried out on 29 *H. erato* and 45 *H. melpomene*. A break-down of the localities these samples originate from can be found in Chapter 3, Table 3.1.

Genomic DNA was extracted from preserved thoraxes of the butterflies, as described in Chapter 3, section 3.2.2. Library preparation and sequencing were carried out by Edinburgh Genomics (University of Edinburgh) for both RAD sequencing and whole genome re-sequencing, details of which are also described in section 3.2.2. The RAD sequencing generated 125 base paired end reads, and we obtained 1,470,287,706 DNA sequence reads for *H. erato*, and 87,892,908 DNA sequence reads for *H. melpomene* in total. The whole genome re-sequencing also generated 125 base paired end reads, and we obtained 1,416,796,324 DNA sequence reads for *H. melpomene*. The raw sequence reads underwent quality checks, and were aligned to their respective reference genomes, as described in section 3.2.2.

4.3.3 *Single-locus genome-wide association studies*

To identify candidate genes associated with iridescence in *H. erato* and *H. melpomene*, we carried out genome-wide association studies (GWAS). Initially, we carried out GWAS using the R package *GenABEL* (Aulchenko *et al.*, 2007), which implements a single locus approach, testing for associations between genetic and phenotypic variation one SNP at a time.

To generate SNP datasets, we followed the protocol outlined in Chapter 3, section 3.2.3. Briefly, this involved computing genotype likelihoods using samtools mpileup (v 1.5), and calling variants with bcftools (v 1.5). It was required that a site had a probability of less than 0.05 of being homozygous to the reference allele to be a variant. Insertions and deletions were ignored,

and sites were assumed to be biallelic. The initially called variants were then filtered to remove sites with a phred quality score lower than 30, sites which lacked sequence data in 50% or more of the individuals, SNPs with a minor allele frequency lower than 0.05, and private variants. For *H. erato*, the SNP dataset included all 297 RAD sequenced individuals, which, after filtering, contained 220,221 SNPs. Due to far fewer *H. melpomene* individuals having been collected on field trips, it was necessary to maximise the sample size, so we decided to combine all RAD and whole-genome re-sequenced individuals, resulting in SNP dataset comprising 66 individuals. To minimise differences due to sequencing type, SNPs were called only from regions present in the RAD sequenced individuals. After filtering, 1,475,053 SNPs were obtained.

Prior to association mapping, further quality checks were implemented using the *GenABEL* function *check.marker*, to check for individuals with unusually high heterozygosity (false discovery rate <1%), and with a high proportion of alleles which are identical-by-state (>=95). No such individuals were identified.

For *H. erato*, we used the *egscore* function, which implements the EIGENSTRAT method (Price *et al.*, 2006), to correct for population structure. This involves carrying out a principal component analysis (PCA) on genotype data and using the resulting continuous axes of variation to account for genetic differences resulting from population stratification, reducing the chances of detecting spurious associations. We computed a distance matrix of genomic kinship, and then performed multidimensional scaling. A plot of the first two axes of genetic variation reveals clear clustering by geography (see supplementary figure S4.1). We used the first three axes of variation from a PCA performed on the genomic kinship distance matrix for adjustment in the GWAS using *egscore*. The GWAS was carried out using the blue score (BR) as a proxy for iridescence. Bonferroni-corrected thresholds, adjusted for genomic inflation factor λ, were used to assess whether SNPs were significantly associated with phenotype. For *H. erato*, the corrected threshold was 2.9×10^{-7}. For *H. melpomene*, the corrected threshold was 3.8×10^{-8}.

To test the efficacy of this analysis, we also performed a GWAS on the hindwing yellow bar pattern, a trait known to be controlled by the gene *cortex* on chromosome 15 (Nadeau *et al.*, 2016), and which varies across the same hybrid zone as iridescence, as explored in detail in Chapter 2.

For *H. melpomene*, we also computed a distance matrix of genomic kinship, and then performed multidimensional scaling. A plot of the first two axes of variation separated out the individuals by both geography and sequencing type (see supplementary figure S4.2). As a result, we decided not to use the EIGENSTRAT method of GWAS on *H. melpomene*, as it would not be able to reliably correct for population structure. Instead, we performed a simple association study using the *qtscore* function in *GenABEL*, which does not correct for population structure. For comparison, we also performed the *qtscore* GWAS on the *H. erato* data, the results of which can be found in the supplementary material (Figure S4.1). Again, these analyses were carried out for both iridescence and the yellow bar phenotype.

4.3.4 *Multi-locus genome-wide association studies*

In addition to the single-locus GWAS, we also used a multi-locus approach, which tests for associations between phenotypic and genetic variation by simultaneously fitting all SNPs to phenotypic variation, allowing for correlations between SNPs to be considered. This was carried out using a Bayesian sparse linear mixed model (BSLMM), implemented in the program *GEMMA* (Zhou *et al.*, 2013). This approach is useful for traits with unknown genetic architectures, as the BSLMM incorporates a linear mixed model, which describes the small effects of SNPs on the phenotype, as well as a sparse regression model which captures the large effects of SNPs on the phenotype. Population structure is controlled for by using an internally computed relatedness matrix as a covariate. It also estimates hyperparameters describing the genetic architecture of a trait, including the proportion of phenotypic variation explained by genetic variation (PVE), the proportion of genetic variation explained by large effect SNPs (PGE), and the number of SNPs with a non-zero effect on the phenotype (n-SNP). SNPs are assigned a posterior inclusion probability (PIP), which is the proportion of Markov chain Monte Carlo (MCMC) iterations in

which the SNP has a non-zero effect on phenotypic variation, that is, SNPs with a larger effect on phenotype than the small polygenic effects which are estimated for every SNP. Using the same SNP datasets for *H. erato* and *H. melpomene* as used in the single locus GWAS, we ran linear BSLMMs in *GEMMA* for both iridescence and the yellow bar in each species. Each analysis was run with 10 independent MCMC chains, for 20 million iterations, with a burn-in of 5 million. Results were averaged across chains. We used a threshold of PIP > 0.1 to determine whether a SNP was associated with the phenotype (Chaves *et al.*, 2016; Armstrong *et al.*, 2018).

4.3.5 *Detecting divergent selection across the genome*

We identified SNPs likely to be under divergent selection using the EigenGWAS approach (Chen *et al.*, 2016), implemented in the software GEAR (https://github.com/gc5k/GEAR/). Whereas traditional approaches to identify genomic regions under divergent selection, such as F_{ST} genome scans, require discrete populations to be defined, EigenGWAS allows divergence to be assessed along a gradient. This is particularly appropriate for our data, which was collected from multiple sites spanning a phenotypic cline. In this method, a principal component analysis is performed on genotype data to quantify population genetic structure. Individual-level eigenvectors are then treated as phenotypes in a single-locus GWAS. SNPs that are associated with population structure may not necessarily be loci under selection, they could also be ancestry-informative markers which have differentiated due to drift. To distinguish between the two, EigenGWAS calculates a genomic inflation factor λ_{GC} for each eigenvector. If λ_{GC} is greater than one, this indicates underlying population stratification. By adjusting *p*-values according to λ_{GC} (Devlin & Roeder, 1999), average genetic drift can be removed, allowing loci under selection to be detected. Using the same SNP datasets as in the previously described GWAS analyses, I carried out EigenGWAS on the first two eigenvectors of genomic relatedness matrix calculated internally by the GEAR software. We used Bonferroni corrected genome-wide significance thresholds of $p < 3.39 \times 10^{-8}$ for *H. melpomene*, and $p < 2.27 \times 10^{-7}$ for *H. erato*, using λ_{GC} adjusted *p*-values to determine whether a SNP was likely to be under selection.

4.3.6 *Identification of candidate genes*

Candidate SNPs were identified by comparing the results from the single and multi-locus GWAS and EigenGWAS analyses. SNPs which showed a strong association in at least two of the analyses were explored in further detail. The genes in closest proximity to candidate SNPs were identified using Lepbase (Challis *et al.*, 2016), which hosts the annotated reference genomes of both species. Information about the predicted genes was recorded. From the gene information, if GO terms were present these were recorded. From the protein information, if descriptions of domains and features were present, these were recorded.

4.4 *Results*

4.4.1 *Single locus genome-wide association studies*

The single locus GWAS using the EIGENSTRAT method did not find any SNPs with a significant association with iridescence in *H. erato*, using a Bonferroni corrected significance threshold of 2.27×10^{-7} (Figure 4.1 A). A single locus GWAS without correction for population structure in *H. melpomene* also did not yield any significantly associated SNPs, using a Bonferroni corrected threshold of 3.8×10^{-8} (Figure 4.2 A). Bonferroni correction can result in overly conservative significance thresholds, since they treat each variant as independent, not taking into account linkage disequilibrium between multiple SNPs, resulting in an increased rate of false negatives (Gao *et al.*, 2010).

To test the efficacy of the single locus GWAS, we repeated the analyses on the yellow bar colour pattern, which is known to be controlled by the gene *cortex*. In *H. erato*, the EIGENSTRAT method found 16 SNPs with a significant association according to the Bonferroni corrected threshold of 2.9×10^{-7} (Table S4.1; Figure 4.3 A). Of these, 14 are located on the scaffold Herato1505 (size: 3,913,891 bp) on chromosome 15, which contains *cortex* (position: 2,074,108 – 2,087,841, based on the *Heliconius erato demophoon* v1 genome annotation accessed on Lepbase) and were between 92,404 and 250,314 base pairs away from *cortex* (Figure 4.3 B). The

remaining two significantly associated SNPs are located on chromosomes 10 and 13, in regions not known to be associated with the yellow bar. It is likely that these are false positives.

For *H. melpomene*, a single locus GWAS without correction for population structure on the yellow bar found no SNPs which surpassed the Bonferroni corrected significance threshold of 3.8×10^{-8} (Figure 4.4 A). However, of the 20 most strongly associated SNPs (Table S4.2), 10 are located on the scaffold Hmel215006 (size: 1,967,117 bp) on chromosome 15, which contains *cortex* (position: 1,205,164–1,324,501 based on the *Heliconius melpomene* Hmel2 genome annotation accessed on Lepbase). Of these, 9 are located inside the gene, and the remaining one is 5,786 base pairs away from the gene (Figure 4.4 B).

4.4.2 *Multi-locus genome-wide association mapping*

In the BSLMM for *H. erato*, a median of 97.8% (credible intervals: 94.8–99.9%) of variation in iridescence can be explained by genetic variation (PVE), of which 98.5% (CI: 91.7–99.9%) is explained by approximately 48 SNPs (n-SNP; CI: 21–102) with relatively large effects (PGE, Table 4.1 A). A total of 27 SNPs have a posterior inclusion probability greater than 0.1, our threshold for identifying SNPs associated with phenotypic variation (Figure 4.1 B).

In the BSLMM for *H. melpomene*, a median of 96.9% (CI: 79.9–99.9%) of variation in iridescence can be explained by genetic variation, of which 58.9% (0.4–98.6%) is explained by approximately 16 (1–242) SNPs with a relatively large effect (Table 4.1 B). However, the credible intervals are very wide for PGE and n-SNP, so these are unlikely to be accurate estimates. There are no SNPs with a PIP greater than 0.1.

We also carried out BSLMMs for the yellow bar in both species. For *H. erato*, 95.9% (87.7–99.9%) of variation in the yellow bar can be explained by genetic variation, of which 97% (89.1–99.9%) is explained by approximately 42 (23–66) SNPs with relatively large effects. A total of 69 SNPs has a PIP greater than 0.1 (Table S4.3; Figure 4.3 C), of which only 7 are on the same scaffold as *cortex* (Herato1505) and are between 250,124 and 1,747,448 base pairs away from the

gene (Figure 4.3 D). There are a high number of false positives. In *H. melpomene*, a median of 99.4% (91.5–99.9%) of the variation in the yellow bar can be explained by genetic variation, of which 91% (73.1–99.6%) can be explained by approximately 5 (1–13) SNPs with relatively large effects. There are 7 SNPs with a PIP greater than 0.1 (Table S4.4; Figure 4.4 C). Of these, 4 are in *cortex* (Figure 4.4 D), and the remaining three are located on chromosome 6.

4.4.3 *Detecting divergent selection across the genome*

We used the EigenGWAS approach to look for SNPs likely to be under divergent selection. In *H. erato*, the first eigenvector separates the Panamanian populations, including the hybrid zone sampling site (Jaque), from the rest of the individuals, and the second eigenvector separates the Ecuadorian populations from the rest of the individuals (Figure 4.5 A). Eigenvector 1 explains a much larger proportion of variation, with an eigenvalue of 19.1, and has a genomic inflation factor λ_{GC} of 11.5, indicating a substantial amount of population structure. Eigenvector 2 has an eigenvalue of 3.96, and a λ_{GC} of 1.92, indicating lower levels of population structure. Using λ_{GC} corrected *p*-values to account for population stratification, and a Bonferroni corrected significance threshold of $p < 2.27 \times 10^{-7}$, EigenGWAS found signatures of selection in 495 SNPs (Figure 4.1 C), in the first eigenvector. In the second eigenvector, signatures of selection were found in 1574 SNPs (supplementary figure S4.3). We used the first eigenvector in the EigenGWAS analysis when identifying possible candidate SNPs for iridescence in *H. erato*, as it separates the iridescent from the non-iridescent populations, therefore it is most likely to detect loci under divergent selection which are associated with iridescence. There were no SNPs significantly associated with eigenvector 1 within *cortex*, however there were two in the scaffold containing *cortex* (Herato1505), which were 432,587 bp and 432,620 bp downstream of the gene. There also were no SNPs significantly associated with eigenvector 2 within *cortex*, but there were 62 SNPs significantly associated with eigenvector 2 on Herato1505, the closest of which is 360,549 bp downstream of *cortex*. Since eigenvector 2 separates the Ecuadorian individuals from the Panamanian and Colombian individuals, it is possible that these SNPs are related to the white

wing margin, which is also controlled by *cortex*, and which is only found in *H. erato cyrbia* from Ecuador.

In *H. melpomene*, the eigenvectors separated out individuals by both geography and sequencing type (Figure 4.5 B). This means that the EigenGWAS results in this species are likely to be confounded, as the eigenvectors will not describe the true underlying population genetic structure. The results from the first eigenvector are reported, as it mostly separates individuals by geography, and will give the best representation of population structure. Eigenvector 1 has an eigenvalue of 4.42, and λ_{GC} is 4.06, indicating lower levels of population stratification than in *H. erato*. Using λ_{GC} corrected *p*-values to account for population stratification, and a Bonferroni corrected significance threshold of $p < 3.39 \times 10^{-8}$, signatures of selection were detected for 406 SNPs (Figure 4.2 C). There were no SNPs significantly associated with eigenvector 1 within *cortex*, however there were 23 in the scaffold containing *cortex* (Hmel215006), the closest being 11,572 bp downstream of the gene.

4.4.4 *Identifying candidate SNPs*

To identify candidate SNPs involved in controlling iridescence, we compared the results of each of the three GWAS approaches. For *H. erato*, the single locus GWAS found no associations between genetic variation and variation in iridescence, therefore comparisons between the results of this analysis, and the results of the multi-locus GWAS and the EigenGWAS provided no potential candidates (Figure 4.1 D & F). Of the 27 SNPs with a PIP greater than 0.1 in the multi-locus BSLMM carried out on iridescence in *H. erato*, 14 SNP are also significant in the EigenGWAS for eigenvector 1 (Figure 4.1 E). These 14 SNPs are therefore both associated with iridescence and are likely to be under divergent selection (Table 4.2). In *H. melpomene*, neither the single nor the multi-locus GWAS yielded any significant results. While the EigenGWAS revealed many loci potentially under divergent selection, since it is a bottom-up approach, it is not phenotype-specific, therefore it cannot be used to identify candidate SNPs without comparison to a traditional GWAS (Figure 4.2 D & E). However, the three SNPs with the

strongest association with iridescence in the single locus GWAS also have a non-zero effect on phenotype in a small proportion of iterations of the BSLMM (Figure 4.1 F; Table 4.3). While it is unknown whether these SNPs might reach genome-wide significance, given a greater sample size, the fact the three SNPs showed an association that was strong relative to other SNPs in both GWAS approaches, makes them worthy of note.

Table 4.1 – BSLMM hyperparameters for iridescence in *H. erato* and *H. melpomene*. Median estimates are given, alongside upper and lower equal-tailed posterior probability intervals (ETPI).

	A. *H. erato*			**B.** *H. melpomene*		
Hyperparameter	Median	Lower 95% ETPI	Upper 95% ETPI	Median	Lower 95% ETPI	Upper 95% ETPI
PVE	0.978	0.948	0.999	0.969	0.799	0.999
PGE	0.985	0.917	0.999	0.589	0.004	0.986
n-SNP	48	21	102	16	1	242

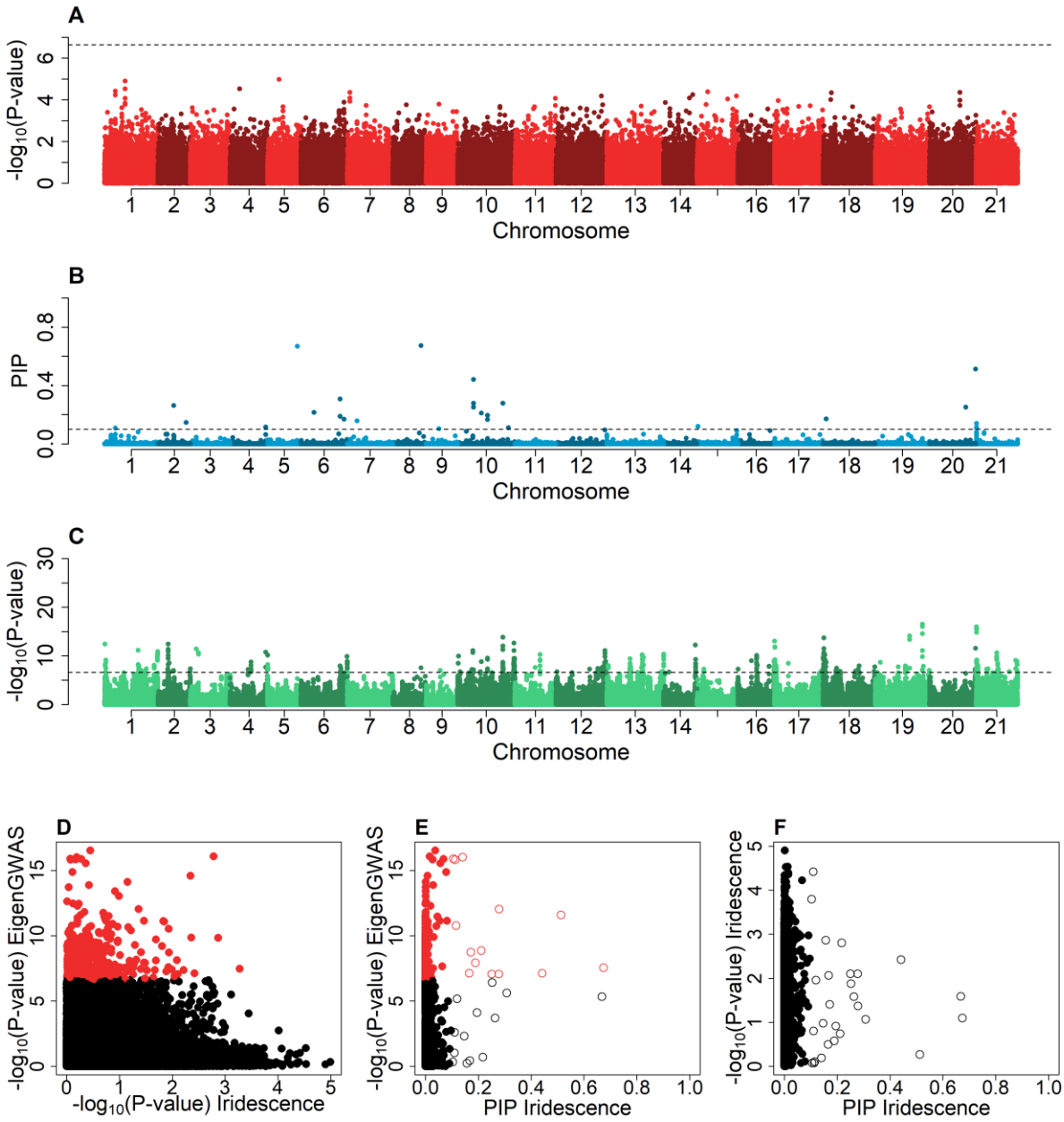

Figure 4.1 – Genetic associations with iridescence in *H. erato*. **(A)** Manhattan plot of the single locus GWAS analysis of iridescence. The dotted horizontal line represents the Bonferroni corrected genome-wide significance threshold. **(B)** Manhattan plot of the BSLMM, the multi-locus GWAS analysis of iridescence. The dotted horizontal line represents the posterior inclusion probability (PIP) threshold of 0.1. **(C)** Manhattan plot of the EigenGWAS results for eigenvector 1. The dotted horizontal line represents the Bonferroni corrected genome-wide significance threshold. **(D)** Comparison between the single locus GWAS and EigenGWAS results. Red points indicate SNPs which have a significant association in the EigenGWAS. **(E)** Comparison between the BSLMM and EigenGWAS results. Red points indicate SNPs which have a significant association in the EigenGWAS. Open circles represent SNPs which pass the PIP threshold in the BSLMM. Red, open circles are put forward as candidate SNPs, and are shown in Table 4.2. **(F)** Comparison between the results of the BSLMM and the single locus GWAS. Open circles represent SNPs which pass the PIP threshold in the BSLMM.

Table 4.2 – Candidate SNPs for iridescence in *H. erato*. Position of the SNP is given as Scaffold:Position. Gene ontology (GO) terms and protein description from Lepbase are given if present.

Chromosome	Position	PIP	*p* (iridescence)	*p* (EigenGWAS)	Protein description	GO terms	Distance (bp)	Gene position
4	Herato0419: 1450216	0.12	0.79	1.69×10^{-11}	Microtubule-associated protein	--	In gene	Herato0419: 1333572-1459662
6	Herato0606: 11547494	0.19	0.27	1.20×10^{-8}	--	--	87	Herato0606: 11547000-11547407
8	Herato0821: 1262218	0.67	0.08	2.88×10^{-8}	--	--	6249	Herato0821: 1250963-1255969
10	Herato1003: 319152	0.44	0.004	7.63×10^{-8}	Serine protease inhibitor	--	In gene	Herato1003: 318928-320163
10	Herato1003: 319224	0.28	0.01	8.66×10^{-8}	Serine protease inhibitor	--	In gene	Herato1003: 318928-320163
10	Herato1003: 319234	0.25	0.01	8.66×10^{-8}	Serine protease inhibitor	--	In gene	Herato1003:

								318928-320163
10	Herato1003: 3652241	0.21	0.18	1.44×10^{-9}	--	Molecular function: nucleic acid binding; zinc ion binding	265	Herato1003: 3650539-3651976
10	Herato1003: 6157592	0.17	0.32	7.50×10^{-8}	Chymotrypsin serine protease	Biological process: proteolysis; Molecular function: serine-type endopeptidase activity	In gene	Herato1003: 6156528-6157784
10	Herato1007: 680659	0.28	0.04	9.36×10^{-13}	--	Molecular function: odorant binding	1511	Herato1007: 682170-694506
18	Herato1801: 1207013	0.17	0.04	1.89×10^{-9}	Integrator complex subunit 7	Molecular function: binding	In gene	Herato1801: 1184323-1213317
20	Herato2001: 19219584	0.51	0.54	2.56×10^{-12}	Protein kinase	Biological process: protein phosphorylation; Molecular function: protein kinase activity, ATP binding	In gene	Herato2001: 19162295-19238271

21	Herato2101: 218945	0.11	0.84	1.57×10^{-16}	Alpha-mannosidase 2	Molecular function: catalytic activity, hydrolase activity, hydrolysing O-glycosyl compounds, alpha-mannosidase activity, zinc ion binding, mannosidase; activity, carbohydrate binding	In gene	Herato2101: 204137-343704
21	Herato2101: 218980	0.11	0.85	1.28×10^{-16}	Alpha-mannosidase 2	(as above)	In gene	Herato2101: 204137-343704
21	Herato2101: 219010	0.14	0.65	9.68×10^{-17}	Alpha-mannosidase 2	(as above)	In gene	Herato2101: 204137-343704

Table 4.3 – SNPs which show a potential association with iridescence in *H. melpomene*. Position of the SNP is given as Scaffold:Position. Gene ontology (GO) terms and protein description from Lepbase are given if present.

Chromosome	Position	PIP	*p* (iridescence)	Protein description	GO terms	Distance (bp)	Gene position
10	Hmel210011: 2590483	0.02	2.22×10^{-5}	Lipase	Molecular function: carboxylic ester hydrolase activity	In gene	Hmel210011: 2589317-2597559
10	Hmel210011: 2590515	0.02	2.22×10^{-5}	Lipase	Molecular function: carboxylic ester hydrolase activity	In gene	Hmel210011: 2589317-2597559
10	Hmel210011: 2590530	0.02	2.42×10^{-5}	Lipase	Molecular function: carboxylic ester hydrolase activity	In gene	Hmel210011: 2589317-2597559

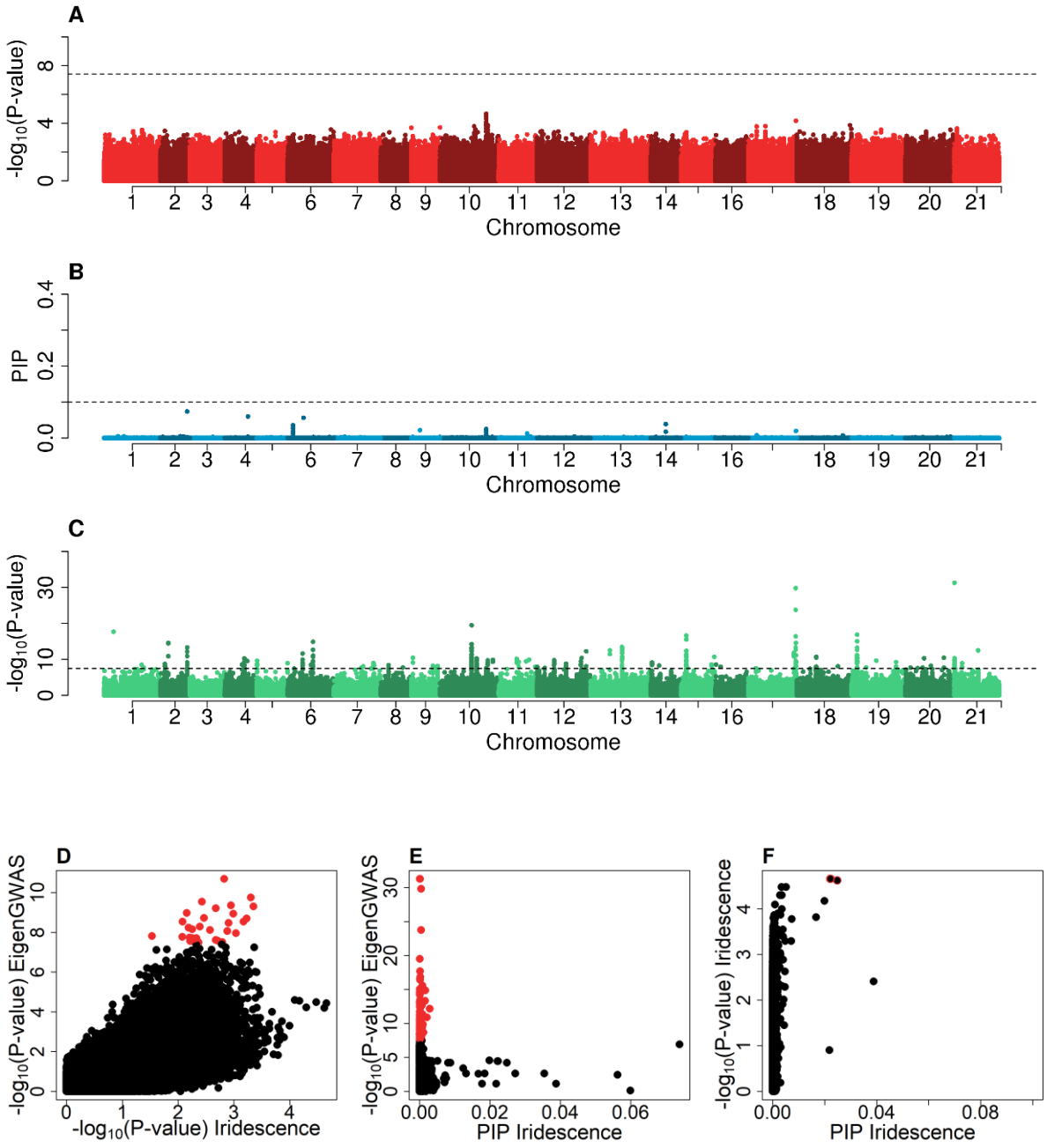

Figure 4.2 – Genetic associations with iridescence in *H. melpomene*. **(A)** Manhattan plot of the single locus GWAS analysis of iridescence. The dotted horizontal line represents the Bonferroni corrected genome-wide significance threshold. **(B)** Manhattan plot of the BSLMM, the multi-locus GWAS analysis of iridescence. The dotted horizontal line represents the posterior inclusion probability (PIP) threshold of 0.1. **(C)** Manhattan plot of the EigenGWAS results for eigenvector 1. The dotted horizontal line represents the Bonferroni corrected genome-wide significance threshold. **(D)** Comparison between the single locus GWAS and EigenGWAS results. Red points indicate SNPs which have a significant association in the EigenGWAS. **(E)** Comparison between the BSLMM and EigenGWAS results. Red points indicate SNPs which have a significant association in the EigenGWAS. **(F)** Comparison between the results of the BSLMM and the single locus GWAS. Black points outlined in red are the SNPs described in Table 4.3.

Table 4.4 – BSLMM hyperparameters for the yellow bar in *H. erato* and *H. melpomene*. Median estimates are given, alongside upper and lower equal-tailed posterior probability intervals (ETPI).

	H. erato			*H. melpomene*		
Hyperparameter	Median	Lower 95% ETPI	Upper 95% ETPI	Median	Lower 95% ETPI	Upper 95% ETPI
PVE	0.959	0.877	0.999	0.994	0.915	0.999
PGE	0.970	0.891	0.999	0.910	0.731	0.996
n-SNP	42	23	66	5	1	13

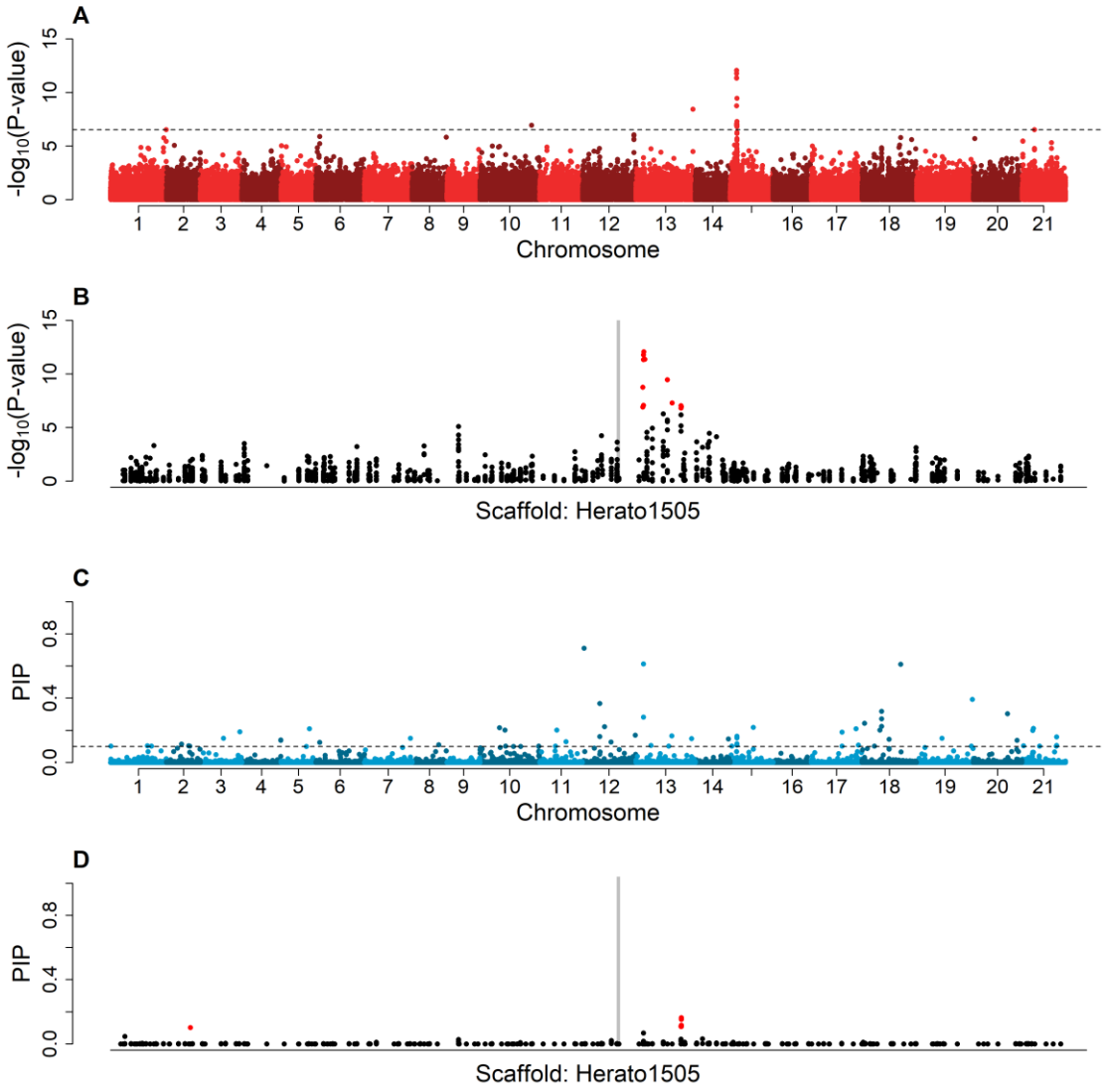

Figure 4.3 – Genetic associations with the yellow bar in *H. erato*. **(A)** Manhattan plot of the single locus GWAS analysis of the yellow bar. The dotted horizontal line represents the Bonferroni corrected genome-wide significance threshold. **(B)** Single locus GWAS results for scaffold Herato1505. The location of *cortex* is indicated by the vertical grey shading. SNPs coloured in red pass the Bonferroni corrected genome-wide significance threshold. **(C)** Manhattan plot of the BSLMM, the multi-locus GWAS analysis of the yellow bar. The dotted horizontal line represents the posterior inclusion probability (PIP) threshold of 0.1. **(D)** Multi-locus GWAS results for scaffold Herato1505. The location of *cortex* is indicated by the vertical grey shading. SNPs coloured in red pass the PIP threshold.

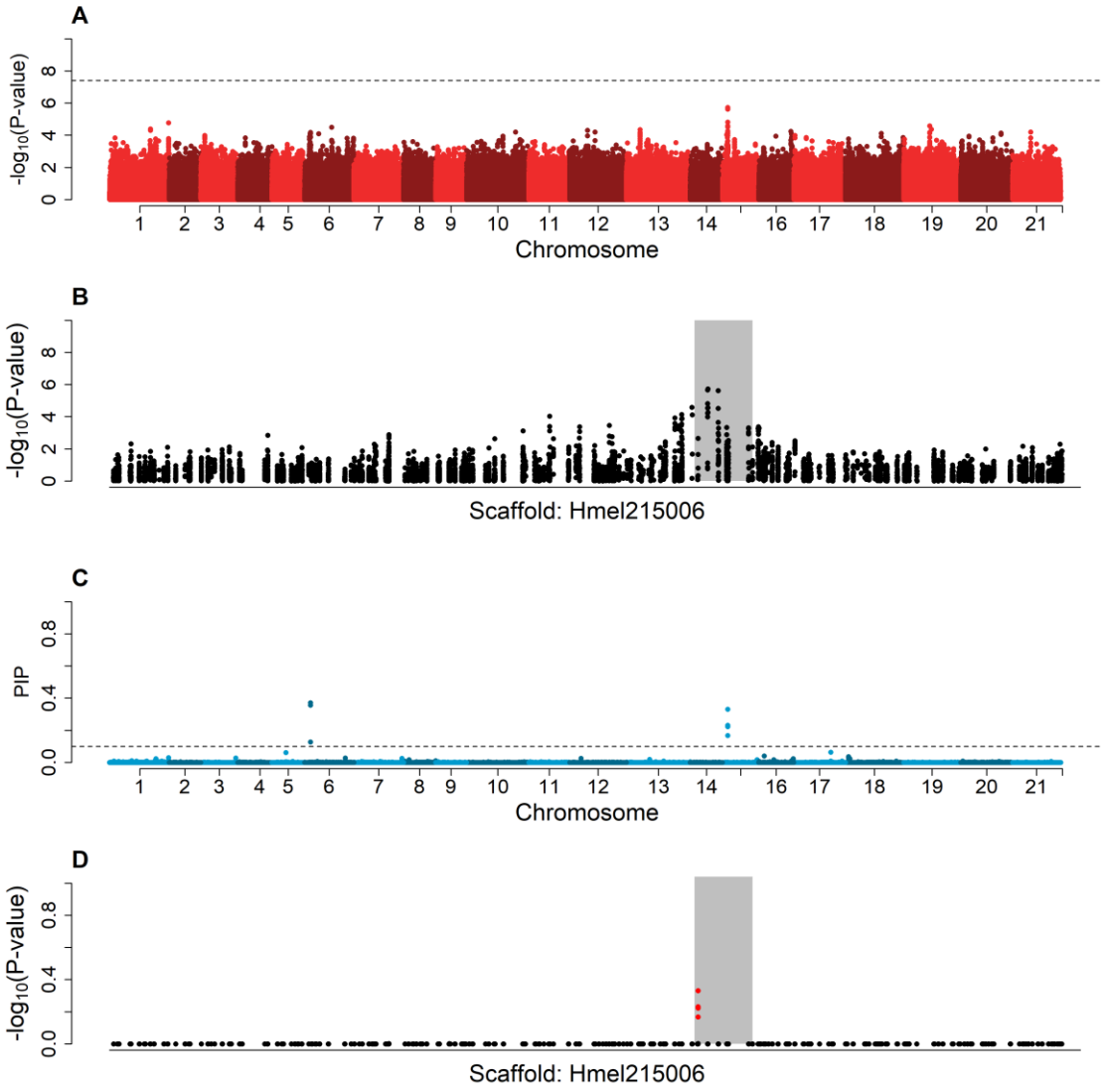

Figure 4.4 – Genetic associations with the yellow bar in *H. melpomene*. **(A)** Manhattan plot of the single locus GWAS analysis of the yellow bar. The dotted horizontal line represents the Bonferroni corrected genome-wide significance threshold. **(B)** Single locus GWAS results for scaffold Hmel215006. The location of *cortex* is indicated by the vertical grey shading. SNPs coloured in red pass the Bonferroni corrected genome-wide significance threshold. **(C)** Manhattan plot of the BSLMM, the multi-locus GWAS analysis of the yellow bar. The dotted horizontal line represents the posterior inclusion probability (PIP) threshold of 0.1. **(D)** Multi-locus GWAS results for scaffold Hmel215006. The location of *cortex* is indicated by the vertical grey shading. SNPs coloured in red pass the PIP threshold.

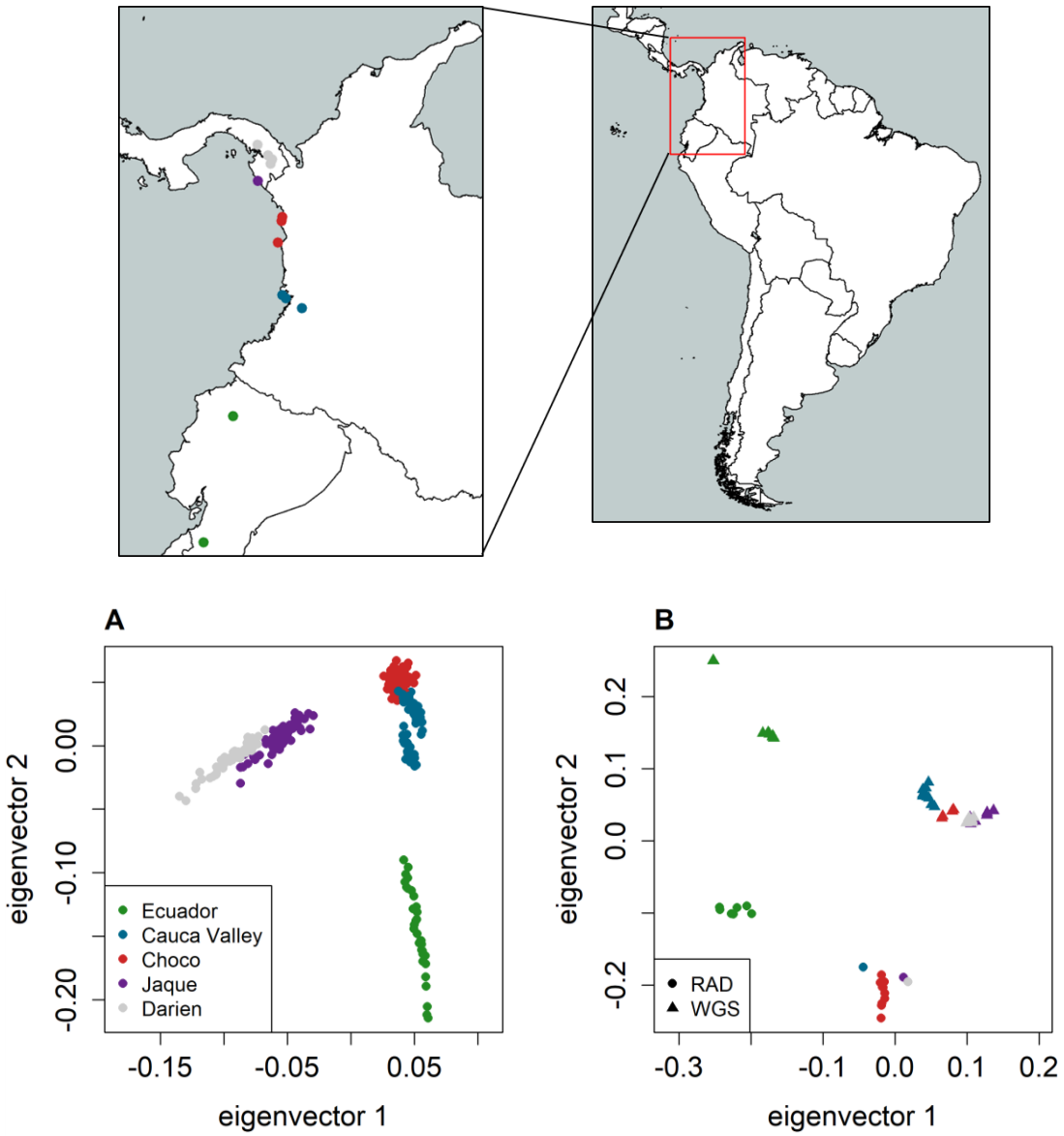

Figure 4.5 – The first two eigenvectors of genotype data, used in the EigenGWAS, in **(A)** *H. erato* and **(B)** *H. melpomene*. The localities of genotyped individuals are indicated on the map.

4.5 *Discussion*

This is the first time that the genetic architecture of iridescent structural colour has been described using genetic and phenotypic variation from natural populations across a hybrid zone. Combining a bottom-up approach to detect loci under selection, and genome-wide association studies, we were able to identify candidate SNPs that both showed an association with variation in iridescence, and that exhibited signatures of selection in *Heliconius erato*. Our results reject a highly polygenic genetic basis of iridescence in *H. erato*, and instead suggest that it is determined by multiple loci of moderate to large effect. Our analyses revealed no SNPs associated with iridescence in *Heliconius melpomene*, according to our genome-wide significance and posterior inclusion probability (PIP) thresholds. We were therefore unable to confidently compare the genetic basis of mimetic iridescence between the two species. Although, if SNPs which show a potential association with iridescence in *H. melpomene*, but which do not reach genome-wide significance, are taken into account, there is some evidence for genetic parallelism.

While the single locus GWAS in *H. erato* found no SNPs with genome-wide significant associations with iridescence, the multi-locus GWAS identified 27 SNPs which passed the PIP threshold, of which 14 were also identified as being under divergent selection. These 14 SNPs were distributed across 7 different chromosomes, suggesting variation in iridescence is determined by multiple independent genes. While the genes closest to candidate SNPs are linked to various processes which may or may not be involved in determining wing scale structure, we have found associations with SNPs under selection on chromosome 21, the Z sex chromosome. Evidence from experimental crosses suggests that iridescence in *H. erato* is sex-linked (Brien et al. submitted; Appendix 1), therefore associations with loci on sex chromosomes is expected. The proportion of variation in iridescence which is explained by SNPs with an effect larger than expected by a highly polygenic model is very high. This suggests that while multiple loci appear to determine iridescence, it is unlikely to be a highly polygenic phenotype. This is different to the genetic architecture of pigment colour in *Heliconius*, where each pattern element is controlled by a single locus (Kronforst *et al.*, 2006; Reed *et al.*, 2011; Martin *et al.*, 2012; Nadeau *et al.*, 2014,

2016; Van Belleghem *et al.*, 2017). Variation in pigment colour patterns appears to be controlled by complex modular variation in the regulatory regions that surround a relatively simple 'genetic tool-kit' of up to five genes (Nadeau, 2016; Van Belleghem *et al.*, 2017). In *Heliconius numata*, multiple colour patterns are controlled by different alleles at a single genetic locus (Le Poul *et al.*, 2014). Our results are also in contrast with a recent study which used CRISPR/Cas9 genome editing to show that a single master gene can act as a switch between iridescent and non-iridescent forms in the nymphalid *Junonia coenia* (Zhang *et al.*, 2017).

We also carried out GWAS on the yellow bar phenotype, which is known to be controlled by the *cortex* gene on chromosome 15 (Joron *et al.*, 2006; Nadeau *et al.*, 2016). This allowed us to test how effective each type of GWAS analysis was using our sequence data. The single locus GWAS resulted in a clear peak of SNPs in the vicinity of *cortex* with genome-wide significant associations with variation in the yellow bar. Two false positives were also detected on chromosomes 10 and 13. The multi-locus BSLMM which was carried out for the yellow bar found 69 SNPs with a PIP greater than 0.1, however only 7 of these were on the same scaffold as *cortex*. This higher rate of false positives suggests that the BSLMM is less effective at accounting for the strong population structure *H. erato* exhibits across the sampling range than the EIGENSTRAT method implemented in the single locus approach. This means that there is a risk that some of the candidate SNPs for iridescence are not actually controlling variation in iridescence but are a consequence of population stratification. Future attempts to map iridescence in *H. erato* might have more success if more sites within the hybrid zone, and directly flanking the hybrid zone, were sampled, as is typical with successful admixture mapping studies (e.g. Brelsford *et al.* 2017). This would maximise phenotypic variation while minimising genetic difference due to geography. This is currently difficult to do, however, as there are security issues across the border of Panama and Colombia, and it is a difficult region to access in general.

The use of restriction-site associated DNA sequencing allows us to obtain sequence data from a large number of individuals, due to its affordability, which increases the statistical power of our analyses. However, as it is a reduced representation sequencing approach, causal loci are less

likely to be sequenced, so we rely on linkage disequilibrium (LD) between causal loci and SNPs in our dataset. If LD does not extend far enough, then we will be unable to detect missed loci. It has been suggested that most genome scans using RAD data will likely miss many loci involved in local adaptation (Lowry *et al.*, 2017). It is possible that this has happened in the present study, as it has been shown that LD in *H. erato* decays rapidly with physical distance for both "pure" populations, and admixed populations in hybrid zones (Counterman *et al.*, 2010). A similar pattern of rapid LD decay is seen in *H. melpomene* for regions not associated with colour patterns, but long range haplotype structure and LD is seen between SNPs associated with wing pattern divergence (Baxter *et al.*, 2010). Despite this, RAD studies have radically improved our understanding of the genomic basis of adaptation (Catchen *et al.*, 2017), particularly in *Heliconius* research (Martin *et al.*, 2012; The Heliconius Genome Consortium, 2012; Nadeau *et al.*, 2014; Huber *et al.*, 2015). Whole-genome re-sequencing will in theory provide complete breadth of coverage, however sequencing enough individuals to gain enough statistical power to detect loci associated with adaptive traits can be prohibitively costly. Additional challenges include the amount of computational power required to handle such large datasets, as well as determining appropriate methods of assessing genome-wide significance (Gao *et al.*, 2010).

In *H. melpomene*, no SNP has genome-wide statistically significant associations with iridescence. This is likely due to the relatively small number of sequenced individuals used in the analysis, due to low numbers of this species being collected during fieldwork. Sample sizes of several hundred to several thousand individuals are often thought to be required for an effective GWAS of traits in natural populations (Kardos *et al.*, 2016), possibly even tens of thousands for mapping polygenic traits (e.g. Lango Allen *et al.*, 2010), and the present analysis only includes 66 individuals. In addition, the MCMC chains from the BSLMM did not converge well. Despite this, the SNPs with the strongest association in the single locus GWAS also had a relatively large effect in the BSLMM, so there was some level of consensus between analyses. These 3 SNPs are on chromosome 10 and fall within a gene (Molecular function: carboxylic ester hydrolase activity). There are no candidate SNPs for *H. erato* within the orthologous gene in the *H. erato demophoon* genome, however there are 6 candidates on chromosome 10, and one on the scaffold

Herato1007, which is 119,444 bp upstream of the orthologue to the potential candidate in *H. melpomene.* If, given a greater sample size, the association between iridescence and the potential candidate locus on chromosome 10 in *H. melpomene* gained genome-wide significance, this could be evidence for the repeated use of similar genomic regions during the convergent evolution of iridescence. Aside from this, we lack the evidence to say whether the genetic basis of iridescence in the co-mimics is parallel, partially parallel, or non-parallel, as it is likely that genes underlying variation in iridescence in both species have not been detected.

A principal component analysis split the *H. melpomene* samples by both geography and sequencing type. One cause of this could be allele dropout in the RAD sequencing data, an issue which occurs when polymorphisms occur within the restriction site, leading to an overestimation of genetic diversity (Gautier *et al.*, 2013). The EIGENSTRAT method was therefore not used for the single locus GWAS in this species, since it uses the principal components of genetic variation to correct for population structure. Despite this, when a simple association test from GenABEL (Aulchenko *et al.*, 2007) without a correction for population structure was carried out to map the genetic basis of the yellow bar in *H. melpomene*, the most strongly associated SNPs in the single locus GWAS are located in and around *cortex*. When this approach was used in *H. erato*, the real association signal with the yellow bar was drowned out by spurious associations due to population structure. The BSLMM for the yellow bar in *H. melpomene* detected SNPs in *cortex* which passed the PIP threshold, but it also yielded a false positive at a locus on chromosome 6. As the yellow bar was scored as a binary trait, it is possible that loci controlling traits which also vary in a binary way between colour pattern races will also be detected. The lower rate of false positive detection, and the recovery of a convincing signal in the single locus GWAS, suggest that the lower levels of population structure in *H. melpomene* make this species more amenable to GWAS approaches than *H. erato.* This is supported by our findings in Chapter 3, which revealed lower genetic differentiation between *H. melpomene* populations across the iridescence cline relative to its co-mimic. Given a larger sample size, and a consistent sequencing type, GWAS might be a promising approach for mapping the genetic basis of iridescence in this species, even when using samples collected across a large geographic area.

We complemented our top-down GWAS approach with a bottom-up approach to look for SNPs exhibiting signatures of selection, using EigenGWAS. In both species this analysis revealed many loci putatively under selection across the genome, although the *melpomene* results should be viewed with caution, since eigenvector decomposition separated out individuals partly due to sequencing type, therefore it may not represent true associations with population structure. Recent studies have used EigenGWAS and GWAS in combination to identify regions under selection which are associated with a phenotype of interest (Bosse *et al.*, 2017; Armstrong *et al.*, 2018). EigenGWAS results have been shown to strongly correlate with F_{ST}-based genome scan approaches (Chen *et al.*, 2016; Bosse *et al.*, 2017), although it may produce overly conservative estimates when applied to a bottlenecked population (Armstrong *et al.*, 2018).

Future attempts to map the genetic basis of iridescence in *Heliconius*, or other butterfly species, might benefit from directly measuring the ultrastructure of the scale, and using this as the phenotype in association studies, rather than measuring colour from photographs. While the colour measurements used in the present study were highly repeatable measurements, which allowed us to effectively model how iridescence in these species varied across the landscape (see Chapter 2), they may not capture some of the subtler phenotypic variation, particularly from sites inside the hybrid zone, which could be key to uncovering how different aspects of variation in iridescence and scale structure segregate with genetic variation.

The photography method might also be prone to introducing variation caused by wing wear and damage, which can mask true phenotypic variation. One promising method of quantifying scale structure is by using small-angle X-ray scattering (SAXS), which can tease apart different structural aspects of the scale which contribute to iridescence (Parnell *et al.*, 2018), and can feasibly be performed on a large number of individuals.

4.6 *Conclusions*

While we were unable to map the genetic basis of iridescence in *Heliconius melpomene*, and therefore could not find out whether this trait evolved using the same complement of genes in each of the co-mimics, we were able to identify some candidate loci for iridescence in *Heliconius erato*, which were also putatively under selection. Estimations of genetic architecture of iridescence in *H. erato* suggest it is controlled by multiple genes, although it is unlikely to be highly polygenic. This suggests a more complex genetic basis for quantitative iridescent colouration, than discrete pigment colour pattern elements in *Heliconius*, which are each controlled by a single gene. This work lays the foundations for future research into the genetic basis of iridescence in *Heliconius*. Combining association mapping with other approaches such as gene expression and QTL analyses will help to narrow down candidate genes for iridescence, paving the way for functional confirmation with technologies such as CRISPR/Cas9 genome editing, and exploration into the developmental basis of iridescent butterfly scales. This will provide a more complete understanding of the genomics of colouration in butterflies.

Table S4.1 – SNPs found to have a significant association with the yellow bar in a single locus GWAS using the EIGENSTRAT method of correction for population structure in *H. erato.* The location of each SNP is given, alongside the *p*-value, corrected for genome inflation factor λ.

chromosome	scaffold	position	*p*
10	Herato1007	2460016	9.65×10^{-8}
13	Herato1301	22972565	3.10×10^{-9}
15	Herato1505	2180245	8.81×10^{-8}
15	Herato1505	2180393	1.32×10^{-9}
15	Herato1505	2184259	8.21×10^{-8}
15	Herato1505	2184268	1.50×10^{-12}
15	Herato1505	2184294	3.96×10^{-12}
15	Herato1505	2184400	9.24×10^{-13}
15	Herato1505	2189012	2.47×10^{-12}
15	Herato1505	2281535	4.00×10^{-10}
15	Herato1505	2300529	4.77×10^{-8}
15	Herato1505	2338040	1.31×10^{-7}
15	Herato1505	2338146	1.95×10^{-7}
15	Herato1505	2338147	1.95×10^{-7}
15	Herato1505	2338149	1.95×10^{-7}
15	Herato1505	2338155	1.95×10^{-7}

Table S4.2 – The top 20 SNPs with the strongest association with the yellow bar in a single locus GWAS without correction for population structure in *H. melpomene*. The location of each SNP is given, alongside the *p*-value, corrected for genome inflation factor λ.

chromosome	scaffold	position	*p*
15	Hmel215006	1232220	1.81×10^{-6}
15	Hmel215006	1232022	2.19×10^{-6}
15	Hmel215006	1253647	2.40×10^{-6}
15	Hmel215006	1231667	1.52×10^{-5}
1	Hmel201019	1701634	1.66×10^{-5}
19	Hmel219003	7261539	2.56×10^{-5}
15	Hmel215006	1199378	2.65×10^{-5}
15	Hmel215006	1232092	2.71×10^{-5}
15	Hmel215006	1231632	2.90×10^{-5}
15	Hmel215006	1253613	3.09×10^{-5}
6	Hmel206009	4216713	3.10×10^{-5}
1	Hmel201009	5911367	4.01×10^{-5}
19	Hmel219005	262144	4.24×10^{-5}
13	Hmel213020	107085	4.55×10^{-5}
13	Hmel213020	107110	4.55×10^{-5}
12	Hmel212001	5115133	4.88×10^{-5}
1	Hmel201009	5911587	5.01×10^{-5}
15	Hmel215006	1232114	5.34×10^{-5}
16	Hmel216015	587085	5.69×10^{-5}
15	Hmel215006	1231855	5.94×10^{-5}

Table S4.3 – SNPs with a posterior inclusion probability (PIP) greater than 0.1 in a BSLMM for the yellow bar in *H. erato*.

chromosome	scaffold	position	PIP
4	Herato0419	2246849	0.14
4	Herato0419	2246846	0.14
10	Herato1003	1578560	0.22
10	Herato1003	4038565	0.10
10	Herato1003	7171629	0.10
10	Herato1007	5288755	0.10
10	Herato1005	2692933	0.10
10	Herato1003	3748150	0.20
12	Herato1202	10781680	0.13
12	Herato1202	8163620	0.22
12	Herato1202	6235260	0.16
12	Herato1202	27880	0.71
12	Herato1202	20529279	0.17
12	Herato1202	6235153	0.37
17	Herato1708	503403	0.21
17	Herato1703	804827	0.10
17	Herato1703	804913	0.19
17	Herato1708	1567919	0.11
15	Herato1505	2338155	0.15
15	Herato1505	326660	0.10
15	Herato1507	4846090	0.22
15	Herato1505	2338149	0.16
15	Herato1505	2338146	0.11
15	Herato1505	2337965	0.11
15	Herato1505	2338028	0.11
15	Herato1505	2338147	0.16
8	Herato0821	218244	0.11
3	Herato0310	3319867	0.15
3	Herato0310	9917498	0.19
19	Herato1904	5896898	0.15
19	Herato1910	5188466	0.39
19	Herato1910	4764318	0.10
11	Herato1108	4574508	0.10
11	Herato1108	8867994	0.13
11	Herato1108	5113565	0.20
18	Herato1805	9371698	0.61
18	Herato1801	988953	0.24

18	Herato1805	1756301	0.32
18	Herato1805	1045970	0.20
18	Herato1805	1756299	0.27
18	Herato1801	4991467	0.10
18	Herato1805	1756278	0.22
18	Herato1805	4760694	0.14
5	Herato0503	8626057	0.10
5	Herato0508	500823	0.21
14	Herato1411	6303223	0.15
6	Herato0601	1407066	0.12
1	Herato0101	14693253	0.10
1	Herato0101	16352207	0.10
1	Herato0101	101008	0.10
13	Herato1301	6059659	0.10
13	Herato1301	3021774	0.61
13	Herato1301	13224588	0.10
13	Herato1301	3021877	0.28
13	Herato1301	14423474	0.17
13	Herato1301	22426826	0.15
2	Herato0211	691038	0.11
2	Herato0214	128156	0.10
2	Herato0214	590352	0.10
21	Herato2101	13871645	0.11
21	Herato2101	4550435	0.21
21	Herato2101	560791	0.10
21	Herato2101	13892443	0.16
21	Herato2101	4306126	0.20
21	Herato2101	7026721	0.10
21	Herato2101	13775839	0.10
20	Herato2001	17488065	0.14
20	Herato2001	13676554	0.30
7	Herato0701	18463393	0.15

Table S4.4 – SNPs with a posterior inclusion probability (PIP) greater than 0.1 in a BSLMM for the yellow bar in *H. melpomene*.

chromosome	scaffold	position	PIP
6	Hmel206006	1151964	0.37
6	Hmel206006	1151950	0.36
15	Hmel215006	1211920	0.33
15	Hmel215006	1212211	0.23
15	Hmel215006	1212203	0.22
15	Hmel215006	1212222	0.17
6	Hmel206006	1151805	0.13

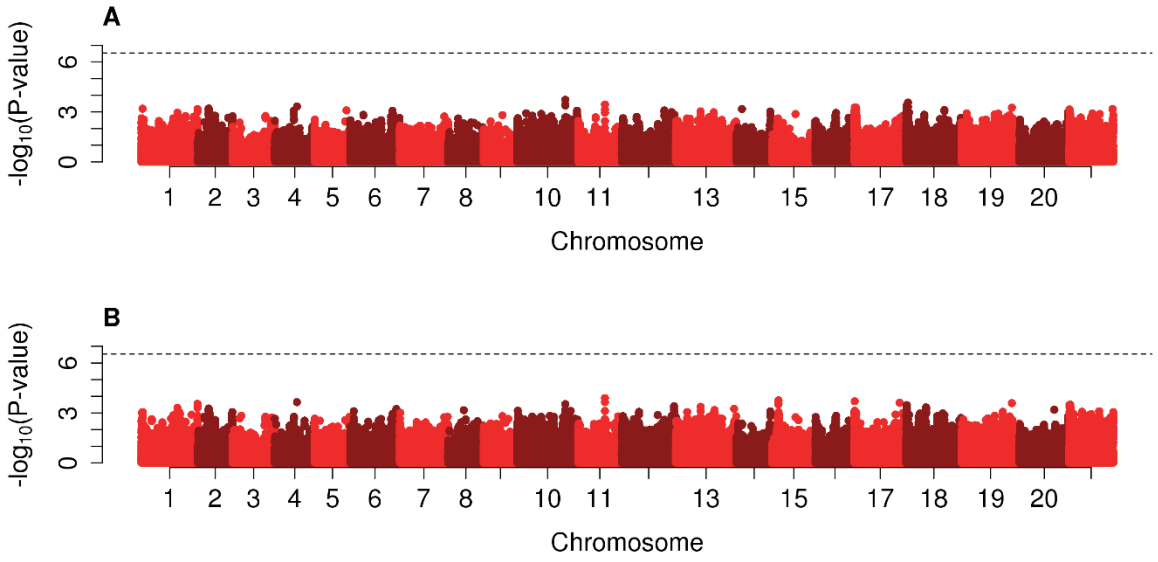

Figure S4.1– Single-locus GWAs results for **(A)** iridescence and **(B)** the yellow bar in *H. erato*, without correcting for population structure.

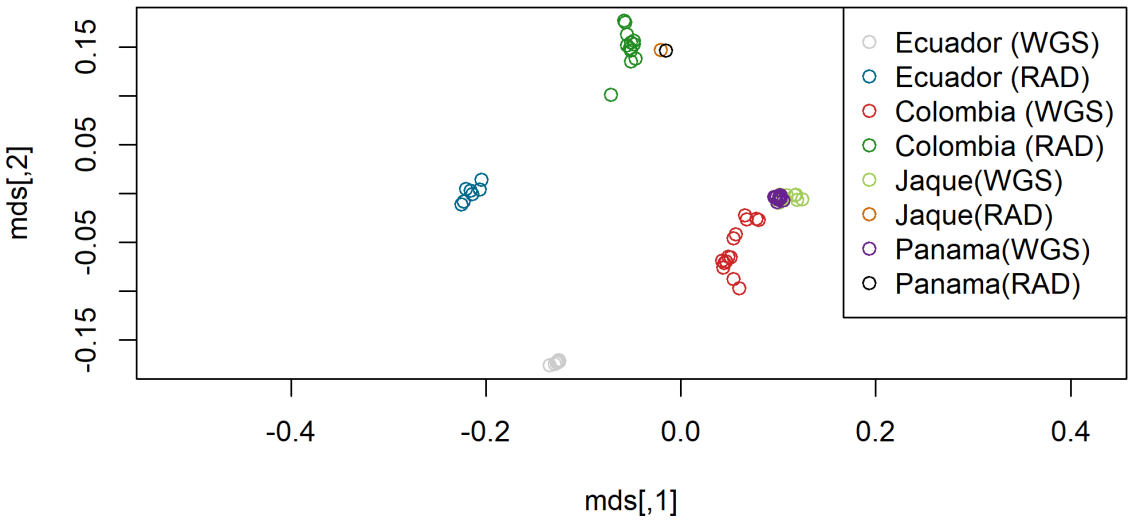

Figure S4.2 – The first two axes of variation of the genomic kinship matrix for *H. melpomene*, generated using GenABEL, on which we performed multidimensional scaling. Whole genome re-sequenced (WGS) individuals separate out from restriction site associated DNA (RAD) sequenced individuals.

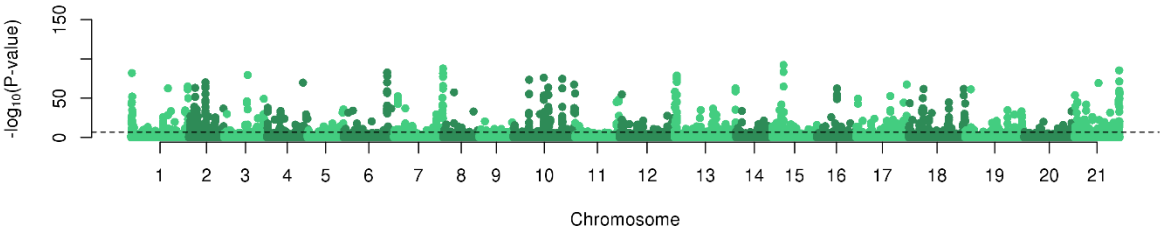

Figure S4.3 – EigenGWAS using the second eigenvector of genetic variation for *H. erato*.

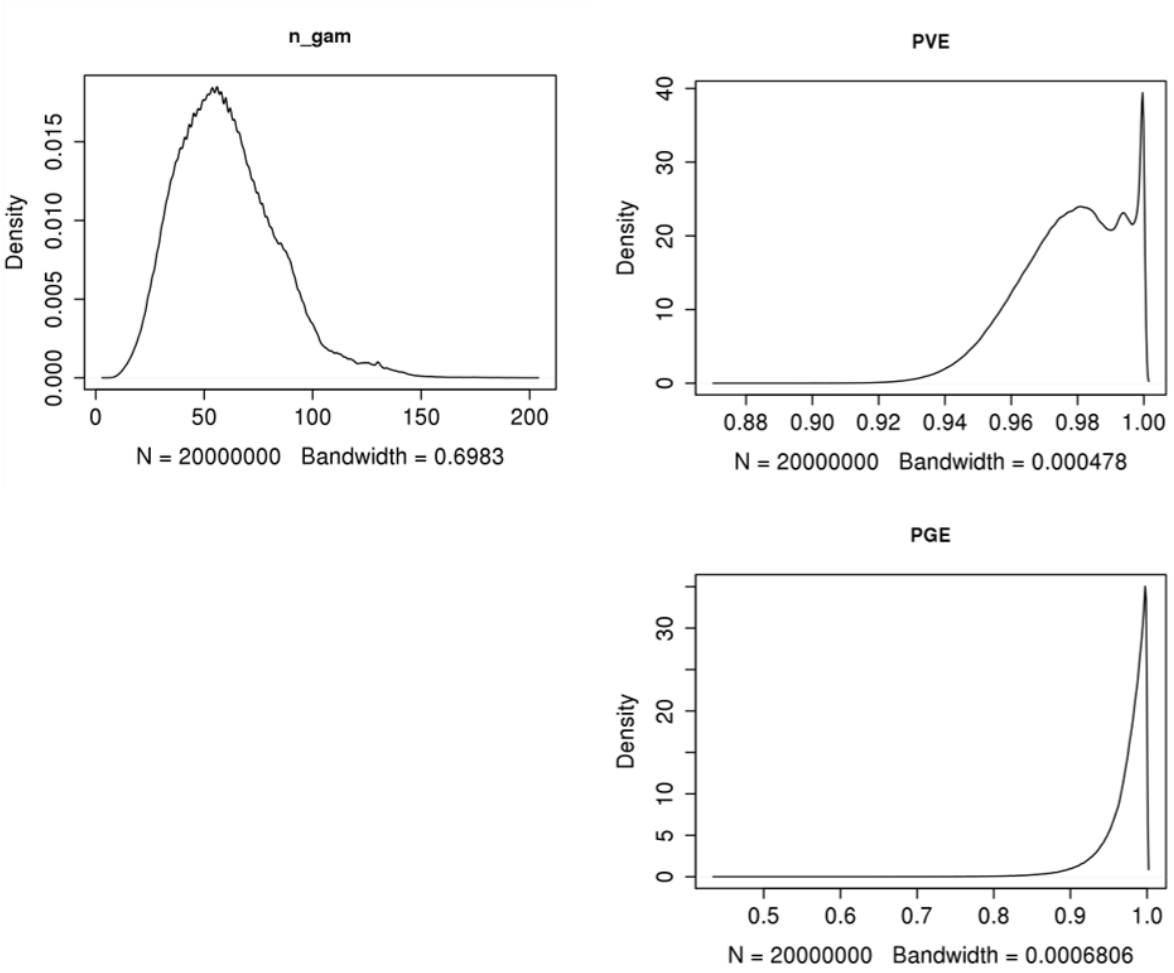

Figure S4.4 – Hyperparameter trace distributions for *H. erato* iridescence (BR) for the number of SNPs with a non-zero effect on phenotype (n_gam), the proportion of phenotypic variation explained by genetic variation (PVE), and the proportion of that genetic variation explained by non-zero effect SNPs (PGE).

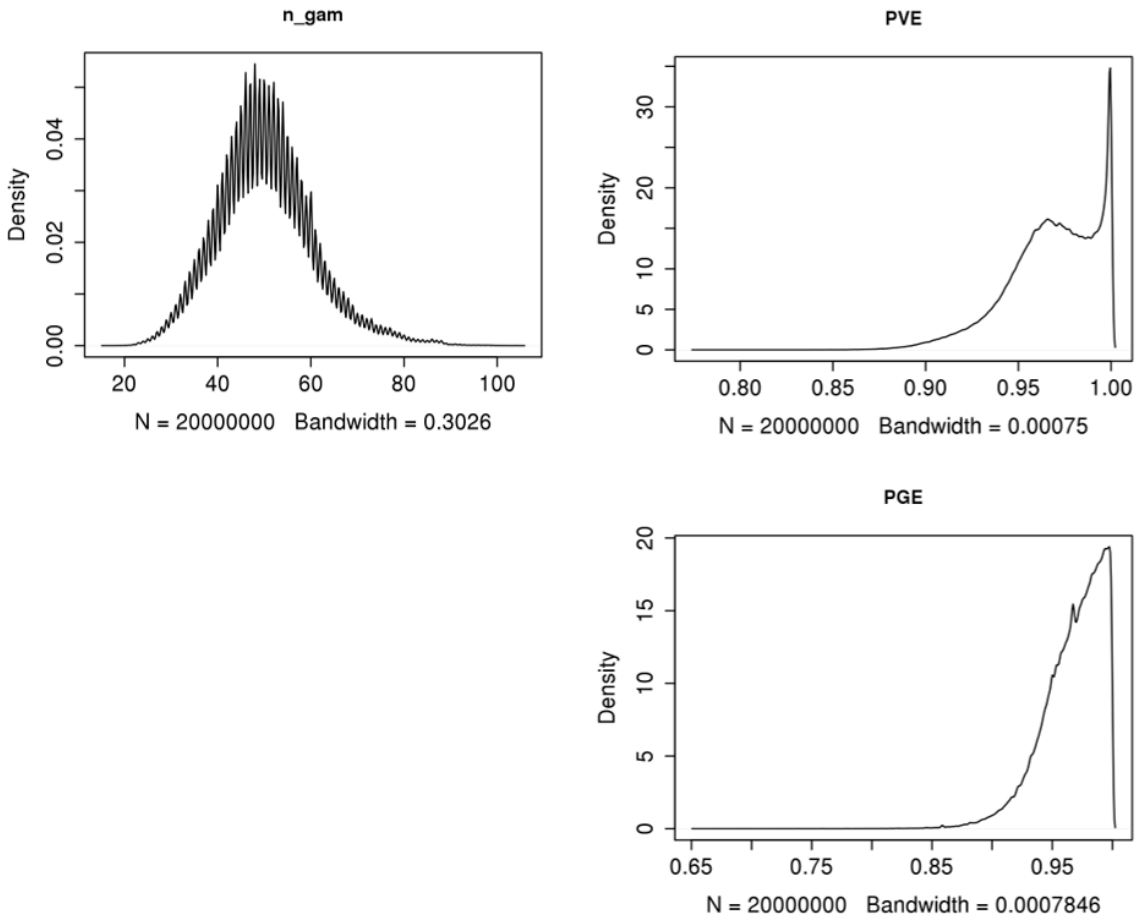

Figure S4.5 – Hyperparameter trace distributions for the yellow bar in *H. erato*, for the number of SNPs with a non-zero effect on phenotype (n_gam), the proportion of phenotypic variation explained by genetic variation (PVE), and the proportion of that genetic variation explained by non-zero effect SNPs (PGE).

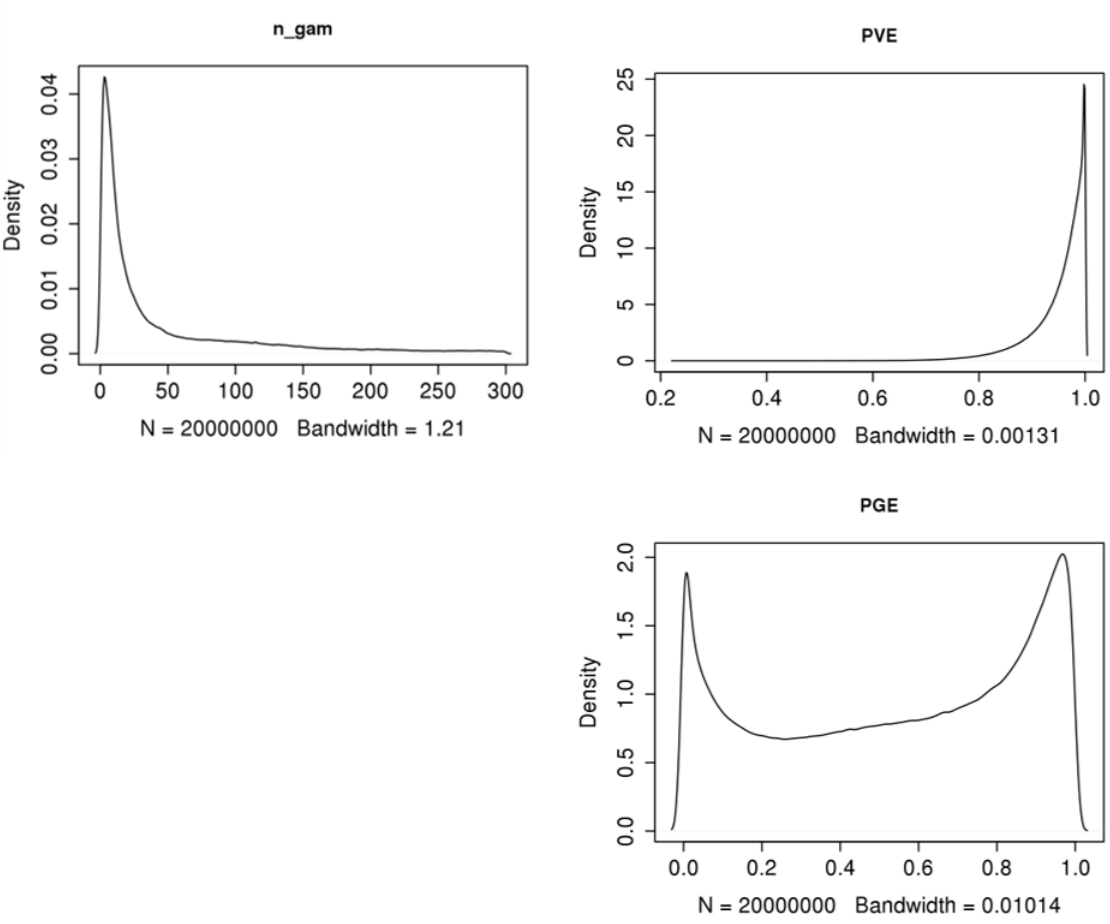

Figure S4.6 – Hyperparameter trace distributions for *H. melpomene* iridescence (BR) for the number of SNPs with a non-zero effect on phenotype (n_gam), the proportion of phenotypic variation explained by genetic variation (PVE), and the proportion of that genetic variation explained by non-zero effect SNPs (PGE).

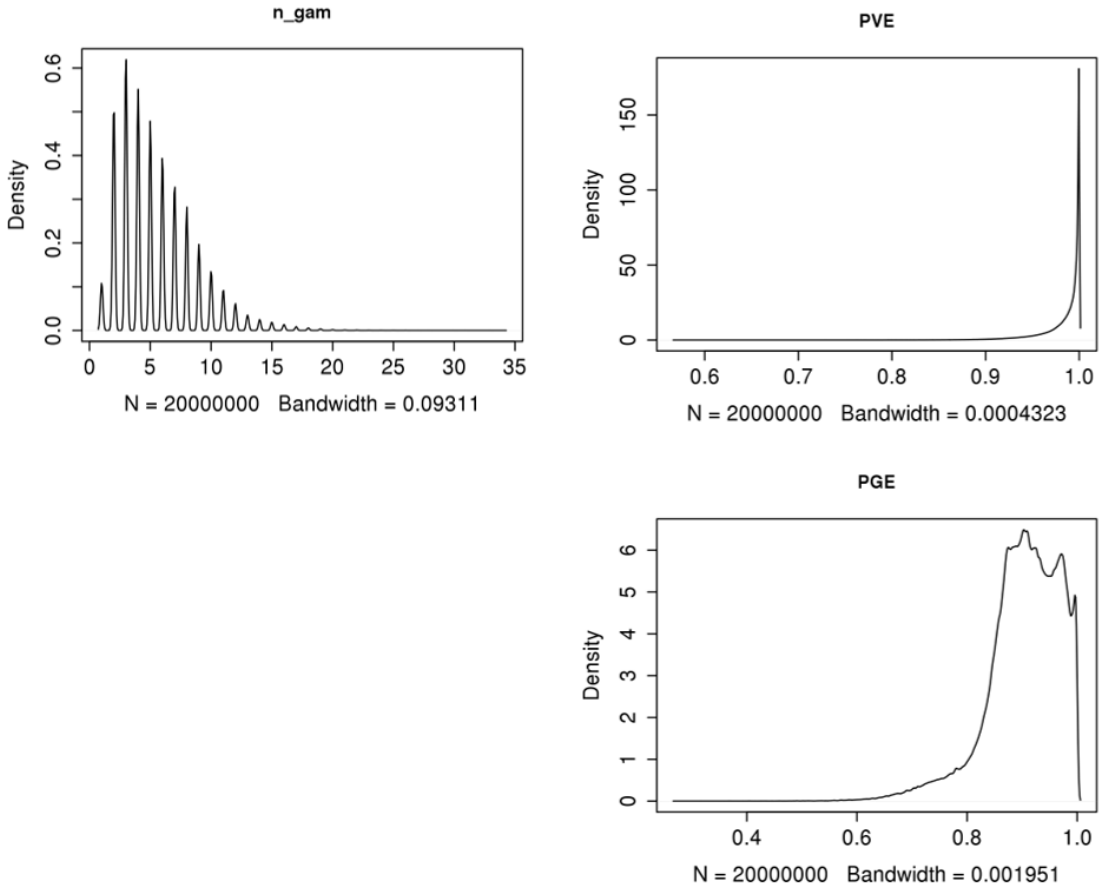

Figure S4.7 – Hyperparameter trace distributions for the yellow bar in *H. melpomene*, for the number of SNPs with a non-zero effect on phenotype (n_gam), the proportion of phenotypic variation explained by genetic variation (PVE), and the proportion of that genetic variation explained by non-zero effect SNPs (PGE).

5

General Discussion

5.1 *Research summary*

Below I provide a summary of the main findings from each data chapter of this thesis.

In Chapter 2, I reconstruct clines in iridescence across a hybrid zone between conspecific colour pattern races in *H. melpomene* and *H. erato*. Iridescence clines are coincident between species, suggesting a common agent of selection. This is likely to be positive frequency dependent selection on warning colour patterns in adjacent colour pattern races, driving selection against less common hybrid phenotypes in the contact zone. This is supported in *H. erato*, as the iridescence cline is coincident with the yellow bar, a pigment colour pattern known to have a warning colour function. However, in *H. melpomene*, the yellow bar and iridescence cline are not coincident, either because of different agents of selection, dominance drive, or weaker direct selection allowing the clines to uncouple. A major finding of this chapter is that the colour pattern clines in *H. melpomene* are much wider than their co-mimic *H. erato*. This suggests that either *H. melpomene* face weaker selection on warning colour, have greater population connectivity, or a combination of the two. Colour pattern clines in both species are considerably wider than other colour pattern clines across *Heliconius* hybrid zones (Mallet *et al.*, 1990; Salazar, 2012). The results of this chapter show how clines in quantitative traits can be maintained by apparently weak selection across large distances.

In Chapter 3, I use reference-aligned genomic data to examine the population genetic structure across the hybrid zones. A comparison of the iridescence clines to clines in average population structure across the hybrid zone show that there is some spatial coupling of genetic structure and iridescence, but that iridescence clines have different centres and widths to clines in population structure. This suggests that, for both species, phenotypic divergence between iridescent and non-

iridescent populations is not simply maintained by genome-wide differentiation and reproductive isolation between races, variation in iridescence is not neutral, and that selection is maintaining the differences despite gene flow. Another major finding of this chapter is the striking difference in population structure between the species. *H. erato* shows clear genetic structure in the population, with strong clustering corresponding to geography. Genetic structure is much less pronounced in *H. melpomene.* This fits with the findings of Chapter 2, that weaker selection against hybrids and greater gene flow between populations is found in *H. melpomene.* I tentatively propose that the greater population structure seen in *H. erato* might indicate a substantial period of allopatry, followed by secondary contact. *H. melpomene* shows weak population structure across its hybrid zone, yet a wide cline in iridescence persists. It is possible that this might indicate phenotypic divergence by primary intergradation in the presence of gene flow. Alternatively, this pattern could be explained by allopatry followed by high levels of gene flow, re-homogenising the genome, except at alleles controlling variation in iridescence.

In Chapter 4, I set out to perform genome-wide association studies to describe the genetic architecture of iridescence and identify candidate loci controlling variation in iridescence in *H. erato* and *H. melpomene,* to ask the extent to which this convergent phenotype is also convergent on the genetic level. The results suggest that the genetic architecture of iridescence in *H. erato* is not highly polygenic but controlled by multiple loci of moderate to large effect, spread across several chromosomes. This genetic architecture is different to that of pigment colour pattern elements, each of which is controlled by a single locus (reviewed in Nadeau, 2016). It is also in contrast with a recent study which suggests a very simple genetic basis for iridescence in a nymphalid butterfly, based on gene knockouts (Zhang *et al.*, 2017). These results in this chapter should be viewed with caution, however, as a GWAS of a colour pattern trait with a known genetic basis, using the same data, revealed many false positives, likely because of the highly structured populations of *H. erato*. A GWAS of iridescence in *H. melpomene* revealed no significantly associated variants. As a result, I was unable to assess whether iridescence has a parallel genetic basis between these species. However, if nonsignificant SNPs which show a potential association with iridescence are taken into account, there is some weak evidence of parallel genetic regions

underlying iridescence in the co-mimics. This study lays the groundwork for future research into the genetic basis of iridescence in natural *Heliconius* populations. I highlight issues, such as the strong genetic structure in *H. erato*, and make recommendations for future studies, regarding the sampling of populations, and the quantification of iridescence. This thesis represents a starting point in addressing the lack of studies on the genomic basis of quantitative variation in structural colours in natural populations (San-Jose & Roulin, 2017).

5.2 *Future directions: The evolution and genetics of iridescence in Heliconius*

The most immediate next steps in understanding the genetic basis of iridescence in *Heliconius* butterflies, are to continue efforts with genetic mapping. In chapter 4, I highlight the limitations which prevented us from successfully identifying candidate loci in both species. The major limitations include high levels of population structure in *H. erato*, and too small a sample size in *H. melpomene*. The best way of overcoming these limitations would be further sampling. For *H. erato*, it would be important to concentrate sampling within, and immediately either side of the hybrid zone, in order to maximise genetic differences due to phenotype, while minimising genetic difference due to geography. Unfortunately, further sampling in the hybrid zone region is dependent on the security situation near the Colombian-Panamanian border improving, as it was too dangerous for us to sample the southern end of the hybrid zone during our major sampling effort in 2015 and 2016. Another way to improve a GWAS of iridescence would be to quantify iridescence by directly measuring scale structures. This will reduce the variation due to environmental effects such as wing wear, rather than real structural differences. Finally, combining GWAS approaches with QTL mapping, and RNA-sequencing experiments will hopefully provide support and consensus of results.

Beyond this, functional confirmation of the most promising candidates could be carried out using CRISPR/Cas9 genome editing, which has already been successfully implemented in *Heliconius* with the effect of altering wing patterning (Zhang *et al.*, 2017). Once it is determined whether similar genes were targeted during the evolution of iridescence in the co-mimics *H. erato*

and *H. melpomene*, it would be interesting to learn about the origin of the genetic changes responsible for iridescence, a phenotype highly localised to the western slopes of the Andes in both species. Introgression of colour patterns have previously been documented between *Heliconius* species (The Heliconius Genome Consortium, 2012), particularly between *H. melpomene* and *H. cydno* (Pardo-Diaz *et al.*, 2012; Enciso-Romero *et al.*, 2017). This could be a potential source of genetic material conferring iridescence, particularly in *H. melpomene*, which overlaps in range on the west of the Andes with *H. cydno*, which also displays iridescence.

To investigate the adaptive significance of iridescence, it will be necessary to carry out behavioural experiments. Structural colour has already been shown to influence mate choice in *Heliconius cydno*, with males preferring females that reflect polarized light (Sweeney *et al.*, 2003). Structural UV colour and iridescent ornamentation have been shown to be sexually selected in butterflies, as structural colour can be an honest, condition-dependent signal (Kemp, 2007; Kemp & Rutowski, 2007). Mate choice experiments could reveal if iridescence has a similar function in *H. erato* and *H. melpomene*. The role of iridescence as a signal of distastefulness should also be tested experimentally. Experiments with butterfly models have been performed to test the role of colour patterns in predator avoidance in the field (Kapan, 2001; Langham, 2004; Dell'aglio *et al.*, 2016), and in enclosed settings using live butterflies and birds (Merrill *et al.*, 2012). To carry out such experiments on iridescent colour, either convincing models capturing the optical properties of real iridescent wings need to be designed, or methods to manipulate the optical properties, such as visible and UV wavelength reflection and polarisation of real wings need to be developed, which may be challenging. Since iridescence has strong angle-dependent effects, movement might also be an important part of the iridescent signal, therefore experiments with stationary wings might not be effective.

5.3 *Beyond Heliconius: Understanding the genetic basis of convergent evolution*

To improve our understanding of the genetic basis of convergent evolution, we need to explore convergent traits with complex genetic architectures. In this thesis I attempted to use

GWAS to compare the genetic basis of a convergent quantitative trait, however successful GWAS on quantitative traits may require very large sample sizes to gain enough statistical power to detect loci of small effect, which I was unable to achieve. With sequencing costs dropping, this will be more feasible, but using alternative methods to traditional GWAS might also be important. For example, Random Forest, a machine learning algorithm (Breiman, 2001), has been proposed as a promising approach to detect loci underlying polygenic traits (Brieuc *et al.*, 2018), and has been used alongside GWAS and selection scans to identify loci involved with killifish adaptation to different osmotic environments (Brennan *et al.*, 2018).

While I have mainly focused on studying instances of convergence in natural populations, experimental evolution has provided important insights into the repeatability of evolution on the genetic level. As this approach is highly controlled, it allows more accurate quantification of convergence, as the generation number is known, and the population size can be controlled (Lenski, 2017). Sequencing individuals from evolution experiments at different time points can reveal the precise genetic changes that occur, and how similar changes are across replicates. This approach is often referred to as 'evolve and resequence' (Long *et al.*, 2015). Replicated experiments selecting for accelerated development in *Drosophila* showed that repeatable genomic changes were likely due to shared standing genetic variation between replicates (Burke *et al.*, 2010). A similar finding was reported in *Saccharomyces*, where standing genetic variation appeared to drive parallel genetic evolution (Burke *et al.*, 2014). This will remain an important source of knowledge regarding the genetic processes underlying convergent phenotypic evolution, as long-term evolution experiments progress through further generations, and new experiments are carried out on more diverse organisms.

Combining studies looking for the genetic underpinnings of adaptive traits in natural populations with experiments to test targets and agents of selection is considered the gold standard when considering the genomic basis of adaptation (Barrett & Hoekstra, 2011). This has been applied to parallel evolution in recent years. Soria-Carrasco *et al.* (2014) examined the repeated emergence of two ecotypes in the stick insect *Timema cristinae* and found both parallel and non-

parallel genetic divergence. An experiment, which involved transplanting ecotypes onto each other's host plant and tracking allele frequency changes across a single generation, revealed strong allele frequency changes in regions of parallel genomic divergence. Similarly, a study comparing natural populations of guppies (*Poecilia reticulata*) adapted to high and low predation environments, to experimental populations which had been transplanted between predation environments, revealed shared genomic regions under selection between different experimental populations (Fraser *et al.*, 2015). Approaches such as these will increase our understanding of parallel genomic evolution in ecologically relevant contexts.

Finally, if gene reuse is pervasive during convergent evolution, it will be interesting to determine what the most common mode of genetic convergence is. Are the same genes repeatedly targeted by independent mutations? Is it a result of selection on shared ancestral genetic variation? Or are adaptive alleles shared through hybridisation events? New methods are being developed to distinguish between these scenarios (Lee & Coop, 2018).

5.4 *Conclusion*

Examining the genetic basis of divergent and convergent colour patterns in *Heliconius* butterflies has been important in expanding our understanding of the genomics of adaptation beyond that of model taxa. This thesis begins to examine the genetic basis of iridescence in the genus for the first time and compares the phenotypic variation in this imperfectly mimetic visual signal between the co-mimics *H. erato* and *H. melpomene.* Iridescence appears to be a quantitative trait, controlled by multiple loci, in sharp contrast with the discrete variation of the pigment colour patterns found on the same wing. This work lays the foundation for a more complete understanding of the genetic basis of all colour pattern variation in the genus. Examining phenotypic and genetic variation in hybrid zones gives us a valuable glimpse into the porous barriers between taxa and provides us an opportunity to witness the active evolutionary forces which are maintaining variation.

References

Abbott, R., Albach, D., Ansell, S., Arntzen, J.W., Baird, S.J.E., Bierne, N., *et al.* 2013. Hybridization and speciation. *J. Evol. Biol.* **26**: 229–246.

Abràmoff, M.D., Magalhães, P.J. & Ram, S.J. 2004. Image processing with imageJ. *Biophotonics Int.* **11**: 36–41.

Alexander, D.H., Novembre, J. & Lange, K. 2009. Fast Model-Based Estimation of Ancestry in Unrelated Individuals. *Genome Res.* **19**: 1655–1664.

Arendt, J. & Reznick, D. 2008. Convergence and parallelism reconsidered: what have we learned about the genetics of adaptation? *Trends Ecol. Evol.* **23**: 26–32.

Armstrong, C., Richardson, D.S., Hipperson, H., Horsburgh, G.J., Küpper, C., Percival-Alwyn, L., *et al.* 2018. Genomic associations with bill length and disease reveal drift and selection across island bird populations. *Evol. Lett.* 22–36.

Aulchenko, Y.S., Ripke, S., Isaacs, A. & van Duijn, C.M. 2007. GenABEL: An R library for genome-wide association analysis. *Bioinformatics* **23**: 1294–1296.

Baldassarre, D.T., White, T.A., Karubian, J. & Webster, M.S. 2014. Genomic and morphological analysis of a semipermeable avian hybrid zone suggests asymmetrical introgression of a sexual signal. *Evolution.* **68**: 2644–2657.

Bálint, Z., Kertész, K., Piszter, G., Vértesy, Z. & Biró, L.P. 2012. The well-tuned blues: the role of structural colours as optical signals in the species recognition of a local butterfly fauna (Lepidoptera: Lycaenidae: Polyommatinae). *J. R. Soc. Interface* **9**: 1745–56.

Barrett, R.D.H. & Hoekstra, H.E. 2011. Molecular spandrels: Tests of adaptation at the genetic level. *Nat. Rev. Genet.* **12**: 767–780.

Barton, N.H. 1979. Gene flow past a cline. *Heredity.* **43**: 333–339.

Barton, N.H. 1983. Multilocus Clines. *Evolution.* **37**: 454.

Barton, N.H. & Gale, K.S. 1993. Genetic analysis of hybrid zones. In: *Hybrid zones and the evolutionary process* (R. G. Harrison, ed), pp. 13–45. Oxford University Press, Oxford, UK.

Barton, N.H. & Hewitt, G.M. 1985. Analysis of Hybrid Zones.

Barton, N.H. & Keightley, P.D. 2002. Understanding quantitative genetic variation. *Nat. Rev. Genet.* **3**: 11–21.

Barton, N.H. & Turelli, M. 2011. Spatial Waves of Advance with Bistable Dynamics: Cytoplasmic and Genetic Analogues of Allee Effects. *Am. Nat.* **178**: E48–E75.

Bates, H.W. 1862. Contributions to an Insect Fauna of the Amazon Valley. Lepidoptera: Heliconidae. *J. Proc. Linn. Soc. London* **6**: 73–77.

Bates, H.W. 1864. *The naturalist on the river Amazons. A record of adventures, habitats of animals, sketches of Brazilian and Indian life and aspects of nature under the equator, during eleven years of travel*. John Murray, London.

Baxter, S.W., Davey, J.W., Johnston, J.S., Shelton, A.M., Heckel, D.G., Jiggins, C.D., *et al.* 2011. Linkage Mapping and Comparative Genomics Using Next-Generation RAD Sequencing of a Non-Model Organism. *PLoS One* **6**: e19315.

Baxter, S.W., Johnston, S.E. & Jiggins, C.D. 2009. Butterfly speciation and the distribution of

gene effect sizes fixed during adaptation. *Heredity.* **102**: 57–65.

Baxter, S.W., Nadeau, N.J., Maroja, L.S., Wilkinson, P., Counterman, B.A., Beltran, M., *et al.* 2010. Genomic Hotspots for Adaptation: The Population Genetics of Müllerian Mimicry in the Heliconius melpomene Clade. *Genetics* **6**: e1000794.

Beldade, P., Saenko, S. V., Pul, N. & Long, A.D. 2009. A gene-based linkage map for Bicyclus anynana butterflies allows for a comprehensive analysis of synteny with the lepidopteran reference genome. *PLoS Genet.* **5**: e1000366.

Benson, W. 1972. Natural Selection for Mullerian Mimicry in Heliconius erato in Costa Rica. *Science*. **176**: 936–939.

Berg, J.J. & Coop, G. 2014. A Population Genetic Signal of Polygenic Adaptation. *PLoS Genet.* **10**: e1004412.

Bhatia, G., Patterson, N., Sankararaman, S. & Price, a. L. 2013. Estimating and interpreting F_{ST}: The impact of rare variants. *Genome Res.* **23**: 1514–1521.

Blum, M.J. 2002. Rapid movement of a Heliconius hybrid zone: evidence for phase III of Wright's shifting balance theory? *Evolution* **56**: 1992–1998.

Bosse, M., Spurgin, L.G., Laine, V.N., Cole, E.F., Firth, J.A., Gienapp, P., *et al.* 2017. Recent natural selection causes adaptive evolution of an avian polygenic trait. *Science.* **368**: 365–368.

Breiman, L. 2001. Random Forests. *Mach. Learn.* **45**: 5–32.

Brelsford, A., Toews, D.P.L. & Irwin, D.E. 2017. Admixture mapping in a hybrid zone reveals loci associated with avian feather coloration. *Proc. R. Soc. B Biol. Sci.* **284**: 20171106.

Brennan, R.S., Healy, T.M., Bryant, H.J., Van La, M., Schulte, P.M. & Whitehead, A. 2018. Integrative population and physiological genomics reveals mechanisms of adaptation in killifish. *Mol. Biol. Evol.*, doi: 10.1093/molbev/msy154/5068378.

Brieuc, M.S.O., Waters, C.D., Drinan, D.P. & Naish, K.A. 2018. A practical introduction to Random Forest for genetic association studies in ecology and evolution. *Mol. Ecol. Resour*. **18**: 755–766.

Brown, K.S. 1981. The biology of Heliconius and related genera. *Annu. Rev. Entomol.* **26**: 427–457.

Brumfield, R.T., Jernigan, R.W., Mcdonald, D.B. & Braun, M.J. 2001. Evolutionary Implications of Divergent Clines in an Avian (Manacus: Aves) Hybrid Zone. *Evolution.* **55**: 2070–2087.

Burg, S.L. & Parnell, A.J. 2018. Self-assembling structural colour in nature. *J. Phys. Condens. Matter* **30**: 413001.

Burke, M.K., Dunham, J.P., Shahrestani, P., Thornton, K.R., Rose, M.R. & Long, A.D. 2010. Genome-wide analysis of a long-term evolution experiment with Drosophila. *Nature* **467**: 587–590.

Burke, M.K., Liti, G. & Long, A.D. 2014. Standing genetic variation drives repeatable experimental evolution in outcrossing populations of saccharomyces cerevisiae. *Mol. Biol. Evol.* **31**: 3228–3239.

Cain, A.J. & Sheppard, P.M. 1954. Natural Selection in *Cepaea*. *Genetics* **39**: 89–116.

Catchen, J.M., Hohenlohe, P.A., Bernatchez, L., Funk, W.C., Andrews, K.R. & Allendorf, F.W. 2017. Unbroken: RADseq remains a powerful tool for understanding the genetics of adaptation in natural populations. *Mol. Ecol. Resour.* **17**: 362–365.

Challis, R.J., Kumar, S., Dasmahapatra, K.K., Jiggins, C.D. & Blaxter, M. 2016. Lepbase: The Lepidopteran genome database. *bioRxiv* 056994.

Chan, Y.F., Marks, M.E., Jones, F.C., Villarreal, G., Shapiro, M.D., Brady, S.D., *et al.* 2010. Adaptive evolution of pelvic reduction in sticklebacks by recurrent deletion of a Pitx1 enhancer. *Science.* **327**: 302–5.

Charlesworth, B., Lande, R. & Slatkin, M. 1982. A Neo-Darwinian Commentary on Macroevolution. *Evolution.* **36**: 474.

Chaves, J.A., Cooper, E.A., Hendry, A.P., Podos, J., De Leon, L.F., Raeymaekers, J.A.M., *et al.* 2016. Genomic variation at the tips of the adaptive radiation of Darwin's finches. *Mol. Ecol.* **25**: 5282–5295.

Chen, G.-B., Lee, S., Zhu, Z.-X., Benyamin, B. & Robinson, M. 2016. EigenGWAS: finding loci under selection through genome-wide association studies of eigenvectors in structured populations. *Heredity.* **117**: 51–61.

Christin, P.-A., Weinreich, D.M. & Besnard, G. 2010. Causes and evolutionary significance of genetic convergence. *Trends Genet.* **26**: 400–405.

Clarke, C.A. & Sheppard, P.M. 1962. The Genetics of the Mimetic Butterfly Papilio Glaucus. *Ecol. Soc. Am.* **43**: 159–161.

Clarke, C.A. & Sheppard, P.M. 1972. The Genetics of the Mimetic Butterfly Papilio polytes L . *Philos. Trans. R. Soc. B Biol. Sci.* **263**: 431–458.

Colombo, M., Diepeveen, E.T., Muschick, M., Santos, M.E., Indermaur, A., Boileau, N., *et al.* 2013. The ecological and genetic basis of convergent thick-lipped phenotypes in cichlid fishes. *Mol. Ecol.* **22**: 670–84.

Colosimo, P.F., Hosemann, K.E., Balabhadra, S., Jr, G.V., Dickson, M., Grimwood, J., *et al.* 2005. Widespread Parallel Evolution in Sticklebacks by Repeated Fixation of Ectodysplasin Alleles. *Science.* **307**: 1928–1933.

Conte, G.L., Arnegard, M.E., Peichel, C.L. & Schluter, D. 2012. The probability of genetic parallelism and convergence in natural populations. *Proc. Biol. Sci.* **279**: 5039–47.

Conway Morris, S. 2003. *Life's solution: inevitable humans in a lonely universe*. Cambridge University Press, Cambridge, UK.

Counterman, B.A., Araujo-Perez, F., Hines, H.M., Baxter, S.W., Morrison, C.M., Lindstrom, D.P., *et al.* 2010. Genomic hotspots for adaptation: The population genetics of Müllerian mimicry in Heliconius erato. *PLoS Genet.* **6**.

Coyne, J.A. & Orr, H.A. 2004. *Speciation*. Sinauer Associates, Inc, Sunderland, MA.

Darwin, C. 1859. *The Origin of Species by Means of Natural Selection, Or The Preservation of Favoured Races in the Struggle for Life*. Modern Library, New York.

Davey, J.W., Chouteau, M., Barker, S.L., Maroja, L., Baxter, S.W., Simpson, F., *et al.* 2016. Major Improvements to the Heliconius melpomene Genome Assembly Used to Confirm 10 Chromosome Fusion Events in 6 Million Years of Butterfly Evolution. *G3 GENES, GENOMES, Genet.* **6**: 695–708.

Dell'aglio, D.D., Stevens, M. & Jiggins, C.D. 2016. Avoidance of an aposematically coloured butterfly by wild birds in a tropical forest. *Ecol. Entomol.* **41**: 627–632.

Dembeck, L.M., Huang, W., Magwire, M.M., Lawrence, F., Lyman, R.F. & Mackay, T.F.C. 2015. Genetic Architecture of Abdominal Pigmentation in Drosophila melanogaster. *PLoS Genet.* **11**: 1–22.

Derryberry, E.P., Derryberry, G.E., Maley, J.M. & Brumfield, R.T. 2013. Hzar: Hybrid zone analysis using an R software package. *Mol. Ecol. Resour.* **14**: 652–663.

Devlin, B. & Roeder, K. 1999. Genomic Control for Association Studies. *Biometrics* **55**: 997–1004.

Dobzhansky, T. 1937. *Genetics and the Origin of Species*. Columbia University Press, New York.

Doucet, S.M. & Meadows, M.G. 2009. Iridescence: a functional perspective. *J. R. Soc. Interface* **6**: S115–S132.

Douglas, J.M., Cronin, T.W., Chiou, T.-H. & Dominy, N.J. 2007. Light habitats and the role of polarized iridescence in the sensory ecology of neotropical nymphalid butterflies (Lepidoptera: Nymphalidae). *J. Exp. Biol.* **210**: 788–799.

Eizirik, E., Yuhki, N., Johnson, W.E., Menotti-Raymond, M., Hannah, S.S. & O'Brien, S.J. 2003. Molecular genetics and evolution of melanism in the cat family. *Curr. Biol.* **13**: 448–453.

Elmer, K.R., Fan, S., Kusche, H., Luise Spreitzer, M., Kautt, A.F., Franchini, P., *et al.* 2014. Parallel evolution of Nicaraguan crater lake cichlid fishes via non-parallel routes. *Nat. Commun.* **5**: 1–8.

Enciso-Romero, J., Pardo-Díaz, C., Martin, S.H., Arias, C.F., Linares, M., Mcmillan, W.O., *et al.* 2017. Evolution of novel mimicry rings facilitated by adaptive introgression in tropical butterflies. *Mol. Ecol.* **26**: 5160–5172.

Endler, J.A. 1977. *Geographic variation, speciation, and clines*. Princeton University Press, Princeton, New Jersey.

Endler, J.A. 1983. Natural and sexual selection on color patterns in poeciliid fishes. *Environ. Biol. Fishes* **9**: 173–190.

Fabricant, S.A., Exnerová, A., Ježová, D. & Štys, P. 2014. Scared by shiny? The value of iridescence in aposematic signalling of the hibiscus harlequin bug. *Anim. Behav.* **90**: 315–325.

Filatov, D.A., Osborne, O.G. & Papadopulos, A.S.T. 2016. Demographic history of speciation in a Senecio altitudinal hybrid zone on Mt. Etna. *Mol. Ecol.* **25**: 2467–2481.

Fisher, R.A. 1930. *The genetical theory of natural selection*. Oxford University Press, Oxford.

Fisher, R.A. 1919. XV.—The Correlation between Relatives on the Supposition of Mendelian Inheritance. *Trans. R. Soc. Edinburgh* **52**: 399–433. Royal Society of Edinburgh Scotland Foundation.

Flaxman, S.M., Wacholder, A.C., Feder, J.L. & Nosil, P. 2014. Theoretical models of the influence of genomic architecture on the dynamics of speciation. *Mol. Ecol.* **23**: 4074–4088.

Ford, E.B. 1977. *Ecological Genetics*. Springer, Dordrecht.

Fox, C.W., Wagner, J.D., Cline, S., Thomas, F.A. & Messina, F.J. 2009. Genetic architecture underlying convergent evolution of egg-laying behavior in a seed-feeding beetle. *Genetica* **136**: 179–87.

Fraser, B.A., Künstner, A., Reznick, D.N., Dreyer, C. & Weigel, D. 2015. Population genomics of natural and experimental populations of guppies (Poecilia reticulata). *Mol. Ecol.* **24**: 389–408.

Gao, X., Becker, L.C., Becker, D.M., Starmer, J.D. & Province, M.A. 2010. Avoiding the high

bonferroni penalty in genome-wide association studies. *Genet. Epidemiol.* **34**: 100–105.

Gautier, M., Gharbi, K., Cezard, T., Foucaud, J., Kerdelhué, C., Pudlo, P., *et al.* 2013. The effect of RAD allele dropout on the estimation of genetic variation within and between populations. *Mol. Ecol.* **22**: 3165–3178.

Gay, L., Crochet, P. a., Bell, D. a. & Lenormand, T. 2008. Comparing clines on molecular and phenotypic traits in hybrid zones: A window on tension zone models. *Evolution.* **62**: 2789–2806.

Gompel, N. & Prud'homme, B. 2009. The causes of repeated genetic evolution. *Dev. Biol.* **332**: 36–47.

Gompert, Z., Fordyce, J.A., Forister, M.L., Shapiro, A.M. & Nice, C.C. 2006. Homoploid hybrid speciation in an extreme habitat. *Science.* **314**: 1923–1925.

Gompert, Z., Mandeville, E.G. & Buerkle, C.A. 2017. Analysis of Population Genomic Data from Hybrid Zones. *Annu. Rev. Ecol. Evol. Syst.* **48**: 207–229.

Gould, S.J. & Lewontin, R.C. 1979. The spandrels of San Marco and the Panglossian paradigrn : a critique of the adaptationist prograrnrne. *Proc. R. Soc. B Biol. Sci.* **205**: 581–598.

Griswold, C.K. 2006. Gene flow's effect on the genetic architecture of a local adaptation and its consequences for QTL analyses. *Heredity.* **96**: 445–453.

Hadfield, J.D., Nutall, A., Osorio, D. & Owens, I.P.F. 2007. Testing the phenotypic gambit: Phenotypic, genetic and environmental correlations of colour. *J. Evol. Biol.* **20**: 549–557.

Hadley, N.F., Savill, A. & Schultz, T.D. 1992. Coloration and its thermal consequences in the New Zealand tiger beetle Neocicindela perhispida. *J. Therm. Biol.* **17**: 55–61.

Härer, A., Meyer, A. & Torres-Dowdall, J. 2018. Convergent phenotypic evolution of the visual system via different molecular routes: How Neotropical cichlid fishes adapt to novel light environments. *Evol. Lett.* **2**:341-354.

Hastings, W.K. 1970. Monte Carlo Sampling Methods Using Markov Chains and Their Applications on. *Biometrika* **57**: 97–109.

Hoekstra, H.E. 2006. Genetics, development and evolution of adaptive pigmentation in vertebrates. *Heredity.* **97**: 222–234.

Hoekstra, H.E., Hirschmann, R.J., Bundey, R.A., Insel, P.A. & Crossland, J.P. 2006. A single amino acid mutation contributes to adaptive beach mouse color pattern. *Science.* **313**: 101–4.

Hoekstra, H.E. & Nachman, M.W. 2003. Different genes underlie adaptive melanism in different populations of rock pocket mice. *Mol. Ecol.* **12**: 1185–1194.

Huber, B., Whibley, A., Poul, Y.L., Navarro, N., Martin, A., Baxter, S., *et al.* 2015. Conservatism and novelty in the genetic architecture of adaptation in Heliconius butterflies. *Heredity.* **114**: 515–524.

Hudson, R.R., Slatkin, M. & Maddison, W.P. 1992. Estimation of levels of gene flow from DNA sequence data. *Genetics* **132**: 583–589.

Hunt, S., Cuthill, I.C., Bennett, A.T.D. & Griffiths, R. 1999. Preferences for ultraviolet partners in the blue tit. *Anim. Behav.* **58**: 809–815.

Ito, K., Katsuma, S., Kuwazaki, S., Jouraku, A., Fujimoto, T., Sahara, K., *et al.* 2016. Mapping and recombination analysis of two moth colour mutations, Black moth and Wild wing spot, in the silkworm Bombyx mori. *Heredity.* **116**: 52–59.

Jiggins, C.D. 2008. Ecological Speciation in Mimetic Butterflies. *Bioscience* **58**: 541.

Johnston, S.E., McEwan, J.C., Pickering, N.K., Kijas, J.W., Beraldi, D., Pilkington, J.G., *et al.* 2011. Genome-wide association mapping identifies the genetic basis of discrete and quantitative variation in sexual weaponry in a wild sheep population. *Mol. Ecol.* **20**: 2555–2566.

Jones, J.S., Leith, B.H. & Rawlings, P. 1977. Polymorphism in Cepaea: A Problem with Too Many Solutions? *Annu. Rev. Ecol. Syst.* **8**: 109–143.

Jones, R.T., Salazar, P.A., Ffrench-Constant, R.H., Jiggins, C.D. & Joron, M. 2012. Evolution of a mimicry supergene from a multilocus architecture. *Proc. R. Soc. B Biol. Sci.* **279**: 316–325.

Joron, M., Frezal, L., Jones, R.T., Chamberlain, N.L., Lee, S.F., Haag, C.R., *et al.* 2011. Chromosomal rearrangements maintain a polymorphic supergene controlling butterfly mimicry. *Nature* **477**: 203–206.

Joron, M., Papa, R., Beltrán, M., Chamberlain, N., Mavárez, J., Baxter, S., *et al.* 2006. A conserved supergene locus controls colour pattern diversity in Heliconius butterflies. *PLoS Biol.* **4**: 1831–1840.

Kapan, D.D. 2001. Three-butterfly system provides a field test of mullerian mimicry. *Nature* **409**: 338–340.

Kardos, M., Husby, A., Mcfarlane, S.E., Qvarnström, A. & Ellegren, H. 2016. Whole-genome resequencing of extreme phenotypes in collared flycatchers highlights the difficulty of detecting quantitative trait loci in natural populations. *Mol. Ecol. Resour.* **16**: 727–741.

Kemp, D.J. 2007. Female butterflies prefer males bearing bright iridescent ornamentation. *Proc. R. Soc. B Biol. Sci.* **274**: 1043–1047.

Kemp, D.J. & Rutowski, R.L. 2007. Condition dependence, quantitative genetics, and the potential signal content of iridescent ultraviolet butterfly coloration. *Evolution.* **61**: 168–183.

Kemp, D.J., Vukusic, P. & Rutowski, R.L. 2006. Stress-mediated covariance between nano-structural architecture and ultraviolet butterfly coloration. *Funct. Ecol.* **20**: 282–289.

Kettlewell, H.B.D. 1955. Selection experiments on industrial melanism in the Lepidoptera. *Heredity.* **9**: 323–342.

Keyser, A.J. & Hill, G.E. 1999. Condition-dependent variation in the blue-ultraviolet coloration of a structurally based plumage ornament. *Proc. R. Soc. B Biol. Sci.* **266**: 771–777.

Korneliussen, T.S., Albrechtsen, A. & Nielsen, R. 2014. ANGSD: Analysis of Next Generation Sequencing Data. *BMC Bioinformatics* **15**: 356.

Kozak, K.M., Wahlberg, N., Neild, A.F.E., Dasmahapatra, K.K., Mallet, J. & Jiggins, C.D. 2015. Multilocus Species Trees Show the Recent Adaptive Radiation of the Mimetic Heliconius Butterflies. *Syst. Biol.* **64**: 505–524.

Kronforst, M.R., Young, L.G., Kapan, D.D., Mcneely, C., Neill, R.J.O. & Gilbert, L.E. 2006. Linkage of butterfly mate preference and wing color preference cue at the genomic location of wingless. *Proc. Natl. Acad. Sci.* **103**: 6575–6580.

Kruuk, L.E.B., Baird, S.J.E., Gale, K.S. & Barton, N.H. 1999. A Comparison of Multilocus Clines Maintained by Environmental Adaptation or by Selection Against Hybrids. *Genetics* **153**: 1959–1971.

Kunte, K., Zhang, W., Tenger-Trolander, A., Palmer, D.H., Martin, A., Reed, R.D., *et al.* 2014. Doublesex is a mimicry supergene. *Nature* **507**: 229–232.

Küpper, C., Stocks, M., Risse, J.E., Dos Remedios, N., Farrell, L.L., McRae, S.B., *et al.* 2015. A supergene determines highly divergent male reproductive morphs in the ruff. *Nat. Genet.* **48**: 79–83.

Langham, G.M. 2004. Specialized Avian Predators Repeatedly Attack Novel Color Morphs of Heliconius Butterflies. *Evolution.* **58**: 2783–2787.

Lango Allen, H., Estrada, K., Lettre, G., Berndt, S.I., Weedon, M.N., Rivadeneira, F., *et al.* 2010. Hundreds of variants clustered in genomic loci and biological pathways affect human height. *Nature* **467**: 832–838.

Le Corre, V. & Kremer, A. 2012. The genetic differentiation at quantitative trait loci under local adaptation. *Mol. Ecol.* **21**: 1548–1566.

Le Poul, Y., Whibley, A., Chouteau, M., Prunier, F., Llaurens, V. & Joron, M. 2014. Evolution of dominance mechanisms at a butterfly mimicry supergene. *Nat. Commun.* **5**: 1–8.

Lee, K.M. & Coop, G. 2018. Distinguishing Among Modes of Convergent Adaptation Using Population Genomic Data. *Genetics* **207**: 1591–1619.

Lenski, R.E. 2017. Convergence and Divergence in a Long-Term Experiment with Bacteria. *Am. Nat.* **190**: S57–S68.

Li, H. 2011. A statistical framework for SNP calling, mutation discovery, association mapping and population genetical parameter estimation from sequencing data. *Bioinformatics* **27**: 2987–2993.

Linnen, C., Poh, Y., Peterson, B., Barrett, R., Larson, J., Jensen, J., *et al.* 2013. Adaptive Evolution of Multiple Traits Through Multiple Mutations at a Single Gene. *Science.* **339**: 1312–1316.

Liu, F., van Duijn, K., Vingerling, J.R., Hofman, A., Uitterlinden, A.G., Janssens, A.C.J.W., *et al.* 2009. Eye color and the prediction of complex phenotypes from genotypes. *Curr. Biol.* **19**: 192–193.

Long, A., Liti, G., Luptak, A. & Tenaillon, O. 2015. Elucidating the molecular architecture of adaptation via evolve and resequence experiments. *Nat. Rev. Genet.* **16**: 567–582.

Losos, J.B. 2011. Convergence, adaptation, and constraint. *Evolution.* **65**: 1827–40.

Lowry, D.B., Hoban, S., Kelley, J.L., Lotterhos, K.E., Reed, L.K., Antolin, M.F., *et al.* 2017. Breaking RAD: an evaluation of the utility of restriction site-associated DNA sequencing for genome scans of adaptation. *Mol. Ecol. Resour.* **17**: 142–152.

MacKay, T.F.C., Stone, E.A. & Ayroles, J.F. 2009. The genetics of quantitative traits: Challenges and prospects. *Nat. Rev. Genet.* **10**: 565–577.

Mallet, J. 1986. Hybrid zones of Heliconius butterflies in Panama and the stability and movement of warning colour clines. *Heredity.* **56**: 191–202.

Mallet, J. 1993. Speciation, raciation, and color pattern evolution in Heliconius butterflies: evidence from hybrid zones. In: *Hybrid zones and the evolutionary process* (R. G. Harrison, ed), pp. 226–260. Oxford University Press, New York.

Mallet, J., Barton, N., Gerardo Lamas, M., Jose Santisteban, C., Manuel Muedas, M. & Eeley, H. 1990. Estimates of selection and gene flow from measures of cline width and linkage disequilibrium in Heliconius hybrid zones. *Genetics* **124**: 921–936.

Mallet, J. & Barton, N.H. 1989. Strong Natural Selection in a Warning-Color Hybrid Zone. *Evoution* **43**: 421–431.

Manceau, M., Domingues, V.S., Mallarino, R. & Hoekstra, H.E. 2011. The Developmental Role

of Agouti in Color Pattern Evolution. *Science.* **331**: 1062–1065.

Marques, D.A., Lucek, K., Haesler, M.P., Feller, A.F., Meier, J.I., Wagner, C.E., *et al.* 2017. Genomic landscape of early ecological speciation initiated by selection on nuptial colour. *Mol. Ecol.* **26**: 7–24.

Martin, A., McCulloch, K.J., Patel, N.H., Briscoe, A.D., Gilbert, L.E. & Reed, R.D. 2014. Multiple recent co-options of Optix associated with novel traits in adaptive butterfly wing radiations. *EvoDevo* **5**: 7.

Martin, A. & Orgogozo, V. 2013. The Loci of repeated evolution: a catalog of genetic hotspots of phenotypic variation. *Evolution.* **67**: 1235–50.

Martin, A., Papa, R., Nadeau, N.J., Hill, R.I., Counterman, B.A., Halder, G., *et al.* 2012. Diversification of complex butterfly wing patterns by repeated regulatory evolution of a Wnt ligand. *Proc. Natl. Acad. Sci.* **109**: 12632–12637.

Martin, S.H., Dasmahapatra, K.K., Nadeau, N.J., Slazar, C., Walters, J.R., Simpson, F., *et al.* 2013. Genome-wide evidence for speciation with gene flow in Heliconius butterflies. *Genome Res.* **23**: 1817–1828.

Mayr, E. 1982. *The growth of biological thought: Diversity, evolution, and inheritance*. Harvard University Press, Cambridge, Massachusetts.

Medina, J.M., Díaz, J.A. & Vukusic, P. 2015. Classification of peacock feather reflectance using principal component analysis similarity factors from multispectral imaging data. *Opt. Express* **23**: 10198.

Meisner, J. & Albrechtsen, A. 2018. Inferring Population Structure and Admixture Proportions in Low Depth Next-Generation Sequencing Data. *bioRxiv* 302463.

Merrill, R.M., Chia, A. & Nadeau, N.J. 2014. Divergent warning patterns contribute to assortative mating between incipient Heliconius species. *Ecol. Evol.* **4**: 911–917.

Merrill, R.M., Dasmahapatra, K.K., Davey, J.W., Dell'Aglio, D.D., Hanly, J.J., Huber, B., *et al.* 2015. The diversification of *Heliconius* butterflies: what have we learned in 150 years? *J. Evol. Biol.* **28**: 1417–1438.

Merrill, R.M., Wallbank, R.W.R., Bull, V., Salazar, P.C.A., Mallet, J., Stevens, M., *et al.* 2012. Disruptive ecological selection on a mating cue. *Proc. R. Soc. B Biol. Sci.* **279**: 4907–4913.

Metropolis, N., Rosenbluth, A.W., Rosenbluth, M.N., Teller, A.H. & Teller, E. 1953. Equation of State Calculations by Fast Computing Machines. *J. Chem. Phys.* **21**: 1087–1092.

Meyer, W.K., Zhang, S., Hayakawa, S., Imai, H. & Przeworski, M. 2013. The convergent evolution of blue iris pigmentation in primates took distinct molecular paths. *Am. J. Phys. Anthropol.* **151**: 398–407.

Milano, E.R., Kenney, A.M. & Juenger, T.E. 2016. Adaptive differentiation in floral traits in the presence of high gene flow in scarlet gilia (Ipomopsis aggregata). *Mol. Ecol.* **25**: 5862–5875.

Moyroud, E., Wenzel, T., Middleton, R., Rudall, P.J., Banks, H., Reed, A., *et al.* 2017. Disorder in convergent floral nanostructures enhances signalling to bees. *Nature*, doi: 10.1038/nature24285.

Müller, F. 1879. Ituna and Thyridia: a remarkable case of mimicry in butterflies. *Trans. Entomol. Soc. London* 20–29.

Mundy, N.I. 2005. A window on the genetics of evolution: MC1R and plumage colouration in birds. *Proc. R. Soc. B Biol. Sci.* **272**: 1633–1640.

Mundy, N.I. 2009. Conservation and convergence of colour genetics: MC1R mutations in brown cavefish. *PLoS Genet.* **5**: 5–6.

Mundy, N.I., Badcock, N.S., Hart, T., Scribner, K., Janssen, K. & Nadeau, N.J. 2004. Conserved Genetic Basis of a Quantitative Plumage Trait Involved in Mate Choice. *Science.* **303**: 1870–1873.

Nachman, M.W., Hoekstra, H.E. & D'Agostino, S.L. 2003. The genetic basis of adaptive melanism in pocket mice. *Proc. Natl. Acad. Sci. U. S. A.* **100**: 5268–73.

Nadeau, N.J. 2016. Genes controlling mimetic colour pattern variation in butterflies. *Current Opinion in Insect Science* **17**:24-31.

Nadeau, N.J., Pardo-Diaz, C., Whibley, A., Supple, M.A., Saenko, S. V., Wallbank, R.W.R., *et al.* 2016. The gene cortex controls mimicry and crypsis in butterflies and moths. *Nature* **534**: 106–110.

Nadeau, N.J., Ruiz, M., Salazar, P., Counterman, B., Medina, J.A., Ortiz-Zuazaga, H., *et al.* 2014. Population genomics of parallel hybrid zones in the mimetic butterflies, H. melpomene and H. erato. *Genome Res.* **24**: 1316–1333.

Nadeau, N.J., Whibley, A., Jones, R.T., Davey, J.W., Dasmahapatra, K.K., Baxter, S.W., *et al.* 2012. Genomic islands of divergence in hybridizing Heliconius butterflies identified by large-scale targeted sequencing. *Philos. Trans. R. Soc. B Biol. Sci.* **367**: 343–353.

Nokelainen, O., Hegna, R.H., Reudler, J.H., Lindstedt, C. & Mappes, J. 2012. Trade-off between warning signal efficacy and mating success in the wood tiger moth. *Proc. R. Soc. B Biol. Sci.* **279**: 257–265.

Orr, H.A. 2005. The genetic theory of adaptation: A brief history. *Nat. Rev. Genet.* **6**: 119–127.

Orr, H.A. 1998. The Population Genetics of Adaptation: The Distribution of Factors Fixed during Adaptive Evolution. *Evolution.* **52**: 935.

Pardo-Diaz, C., Salazar, C., Baxter, S.W., Merot, C., Figueiredo-Ready, W., Joron, M., *et al.* 2012. Adaptive introgression across species boundaries in Heliconius butterflies. *PLoS Genet.* **8**: e1002752.

Parnell, A.J., Bradford, J.E., Curran, E. V., Washington, A.L., Adams, G., Brien, M.N., *et al.* 2018. Wing scale ultrastructure underlying convergent and divergent iridescent colours in mimetic *Heliconius* butterflies. *J. R. Soc. Interface* **15**: 20170948.

Poelstra, J.W., Vijay, N., Bossu, C.M., Lantz, H., Ryll, B., Muller, I., *et al.* 2014. The genomic landscape underlying phenotypic integrity in the face of gene flow in crows. *Science.* **344**: 1410–1414.

Price, A.L., Patterson, N.J., Plenge, R.M., Weinblatt, M.E., Shadick, N. a & Reich, D. 2006. Principal components analysis corrects for stratification in genome-wide association studies. *Nat. Genet.* **38**: 904–909.

Protas, M.E., Hersey, C., Kochanek, D., Zhou, Y., Wilkens, H., Jeffery, W.R., *et al.* 2006. Genetic analysis of cavefish reveals molecular convergence in the evolution of albinism. *Nat. Genet.* **38**: 107–11.

Protas, M.E. & Patel, N.H. 2008. Evolution of Coloration Patterns. *Annu. Rev. Cell Dev. Biol.* **24**: 425–446.

Prud'homme, B., Gompel, N. & Carroll, S.B. 2007. Emerging principles of regulatory evolution. *Proc. Natl. Acad. Sci. U. S. A.* **104 Suppl**: 8605–12.

Reed, R.D., Papa, R., Martin, A., Hines, H.M., Counterman, B. a, Pardo-Diaz, C., *et al.* 2011. Optix Drives the Repeated Convergent Evolution of Butterfly Wing Pattern Mimicry.

Science. **333**: 1137–41.

Rockman, M. V. 2011. The QTN program and the alleles that matter for evolution: all that's gold does not glitter. *Evolution* **66**: 1–17.

Römpler, H., Rohland, N. & Lalueza-Fox, C. 2006. Nuclear gene indicates coat-color polymorphism in mammoths. *Science.* **313**: 62.

Rosenblum, E.B., Hoekstra, H.E. & Nachman, M.W. 2004. Adaptive Reptile Color Variation and the Evolution of the Mc1R Gene. *Evolution.* **58**: 1794.

Rosser, N., Dasmahapatra, K.K. & Mallet, J. 2014. Stable Heliconius butterfly hybrid zones are correlated with a local rainfall peak at the edge of the Amazon basin. *Evolution.* **68**: 3470–3484.

Rosser, N., Phillimore, A.B., Huertas, B.C., Willmott, K.R. & Mallet, J. 2012. Testing historical explanations for gradients in species richness in heliconiine butterflies of tropical America. *Biol. J. Linn. Soc.* **105**: 479–497.

Roulin, A. 2004. The evolution, maintenance and adaptive function of genetic colour polymorphism in birds. *Biol. Rev. Camb. Philos. Soc.* **79**: 815–848.

Salazar, P.A. 2012. Hybridization and the genetics of wing colour-pattern diversity in Heliconius butterflies. PhD thesis. University of Cambridge.

San-Jose, L.M. & Roulin, A. 2017. Genomics of coloration in natural animal populations. *Philos. Trans. R. Soc. B Biol. Sci.* **372**: 20160337.

Sandoval, C.P. 1994. Differential visual predation on morphs of *Timema cristinae* (Phasmatodeae:Timemidae) and its consequences for host range. *Biol. J. Linn. Soc.* **52**: 341–356.

Santos, J.C., Coloma, L.A. & Cannatella, D.C. 2003. Multiple, recurring origins of aposematism and diet specialization in poison frogs. *Proc. Natl. Acad. Sci.* **100**: 12792–12797.

Schluter, D. & Nagel, L.M. 1995. Parallel speciation by natural selection. *Am. Nat.* **146**: 292–301.

Scordato, E.S.C., Wilkins, M.R., Semenov, G., Rubtsov, A.S., Kane, N.C. & Safran, R.J. 2017. Genomic variation across two barn swallow hybrid zones reveals traits associated with divergence in sympatry and allopatry. *Mol. Ecol.* **26**: 5676–5691.

Seehausen, O., Butlin, R.K., Keller, I., Wagner, C.E., Boughman, J.W., Hohenlohe, P.A., *et al.* 2014. Genomics and the origin of species. *Nat. Rev. Genet.* **15**: 176–192.

Seehausen, O., Terai, Y., Magalhaes, I.S., Carleton, K.L., Mrosso, H.D.J., Miyagi, R., *et al.* 2008. Speciation through sensory drive in cichlid fish. *Nature* **455**: 620–626.

Shawkey, M.D. & Alba, L.D. 2017. Interactions between colour-producing mechanisms and their effects on the integumentary colour palette. *Philos. Trans. R. Soc. B Biol. Sci.* **372**.

Shawkey, M.D., Morehouse, N.I. & Vukusic, P. 2009. A protean palette: colour materials and mixing in birds and butterflies. *J. R. Soc. Interface* **6**: S221–S231.

Silberglied, R.E. 1984. Visual communication and sexual selection among butterflies. In: *The biology of butterflies* (R. I. Vane-Wright & P. E. Ackery, eds), pp. 207–223. Academic Press, London.

Slate, J. 2005. Quantitative trait locus mapping in natural populations: Progress, caveats and future directions. *Mol. Ecol.* **14**: 363–379.

Song, Y., Endepols, S., Klemann, N., Richter, D., Matuschka, F.R., Shih, C.H., *et al.* 2011. Adaptive introgression of anticoagulant rodent poison resistance by hybridization between

old world mice. *Curr. Biol.* **21**: 1296–1301.

Soria-Carrasco, V., Gompert, Z., Comeault, A. a, Farkas, T.E., Parchman, T.L., Johnston, J.S., *et al.* 2014. Stick insect genomes reveal natural selection's role in parallel speciation. *Science.* **344**: 738–42.

Soria-Carrasco, V. 2018. Delimitation of contiguous regions of differentiation using Hidden Markov Models. Github repository, https://github.com/visoca/popgenomworkshop-hmm

Srinivasarao, M. 1999. Nano-Optics in the Biological World: Beetles, Butterflies, Birds, and Moths. *Chem. Rev.* **99**: 1935–1962.

Stankowski, S., Sobel, J.M. & Streisfeld, M.A. 2015. The geography of divergence with gene flow facilitates multitrait adaptation and the evolution of pollinator isolation in Mimulus aurantiacus. *Evolution.* **69**: 3054–3068.

Stemshorn, K.C., Reed, F.A., Nolte, A.W. & Tautz, D. 2011. Rapid formation of distinct hybrid lineages after secondary contact of two fish species (Cottus sp.). *Mol. Ecol.* **20**: 1475–1491.

Stern, D.L. 2013. The genetic causes of convergent evolution. *Nat. Rev. Genet.* **14**: 751–64.

Storz, J.F. 2002. Contrasting patterns of divergence in quantitative traits and neural DNA markers: analysis in clinal variation. *Mol. Ecol.* **11**: 2537–2551.

Supple, M.A., Hines, H.M., Dasmahapatra, K.K., Lewis, J.J., Nielsen, D.M., Lavoie, C., *et al.* 2013. Genomic architecture of adaptive color pattern divergence and convergence in Heliconius butterflies. *Genome Res.* **23**: 1248–1257.

Sweeney, A., Jiggins, C. & Johnsen, S. 2003. Polarized light as a butterfly mating signal. *Nature* **423**: 31–32.

Szymura, J.M. & Barton, N.H.. 1986. Genetic Analysis of a Hybrid Zone Between the Fire-Bellied Toads, Bombina bombina and B. variegata, Near Cracow in Southern Poland. *Evolution* **40**: 1141–1159.

Szymura, J.M. & Barton, N.H. 1991. The genetic structure of the hybrid zone between the fire-bellied toads *Bombina bombina* and *B. variegata*: comparisons between transects and between loci. *Evolution.* **45**: 237–261.

Taylor, E.B., Boughman, J.W., Groenenboom, M., Sniatynski, M., Schluter, D. & Gow, J.L. 2006. Speciation in reverse: Morphological and genetic evidence of the collapse of a three-spined stickleback (Gasterosteus aculeatus) species pair. *Mol. Ecol.* **15**: 343–355.

The Heliconius Genome Consortium. 2012. Butterfly genome reveals promiscuous exchange of mimicry adaptations among species. *Nature* **487**: 94–8.

Theron, E., Hawkins, K., Bermingham, E., Ricklefs, R. & Mundy, N. 2001. The molecular basis of an avian plumage polymorphism in the wild: a point mutation in the melanocortin-1 receptor is perfectly associated with melanism in the bananaquit (Coereba flaveola). *Curr. Biol.* **11**: 550–557.

Thurber, C.S., Jia, M.H., Jia, Y. & Caicedo, A.L. 2013. Similar traits, different genes? Examining convergent evolution in related weedy rice populations. *Mol. Ecol.* **22**: 685–98.

Thurman, T.J. & Seymoure, B.M. 2016. A bird's eye view of two mimetic tropical butterflies: Coloration matches predator's sensitivity. *J. Zool.* **298**: 159–168.

Toews, D.P.L., Taylor, S.A., Vallender, R., Brelsford, A., Butcher, B.G., Messer, P.W., *et al.* 2016. Plumage Genes and Little Else Distinguish the Genomes of Hybridizing Warblers. *Curr. Biol.* **26**: 2313–2318.

Ungerer, M.C., Baird, S.J.E., Pan, J. & Rieseberg, L.H. 1998. Rapid hybrid speciation in wild sunflowers. *Proc. Natl. Acad. Sci.* **95**: 11757–11762.

Van't Hof, A.E., Edmonds, N., Dalíková, M., Marec, F. & Saccheri, I.J. 2011. Industrial melanism in british peppered moths has a singular and recent mutational origin. *Science.* **332**: 958–960.

Van Belleghem, S.M., Rastas, P., Papanicolaou, A., Martin, S.H., Arias, C.F., Supple, M.A., *et al.* 2017. Complex modular architecture around a simple toolkit of wing pattern genes. *Nat. Ecol. Evol.* **1**: 1–12.

Vines, T.H., Dalziel, A.C., Albert, A.Y.K., Veen, T., Schulte, P.M. & Schluter, D. 2016. Cline coupling and uncoupling in a stickleback hybrid zone. *Evolution.* **70**: 1023–1038.

Vukusic, P., Hallam, B. & Noyes, J. 2007. Brilliant whiteness in ultrathin beetle scales. *Science.* **315**: 348.

Vukusic, P., Sambles, J.R. & Lawrence, C.R. 2000. Colour mixing in wing scales of a butterfly. *Nature* **404**: 457.

Vukusic, P., Sambles, J.R., Lawrence, C.R. & Wootton, R.J. 1999. Quantified interference and diffraction in single Morpho butterfly scales. *Proc. R. Soc. B Biol. Sci.* **266**: 1403.

Wake, D. 1991. Homoplasy: the result of natural selection, or evidence of design limitations? *Am. Nat.* **138**: 543–567.

Waldron, S.J., Endler, J.A., Valkonen, J.K., Honma, A., Dobler, S. & Mappes, J. 2017. Experimental evidence suggests that specular reflectance and glossy appearance help amplify warning signals. *Sci. Rep.* **7**: 1–10.

Wasik, B.R., Liew, S.F., Lilien, D. a., Dinwiddie, a. J., Noh, H., Cao, H., *et al.* 2014. Artificial selection for structural color on butterfly wings and comparison with natural evolution. *Proc. Natl. Acad. Sci.* **111**: 12109–12114.

Weinreich, D.M., Delaney, N.F., DePristo, M.A. & Hartl, D.L. 2006. Darwinian Evolution Can Follow Only Very Few Mutational Paths to Fitter Proteins. *Science.* **312**: 111–114.

Westram, A.M., Rafajlović, M., Chaube, P., Faria, R., Larsson, T., Panova, M., *et al.* 2018. Clines on the seashore: The genomic architecture underlying rapid divergence in the face of gene flow. *Evol. Lett.* **2**: 297–309.

Whitlock, M.C. & Schluter, D. 2009. *The Analysis of Biological Data*. Roberts and Company Publishers, Greenwood Village, Colorado.

Wilts, B.D., Sheng, X., Holler, M., Diaz, A., Guizar-Sicairos, M., Raabe, J., *et al.* 2018. Evolutionary-Optimized Photonic Network Structure in White Beetle Wing Scales. *Adv. Mater.* **30**: 1–6.

Wilts, B.D., Vey, A.J.M., Briscoe, A.D. & Stavenga, D.G. 2017. Longwing (Heliconius) butterflies combine a restricted set of pigmentary and structural coloration mechanisms. *BMC Evol. Biol.* **17**: 226.

Wittkopp, P.J., Carroll, S.B. & Kopp, A. 2003. Evolution in black and white: Genetic control of pigment patterns in Drosophila. *Trends Genet.* **19**: 495–504.

Wu, C.I. 2001. The genic view of the process of speciation. *J. Evol. Biol.* **14**: 851–865.

Yeaman, S. & Whitlock, M.C. 2011. The genetic architecture of adaptation under migration-selection balance. *Evolution.* **65**: 1897–1911.

Zhang, L., Mazo-Vargas, A. & Reed, R.D. 2017. Single master regulatory gene coordinates the evolution and development of butterfly color and iridescence. *Proc. Natl. Acad. Sci.* **114**:

201709058.

Zhen, Y., Aardema, M.L., Medina, E.M., Schumer, M. & Andolfatto, P. 2012. Parallel molecular evolution in an herbivore community. *Science*. **337**: 1634–1637.

Zhou, X., Carbonetto, P. & Stephens, M. 2013. Polygenic Modeling with Bayesian Sparse Linear Mixed Models. *PLoS Genet.* **9**.

Zi, J., Yu, X., Li, Y., Hu, X., Xu, C., Wang, X., *et al.* 2003. Coloration strategies in peacock feathers. *Proc. Natl. Acad. Sci.* **100**: 12576–12578.

Appendix 1

Manuscript as submitted to the journal Interface Focus

Phenotypic variation in *Heliconius erato* crosses shows iridescent structural colour is sex-linked and controlled by multiple genes

Melanie N. Brien[1], Juan Enciso Romero[1,2], Andrew J. Parnell[3], Patricio A. Salazar[1,4], Carlos Morochz[5], Darwin Chalá[5], Hannah E. Bainbridge[1], Thomas Zinn[6], Emma V. Curran[1], Nicola J. Nadeau[1]

[1]Department of Animal and Plant Sciences, The University of Sheffield, Alfred Denny Building, Western Bank, Sheffield, S10 2TN, United Kingdom;

[2]Biology Program, Faculty of Natural Sciences and Mathematics, Universidad del Rosario, Bogota, Colombia;

[3]Department of Physics and Astronomy, The University of Sheffield, Hicks Building, Hounsfield Road, Sheffield, S3 7RH, United Kingdom;

[4]Centro de Investigación en Biodiversidad y Cambio Climático (BioCamb), Universidad Tecnológica Indoamérica, Quito, Ecuador;

[5]Mashpi Reserve, Ecuador;

[6]ESRF - The European Synchrotron, 38043, Grenoble Cedex 9, France.

Corresponding authors: Melanie Brien (mnbrien1@sheffield.ac.uk), Nicola Nadeau (n.nadeau@sheffield.ac.uk)

Abstract

Bright, highly reflective iridescent colours can be seen across nature and are produced by the scattering of light from nanostructures. *Heliconius* butterflies have been widely studied for their diversity and mimicry of wing colour patterns. Despite iridescence evolving multiple times in this genus, little is known about the genetic basis of the colour and the development of the structures which produce it. *Heliconius erato* can be found across Central and South America, but only races found in Western Ecuador and Colombia have developed blue iridescent colour. Here, we use crosses between iridescent and non-iridescent races of *H. erato* to study phenotypic variation in the resulting F2 generation. Using measurements of blue colour from photographs, we find that iridescent structural colour is a quantitative trait controlled by multiple genes, with strong evidence for loci on the Z sex chromosome. Iridescence is not linked to the Mendelian colour pattern locus that also segregates in these crosses (controlled by the gene *cortex*). Small angle X-ray scattering data shows that spacing between longitudinal ridges on the scales, which affects the intensity of the blue reflectance, also varies quantitatively in F2 crosses.

Keywords

Structural colour, *Heliconius*, butterflies, iridescence, evolution, quantitative genetics

1. Introduction

Structural colours are bright and highly reflective colours produced by the interaction of light with nanostructures. They can be seen across a range of taxa, including fish, birds, molluscs and insects, and have numerous functions covering visual communication and recognition, mate choice and thermoregulation [1–3]. Despite this, little is known about the genetic basis of structural colour, or how genetic variation translates into developmental differences of the nanostructures.

Examples of the different ways structural colour is produced can be seen across butterfly species. Multilayer reflectors produce the bright blue colour in *Morpho* butterflies [4], while *Callophrys rubi* have a highly connected gyroid structure contained within the upper and lower lamina [5]. scales on butterfly wings are formed as a long, flattened extension of the cuticle. Generally, they are composed of longitudinal ridges which are linked transversely by cross-ribs (Figure 1). These nanostructures make up a variety of repeating elements which can vary in thickness and patterning, producing different effects. F-actin filaments are important in the development of wing scale cells, and appear to pre-pattern where the ridges will form [6].

The neotropical *Heliconius* butterflies (Nymphalidae) are well-known for the diversity in their wing colour patterns and mimicry between species [7]. Many of these colour patterns are formed by chemical pigments, but several species also exhibit iridescent colour, an angle-dependent, structurally produced blue reflectance. *Heliconius* butterflies can produce iridescent colour by thin film interference using different features on their scales. Longwing *H. doris,* for example, display hindwing colour reflected by their lower lamina; the resulting colour can be blue or green depending on the absence or presence of the yellow pigment 3-OH-kynurenine [8]. Several other species, including *Heliconius erato,* produce iridescent colours using layered lamellae that make up their scale ridges; density of the ridges, the curvature and layering of the lamellae affect the intensity of the structural colour, with denser ridge spacing producing higher reflectance. Brightness and wavelength of peak reflectance change with angle [9].

Heliconius erato is found across Central and South America and has evolved more than 25 races with a diversity of colour patterns. These aposematic patterns are mimetic with *Heliconius melpomene* and are an example of Müllerian mimicry. Variation in pigment colour patterns have been found to map to a handful of loci that control a diversity of patterns in several distantly related species [10–13]. Despite iridescent colour evolving multiple times in *Heliconius*, the genetics of this trait have not been studied to the same extent as pigment colour patterns, likely due to the difficulty of measuring the trait. Iridescent *H. erato cyrbia* is found on the Western slopes of the Andes in Ecuador. *H. erato* races found further north in Panama lack this structural colour, and hybrid zones arise between the iridescent and non-iridescent races, where

populations with intermediate levels of iridescence can be found. Previous researchers have noted that levels of iridescence vary in F2 hybrid crosses and appear to do so in a continuous manner [12,14] but have not attempted to quantify the variation. Continuous variation in the F2 would suggest that the trait is controlled by multiple loci and therefore not controlled by the "tool kit" of major effect loci that regulate pigment colour patterns. The genes controlling variation in iridescence may perhaps be those directly controlling the formation of scale structure.

Experimental genetic crosses can be used to estimate the number of genes involved in controlling a trait by investigating the distribution of the phenotype across segregating generations [15]. Traits that are controlled by a single locus of major effect will segregate according to Mendelian ratios, with 50-100% of individuals in the F2 generation having phenotypes the same as one or other of their parents (depending on dominance of the alleles). The more individuals there are with intermediate phenotypes, the more loci are likely to be involved, as a greater number of allele combinations will be possible. We can also estimate positions of loci in the genome by looking for links to known loci which control other phenotypes, and by looking for patterns of sex linkage.

Here, we aim to determine whether iridescence in *Heliconius erato* is a quantitative trait controlled by multiple genes, and if any of these genes are sex-linked or linked to known colour pattern loci, by looking at the segregation of the trait in F2 crosses between different races. *H. erato demophoon* from Panama is black with red and yellow bands. This race was crossed to *H. erato cyrbia* from Ecuador, which has a similar colour pattern but has an iridescent blue colour instead of being matt black (Figure 2). The only major colour pattern differences between these races are the white margin on the hindwing of *H. erato cyrbia* and the yellow bar on the dorsal hindwing of *H. erato demophoon.* Based on previous crosses, these are likely to be controlled by alternative alleles of the *Cr* locus on linkage group 15, which is homologous to three tightly linked loci (*Yb*, *Sb* and *N*) in *H. melpomene* [10], and corresponds to the gene *cortex* [16]. A gene found on chromosome 10, *WntA*, controls various colour pattern characteristics by determining the size and shape of black pattern elements which in turn affect the appearance of the red, yellow and white areas [17,18]. Differences in the size and position of the red forewing band between *cyrbia* and *demophoon* are due to variation around this locus. We also use small angle X-ray scattering (SAXS) to quantify ridge spacing in broods. As several aspects of scale morphology are known to vary between the iridescent and non-iridescent races [9] it is possible that apparent continuous variation in the reflectance in the F2 could be due to independent segregation of these different features, each of which may be controlled by a major effect gene. Therefore, we also test whether ridge spacing shows continuous variation in the F2 generation.

2. Methods

2.1 Crossing Experiments

Experimental crosses were performed between geographical races of *Heliconius erato* at the insectary in Mashpi Reserve, Ecuador, over a period of 2 years. *H. erato demophoon* was collected from Gamboa, Panama (9.12° N, 79.67° W) in May 2014, then transported to Mashpi, Ecuador (0.17° N, 78.87° W), where they were kept as stocks. Iridescent *H. erato cyrbia* were collected from the area around Mashpi. *H. e. demophoon* were crossed with *H. e. cyrbia*, and the F1 generation crossed together, along with the addition of 2 backcrosses (BC) between the F1 and *cyrbia* (Figure 2). Crosses were reciprocal, so that in roughly half of the first generation crosses the female was the iridescent race and the male non-iridescent, and vice versa. In line with previous studies with intraspecific *Heliconius* hybrids [12,19], races readily hybridised and we did not observe any evidence of hybrid inviability or differing success between the reciprocal crosses. *Passiflora* species were provided as larval food plants and for oviposition, and butterflies were given *Lantana camara* and other locally collected flowers, plus sugar solution (10%) and pollen to feed. The bodies of the parents and offspring were preserved in NaCl saturated 20% dimethyl sulfoxide (DMSO) 0.25M EDTA solution to preserve the DNA, and the wings stored separately in glassine envelopes. A total of 302 individuals obtained from 14 crosses were used in the analysis (Table 1).

2.2 Phenotypic Colour Analysis

All butterfly wings were photographed flat under standard lighting conditions using a mounted Nikon D7000 DSLR camera with a 40mm f/2.8 lens set to an aperture of f/10, shutter speed of 1/60 and ISO of 100. Lights were mounted at a fixed angle of 45 degrees to maximise the observed blue reflection from the iridescent wing regions. All photographs also included an X-Rite Colour Checker to help standardise the colour of the images. RAW format images were standardised using the levels tool in Adobe Photoshop CS2 (Version 9.0). Using the colour histogram plugin in ImageJ [20,21], red-green-blue (RGB) values were recorded from 2 sections of the wings and averaged (Figure 3). These areas were chosen because the scales on these sections of the wings close to the body tended to be the least damaged and worn, so a more accurate measurement of the colour could be taken, and the wing venation was used as a marker to allow the same areas to be measured each time.

Blue reflection from the iridescent wing regions was measured as variation in blue-red (BR) colour. This was calculated as (B-R)/(B+R), with -1 being completely red and 1 being completely blue. The level of UV reflectance could not be measured from our photographs. Previous spectral measurements of the wing reflectance show that peak reflectance for *H. erato cyrbia* is just below the visible range at about 360-370nm, with much of the reflectance being

within the human visible range, while *H. erato demophoon* reflects very little but tends to show highest reflectance in the red-infrared range [9]. Therefore, the colour values will allow variation in colour and reflectance to be measured but will not represent butterfly visual systems. Repeatability of the colour measurements was tested using the repeatability equation of Whitlock and Schluter [22] by taking 5 measurements each on 5 randomly selected individuals. This estimates the fraction of total variance that is among groups in a random-effects ANOVA. We used the Castle-Wright estimator:

$$n_e = \frac{[\mu(P_1) - \mu(P_2)]^2 - Var[\mu(P_1)] - Var[\mu(P_2)]}{8Var(S)}$$

where $S = Var(F_2) - Var(F_1)$, to estimate the effective number of genetic loci (n_e) contributing to variation in the trait [15,23,24]. This is the difference between the mean BR values of the parental races squared, then the subtraction of the two variance terms, which corrects for sampling error of the estimates of the parental means (P_1 and P_2).

The genotype at the *Cr* locus was scored in 286 individuals based on the presence and absence of the white hind-wing margin and the dorsal hind-wing yellow bar, under the assumption that these pattern elements are controlled by alternative alleles of the *Cr* locus [10,25]. The *demophoon* genotype has the yellow bar present and is scored as Cr^dCr^d, a white margin indicates the *cyrbia* genotype and this is scored as Cr^cCr^c, and the Cr^dCr^c heterozygous genotype has neither of these elements (Figure 2). To look for association between variation in the red band and blue colour, we took four measurements of forewing band size in 71 F2 individuals and three further measurements to adjust for wing size (Figure 4), based on methods from Baxter *et al.* [26]. Using ImageJ, band measurements were carried out on the dorsal side of the wing and repeated for both the left and right wings. The average of these two measurements was divided by the average of the three standardising wing measurements.

All statistical analyses were carried out in the R statistical package version 3.4.2 [27]. Welch's t-tests were used for analysis of differences between sexes and reciprocal crosses. ANOVA models were used to compare blue values to *Cr* genotypes. Yellow bar and white margin traits were tested for departures from the expected segregation ratios, based on the above hypothesis of the linkage and Mendelian inheritance, using a chi-squared test. Correlations between BR values and ridge spacing, cross-rib spacing, and forewing red band measurements were tested with the Pearson correlation coefficient.

2.3 Small angle X-ray scattering data collection

We estimated the size of the spacing between scale ridges and between cross-ribs (Figure 1) using small angle X-ray scattering (SAXS) carried out at the ID02 beamline at the European

Synchrotron (ESRF), Grenoble, France [28]. The detector was a high-sensitivity FReLon 16M Kodak CCD with an effective area of 2048 x 2048 pixels (24 µm). The X-ray wavelength λ was 0.0995 nm (12.45 keV), the beam was collimated to 50 µm x 50 µm and the accessible q-range was from 0.0017 to 0.07 nm-1 at 30.7m sample-to-detector distance. All 2D images were corrected for dark, spatial distortion, normalised by transmitted flux and masked to account for the beam stop and the edges of the detector. We azimuthally integrated the 2D images to obtain one dimensional patterns of scattered intensity *I* as a function of the momentum transfer vector *q*, where $q = (4\pi \sin \theta)/\lambda$. Here 2θ is the scattering angle. A typical scattering profile is shown in Figure 5.

Wings were mounted in a frame that could be rotated to precisely align the samples. We collected between 33 and 113 measurements over 10-20 mm between two of the wing veins on the forewing (Figure 3) of 69 *H. erato* individuals: 8 *cyrbia*, 1 *demophoon*, 6 F1 (from 2 crosses in reciprocal directions) and 59 F2 (all from a single cross). In addition, we measured 4 *Heliconius erato hydara* individuals to be analysed alongside the *demophoon. H. e. hydara* do not have iridescent colour and differ only in the lack of yellow hindwing bar. To obtain estimates of the ridge spacing, we fitted the peak positions in the one dimensional scattered intensity to a composite Lorentzian + linear profile using the lmfit Python module [29]. We then used the centre of each fitted profile to calculate ridge spacing using the expression $D = 2\pi/q$ and averaged these to obtain a single estimate per individual. The average distances between ridges are in good agreement with those previously reported for *H. erato* [9].

3. Results

3.1 Segregation of blue colour

Measurements of blue scores were shown to be repeatable, with 99% of variation due to differences between individuals and 1% due to measurement error ($R^2 = 0.99$, $F_{4,20} = 54159$, $p < 0.001$; Table S3). *H. erato demophoon* showed very little blue colour with an average BR value of -0.56 ± 0.08 compared to iridescent *H. erato cyrbia* which had a mean value of 0.97 ± 0.05 (Table 2). The mean for the F2 generation fell midway between the 2 parental races (Figure 6), suggesting additive effects of alleles. The mean of the F1 was slightly skewed towards *demophoon*, although the median was in a similar position to the F2 (0.13 and 0.14). The mean BR value of the backcrosses did not fall halfway between that of the F1 and the parental race, which they were crossed with, but were skewed towards *cyrbia*, the Ecuadorian race. This suggests that the effects of the alleles are not completely additive, and there may be some dominance of the *cyrbia* alleles or epistatic interactions between loci.

The lack of discrete groups in the F2 generation suggests that variation in the trait is controlled by more than one locus. Using the Castle-Wright estimator, with mean BR values and variances

from only one cross direction to reduce variation due to sex linkage (see subsequent results), we obtained an estimate of 4.6 loci contributing to the trait. While this formula assumes that crosses started with inbred lines, it is generally robust to deviations from the assumptions [30]. However, it likely underestimates the total number of loci as it assumes loci all have equal effects. It is therefore perhaps best interpreted as the likely number of loci with medium to large effects on the phenotype. In addition, the F1 individual wings that we measured were of varying age and condition, which may have increased the variance and decreased the mean of blue reflectance seen in these individuals relative to the F2 individuals, which were all preserved soon after emergence. This could influence the estimation of the number of loci.

3.2 Sex linkage

Sex linkage leads to a difference in the trait between reciprocal crosses in the F1 generation, which is confined to the heterogametic sex, or a difference between reciprocal crosses in the F2 generation in the homogametic sex [31]. As in birds, female butterflies are the heterogametic sex; they have ZW sex chromosomes whereas males have ZZ. Differences would occur depending on which parent or grandparent the Z or W is inherited from (Figure 7). If the sex difference is present in the parental population, or the pattern is the same in reciprocal crosses, this would indicate a sex-limited trait (i.e. an autosomal trait that is expressed differently between the sexes).

Comparing the F1 offspring of reciprocal crosses suggested some sex linkage (Figure 8; Table 3). Offspring of crosses with a male *cyrbia* parent had significantly higher blue values than those which had a female *cyrbia* parent. Separated by sex, there was no difference between the males from reciprocal F1 crosses, which had a mean of 0.23 and 0.25 respectively ($t(11) = -0.19$, $p = 0.85$). The variation was amongst the female offspring which had means of -0.03 and 0.26 ($t(44) = -5.55$, $p<0.001$; Table 4). This pattern would be expected if there were one or more loci controlling iridescence on the Z chromosome. In each case, males will be receiving one Z chromosome from an iridescent parent, and the other from a non-iridescent parent. The female offspring, in contrast, will only receive a Z chromosome from their father (Figure 7). To confirm that these results were not biased by a particular cross, individual crosses were plotted and the same pattern was found (Figure S1). We did not find any difference in blue score between the sexes in pure *H. erato cyrbia* (Table 3), demonstrating that the difference between the sexes in the crosses is not due autosomally mediated sexual dimorphism.

If blue colour was controlled only by genes on the Z chromosome, we would expect that females from crosses with a non-iridescent father would have the same phenotype as *demophoon* females. However, they are significantly bluer than wild *demophoon*, supporting the

hypothesis that the colour is controlled by multiple loci on different chromosomes (-0.03 ± 0.2 and -0.56 ± 0.1, $t(25) = -10.6$, $p<0.001$).

In the F2 generation, sex linkage would be shown as males with an iridescent maternal grandfather being more blue than those with an iridescent maternal grandmother. The results point towards this pattern, however the differences between the male groups are not significant, possibly due to small sample sizes in the first group (Figure 9; Table 4). There was little difference in females. Overall, however, offspring with an iridescent maternal grandfather were bluer than those with black maternal grandfather. This is consistent with sex linkage, due to the greater number of "*cyrbia"* Z chromosomes present in the F2 offspring (Figure 7). Within the offspring with an iridescent maternal grandfather, males were bluer than females, while this was not the case for crosses with a black maternal grandfather, also supporting Z linkage (Table 3).

Using the standard wing measurements, we can see that there is no dimorphism in wing size between males (11.2 ± 0.5mm) and females (10.9 ± 0.6mm) in the F2 ($t = -1.82$, d.f. = 68.33, $p = 0.07$).

In summary, F1 females were bluer than males when they had an iridescent father, and males were bluer in the F2 when they had an iridescent maternal grandfather. There were no differences in BR values between males and females in the parental races, *H. e. demophoon* and *H. e. cyrbia*. These results support the presence of loci controlling iridescence in the Z chromosome.

3.3 Links to other colour pattern loci

In *H. erato*, the *Cr* locus controls the presence of a yellow forewing bar in *demophoon* and a white margin in *cyrbia*. There were 3 observed phenotypes in the F2 generation – yellow bar present, white margin present, and both absent (Figure 2). Consistent with the hypothesis that these two features are controlled by recessive, tightly linked loci or are alternative alleles of the same locus, we did not find any individuals that had both a yellow dorsal bar and a white margin present. The ratio of these traits was also consistent with a 1:2:1 ratio as expected under the assumption that the individuals lacking both features were heterozygous at this locus ($x^2 = 2.1$, d.f. = 2, $p = 0.35$). There was no significant difference in BR values between individuals with different *Cr* genotypes ($F_{2,107} = 2.05$, $p = 0.133$) (Figure 10), suggesting that *cortex* is not one of the genes controlling iridescence, nor are there any major effect loci linked to this region on *Heliconius* chromosome 15. In the F2, there were also no significant correlations between blue colour and any of the linear measurements used to determine shape of the red forewing band (Table 5).

3.4 Nanostructure variation

As we expected, there was a negative correlation between longitudinal ridge spacing and BR values (r^2 = -0.52, p<0.001; Figure 11), indicating that blue reflectance increases with increasing density of ridges on the scale. The lack of a strong correlation shows that ridge spacing is only one factor which is affecting the intensity of iridescence, and that other aspects of scale morphology that determine blue reflectance may segregate somewhat independently in the crosses. BR values also declined with increasing cross-rib spacing, although not significantly (r^2 = -0.20, p = 0.09; Figure 11). Ridge spacing and cross-rib spacing were highly correlated with each other (r^2 = 0.34, p = 0.002; Figure 11) suggesting a genetic correlation between these traits. Therefore, the correlation between cross-rib spacing and BR value is likely due to this association between ridge and cross-rib spacing, as we do not expect the cross-ribs to directly affect colour.

Consistent with previous findings [9], *H. erato cyrbia* had closer ridge spacing than *H. erato demophoon* (Table 6). Like the BR values, measurements of ridge spacing in the F2 generation fell between the parental races (Figure 12) and was fairly continuous, consistent with the action of multiple genes. Interestingly, ridge spacing in the F1 generation was highly variable between individuals. This could indicate variation in epistatically acting alleles in the parental populations that segregate in the F1 generation, or may suggest environmental effects. However, the phenotyped F1 individuals in this comparison were from two different reciprocal crosses, with apparent differences between these two groups. Therefore, some of the variation that is observed may be due to cross-specific genetic effects and possibly sex-linkage, but we have data from too few individuals to fully dissect these effects.

Cross-rib spacing in the F2 generation appears to extend beyond the range of the parental races (Figure 13), again possibly indicating epistatically acting alleles in the parental populations, although not all parental individuals were measured. Large variation in cross-rib spacing may be expected as it is not predicted to have an effect on colour, so may be under weaker selection. In the F2 generation, males had narrower longitudinal ridge spacing than females, which was similar to the differences seen in this generation in blue values, and may suggest sex linkage of loci controlling ridge spacing ($t(57) = 3.80$, $p < 0.001$; Figure 14). Cross-rib spacing was also smaller in males ($t(43) = 4.95$, $p < 0.001$), supporting the idea that ridge spacing and cross-rib spacing may be genetically correlated. Overall, ridge spacing appears to have a very similar genetic architecture to that of the BR colour values, suggesting that it is also controlled by multiple loci.

4. Discussion

Our phenotypic analysis of crosses between iridescent and non-iridescent races shows that iridescence is controlled by multiple loci in *H. erato* with convincing evidence for loci on the Z chromosome. There is an extensive history of using experimental crosses in *Heliconius* to investigate the genes controlling colour and pattern, but although iridescence had been shown to segregate in crosses, the trait has not been investigated due to the difficulty of quantifying the continuous phenotype. We show that standardised photographs and the BR ratio is an effective method of estimating variation in blue iridescent reflectance. As expected, iridescent *H. erato cyrbia* gave the highest blue values, and non-iridescent *H. e. demophoon* the lowest. BR values correlated with longitudinal ridge spacing, which has previously been shown to have an effect on the brightness of the blue iridescent colour [9]. The distribution of blue values in the F2 generation suggests that variation in the trait is not controlled by a single locus.

The differences in blue values found between sexes in the F1 reciprocal *erato* crosses suggest that there could be a major effect locus involved in iridescent colour on the Z chromosome. We may expect that genes on the sex chromosomes will control sexually selected traits [32]. Reinhold [33] calculated that in *Drosophila* around a third of phenotypic variation in sexually selected traits was caused by X-linked genes, and that X-linked genes only influenced traits classified as under sexual selection. Iridescent structural colours are used as sexual signals in many butterfly species [2,34,35]. Work with *Colias* butterflies has found many wing pattern elements are sex-linked, including melanisation, UV reflectance and yellow wing pigmentation [36,37]. These studies found that sex linkage was important in prezygotic isolation and species differentiation. Therefore, sex linkage of iridescence in *Heliconius* may have contributed to the differentiation of this trait between geographical races.

Unlike some Lepidoptera, *Heliconius* do not show complete sex chromosome dosage compensation. Analysis of *H. cydno* and *H. melpomene* gene expression showed a modest dosage effect on the Z chromosome, and overall reduced expression compared to autosomes [38]. Sex linkage of iridescence may therefore be explained by this incomplete dosage compensation.

The three *erato* phenotypes controlled by the *Cr* locus did not show any correlation with iridescent colour values. The gene *cortex*, found in this genomic region, has been shown to underlie these colour pattern differences [16]. There are several reasons why major colour patterning genes could have been hypothesised to also control structural colour variation in *Heliconius*. Knockouts of one of the genes that control colour pattern in *Heliconius*, *optix*, in *Junonia coenia* butterflies resulted in a change in pigmentation, and the gain of structural colour [39], although this was not observed in the same tests with *Heliconius erato*. In addition,

linkage between divergently selected loci would be expected under ‘divergence hitchhiking’, in which genomic regions around key divergently selected loci are protected from recombination during speciation [40]. Hitchhiking regions can be small in natural populations unless recombination is reduced, but in Lepidoptera there is no recombination in the female germ-line. Furthermore, for highly polygenic traits we would expect many loci to be distributed throughout the whole genome, so that for any genetic marker there will be some phenotypic association. Individuals with homozygous *Cr* phenotypes, for example, will have inherited an entire chromosome 15 from either an iridescent or non-iridescent grandparent, due to the lack of female recombination. Therefore, any combination of a single major effect locus or multiple smaller effect loci on chromosome 15 would have been seen as a difference in iridescence between individuals with different *Cr* phenotypes. The fact that we find no association with *Cr* suggests that structural colour is not highly polygenic, but controlled by a moderate number of loci, none of which are located on chromosome 15. It is also consistent with it being controlled independently of colour pattern. Similarly, we see no association with variation in forewing red band size, which is largely determined by the gene *WntA*. This region on chromosome 10 controls forewing band shape in multiple races of *H. erato*, as well as other *Heliconius* species [12].

In *Heliconius* pigment colour patterns, a small set of major effect genes have been well studied but a larger set of “modifier” loci have also been found which adjust colour pattern [12]. It is possible that the iridescence genes have a similar distribution of effect sizes, with a small number of major effect genes, including one on the Z chromosome, and a distribution of other smaller effect genes. This supports the existing evidence of the importance of major effect loci in adaptive change [10–12]. Future work with the co-mimic of *erato*, *Heliconius melpomene*, will allow us to compare the genetic basis of iridescence between the two species. Following the two-step process of Müllerian mimicry described by Turner [41,42], a large effect mutation, such as the one we have found on the Z chromosome, allows an adaptive phenotypic change large enough for the population to resemble those in the mimicry ring and survive, then smaller changes will produce incremental improvements in mimicry.

Longitudinal ridge spacing also appears to have a polygenic architecture. The continuous variation that is observed in blue colour in the F2 broods does not seem to be due to major effect loci with discrete effects on different aspects of scale structure. Rather it seems that multiple interacting genes are involved in controlling scale morphology. The correlation between ridge and cross-rib spacing suggests that some of these loci produce correlated effects on various aspects of scale morphology. There is wide variation in the SAXS measurements and this is most likely because this method will detect variation in structures other than ridge and cross-rib spacing, such as layering of the lamellae. The values are averaged from multiple measurements

per individual so there will also be variation within individuals. The fact that we do not see a perfect correlation between ridge and cross-rib spacing and blue colour suggests that there is some independent segregation of other aspects of scale morphology that contribute to the colour. Measurements of other aspects of scale morphology, such as ridge curvature and layering, will be needed to confirm this.

Conclusions

Crosses are ideal for investigating the genetic basis of colour and pattern as traits will segregate in following generations. Crossing iridescent and non-iridescent *Heliconius erato* has allowed us to quantify variation in the colour and determine that it is sex-linked and controlled by multiple loci.

Data accessibility

SAXS data (doi:10.15131/shef.data.6839315) and accompanying code (doi: 10.15131/shef.data.6837905) have been uploaded to an online repository. Colour measurements, repeatability measurements and cross pedigree information can be found as part of the electronic supplementary material.

Authors' contributions

MNB collected the colour data, performed the genetic analysis and wrote the manuscript. JER analysed the SAXS data under the supervision of AJP. The crosses were performed by PAS, CM, DC, MNB, NJN and EVC. The SAXS data was collected by AJP, TZ, EVC, NJN and MNB. The study was devised and co-ordinated by NJN. AJP co-ordinated collection of the SAXS data. All authors read and commented on the manuscript.

Competing Interests

We declare we have no competing interests.

Funding

This work was funded by the UK Natural Environment Research Council (NERC) through an Independent Research Fellowship (NE/K008498/1) to NJN. MNB and EVC are funded by the NERC doctoral training partnership, ACCE. JER is funded through the Leverhulme Centre for Advanced Biological Modelling as well as scholarships from Universidad del Rosario and the University of Sheffield.

Acknowledgements

We thank the governments of Ecuador and Panama for permission to collect butterflies. Thanks to Juan López and Gabriela Irazábal for their assistance with the crosses. We are grateful to the European Synchrotron Radiation Facility for provision of X-ray beamtime under proposal LS2720 and to Andrew Dennison for assistance with SAXS data collection.

References

1. Bálint Z, Kertész K, Piszter G, Vértesy Z, Biró LP. 2012 The well-tuned blues: the role of structural colours as optical signals in the species recognition of a local butterfly fauna (Lepidoptera: Lycaenidae: Polyommatinae). *J. R. Soc. Interface* **9**, 1745–56. (doi:10.1098/rsif.2011.0854)

2. Sweeney A, Jiggins C, Johnsen S. 2003 Insect communication: Polarized light as a butterfly mating signal. *Nature* **423**, 31–32. (doi:10.1038/423031a)

3. Hadley NF, Savill A, Schultz TD. 1992 Coloration and its thermal consequences in the New Zealand tiger beetle Neocicindela perhispida. *J. Therm. Biol.* **17**, 55–61.

4. Vukusic P, Sambles JR, Lawrence CR, Wootton RJ. 1999 Quantified interference and diffraction in single Morpho butterfly scales. *Proc. R. Soc. B Biol. Sci.* **266**, 1403. (doi:10.1098/rspb.1999.0794)

5. Winter B, Butz B, Dieker C, Schröder-Turk GE, Mecke K, Spiecker E. 2015 Coexistence of both gyroid chiralities in individual butterfly wing scales of Callophrys rubi *Proc. Natl. Acad. Sci.* **112**, 12911 LP-12916.

6. Dinwiddie A, Null R, Pizzano M, Chuong L, Leigh Krup A, Ee Tan H, Patel NH. 2014 Dynamics of F-actin prefigure the structure of butterfly wing scales. *Dev. Biol.* **392**, 404–418. (doi:10.1016/j.ydbio.2014.06.005)

7. Merrill RM *et al.* 2015 The diversification of *Heliconius* butterflies: what have we learned in 150 years? *J. Evol. Biol.* **28**, 1417–1438. (doi:10.1111/jeb.12672)

8. Wilts BD, Vey AJM, Briscoe AD, Stavenga DG. 2017 Longwing (Heliconius) butterflies combine a restricted set of pigmentary and structural coloration mechanisms. *BMC Evol. Biol.* **17**, 1–12. (doi:10.1186/s12862-017-1073-1)

9. Parnell AJ *et al.* 2018 Wing scale ultrastructure underlying convergent and divergent iridescent colours in mimetic *Heliconius* butterflies. *J. R. Soc. Interface* **15**, 20170948. (doi:10.1098/rsif.2017.0948)

10. Joron M *et al.* 2006 A Conserved Supergene Locus Controls Colour Pattern Diversity in Heliconius Butterflies. *PLoS Biol.* **4**, 1831–1840. (doi:10.1371/journal.pbio.0040303)

11. Baxter SW, Papa R, Chamberlain N, Humphray SJ, Joron M, Morrison C, ffrench-Constant RH, McMillan WO, Jiggins CD. 2008 Convergent Evolution in the Genetic Basis of Mullerian Mimicry in Heliconius Butterflies. *Genetics* **180**, 1567–1577. (doi:10.1534/genetics.107.082982)

12. Papa R, Kapan DD, Counterman BA, Maldonado K, Lindstrom DP, Reed RD, Nijhout HF, Hrbek T, McMillan WO. 2013 Multi-Allelic Major Effect Genes Interact with Minor Effect QTLs to Control Adaptive Color Pattern Variation in Heliconius erato. *PLoS One* **8**, e57033. (doi:10.1371/journal.pone.0057033)

13. Nadeau NJ. 2016 Genes controlling mimetic colour pattern variation in butterflies. *Curr. Opin. Insect Sci.* **17**, 24–31. (doi:10.1016/j.cois.2016.05.013)

14. Emsley M. 1965 The geographical distribution of the color-pattern components of Heliconius erato and Heliconius melpomene with genetical evidence for the systematic relationship between the two species. *Zoologica* **49**, 245–286.

15. Lynch M, Walsh B. 1998 Analysis of Line Crosses. In *Genetics and Analysis of Quantitative Traits*, pp. 205–250. Sinauer Associates, Massachusetts.

16. Nadeau NJ *et al.* 2016 The gene cortex controls mimicry and crypsis in butterflies and moths. *Nature* **534**, 106–110. (doi:10.1038/nature17961)

17. Martin A *et al.* 2012 Diversification of complex butterfly wing patterns by repeated regulatory evolution of a Wnt ligand. *Proc. Natl. Acad. Sci.* **109**, 12632–12637. (doi:10.1073/pnas.1204800109)

18. Mazo-Vargas A *et al.* 2017 Macroevolutionary shifts of *WntA* function potentiate butterfly wing-pattern diversity. *Proc. Natl. Acad. Sci.* , 201708149. (doi:10.1073/pnas.1708149114)

19. Mallet J. 1989 The Genetics of Warning Colour in Peruvian Hybrid Zones of Heliconius erato and H. melpomene. *Proc. R. Soc. B Biol. Sci.* **236**, 163–185. (doi:10.1098/rspb.1989.0019)

20. Abramoff, M.D., Magalhaes PJ, Ram SJ. 2004 Image Processing with ImageJ. *Biophotonics Int.* **11**, 36–42.

21. Comeault AA, Carvalho CF, Dennis S, Soria-Carrasco V, Nosil P. 2016 Color phenotypes are under similar genetic control in two distantly related species of Timema stick insect. *Evolution (N. Y).* **70**, 1283–1296. (doi:10.1111/evo.12931)

22. Michael C Whitlock. 2007 *The analysis of biological data*. 1st Editio. Roberts & Company Publishers. (doi:10.1080/03610927808827682)

23. Cockerham CC. 1986 Modifications in estimating the number of genes for a quantitative character. *Genetics* **114**, 659–664.

24. Otto SP, Jones CD. 2000 Detecting the undetected: estimating the total number of loci inderlying a quantitative trait. *Genetics* **156**, 2093–2107. (doi:10.1007/s001220050781)

25. Mallet J. 1986 Hybrid zones of heliconius butterflies in panama and the stability and movement of warning colour dines. *Heredity (Edinb).* **56**, 191–202. (doi:10.1038/hdy.1986.31)

26. Baxter S, Johnston S, Jiggins C. 2009 Butterfly speciation and the distribution of gene effect sizes fixed during adaptation. *Heredity (Edinb).* **102**, 57–65. (doi:10.1038/hdy.2008.109)

27. R Core Team. 2018 R: A language and environment for statistical computing.

28. Van Vaerenbergh P, L??onardon J, Sztucki M, Boesecke P, Gorini J, Claustre L, Sever F, Morse J, Narayanan T. 2016 An upgrade beamline for combined wide, small and ultra small-angle x-ray scattering at the ESRF. *AIP Conf. Proc.* **1741**. (doi:10.1063/1.4952857)

29. Newville M, Stensitzki T, Allen DB, Ingargiola A. 2014 LMFIT: Non-Linear Least-Square Minimization and Curve-Fitting for Python. *Astrophys. Source Code Libr.*

30. Lande R. 1981 The minimum number of genes contributing to quantitative variation between and within populations. *Genetics* **99**, 541–553.

31. Mather K, Jinks JL. 1982 *Biometrical Genetics*. 3rd edn. Cambridge University Press.

32. Fairbairn DJ, Roff D a. 2006 The quantitative genetics of sexual dimorphism: assessing the importance of sex-linkage. *Heredity (Edinb).* **97**, 319–328. (doi:10.1038/sj.hdy.6800895)

33. Reinhold K. 1998 Sex linkage among genes controlling sexually selected traits. *Behav. Ecol. Sociobiol.* **44**, 1–7.

34. Kemp DJ. 2007 Female butterflies prefer males bearing bright iridescent ornamentation. *Proc. R. Soc. B Biol. Sci.* **274**, 1043–1047. (doi:10.1098/rspb.2006.0043)

35. Rajyaguru PK, Pegram K V., Kingston ACN, Rutowski RL. 2013 Male wing color properties predict the size of nuptial gifts given during mating in the Pipevine Swallowtail butterfly (Battus philenor). *Naturwissenschaften* **100**, 507–513. (doi:10.1007/s00114-013-1046-1)

36. Silberglied RE. 1979 Communication in the Ultraviolet. *Annu. Rev. Ecol. Syst.* **10**, 373–398. (doi:10.1146/annurev.es.10.110179.002105)

37. Ellers J, Boggs CL. 2002 The Evolution of Wing Color in Colias Butterflies : Heritability , Sex Linkage , and Population Divergence. *Evolution (N. Y).* **56**, 836–840.

38. Walters JR, Hardcastle TJ, Jiggins CD. 2015 Sex chromosome dosage compensation in heliconius butterflies: Global yet still incomplete? *Genome Biol. Evol.* **7**, 2545–2559. (doi:10.1093/gbe/evv156)

39. Zhang L, Mazo-Vargas A, Reed RD. 2017 Single master regulatory gene coordinates the evolution and development of butterfly color and iridescence. *Proc. Natl. Acad. Sci.* , 201709058. (doi:10.1073/pnas.1709058114)

40. Via S, West J. 2008 The genetic mosaic suggests a new role for hitchhiking in ecological speciation. *Mol. Ecol.* **17**, 4334–4345. (doi:10.1111/j.1365-294X.2008.03921.x)

41. Turner J. 1977 Butterfly mimicry: the genetical evolution of an adaptation. *Evol. Biol.* **10**, 163–206.

42. Turner JRJ. 1981 Adaptation and Evolution in Heliconius: A Defense of NeoDarwinism. *Annu. Rev. Ecol. Syst.* **12**, 99–121.

Figure Legends

Figure 1. Scanning Electron Microscope image showing the structures on a *Heliconius* wing scale. Longitudinal ridges, composed of overlapping lamellae, are connected by cross-ribs.

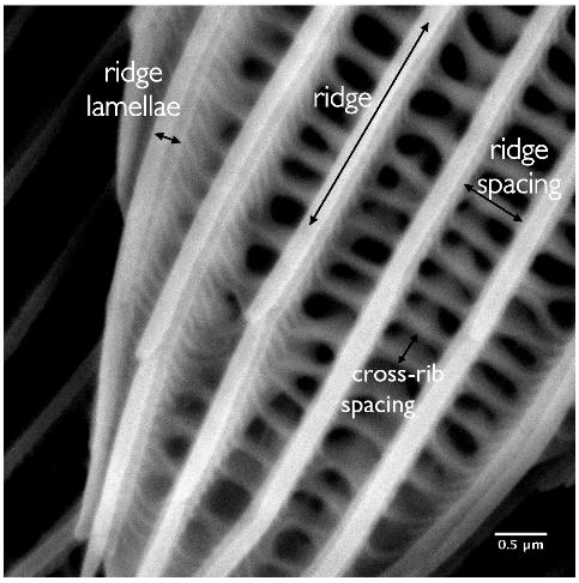

Figure 2. Cross design and examples of colour pattern variation in *H. erato* F1, F2, and backcross generations. Examples of the *Cr* genotypes are shown in the F2 generation.

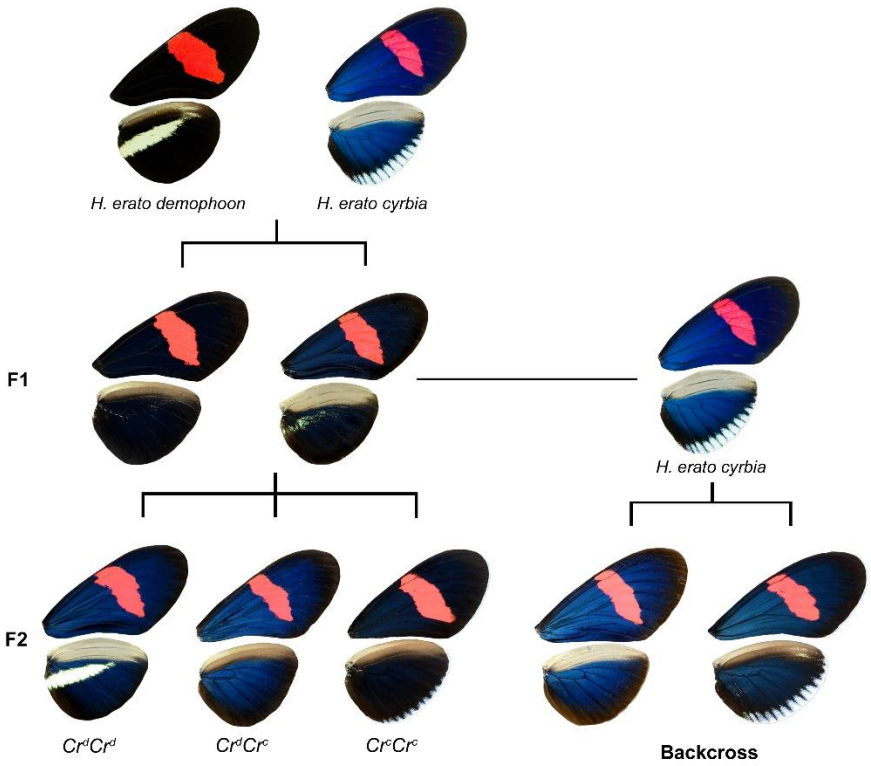

Figure 3. RGB values were measured in the hatched areas highlighted on the right wings and averaged for each butterfly. Left wings were used when the right side were too damaged. Small angle X-ray scattering (SAXS) measurements were taken along the dotted line shown on the left forewing.

Figure 4. Four measurements of forewing band width were taken (bold arrows) along with three further measurements to standardise wing size (dotted arrows), using wing veins as points of reference.

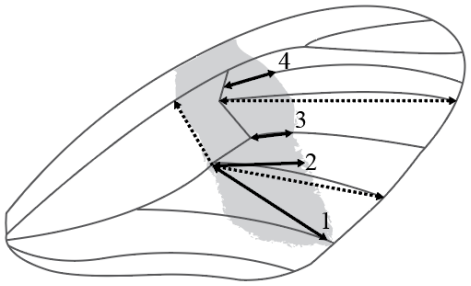

Figure 5. Representative small angle X-ray scattering patterns for a single frame of a male *H. e. cyrbia* parent. (A) The 2D pattern reveals approximately perpendicular scattering intensity from scale features. From their orientation, length scales of the scattered intensity and previous interpretations, we infer that they correspond to the spacing between ridges and cross-ribs. (B) Full azimuthal integration of the scattered intensity as a function of the magnitude of the momentum transfer vector *q*. The peaks corresponding to ridge and cross-rib spacing are indicated together with the measurements in real space.

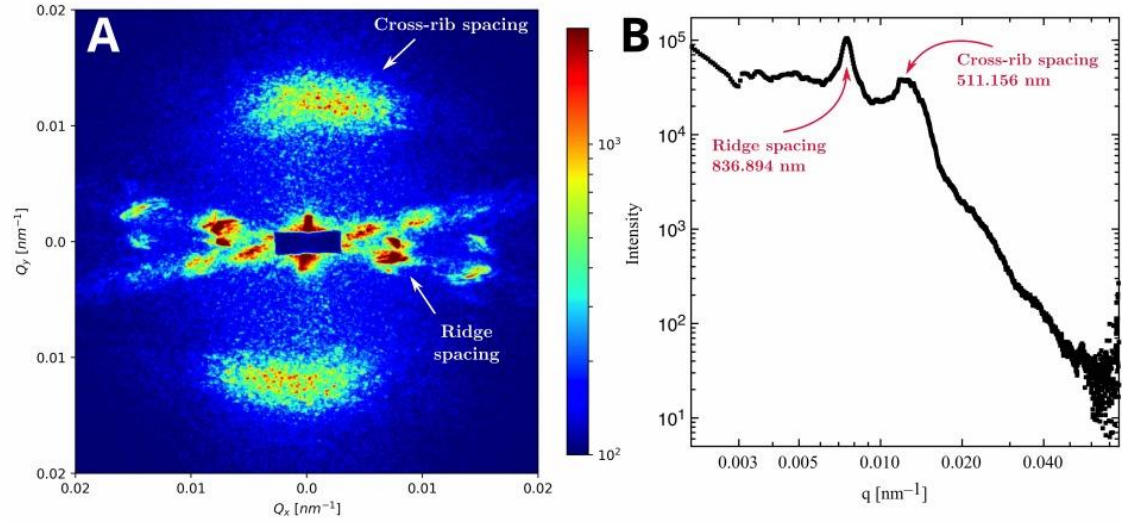

Figure 6. Mean BR values across *H. erato* generations. F1 and F2 individuals largely fall between the parental Panama (*demophoon*) and Ecuador (*cyrbia*) races. The backcross generation (BC) are highly skewed towards *cyrbia*, which is the race they were crossed with.

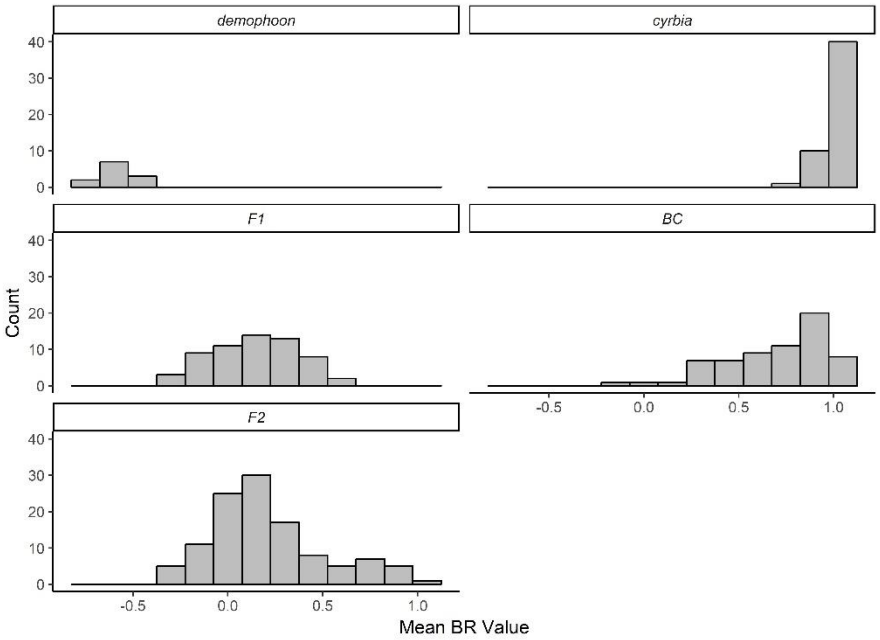

Figure 7. If there are loci of interest on the Z chromosome, F1 females with an iridescent *cyrbia* father will be bluer than those with a non-iridescent *demophoon* father because they inherit an

"*cyrbia*" Z chromosome. In the F2, males always inherit a complete, non-recombined Z chromosome from their maternal grandfather, so if he is iridescent they will be bluer than offspring from the reciprocal cross.

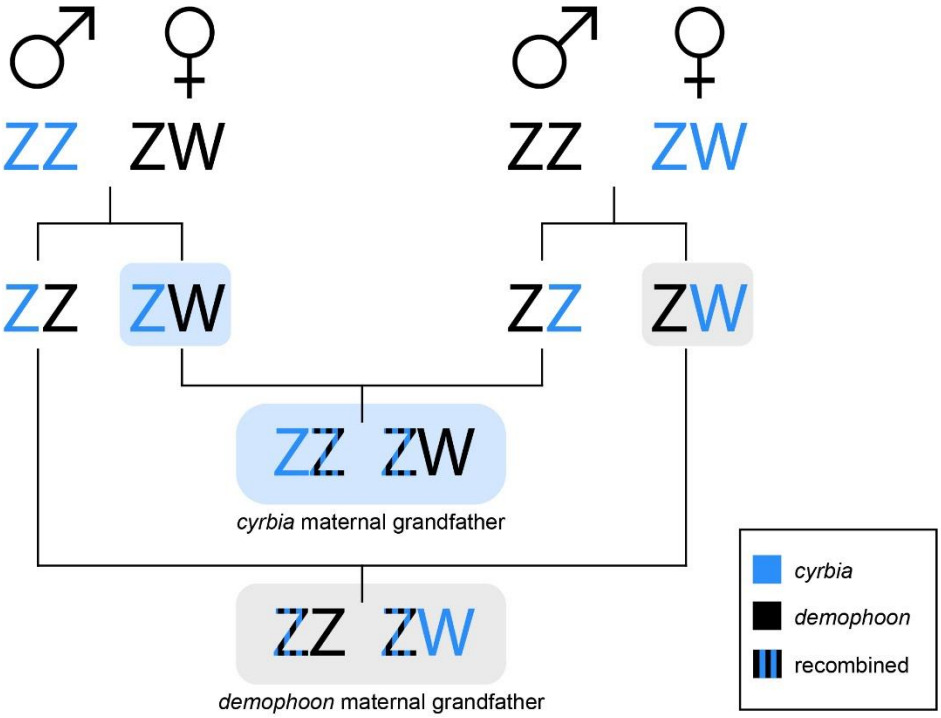

Figure 8. F1 females with an iridescent *cyrbia* father were significantly bluer than those with a *demophoon* father. There were no differences in males.

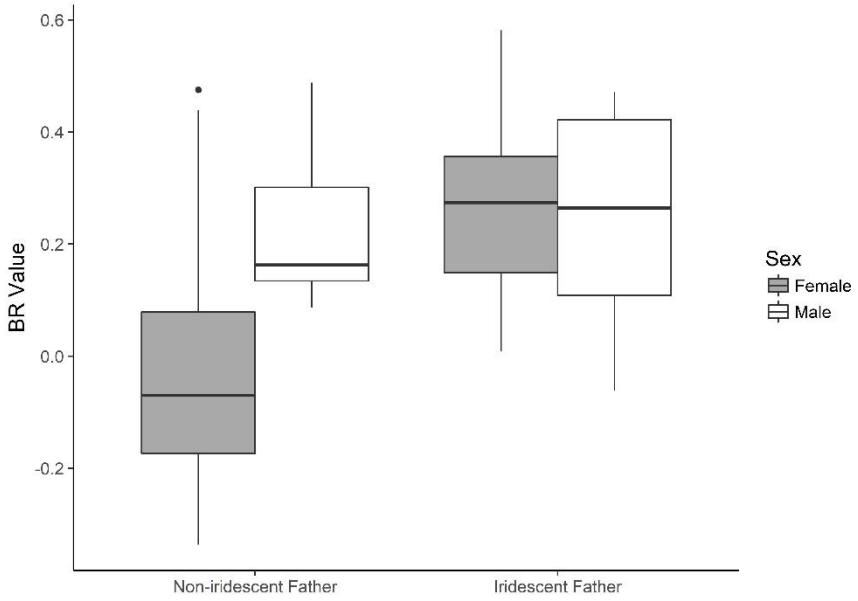

Figure 9. Mean BR values for F2 males with an iridescent maternal grandfather (MGF) were higher than those with an iridescent maternal grandmother, although not significantly. Females in both groups had similar BR values.

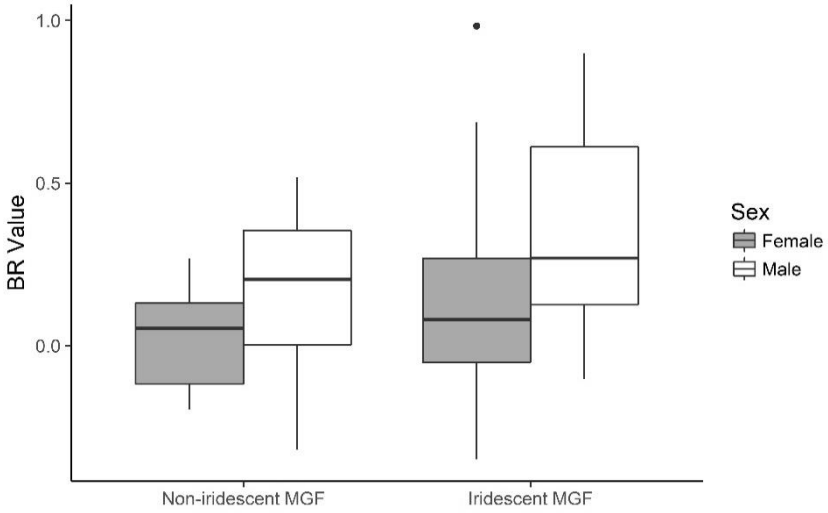

Figure 10. In the F2 generation, BR values did not differ with the different *Cr* phenotypes. Cr^dCr^d represents the *demophoon* genotype with the yellow bar present, and Cr^cCr^c is the *cyrbia* genotype with the white margin. Cr^dCr^c is heterozygous and has neither of these elements.

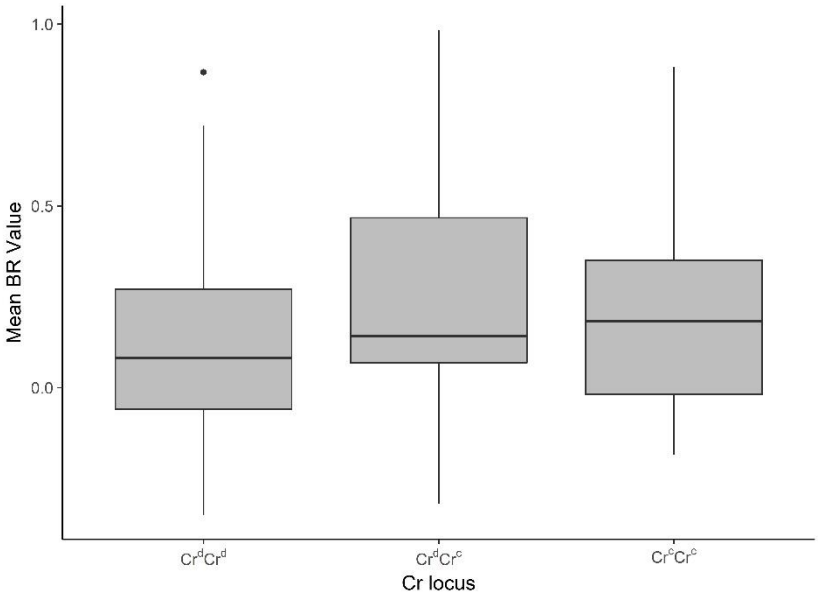

Figure 11. An increase in longitudinal ridge spacing correlated with a decrease in BR values. Blue colour slightly decreased with cross-rib spacing, but ridge spacing and cross-rib spacing were highly correlated.

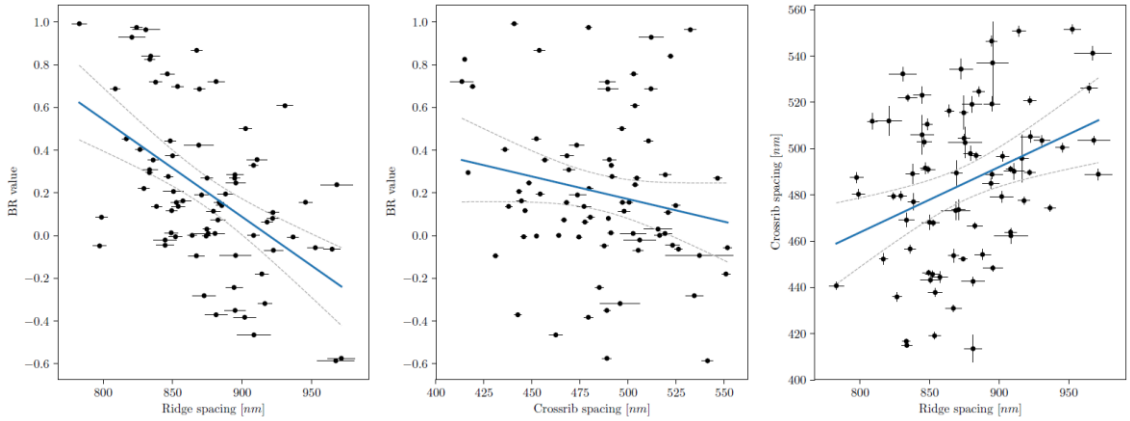

Figure 12. Variation in longitudinal ridge spacing in the F2 suggests it is controlled by multiple genes. In the F1, those with an iridescent father had lower ridge spacing, reflecting the higher BR values seen in this cross.

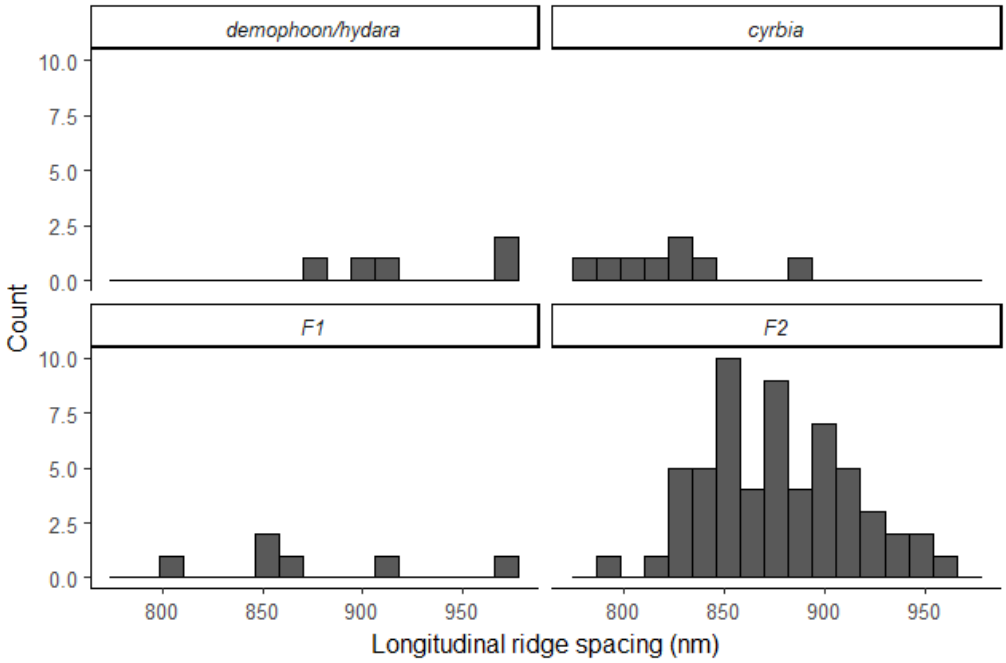

Figure 13. Cross-rib spacing also shows continuous variation in the F2 generation, and extremes extended beyond the values of the few parental individuals which were measured.

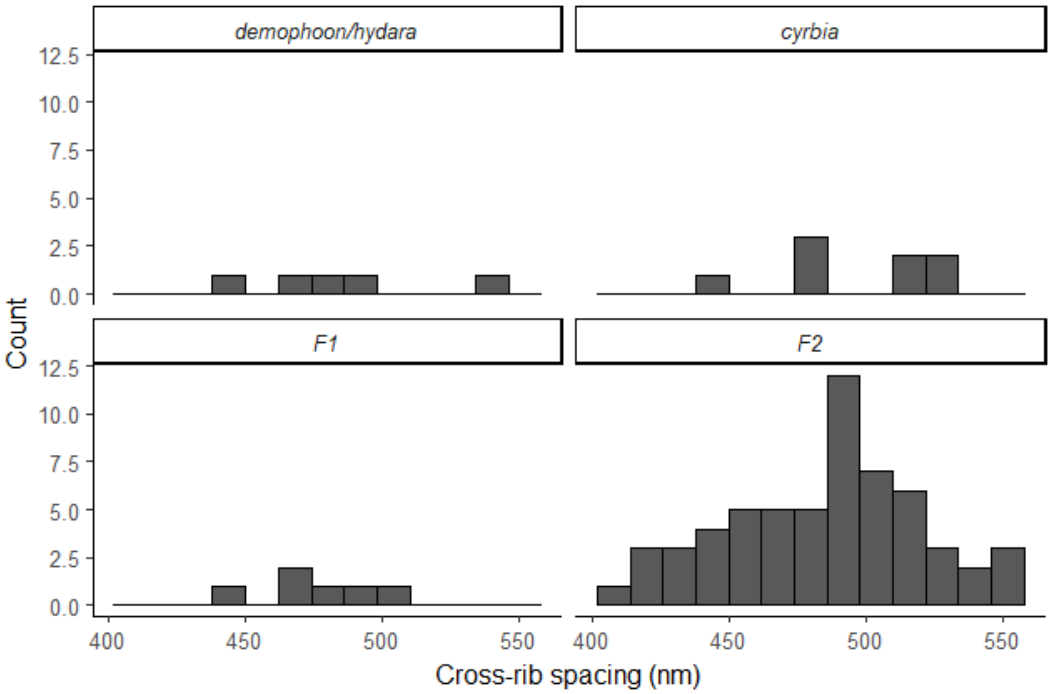

Figure 14. Males have narrower longitudinal ridge spacing than females in the F2, but not in the parental races. Significant differences in cross-rib spacing were seen in *cyrbia* and in the F2,

with males again having narrower spacing. These results are consistent with the finding that males have higher measures of blue colour.

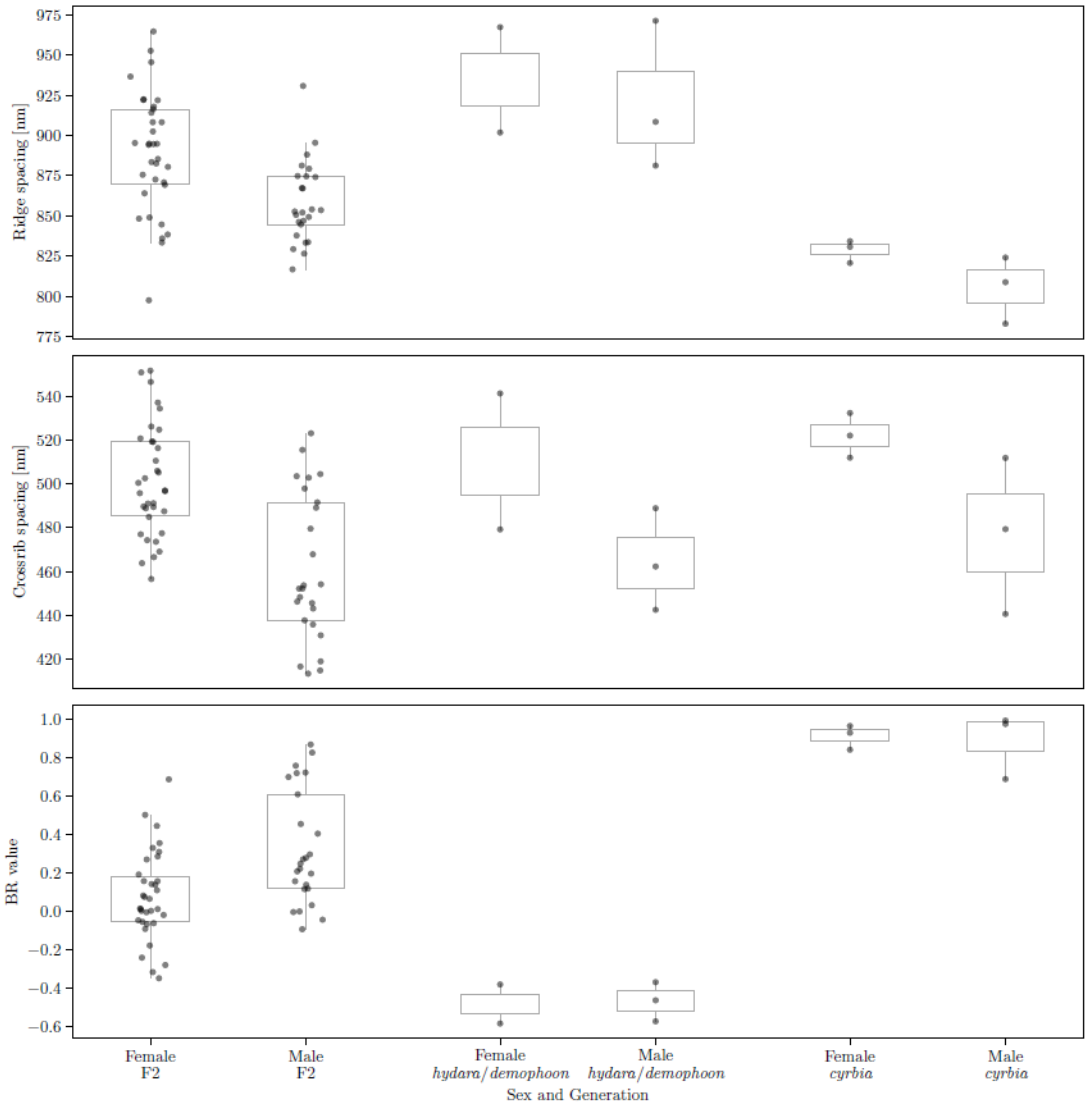

Table Legends

Table 1. *H. erato* crosses performed and the number of offspring produced from each. See supplementary Table S2 for details of each cross.

Cross type	Number of crosses	Number of offspring phenotyped for blue values	Number of offspring phenotyped for ridge spacing
F1: *demophoon* ♂ x *cyrbia* ♀	2	37	3
F1*: cyrbia* ♂ x *demophoon* ♀	3	33	3
F2: *cyrbia* maternal grandfather	3	100	59
F2: *demophoon* maternal grandfather	3	14	0
Backcross: *cyrbia* ♂ x (*demophoon* ♂ x *cyrbia* ♀)	2	16	0
Backcross: *cyrbia* ♀ x (*cyrbia* ♂ x *demophoon* ♀)	1	49	0

Table 2. Summary statistics for BR values in each generation of *H. erato*.

Generation	Mean BR value	Standard deviation	Variance	Sample size
demophoon	-0.56	0.08	0.01	12
F1	0.13	0.23	0.05	60
Backcross	0.69	0.28	0.08	65
F2	0.21	0.30	0.09	114
cyrbia	0.97	0.05	0.00	51

Table 3. Comparison of BR values (± SD) between females and males in each *H. erato* generation. Males are bluer than females in crosses with a *demophoon* father or *cyrbia* maternal grandfather (MGF). Males are also bluer in backcrosses with a *cyrbia* MGF. There are no differences in the parental races.

Generation	Female BR value	Female sample size	Male BR value	Male sample size	t statistic	d.f.	p-value
demophoon	-0.56 ± 0.1	6	-0.56 ± 0.1	6	-0.06	9.0	0.955
All F1	0.10 ± 0.3	46	0.24 ± 0.2	14	-2.37	28.9	0.025*

F1 *cyrbia* father	0.26 ± 0.2	21	0.25 ± 0.2	7	0.17	8.4	0.872
F1 *demo*. father	-0.03 ± 0.2	25	0.23 ± 0.1	7	-3.80	13.3	0.0021*
All F2	0.10 ± 0.3	63	0.33 ± 0.3	51	-4.28	96.4	<0.001*
F2 *cyrbia* MGF	0.12 ± 0.3	53	0.35 ± 0.3	47	4.00	92.1	<0.001*
F2 *demo.* MGF	0.02 ± 0.2	10	0.15 ± 0.4	4	-0.72	3.5	0.512
All BC	0.60 ± 0.3	35	0.79 ± 0.2	30	-2.93	62.9	0.005*
BC *cyrbia* MGF	0.58 ± 0.3	24	0.83 ± 0.2	25	-3.86	42.7	<0.001*
BC *demo.* MGF	0.65 ± 0.4	11	0.62 ± 0.4	5	0.16	7.6	0.877
cyrbia	0.98 ± 0.02	16	0.97 ± 0.1	35	0.79	48.2	0.431

Table 4. Comparison of BR values for offspring from reciprocal F1 crosses, which had either an iridescent mother or iridescent father, and for F2 crosses, which had either an iridescent maternal grandfather or grandmother. Mean values and sample sizes are shown in Table 3.

F1 *cyrbia* or *demophoon* father				**F2 *cyrbia* or *demophoon* maternal grandfather**			
	t	**d.f.**	**p-value**		**t**	**d.f.**	**p-value**
Female	-5.55	43.6	<0.0001*	**Female**	-1.64	19.5	0.118
Male	-0.19	10.8	0.85	**Male**	-1.06	3.4	0.357
All	-4.67	56.8	<0.0001*	**All**	-2.53	20.2	0.02*

Table 5. There are no significant correlations between the forewing red band measurements and BR colour in the F2 generation. Measurements are ratios of band measurements to wing size. Degrees of freedom = 69. N = 71.

Measurement	Mean	SD	Variance	t	r^2	p-value
Linear 1	0.76	0.08	0.006	-1.65	-0.20	0.10
Linear 2	0.55	0.06	0.003	-1.41	-0.17	0.16
Linear 3	0.35	0.05	0.002	-1.69	-0.20	0.10
Linear 4	0.41	0.05	0.003	0.38	0.05	0.71

Table 6. Mean spacing (±SD) between longitudinal ridges and between cross-ribs. The narrower ridge spacing in *cyrbia* results in a brighter iridescent colour. The mean values for the F1 and F2 generations fell between the values for the parental races.

Generation	Mean longitudinal ridge spacing (nm)	Mean cross-rib spacing (nm)	Sample size (Male, Female)
demophoon	967.36	541.26	1 (0, 1)
F1	875.64 ± 57.8	476.66 ± 20.0	6 (4, 2)
F2	876.25 ± 36.0	484.46 ± 35.0	59 (25, 34)
cyrbia	818.95 ± 40.0	478.46 ± 25.3	5 (5, 0)

Paper in the format published in the journal Interface

Downloaded from http://rsif.royalsocietypublishing.org/ on December 5, 2018

INTERFACE

rsif.royalsocietypublishing.org

Research

Cite this article: Parnell AJ *et al*. 2018 Wing scale ultrastructure underlying convergent and divergent iridescent colours in mimetic *Heliconius* butterflies. *J. R. Soc. Interface* **15**: 20170948.
http://dx.doi.org/10.1098/rsif.2017.0948

Received: 17 December 2017
Accepted: 26 March 2018

Subject Category:
Life Sciences–Physics interface

Subject Areas:
biophysics, evolution, biomaterials

Keywords:
structural colour, biophotonics, butterflies, iridescence, *Heliconius*, mimicry

Electronic supplementary material is available online at https://dx.doi.org/10.6084/m9.figshare.c.4058795.

THE ROYAL SOCIETY PUBLISHING

Wing scale ultrastructure underlying convergent and divergent iridescent colours in mimetic *Heliconius* butterflies

Andrew J. Parnell[1], James E. Bradford[1], Emma V. Curran[2], Adam L. Washington[1,3], Gracie Adams[2], Melanie N. Brien[2], Stephanie L. Burg[1], Carlos Morochz[4], J. Patrick A. Fairclough[3], Pete Vukusic[5], Simon J. Martin[6], Scott Doak[6] and Nicola J. Nadeau[2]

[1]Department of Physics and Astronomy, University of Sheffield, Hicks Building, Hounsfield Road, Sheffield S3 7RH, UK
[2]Department of Animal and Plant Sciences, University of Sheffield, Alfred Denny Building, Western bank, Sheffield S10 2TN, UK
[3]Department of Mechanical Engineering, University of Sheffield, Sheffield S3 7HQ, UK
[4]Mashpi Reserve, Quito, Ecuador
[5]Department of Physics and Astronomy, University of Exeter, Stocker Road, Exeter EX4 4QL, UK
[6]Department of Materials, Loughborough University, Loughborough LE11 3TU, UK

AJP, 0000-0001-8606-8644; NJN, 0000-0002-9319-921X

Iridescence is an optical phenomenon whereby colour changes with the illumination and viewing angle. It can be produced by thin film interference or diffraction. Iridescent optical structures are fairly common in nature, but relatively little is known about their production or evolution. Here we describe the structures responsible for producing blue-green iridescent colour in *Heliconius* butterflies. Overall the wing scale structures of iridescent and non-iridescent *Heliconius* species are very similar, both having longitudinal ridges joined by cross-ribs. However, iridescent scales have ridges composed of layered lamellae, which act as multilayer reflectors. Differences in brightness between species can be explained by the extent of overlap of the lamellae and their curvature as well as the density of ridges on the scale. *Heliconius* are well known for their Müllerian mimicry. We find that iridescent structural colour is not closely matched between co-mimetic species. Differences appear less pronounced in models of *Heliconius* vision than models of avian vision, suggesting that they are not driven by selection to avoid heterospecific courtship by co-mimics. Ridge profiles appear to evolve relatively slowly, being similar between closely related taxa, while ridge density evolves faster and is similar between distantly related co-mimics.

1. Introduction

Structural colour and in particular iridescent structural colour is widely distributed in nature, for example, in beetle elytra, the shells of molluscs, bird feathers, plants and butterfly wings [1]. It most often arises from one of two phenomena, diffraction or thin-film interference. In most butterflies studied to date, structural colours are produced by thin-film interference [2–4], when light is reflected off the upper and lower surfaces of thin films of material, in this case cuticle, composed of chitin [5], with a different refractive index ($n = 1.56$) from that of the surrounding medium (air). This creates an optical path difference between scattered light waves that gives rise to interference. The reflected colour will depend on the angle of incidence and thickness of the air and chitin layers. On butterfly wings these thin cuticle layers are present within flat scales around 100 µm in size, arranged in rows of, usually, two different forms of scale: cover scales overlapping

© 2018 The Authors. Published by the Royal Society under the terms of the Creative Commons Attribution License http://creativecommons.org/licenses/by/4.0/, which permits unrestricted use, provided the original author and source are credited.

Downloaded from http://rsif.royalsocietypublishing.org/ on December 5, 2018

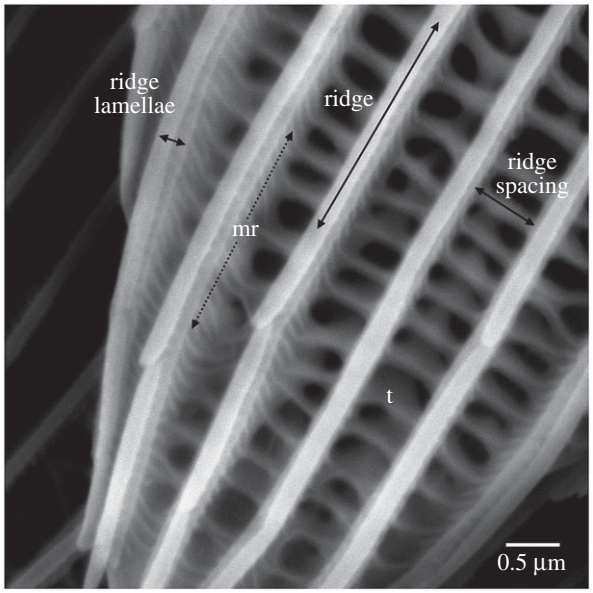

Figure 1. The general structures seen on a *Heliconius* wing scale. The dominant structures are the ridges, these in turn comprise the ridge lamellae, which can be overlapping as is seen in this instance. Micro ribs (mr) are found on the walls of the ridges, some continue as cross ribs, connecting the ridges together. The trabeculae (t) act as connections to the lower lamina. Image is of the tip region of a blue *H. eleuchia* wing scale, but these broad features were found on all scales.

ground scales. The surface of each scale comprises a lattice of raised longitudinal ridges joined together by cross-ribs (figure 1) [2]. The longitudinal ridges can be composed of layered lamellae, which are responsible for producing iridescence in some butterflies [3,6,7]. Little is known about the developmental processes that give rise to layered thin film structures in butterflies [7]. By comparing closely related species that differ in their structural colour we can identify how aspects of scale structure and development have evolved to optimize the reflected colour appearance [8]. An improved understanding of scale structure development could provide useful insights for replicating biological nanostructures for commercial or technological applications [9].

The neotropical *Heliconius* butterflies have been widely studied over the last 150 years, largely because of their intriguing diversity in colour and pattern and the near perfect mimicry between closely related species [10]. These studies have demonstrated that *Heliconius* colour patterns are under strong positive frequency-dependent selection due to predator avoidance of local warning patterns [11,12], which also drives mimicry between species. Colour patterns also have an important role in mate choice and mate recognition in these species, with changes in colour pattern resulting in divergent mate preference and also playing a role in driving speciation in this system [13]. The diversity of colour and pattern in this group also makes them an ideal system for understanding the mechanisms and genetic pathways controlling colour and pattern production [14,15]. The culmination of many years of genetic work has been the identification of a small number of genes that, between them, explain most of the diversity in pigmentation patterning both within and between species [16–19].

By contrast, very little is known about the production of structural colours in *Heliconius*. Several species exhibit an angle-dependent iridescent blue or green colour that is also mimetic between species [20,21] and involved in mate

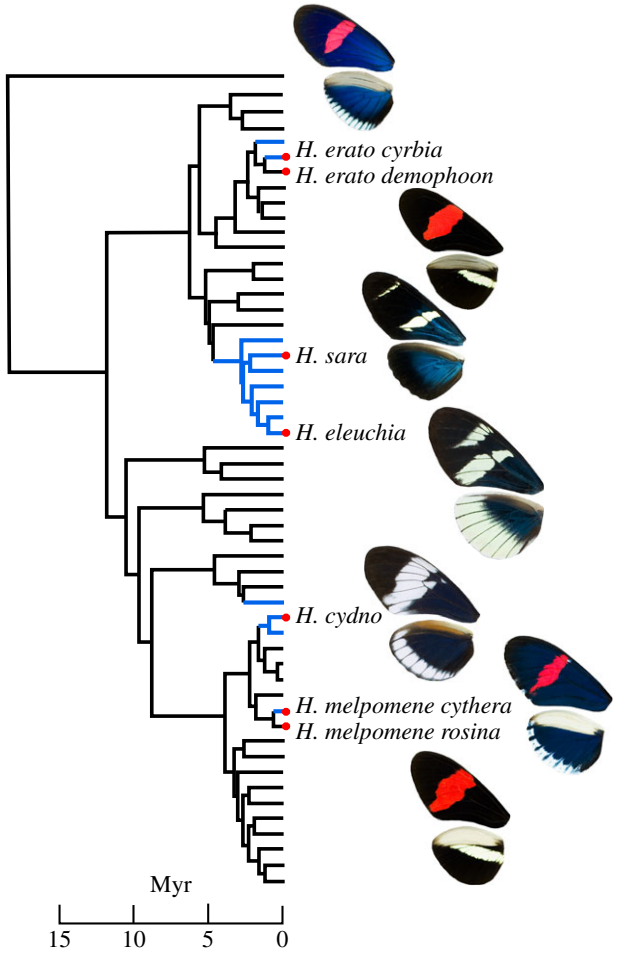

Figure 2. Phylogenetic relationships of the species and subspecies investigated in this work (based on [23]). Blue branches indicate the inferred presence of iridescent blue colour. Note the mimicry between distantly related species pairs *H. cydno* and *H. eleuchia*, and between *H. melpomene* and *H. erato*. Wing photographs were taken with consistent lighting conditions and camera settings. Here we focus on the blue/black wing regions only.

choice [22]. These colours are relatively uncommon within the greater than 40 species of *Heliconius* and appear to have evolved multiple times [23]. Iridescent blue colour is found in all members of one monophyletic group of seven species, the 'iridescent specialists' (*Heliconius antiochus*, *H. leuchadia*, *H. sara*, *H. hewitsoni*, *H. sapho*, *H. congener* and *H. eleuchia*), suggesting that it likely evolved in the common ancestor of this group between 2 and 5 million years ago (figure 2) [23,24]. Similar colours in other *Heliconius* species likely have a more recent origin. For example, *H. cydno* has an iridescent blue colour, which is largely absent from its sister species (*H. timareta* and *H. melpomene*). This suggests it evolved recently in this species (fewer than 1 million years ago), likely as a result of the co-mimicry between *H. cydno* and *H. sapho* or *H. eleuchia*. Furthermore, subspecies of the co-mimics *H. erato* and *H. melpomene* from the western slopes of the Andes in Colombia and Ecuador both have an iridescent blue colour, which is absent from all other populations of these species that are widespread across South and Central America, suggesting a very recent origin (probably within the last 100 000 years [22,23]). The differences in structural colour between subspecies of *H. erato*/*melpomene* are genetically determined and not plastic responses to environmental differences, as they are maintained when the butterflies are reared under common conditions in captivity and hybrids between subspecies are intermediate in colour [25].

Downloaded from http://rsif.royalsocietypublishing.org/ on December 5, 2018

Here we characterize the structures responsible for producing iridescence in five subspecies, *Heliconius erato cyrbia* (Godart, 1819), *Heliconius sara sprucei* Bates, 1864, *Heliconius eleuchia primularis* Butler, 1869, *Heliconius cydno alithea* (Hewitson, 1869) and *Heliconius melpomene cythera* (Hewitson, 1869), likely corresponding to four independent evolutionary origins of this type of colour. The sampled individuals were from western Ecuador where there are mimetic relationships between *H. cydno alithea* and *H. eleuchia primularis* and between *H. erato cyrbia* and *H. melpomene cythera*. We also investigated the non-iridescent subspecies *Heliconius erato demophoon* Ménétriés, 1855 and *Heliconius melpomene rosina* (Boisduval, 1870) from Panama, which are the most closely related non-iridescent populations of *H. erato* and *H. melpomene* [26], to identify the structural transitions that have occurred and give rise to iridescence in these two species. The apparent multiple recent evolutionary origins of iridescence make this group ideal to address the question of how iridescent colours evolve. In addition, the presence of mimicry between species allows us to ask how easily such colours can evolve towards a single evolutionary optimum structure or if there are subtle differences in architecture that give similar iridescent optical effects.

2. Material and methods

2.1. Butterfly specimens

Specimens of the iridescent butterflies, *H. erato cyrbia*, *H. sara*, *H. eleuchia*, *H. cydno alithea* and *H. melpomene cythera*, were collected in and around the Mashpi reserve in Ecuador (0.17° N, 78.87° W) between May 2014 and February 2017. One *Heliconius sara sara* (Fabricius, 1793) individual was also collected from Gamboa, Panama (9.12° N, 79.70° W), along with specimens of the non-iridescent *H. melpomene rosina* and *H. erato demophoon*. Species and subspecies identification was based on Brown [27] and Warren *et al*. [28]. For comparison, we also obtained a species with a known lower lamina reflector, the peacock butterfly (*Aglais io*), obtained from the company World of Butterflies and Moths (UK). All remaining specimens are preserved at the University of Sheffield.

2.2. Optical microscopy

We obtained images using a Nikon Eclipse ME600 optical microscope, using 20× or 50× objective lenses and a PixeLINK PL-A742 camera. A calibration grid (Reichert) was used to calibrate the length scales in the images. For the peacock butterfly, we used a mercury vapour lamp to give sufficient intensity in the UV/blue part of the spectrum.

We also obtained images of the *Heliconius* species using a Zeiss Axioscope optical microscope with a 100× objective lens and mounted AxioCam MR5. AxioVision software was used to obtain extended focus images by integrating information taken from images at multiple focal planes. We imaged the surface of *H. erato cyrbia* further using a Zeta-20 Optical Profiler, which characterizes the colour and the three-dimensional surface structure.

2.3. Scanning electron microscopy

Scanning electron microscopy (SEM) samples were prepared by cutting small regions of the wings and adhering them to SEM stubs using conductive silver paint (AGAR, UK). These were coated with a few nanometres of gold (AGAR) using vacuum evaporation and imaged on a JEOL JSM-6010LA together with InTouchScope software.

We made cross sections through the vertical ridge profile of *H. erato demophoon* and *H. sara*, as representative non-iridescent and iridescent *Heliconius* structures, respectively. The samples were sputter coated with a few nanometres of gold–palladium prior to mounting in a FEI Nova 600 Nanolab dual-beam focused ion beam (FIB) and SEM. Initial studies on these samples showed marked charging effects so individual scales were removed by bonding them to the lift-out needle of the FIB and transferring them to a clear section of the stubs. A protective layer of platinum was deposited by evaporation on the surface of each scale using FIB-induced deposition. The scales were then sectioned using a gallium ion beam and imaged using the SEM column of the system.

2.4. Raman microscopy

To assess the pigment content of the scales, we performed Raman microscopy on single cover scales, using a Renishaw inVia measurement system (Renishaw, UK). The butterfly scales were brought into focus using the white light source and then fine-adjusted to optimize the signal counts for the focus using the argon-ion laser (514.5 nm) source.

2.5. Scanning probe microscopy

A Digital Instruments Dimension 3100 scanning probe microscope (SPM) was used in atomic force microscopy (AFM) tapping mode, together with either a Nanoscope® IIIa or IV controller. AFM data were taken using standard tapping mode tips (Bruker) with a resonance near 320 kHz, lowered down on either the centre or the edge of a single undamaged wing scale in the sample. The data were subsequently flattened and analysed, to produce two-dimensional surface topography height images (with height represented as a colour scale) and rendered three-dimensional surfaces using the software Gwyddion and ImageSXM. Fourier analysis was performed on the scale SPM scans and the ridge spacing extracted from the integrated Fourier transform to give an image-averaged ridge spacing over the 10 µm square image.

2.6. Small angle X-ray scattering

Transmission small angle X-ray scattering (SAXS) of the butterfly wings was measured at the ID02 beamline (ESRF—the European synchrotron, Grenoble, France). The camera was a Rayonix MX-170HS CCD detector and we used X-rays with a wavelength of 0.1 nm, a beam size of 20 µm by 20 µm and a sample-to-detector distance of 30.98 m. Between 8 and 17 measurements were collected over 10–20 mm from one wing of each species/subspecies.

The two-dimensional detector images were masked to account for the beam stop and edges of the detector, corrected for dark, spatial distortion, normalized by transmitted flux and subsequently radially integrated to give the one-dimensional scattering plots of scattered intensity, I, as a function of momentum transfer q, where $q = (4\pi\sin\theta)/\lambda$, 2θ being the scattering angle. Based on our interpretation of the scale structure (figure 1) and correlating this with the X-ray scattering pattern, we were able to use a particular peak position in the one-dimensional scattering pattern to measure the ridge spacing (as shown in electronic supplementary material, figure S1).

2.7. Optical reflectance spectroscopy

Reflectance measurements were taken for four individuals of each taxon from both the hindwing and forewing. Samples were prepared by sticking either whole wings or pieces of wings to glass slides using a cyanoacrylate-based adhesive. The sample slide was fixed to an optical mount on a rotation stage. Measurements were taken at normal incidence and at

Downloaded from http://rsif.royalsocietypublishing.org/ on December 5, 2018

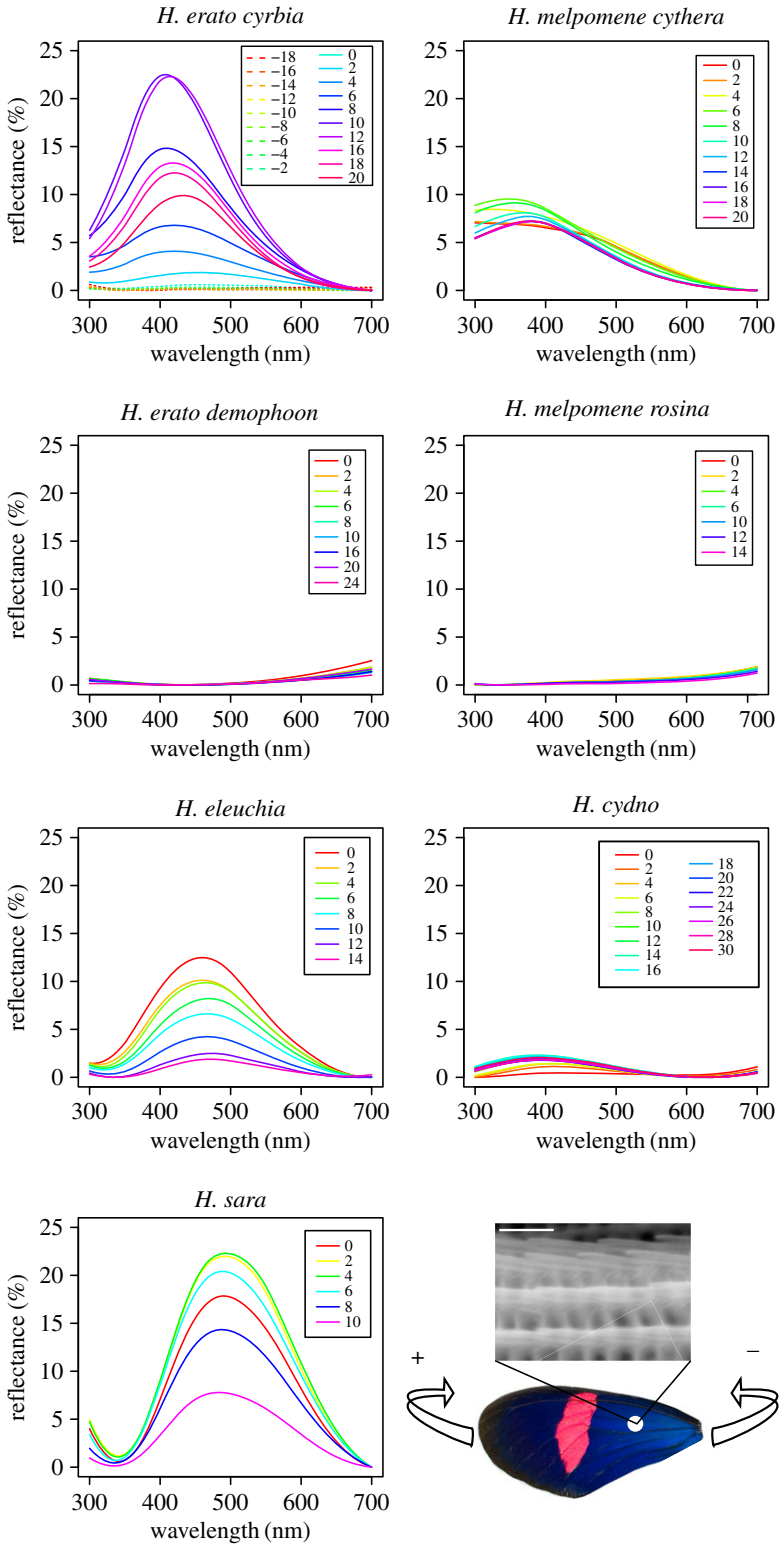

Figure 3. Representative reflectance profiles taken from one individual forewing of each of the seven taxa with varying angles. Angles are relative to incident with wings rotated along an anterior–posterior axis and positive angles being towards the proximal end of the wing and negative angles towards the distal end, as shown in the lower right panel. Negative angles are only shown for *H. erato cyrbia* to illustrate that the patterns are not symmetrical, due to the asymmetry of the structures when rotated along this axis.

angles parallel to the orientation of the wing scales (determined by optical microscopy as being parallel to the wing veins). Rotations were performed so that the distal part of the wing moved away from the probe, because this produced the brightest reflectance (figure 3). Measurements were taken every 2°–5° to determine the angle of brightest peak reflection for each specimen.

Reflectance spectra were captured using a spectrometer (Ocean Optics USB2000+, USA) connected through a bifurcated fibre-optic probe to a PX-2 pulsed xenon light source, the third end of the probe clamped perpendicular to the wing. Measurements were normalized to the reflectance of a diffuse white standard (polytetrafluoroethylene, Labsphere Spectralon 99% at 400–1600 nm). The SpectraSuite (Ocean Optics) software was used to collect and average 20 individual scans, with a boxcar width of 4 nm and an integration time of 1 s per scan for all sample reflectance measurements.

Downloaded from http://rsif.royalsocietypublishing.org/ on December 5, 2018

2.8. Analysis of spectral data and visual system modelling

Processing and visualization of the reflectance spectra were performed using the R package PAVO v. 1.1 [29]. The data were smoothed (using the *procspec* function with *fixneg* set to zero and *span* set to 0.3) and then normalized by subtracting the minimum reflectance of a spectrum from all wavelengths (i.e. setting the minimum to zero, using *procspec*, '*min*'). For some individuals, we had multiple measurements per wing, in which case we averaged these measurements using the *aggspec* function.

We used bird and butterfly visual models to compare the reflectance spectra and determine how similar the iridescent colour of different species appears to the butterflies themselves and their predators. We calculated von Kries-transformed receptor quantum catches (using *vismodel*), for two visual systems [30]. Firstly, the average avian violet sensitive model within PAVO v. 1.1, which has four photoreceptors (peak sensitivities 416, 478, 542 and 607 nm). Most avian predators of *Heliconius* are thought to have this type of visual system [21]. The model also included transmission through blackbird ocular media [31], although this had little effect on the results. Secondly, we used a *Heliconius* visual system model, which has four photoreceptors [32], with receptor sensitivities from intracellular recordings by McCulloch *et al*. [33] (peak sensitivities 355 nm—UV1, 390 nm—UV2, 470 nm—B and 555 nm—L). We first calculated relative receptor quantum catches under standard daylight for both systems, which were used for tetrahedral colour space analysis [34].

Secondly, absolute receptor quantum catches were used to calculate discriminability between each butterfly individual for forewings and hindwings separately under standard daylight (illum = 'D65') and forest shade (illum = 'forestshade'). We used five different visual models: avian violet sensitive, *Heliconius* type I (tetrachromatic, *H. erato* female type), *Heliconius* type II (trichomatic, *H. erato* and *H. sara* male type), *Heliconius* type III (tetrachromatic, *H. sara* female type) and *Heliconius* type IV (trichomatic, *H. melpomene* type) [35]. For the avian and *Heliconius* type I and II models we followed Finkbeiner *et al*. [36]. Specifically, for the avian visual model, we used a Weber fraction of 0.06 and relative cone abundances of VS = 0.25, S = 0.5, M = 1, L = 1. For the *Heliconius* models, we used a Weber fraction of 0.05 and relative photoreceptor abundances of UV1 = 0.09, UV2 = 0.07, B = 0.17, L = 1 for type I, and UV2 = 0.13, B = 0.2, L = 1 for type II. Type III and IV relative photoreceptor abundances were calculated from the percentages of ommatidial types multiplied by the proportion of photoreceptor types within each ommatitial type, from McCullock *et al*. [35]. For type III these were UV1 = 0.09, UV2 = 0.13, B = 0.2, L = 1 and for type IV these were UV1 = 0.07, B = 0.26, L = 1. Achromatic discriminability was based on the long wavelength photoreceptor in all cases.

2.9. Genotyping *Heliconius sara* individuals

To confirm the taxonomic identity of the *H. sara* individuals we sequenced a 745-bp fragment of the mitochondrial *CoI* gene, which has previously been shown to be species diagnostic for most *Heliconius* species [37], for five individuals sampled in Ecuador and one sampled in Panama (including all those used for reflectance and scale structure measurements). We used previously described protocols for polymerase chain reaction amplification with oligonucleotide primers Patlep and Jerry followed by Sanger sequencing [38]. These were then aligned with existing sequences from GenBank using BioEdit Sequence Alignment Editor v. 7.2.5. We generated a phylogenetic tree using the neighbour joining method in MEGA v. 6.06 with 1000 bootstrap replicates.

3. Results and discussion

3.1. Structural features responsible for iridescent colour in *Heliconius*

As expected, reflectance measurements taken from the blue/black region of the wings of all five species showed strong angle-dependent effects, with both brightness and wavelength of peak reflectance changing with angle (figure 3). In contrast, the 'non-iridescent' subspecies, *H. erato demophoon* and *H. melpomene rosina*, had very little visible light reflected from their wings, which changed very little with angle. In general, reflectance from both the fore- and hindwing was similar (figures 4 and 5), suggesting that similar structures are responsible, although the forewing was generally brighter than the hindwing, perhaps suggesting some slight structural difference between the wings or possibly a difference in the density of scales on the wings or a pigmentation difference.

The general layout of an iridescent scale is shown in figure 1, with the long continuous ridges spaced by perpendicular cross-ribs. It is possible to see the trabeculae, which extend down into the scale. The ridges are structured with micro-ridges (mr) perpendicular to the length of the ridge. In the vertical axis, we see ridge lamellae. In general, the overall scale morphology was similar between iridescent blue and black scales (figures 4 and 5). However, the iridescent scales have ridge lamellae that appear to overlap in vertical layers, which is not observed in the non-iridescent taxa. It is this series of chitin/air/chitin lamellae repeat structures that we propose causes the iridescence in the *Heliconius* butterflies we have examined. This is in agreement with a recent analysis of wing scale structure in *H. sara* [39]. This type of structure has been described in other butterfly species previously [2], most notably as producing the bright blue colour of *Morpho* butterflies [3].

Optical microscopy showed that reflected blue colour in all five *Heliconius* species was highly localized to the ridges (figure 6; electronic supplementary material, figure S2). In some other nymphalid butterflies, such as the peacock butterfly, *Aglais io*, the lower lamina of the scale has been shown to act as an optical thin film and reflect blue light [40]. Optical microscope images from the blue eye spots of the peacock butterfly were very different from those taken from the five *Heliconius* species, with reflected colour seen in many places across the scale rather than localized to the ridges, supporting our assertion that the blue colour seen in these *Heliconius* species is not due to lower lamina reflection. In addition, Raman spectra of the blue *Heliconius* cover scales show a high amount of melanin present, of a similar order to that seen in the black wing regions of the non-iridescent taxa (figure 7), which is also consistent with the fact that the iridescent wing regions appear black at certain angles (figure 3). This melanin would likely inhibit any reflection being discernible from the lower lamina; indeed, most butterfly scales that derive blue colour from the lower lamina have little or no pigment present [42].

Images of individual *H. erato cyrbia* scales show that both cover and ground scale types are similar in appearance and reflect blue colour equally (electronic supplementary material, figure S2), suggesting that layering of the scales on the wing does not have a major influence on colour production, as it does in some butterflies [3,39].

To examine the ridges in cross section, we used a focused ion beam to section them without the need macroscopically

Downloaded from http://rsif.royalsocietypublishing.org/ on December 5, 2018

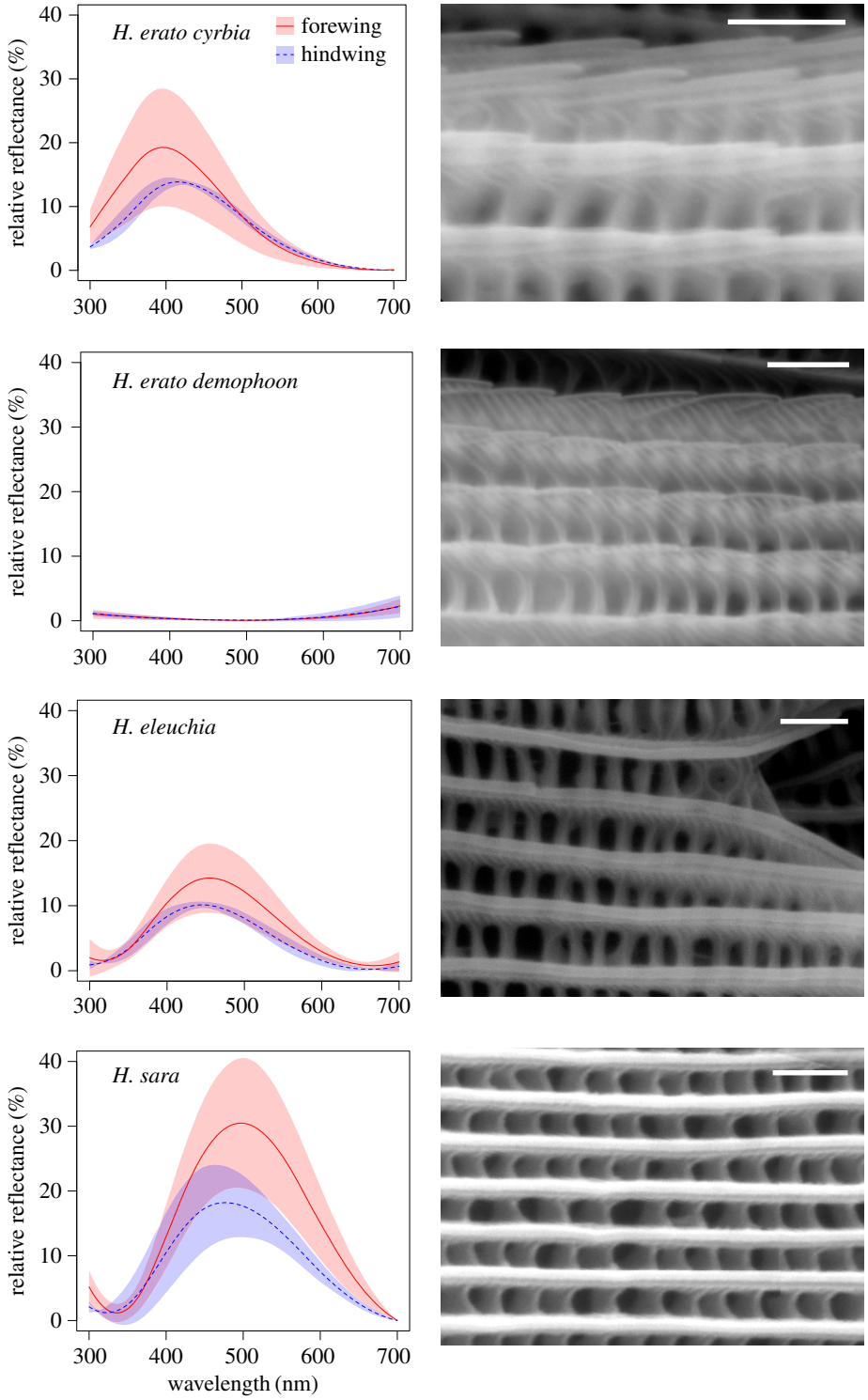

Figure 4. Reflectance spectra and scanning electron micrographs of wing scales for *H. erato* group species. Reflectance spectra are from the angle of maximum reflectance and are shown as the mean and standard deviation of measurements from four individuals, for both the forewing (red/solid line) and hindwing (blue/dashed line) for each species/subspecies. Scanning electron micrographs show one representative region for each species. White bars are 1 µm. (Online version in colour.)

to cut and possibly damage the scale structure. The ridge structure of the non-iridescent *H. erato demophoon* appears non-periodic with a near-smooth triangular profile (figure 8*a*,*c*). In contrast, the ridge structure of bright iridescent *H. sara* showed approximately two regular periodic chitin protrusions (figure 8*b*,*d*), which we propose are responsible for the iridescence. The air space and chitin layers were 119 ± 6 nm and 85 ± 7 nm, respectively. In total, this reveals the period for the structure to be 204 ± 10 nm and yields an effective (average) refractive index of 1.22. These values can be used to give the reflected wavelength of 499 ± 18 nm [43], in good agreement with the measured reflectance peak for *H. sara* (Ecuador, figure 4 and table 1).

3.2. Comparison of optical and structural features between *Heliconius* species

Optical microscopy also revealed differences between iridescent *Heliconius* species. *Heliconius sara* has long near-continuous lines of colour whereas *H. erato cyrbia*, *H. melpomene cythera* and *H. cydno* have punctuated colour along the length of the ridges (figure 6; electronic supplementary material, figure S2). These optical differences can be explained by observed

Downloaded from http://rsif.royalsocietypublishing.org/ on December 5, 2018

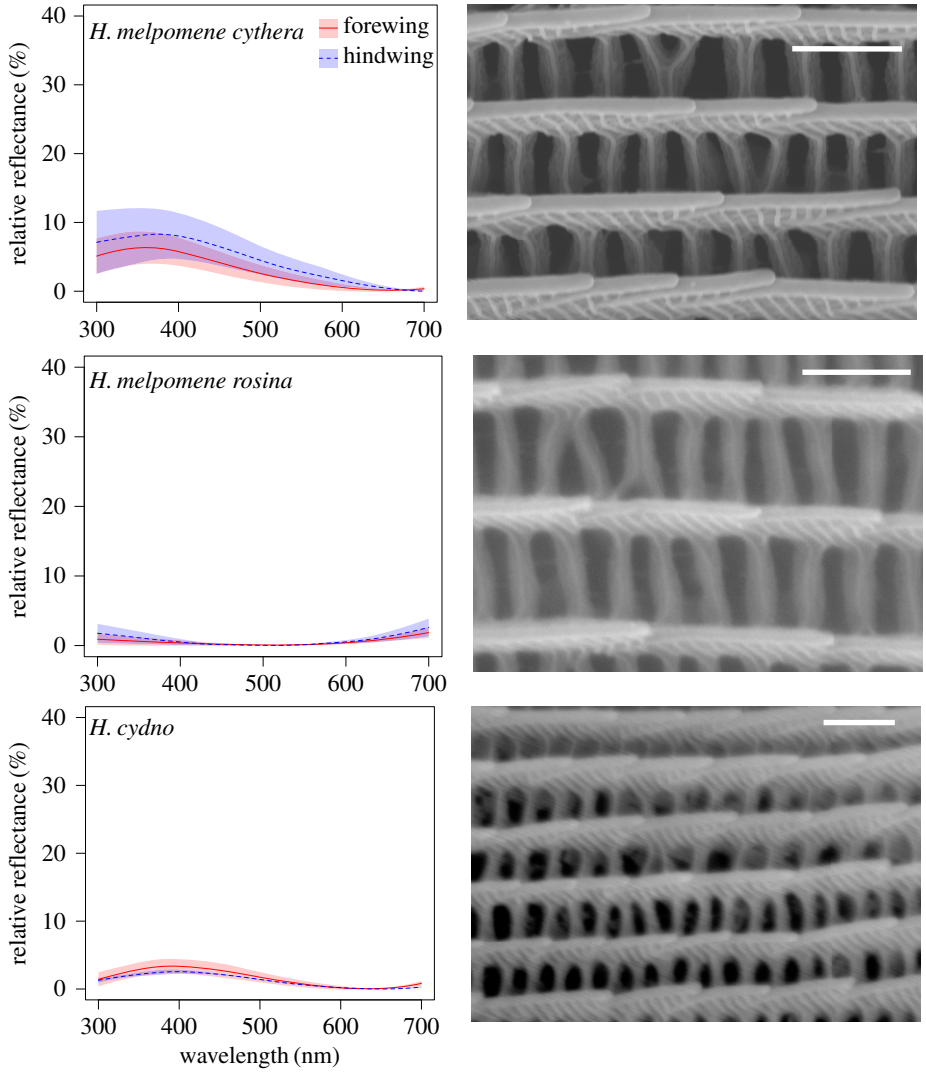

Figure 5. Reflectance spectra and scanning electron micrographs of wing scales for *H. melpomene* group species. See figure 4 caption for details. (Online version in colour.)

differences in ridge morphology between species. In the SEM images of *H. sara* the ridges are essentially flat and uninterrupted, while in all other taxa the ridge lamellae are more steeply sloped and hence are not continuous and appear to have a variable number of layers of lamellae long their length (figure 4). This suggests that the observed breaks in the lines of colour along the ridges are due to parts of the ridges where the lamellae either do not overlap or where the spacing of the overlapping layers is not of the correct periodicity to cause constructive interference of a visible wavelength.

There was substantial variation between individuals within some of the species for the angle at which maximum reflectance was observed (table 1). This is most likely due to the wing surfaces being uneven. Nevertheless, there were some apparent differences between species, with *H. eleuchia* and *H. sara* generally showing maximum reflectance at angles closer to normal incidence (0°) than *H. erato cyrbia* and *H. melpomene cythera*. Figure 9*a* shows ridge profiles for each of the seven taxa extracted from SPM data from wings in their natural state. For *H. sara* and *H. eleuchia* the structures were fairly flat, which likely explains why the angle of maximum reflection is close to normal incidence. *H. erato cyrbia* and *H. melpomene cythera* have more angled ridge lamellae, with the angle of peak reflectance occurring when the wing is rotated such that the beam and detector are perpendicular to these. Rotating the wing in the opposite direction produced very low reflection (figure 3), as in this direction the light beam does not fall perpendicular to the lamellae.

There were also considerable differences in brightness between the five iridescent taxa, with *H. sara* and *H. erato cyrbia* being the brightest and *H. cydno* showing the weakest reflectance (figures 4, 5 and table 1). The SPM data suggested two major features of scale morphology giving rise to this variation. Firstly, as noted above, the planar nature of the *H. sara* ridges likely contributes to the brighter overall optical effect, because colour is reflected across the entire length of the ridge, with good uniformity in the ridge optical nanostructure. The taxa with the weakest iridescent colour, *H. cydno* and *H. melpomene cythera*, have curved ridge profiles, which reduces the uniformity of the lamellae layers. In this respect, they are somewhat similar to the non-iridescent taxa, which also have highly curved ridge profiles (figure 9*a*). Secondly, ridge reflectors were much more densely packed in *H. sara* (ridge spacing at 723 nm) and *H. erato cyrbia* (887 nm) than the other species, where spacing was above 1 µm, when measured using SPM over 100 μm^2 (table 1). The SPM data show that the ridge height is fairly consistent between taxa (figure 9*c–f*), suggesting that these species do not produce brighter colours by substantially increasing the number of layers of lamellae.

Downloaded from http://rsif.royalsocietypublishing.org/ on December 5, 2018

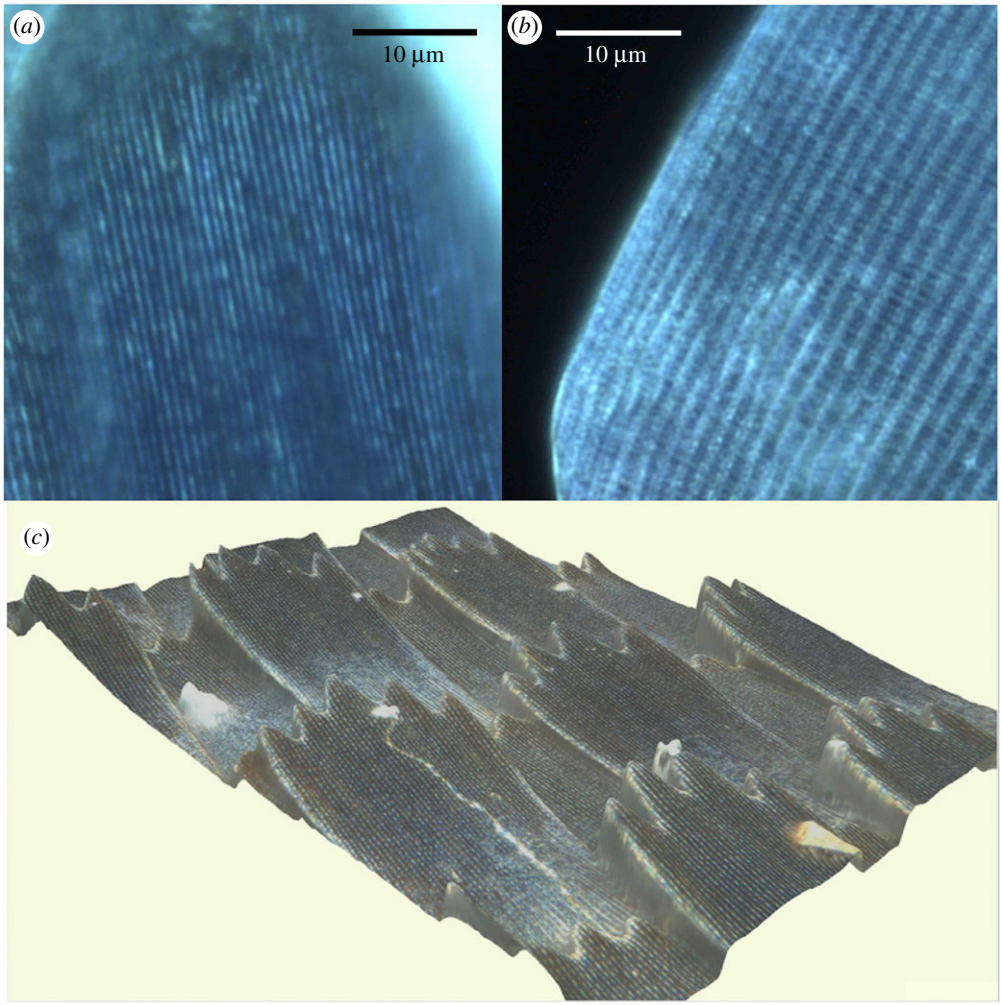

Figure 6. Optical microscope images showing that the blue colour localizes to the ridge structures in *Heliconius*. (*a*) Extended focus, dark field microscopy image of part of two scales on a *H. erato cyrbia* wing. (*b*) For comparison, part of two blue scales on the wing of *Aglais io*, a known lower lamina reflector. (*c*) True colour three-dimensional image from the Zeta-20 Optical Profiler, of scales on a *H. erato cyrbia* wing.

Ridge spacing was also inferred from the SAXS patterns (electronic supplementary material, figure S1), and correlated with peak reflectance (Pearson correlation from mean values, $r = -0.829$, $p = 0.021$; table 1 and figure 10). These ridge spacing values were derived from many measurements, each an average over 400 μm^2, so are likely to be better estimates of the average ridge spacing than the SPM measurements, which will be subject to individual scale variability. This comparison also confirmed that the *H. melpomene* clade species (*H. cydno* and *H. melpomene cythera*) achieve lower reflectance for a given ridge density than the *H. erato* clade species (*H. sara*, *H. eleuchia* and *H. erato cyrbia*).

There were also differences between species in the wavelength of the peak reflectance (hue), with *H. sara* being the greenest (figure 4 and table 1). These differences are presumably due to differences in the spacing of the ridge lamellae layers, although data from further cross sections of the ridge structures are needed to confirm this. Our prediction is that the spacing of the lamellae layers will be greater in *H. sara* than in the other iridescent species, leading to constructive interference of longer wavelengths.

3.3. Colour differences between species and visual modelling

Our measured wavelength of peak reflectance for *H. sara* was considerably longer than that reported previously for samples collected from Panama [21]. We, therefore, measured a *H. sara sara* from Panama, which had a wavelength peak similar to those measured by Thurman & Seymour [21] (electronic supplementary material, figure S3), suggesting that this is a regional difference in *H. sara*. To confirm that we were not in fact measuring two different species, we genotyped our *H. sara* individuals from Ecuador and Panama for the COI gene and compared them to existing *Heliconius* sequences for this gene. Of the five genotyped *H. sara* individuals from Ecuador, three were identical to the reference *H. sara* sequence on GenBank, and they showed between 98.3% and 98.5% identity to the individual from Panama. In addition, all sampled *H. sara* individuals grouped together robustly in a phylogenetic tree (electronic supplementary material, figure S4), strongly supporting a single species designation.

Heliconius sara may have shifted to being more green in appearance in this population west of the Andes in Ecuador because none of its main co-mimics (*H. leucadia*, *H. antiochus* and *H. congener* and *H. wallacei*) are present in this area [27,44]. The only mimic that is present is *H. doris*, but the blue colour in this species is not of the same type [39]. *Heliconius doris* is also polymorphic, with blue, green and red forms.

In order to better understand the selective pressures driving the evolution of these traits, we used visual models to assess and quantify the extent of similarity in colour between co-mimetic taxa. Birds are thought to be the main visual predators of *Heliconius* and as such to be the main force driving

Downloaded from http://rsif.royalsocietypublishing.org/ on December 5, 2018

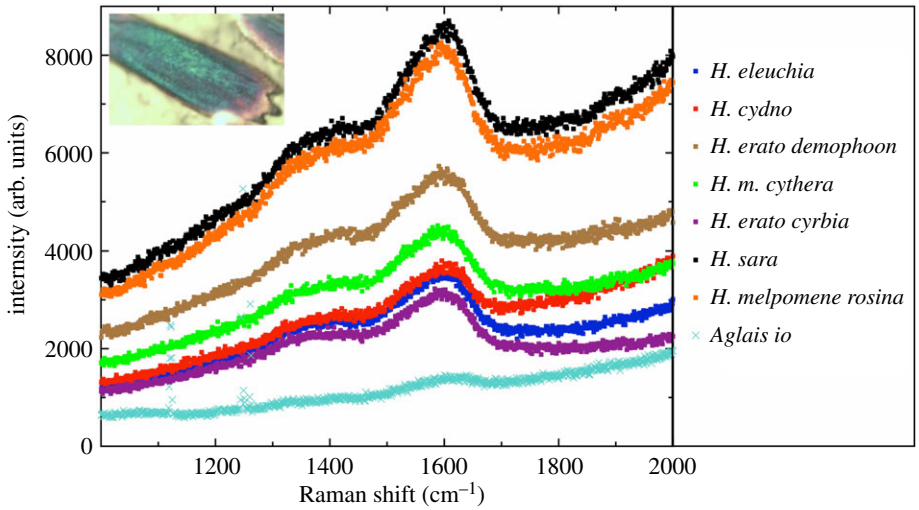

Figure 7. Single scale Raman spectra measurements from cover scales. The melanin peak appears at wavenumbers 1588 and 1408 cm^{-1} [41], this signal being due to the in-plane stretching of the aromatic rings and linear stretching of the C–C bonds within the rings, and is also accompanied by components from the C–H vibrations in both the methyl and methylene groups. The measured blue wing regions of *H. erato cyrbia*, *H. cydno* and *H. eleuchia* contain similar melanin concentrations to the black wing regions of *H. erato demophoon* and *H. melpomene rosina*.

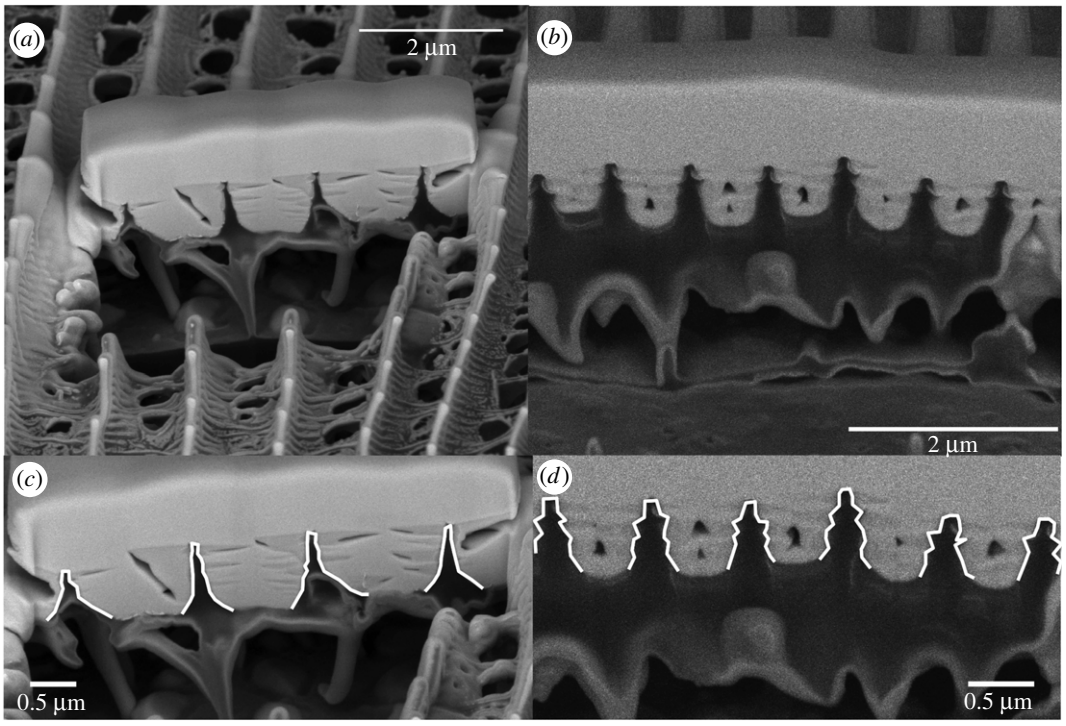

Figure 8. Focused ion beam interrogation of the surface of a *H. erato demophoon* cover scale (*a*) and a *H. sara* cover scale (*b*) showing crenelated like structures perpendicular to the ridge surface. In (*c*) and (*d*) the vertical ridge profile is highlighted in white to appreciate the difference between non-iridescent *H. erato demophoon* (*c*) and iridescent *H. sara* (*d*).

mimicry between species [10,45]. Birds are tetrachromatic, with four different photoreceptor types that allow colour discrimination along four axes. Avian visual systems can be broadly classed into two types, violet and UV sensitive, based on the peak absorbance of their shortest wavelength sensitive opsin [46,47]. The main butterfly predators in South America belong to the tyrant flycatcher (Tyrannidae) and jacamar (Galbulidae) families [45], both of which have visual systems that are sensitive to violet but not ultraviolet colours [46].

Wing colours are also important cues for the butterflies themselves, particularly in mate choice [10]. The visual systems of butterflies are very different from those of birds [33]. In particular, the *Heliconius* butterflies have undergone a duplication of the UV sensitive opsin, allowing them to see additional colours in the UV range [32]. This raises the possibility that some differences in colour between co-mimics may be visible to the butterflies but not avian predators. This would presumably be a selective advantage, allowing the butterflies to distinguish conspecifics from mimics, and so prevent wasted effort courting non-conspecifics, while gaining the protection benefits of mimicry. We would, therefore, predict co-mimics to be less discriminable in models of bird vision when compared to butterfly vision. However, the results of visual modelling found the opposite to be the case (figure 11). Under both ideal daylight and forest shade lighting

Downloaded from http://rsif.royalsocietypublishing.org/ on December 5, 2018

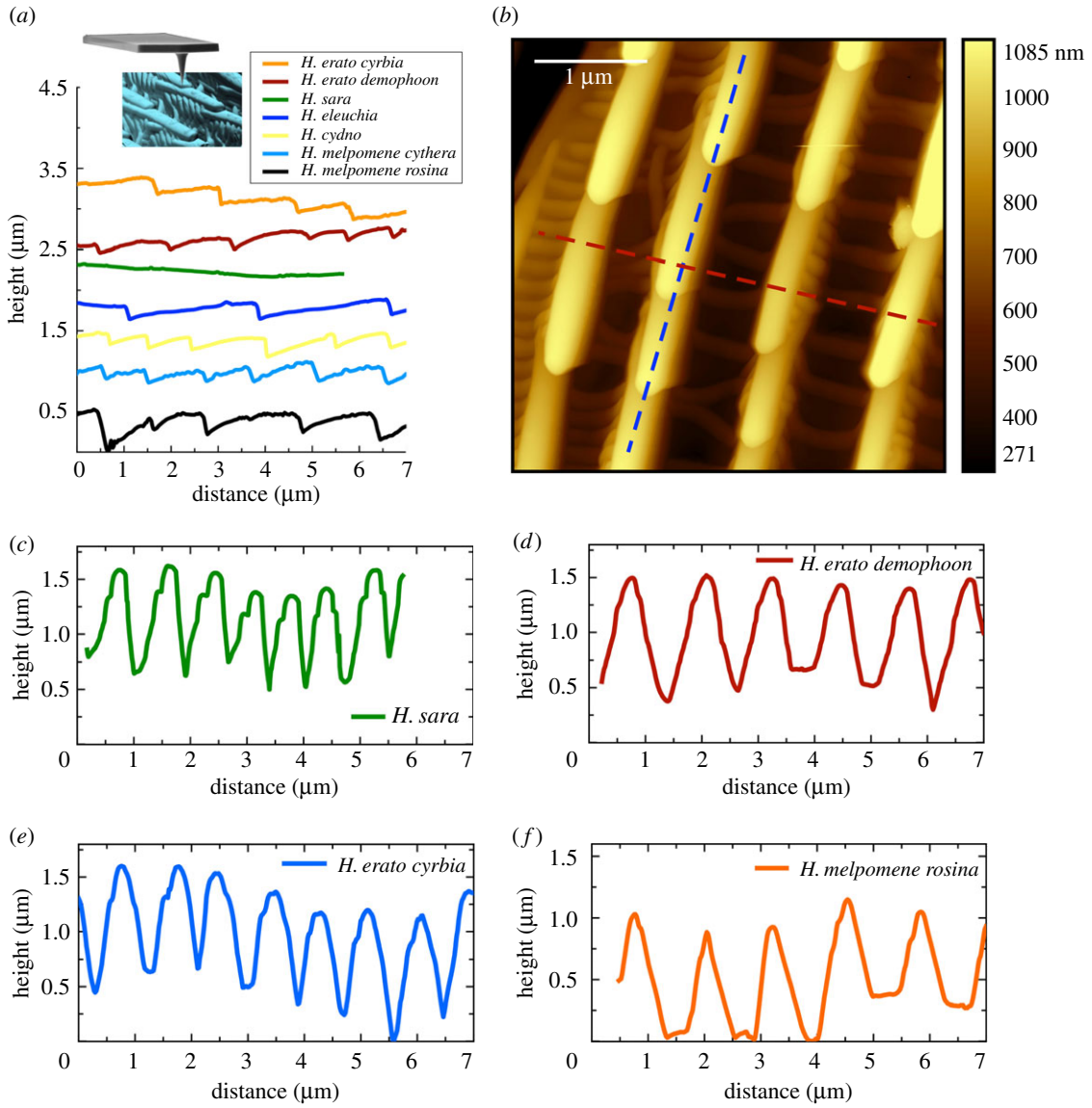

Figure 9. (*a*) The ridge profile extracted from a single ridge for each of the seven taxa using AFM scans. The inset shows an AFM tip scanning along a cover scale ridge structure. (*b*) A representative AFM image of the surface of a blue iridescent region for *H. cydno* showing the saw tooth like ridge discontinuities. The blue dashed line highlights the ridge profile shown in (*a*), while the orange dashed line shows the ridge heights, shown in (*c*–*f*) for two iridescent and two non-iridescent subspecies. (Online version in colour.)

Table 1. Summary of reflectance parameters and ridge spacing measurements for all taxa.

species	ridge spacing from AFM (nm)	ridge spacing from SAXS (nm)[b]	wavelength of peak reflectance[a] (nm)	full width at half maximum[a] (nm)	angle of maximum reflectance (°)[a]	maximum reflectance value[a] (%)[b]
H. erato cyrbia	887	812 ± 28	369 ± 8	177 ± 12	11.8 ± 4.9	19.4 ± 9.3
H. erato demophoon	1149	1063 ± 39	~700	n.a.	n.a.	2.4 ± 1.4
H. sara (Ecuador)	723	742 ± 28	497 ± 7	191 ± 5	10.0 ± 7.2	30.6 ± 10.1
H. sara (Panama)	—	—	443 ± 3	274 ± 2	3.5 ± 0.7	15.9 ± 2.1
H. eleuchia	1159	889 ± 73	455 ± 12	172 ± 1	6.0 ± 3.5	14.4 ± 5.3
H. cydno	1143	929 ± 58	390 ± 2	192 ± 20	6.7 ± 3.0	3.4 ± 1.1
H. melpomene cythera	1242	823 ± 22	362 ± 10	180 ± 9	16.7 ± 4.6	6.4 ± 2.4
H. melpomene rosina	1253	1025 ± 82	~700	n.a.	n.a.	1.9 ± 0.7

[a]Measurements are from within the bird/butterfly visible range (300–700 nm) from forewings given as mean values from four individuals ± s.d., except for *H. sara* from Panama, where only a single individual was measured and values are means of three measurements.
[b]These values are plotted in figure 10.

Downloaded from http://rsif.royalsocietypublishing.org/ on December 5, 2018

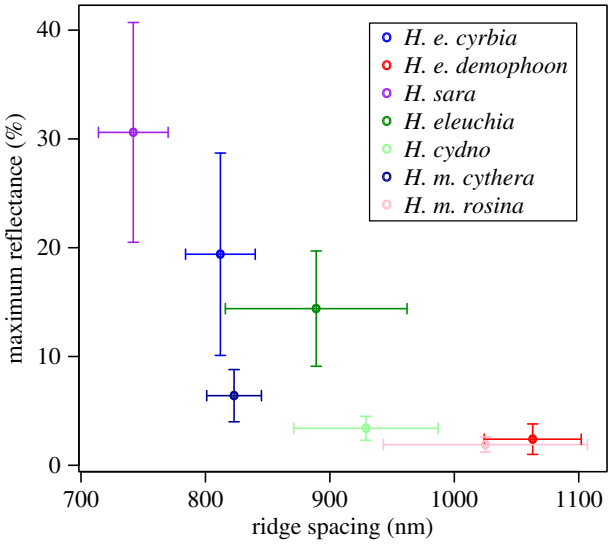

Figure 10. Taxa with lower ridge spacing (higher ridge density) have higher peak reflectance. The slope of the relationship is greater for taxa in the *H. erato* group (*H. e. demophoon, H. e. cyrbia, H. sara, H. eleuchia*) than for taxa in the *H. melpomene* group (*H. cydno, H. m. cythera, H. m. rosina*), likely due to differences in the structure of the ridges themselves, as observed with SEM and AFM. Co-mimetic pairs *H. e. cyrbia/H. m. cythera* and *H. eleuchia/H. cydno* have similar ridge density. Values are mean ± s.d. for each species/subspecies, as shown in table 1. Ridge spacing is calculated from SAXS data from 8–17 measurements across one wing of each species/subspecies. Reflectance values are from four individuals of each species/subspecies.

and for both forewings and hindwings, co-mimetic species were more discriminable with the avian visual model than any of the *Heliconius* models. Achromatic discriminabilites were similar for the birds and butterflies, but very high for both taxa, suggesting that both visual systems could easily discriminate species based on brightness. This suggests that the lack of perfect mimicry between species is not due to selection for conspecific recognition, and instead may be due to developmental constraint in the ability to rapidly evolve specific photonic structures.

This result is surprising, given that the *Heliconius* species largely differ along the blue–UV axis. This can be seen in a colour space analysis, where the species do appear more distinct in *Heliconius* visual space than in avian visual space (electronic supplementary material, figure S5). The reason the discriminability analysis finds poorer discrimination with the *Heliconius* visual systems is that it takes into account relative photoreceptor densities: the *Heliconius* visual system has relatively fewer photoreceptors sensitive in the blue/UV range, even though it has more types within this range. Nevertheless, the visual models are a simplification of the visual systems and little is known about precisely how the relative abundances and distribution of photoreceptor types will influence colour discrimination [48,49].

Recent work by McCulloch *et al.* [35] has shown that a change occurred in the visual system on the branch leading to the 'iridescent specialists' including *H. sara* and *H. eleuchia*, suggesting that the evolution of iridescence and the change of the visual system occurred around the same time. This change only occurred in the female visual systems: the males of both *H. erato* and *H. sara* do not express the UV1 opsin (type II visual system), while females of both species do (type I and type III visual systems in *H. erato* and *H. sara* females respectively) [35]. In the visual models, the male type II system is less able to discriminate the co-mimics (figure 11; electronic supplementary material, figure S5), suggesting that iridescent colour may have a more important role in female than male mate choice. In the *H. melpomene* clade, both sexes have a trichromatic visual system, lacking the UV2 opsin (type IV visual system) [35], but their predicted discrimination ability is better than the type II visual systems, suggesting that the UV1 opsin is more useful for discriminating these colours. We also note that the discrimination ability of the *Heliconius* visual systems is slightly better under forest shade lighting conditions than under standard daylight, while the opposite is true of the avian visual system (figure 11), which may suggest an advantage to these types of colours in more shaded environments.

There are other aspects of these iridescent signals that are not captured by visual modelling. Firstly, both the brightness and wavelength of peak reflectance change with angle (figure 3). This may mean that differences that are obvious to predators when measured on stationary wings may not be perceived as such on live, moving individuals. Secondly, the layered thin film reflectors that produce the iridescent colour are also known to produce polarization of the reflected light [22,24,49,50]. This can be detected by butterflies [22,51,52], but probably not by avian predators. Therefore, the differences in the ridge reflectors that we have documented between species could allow species discrimination by producing different polarization signals, even though the colours seem less readily discriminated by the butterflies than avian predators.

3.4. Evolutionary insights into the biological process of constructing a ridge reflector

Within *Heliconius* it appears that modification of the scale ridges to produce multilayer reflectors has occurred multiple times. Nevertheless, co-mimetic species do not appear to have achieved perfect mimicry in these structural colours, suggesting that there are developmental constraints in the evolutionary ability to modify the ridge reflectors. The brightest iridescence and highest degree of modification of the scale ridges is seen in *H. sara*, which belongs to a clade of all iridescent species, which likely evolved iridescence several million years ago. This suggests that structural changes have accumulated gradually over evolutionary time to produce brighter structural colour in this group. In contrast, *H. erato* is remarkable in that it appears to have very recently evolved relatively bright structural colour.

There appear to be three key features that determine the variation in hue and brightness of structural colour in these species: ridge density, curvature of the lamellae that make up the ridges and layering of the lamellae. Ridge density appears to evolve relatively rapidly, with mimetic species having similar ridge density (table 1 and figure 10). In contrast, ridge curvature appears to be more slowly evolving in these species, with distinct differences observed between the two major clades: the *H. erato* clade species (*H. erato, H. eleuchia* and *H. sara*) all appear to have flatter ridge profiles, while the *H. melpomene* clade species (*H. melpomene* and *H. cydno*) have more curved ridge profiles (figure 9). This also holds for the non-iridescent taxa: *H. erato demophoon* appears to have a less curved ridge profile than *H. melpomene rosina*. This may explain why *H. erato cyrbia* was able to rapidly evolve bright iridescent

Downloaded from http://rsif.royalsocietypublishing.org/ on December 5, 2018

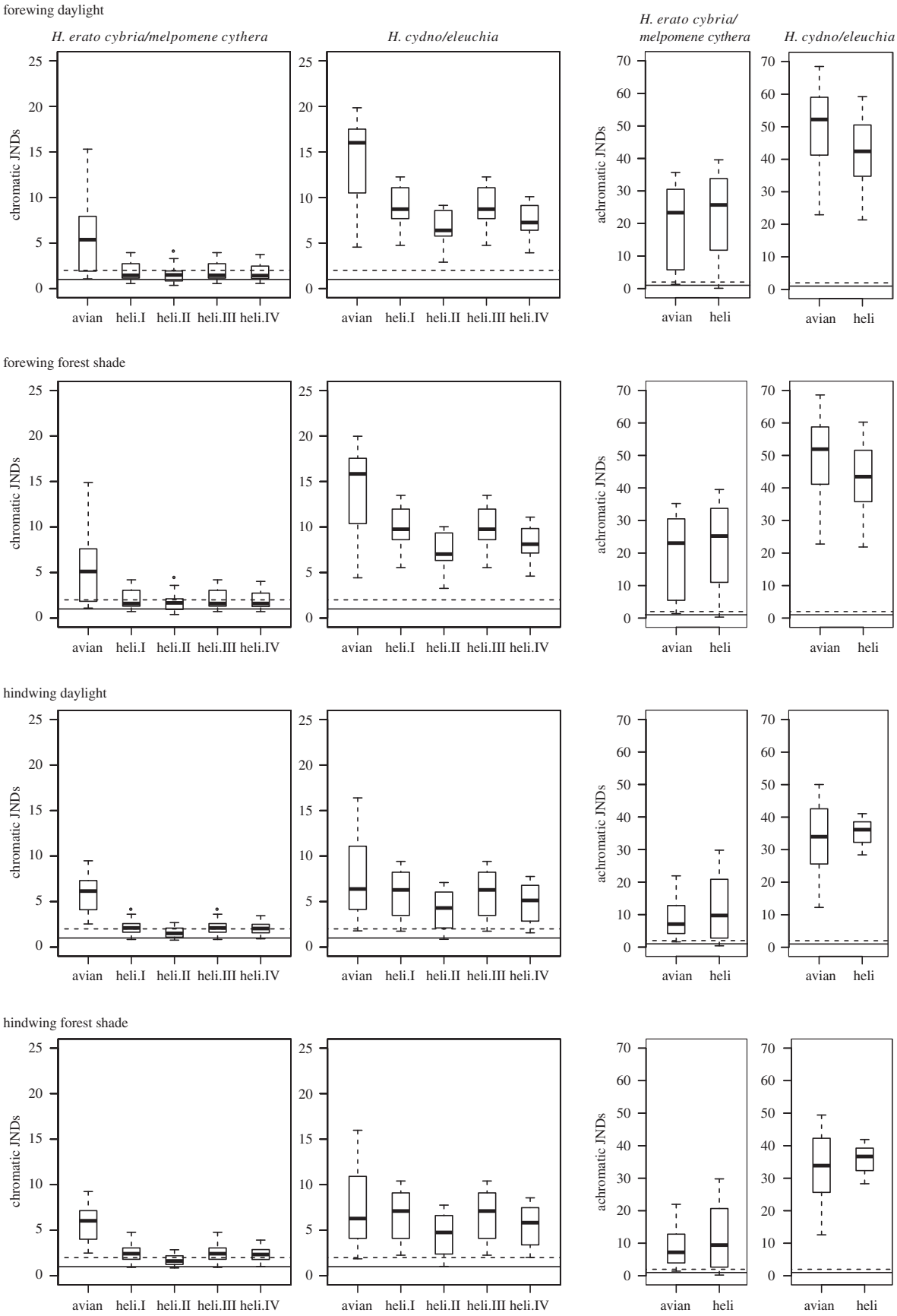

Figure 11. Discriminabilities of co-mimetic species pairs (*H. erato cyrbia* versus *H. melpomene cythera* and *H. cydno* versus *H. eleuchia*) for iridescent forewing and hindwing regions under ideal daylight and forest shade. The left plots give chromatic (colour) discrimination and the right plots give achromatic (brightness) discrimination. Units are just noticeable differences (JNDs), with values above 1 indicating that the colours can be discriminated (solid line threshold in plots; a threshold of 2 is also indicated with a dotted line). Five visual systems are compared: avian violet sensitive (avian), *Heliconius* type I (heli.I, tetrachromatic, *H. erato* female type), *Heliconius* type II (heli.II, trichomatic, *H. erato, H. sara* and presumed *H. eleuchia* male type), *Heliconius* type III (heli.III, tetrachromatic, *H. sara* and presumed *H. eleuchia* female type) and *Heliconius* type IV (heli.IV, trichomatic, *H. melpomene* type). Boxes indicate the upper and lower quartiles and median of all pairwise comparisons between individuals of each species ($n = 16$). Tails indicate the maximum and minimum values excluding outliers (if present, shown as points).

Downloaded from http://rsif.royalsocietypublishing.org/ on December 5, 2018

structural colour, while *H. melpomene cythera* and *H. cydno* appear not to have been able to.

Previous work on other butterflies has shown that the ridges form between longitudinal actin filaments during development [54–56]. Less is known about what causes folding of the ridges in order to produce the ridge lamellae. Ghiradella [56,57] has proposed that they could be produced by buckling of the ridges under mechanical stress and that the actin filaments may also be responsible for producing this stress. This would be consistent with results from Dinwiddie *et al.* [54] who showed that actin also played a critical role in the elongation of the cell. The *Heliconius* butterflies provide an ideal system to understand these processes better through comparisons of scale development and molecular genetics.

Data accessibility. The datasets supporting this article have been uploaded as part of the electronic supplementary material.

Authors' contributions. The majority of the data was collected by A.J.P. and J.E.B. N.J.N. and A.J.P. conceived and coordinated the study and prepared the manuscript. N.J.N. performed the visual system analysis. All other authors contributed to specific aspects of data collection and analysis, and provided comments on the manuscript.

Competing Interests. We declare we have no competing interests.

Funding. This work was funded by a Natural Environment Research Council (NERC) fellowship (NE/K008498/1) to N.J.N. J.E.B. was funded under the NERC Research Experience Placements (REP) scheme. E.C. and M.B. are funded by the NERC doctoral training partnership, ACCE. A.L.W. was funded via InnovateUK.

Acknowledgements. We thank the governments of Ecuador and Panama for giving permission to collect butterflies; Owen McMillan and Elizabeth Evans their help in Panama; and Patricio Salazar and Caroline Bacquet for their help in Ecuador. We are grateful to Dr Alan Dunbar for use of the scanning electron microscope, which was made possible by the EPSRC 4CU grant no. EP/K001329/1. We also thank Anna Puttick for taking some of the reflectance measurements, Caroline Pouya for her help in the laboratory in Exeter, and Dan Wesley and Richard Archer for metal coating some of the samples used in the SEM studies. We are grateful to Adriana Briscoe for her guidance in the *Heliconius* visual modelling. We acknowledge the European Synchrotron Radiation Facility for provision of synchrotron radiation facilities at ID02 and we are particularly grateful to Dr Sylvain Prevost for his expertise and skill in helping us measure the SAXS patterns of these scales.

References

1. Vukusic P, Sambles JR. 2003 Photonic structures in biology. *Nature* **424**, 852–855. (doi:10.1038/nature01941)
2. Ghiradella H. 1991 Light and color on the wing: structural colors in butterflies and moths. *Appl. Opt.* **30**, 3492–3500. (doi:10.1364/AO.30.003492)
3. Vukusic P, Sambles JR, Lawrence CR, Wootton RJ. 1999 Quantified interference and diffraction in single Morpho butterfly scales. *Proc. R. Soc. Lond. B* **266**, 1403–1411. (doi:10.1098/rspb.1999.0794)
4. Prum RO, Quinn T, Torres RH. 2006 Anatomically diverse butterfly scales all produce structural colours by coherent scattering. *J. Exp. Biol.* **209**, 748–765. (doi:10.1242/jeb.02051)
5. Leertouwer HL, Wilts BD, Stavenga DG. 2011 Refractive index and dispersion of butterfly chitin and bird keratin measured by polarizing interference microscopy. *Opt. Express* **19**, 24 061–24 066. (doi:10.1364/OE.19.024061)
6. Kemp DJ, Vukusic P, Rutowski RL. 2006 Stress-mediated covariance between nano-structural architecture and ultraviolet butterfly coloration. *Funct. Ecol.* **20**, 282–289. (doi:10.1111/j.1365-2435.2006.01100.x)
7. Ghiradella H. 1989 Structure and development of iridescent butterfly scales: lattices and laminae. *J. Morphol.* **202**, 69–88. (doi:10.1002/jmor.1052020106)
8. Wickham S, Large MCJ, Poladian L, Jermiin LS. 2006 Exaggeration and suppression of iridescence: the evolution of two-dimensional butterfly structural colours. *J. R. Soc. Interface* **3**, 99–109. (doi:10.1098/rsif.2005.0071)
9. Parker AR, Townley HE. 2007 Biomimetics of photonic nanostructures. *Nat. Nanotechnol.* **2**, 347–353. (doi:10.1038/nnano.2007.152)
10. Merrill RM *et al.* 2015 The diversification of *Heliconius* butterflies: what have we learned in 150 years? *J. Evol. Biol.* **28**, 1417–1438. (doi:10.1111/jeb.12672)
11. Merrill RM, Wallbank RWR, Bull V, Salazar PCA, Mallet J, Stevens M, Jiggins CD. 2012 Disruptive ecological selection on a mating cue. *Proc. R. Soc. B* **279**, 4907–4913. (doi:10.1098/rspb.2012.1968)
12. Mallet J, Barton NH. 1989 Strong natural selection in a warning-color hybrid zone. *Evolution* **43**, 421–431. (doi:10.2307/2409217)
13. Jiggins CD, Naisbit RE, Coe RL, Mallet J. 2001 Reproductive isolation caused by colour pattern mimicry. *Nature* **411**, 302–305. (doi:10.1038/35077075)
14. Joron M, Jiggins CD, Papanicolaou A, McMillan WO. 2006 Heliconius wing patterns: an evo-devo model for understanding phenotypic diversity. *Heredity* **97**, 157–167. (doi:10.1038/sj.hdy.6800873)
15. Ferguson LC, Jiggins CD. 2009 Shared and divergent expression domains on mimetic *Heliconius* wings. *Evol. Dev.* **11**, 498–512. (doi:10.1111/j.1525-142X.2009.00358.x)
16. Reed RD *et al.* 2011 *optix* drives the repeated convergent evolution of butterfly wing pattern mimicry. *Science* **333**, 1137–1141. (doi:10.1126/science.1208227)
17. Martin A *et al.* 2012 Diversification of complex butterfly wing patterns by repeated regulatory evolution of a Wnt ligand. *Proc. Natl Acad. Sci. USA* **109**, 12 632–12 637. (doi:10.1073/pnas.1204800109)
18. Nadeau NJ *et al.* 2016 The gene cortex controls mimicry and crypsis in butterflies and moths. *Nature* **534**, 106–110. (doi:10.1038/nature17961)
19. Nadeau NJ. 2016 Genes controlling mimetic colour pattern variation in butterflies. *Curr. Opin. Insect Sci.* **17**, 24–31. (doi:10.1016/j.cois.2016.05.013)
20. Chamberlain NL, Hill RI, Kapan DD, Gilbert LE, Kronforst MR. 2009 Polymorphic butterfly reveals the missing link in ecological speciation. *Science* **326**, 847–850. (doi:10.1126/science.1179141)
21. Thurman TJ, Seymoure BM. 2016 A bird's eye view of two mimetic tropical butterflies: coloration matches predator's sensitivity. *J. Zool.* **298**, 159–168. (doi:10.1111/jzo.12305)
22. Sweeney A, Jiggins C, Johnsen S. 2003 Insect communication: polarized light as a butterfly mating signal. *Nature* **423**, 31–32. (doi:10.1038/423031a)
23. Kozak KM, Wahlberg N, Neild AFE, Dasmahapatra KK, Mallet J, Jiggins CD. 2015 Multilocus species trees show the recent adaptive radiation of the mimetic *Heliconius* butterflies. *Syst. Biol.* **64**, 505–524. (doi:10.1093/sysbio/syv007)
24. Douglas JM, Cronin TW, Chiou T-H, Dominy NJ. 2007 Light habitats and the role of polarized iridescence in the sensory ecology of neotropical nymphalid butterflies (Lepidoptera: Nymphalidae). *J. Exp. Biol.* **210**, 788–799. (doi:10.1242/jeb.02713)
25. Emsley MG. 1965 The geographical distribution of the color-pattern components of *Heliconius erato* and *Heliconius melpomene* with genetical evidence for the systematic relationship between the two species. *Zoologica* **49**, 245–286.
26. Flanagan NS, Tobler A, Davison A, Pybus OG, Kapan DD, Planas S, Linares M, Heckel D, McMillan WO. 2004 Historical demography of Müllerian mimicry in the neotropical *Heliconius* butterflies. *Proc. Natl Acad. Sci. USA* **101**, 9704–9709. (doi:10.1073/pnas.0306243101)
27. Brown KS. 1979 *Ecologia Geográfica e Evolução nas Florestas Neotropicais*. Campinas, Brazil: Universidade Estadual de Campinas.
28. Warren AD, Davis KJ, Stangeland EM, Pelham JP, Willmott KR, Grishin NV. 2016 Illustrated lists of American butterflies. See http://www.butterfliesofamerica.com (accessed on 2 August 2017).

Downloaded from http://rsif.royalsocietypublishing.org/ on December 5, 2018

29. Maia R, Eliason CM, Bitton P-P, Doucet SM, Shawkey MD. 2013 pavo: an R package for the analysis, visualization and organization of spectral data. *Methods Ecol. Evol.* **4**, 906–913. (doi:10.1111/2041-210X.12069)
30. Vorobyev M, Osorio D, Bennett ATD, Marshall NJ, Cuthill IC. 1998 Tetrachromacy, oil droplets and bird plumage colours. *J. Comp. Physiol. A* **183**, 621–633. (doi:10.1007/s003590050286)
31. Hart NS, Partridge JC, Cuthill IC, Bennett ATD. 2000 Visual pigments, oil droplets, ocular media and cone photoreceptor distribution in two species of passerine bird: the blue tit (*Parus caeruleus* L.) and the blackbird (*Turdus merula* L.). *J. Comp. Physiol. A* **186**, 375–387. (doi:10.1007/s003590050437)
32. Bybee SM, Yuan F, Ramstetter MD, Llorente-Bousquets J, Reed RD, Osorio Daniel, Briscoe AD. 2012 UV photoreceptors and UV-yellow wing pigments in *Heliconius* butterflies allow a color signal to serve both mimicry and intraspecific communication. *Am. Nat.* **179**, 38–51. (doi:10.1086/663192)
33. McCulloch KJ, Osorio D, Briscoe AD. 2016 Determination of photoreceptor cell spectral sensitivity in an insect model from in vivo intracellular recordings. *J. Vis. Exp.* e53829. (doi:10.3791/53829)
34. Stoddard MC, Prum RO. 2008 Evolution of avian plumage color in a tetrahedral color space: a phylogenetic analysis of new world buntings. *Am. Nat.* **171**, 755–776. (doi:10.1086/587526)
35. McCulloch KJ, Yuan F, Zhen Y, Aardema ML, Smith G, Llorente-Bousquets J, Andolfatto P, Briscoe AD. 2017 Sexual dimorphism and retinal mosaic diversification following the evolution of a violet receptor in butterflies. *Mol. Biol. Evol.* **34**, 2271–2284. (doi:10.1093/molbev/msx163)
36. Finkbeiner SD, Fishman DA, Osorio D, Briscoe AD. 2017 Ultraviolet and yellow reflectance but not fluorescence is important for visual discrimination of conspecifics by *Heliconius erato*. *J. Exp. Biol.* **220**, 1267–1276. (doi:10.1242/jeb.153593)
37. Nadeau NJ *et al.* 2014 Population genomics of parallel hybrid zones in the mimetic butterflies, H. melpomene and H. erato. *Genome Res.* **24**, 1316–1333. (doi:10.1101/gr.169292.113)
38. Dasmahapatra KK, Silva-Vásquez A, Chung J-W, Mallet J. 2007 Genetic analysis of a wild-caught hybrid between non-sister *Heliconius* butterfly species. *Biol. Lett.* **3**, 660–663. (doi:10.1098/rsbl.2007.0401)
39. Wilts BD, Vey AJM, Briscoe AD, Stavenga DG. 2017 Longwing (*Heliconius*) butterflies combine a restricted set of pigmentary and structural coloration mechanisms. *BMC Evol. Biol.* **17**, 226. (doi:10.1186/s12862-017-1073-1)
40. Stavenga DG, Leertouwer HL, Wilts BD. 2014 Coloration principles of nymphaline butterflies: thin films, melanin, ommochromes and wing scale stacking. *J. Exp. Biol.* **217**, 2171–2180. (doi:10.1242/jeb.098673)
41. Parnell AJ *et al.* 2015 Spatially modulated structural colour in bird feathers. *Sci. Rep.* **5**, 18317. (doi:10.1038/srep18317)
42. Stavenga DG, Matsushita A, Arikawa K. 2015 Combined pigmentary and structural effects tune wing scale coloration to color vision in the swallowtail butterfly *Papilio xuthus*. *Zool. Lett.* **1**, 14. (doi:10.1186/s40851-015-0015-2)
43. Kinoshita S. 2008 *Structural colors in the realm of nature*, pp. 215–263. Singapore: World Scientific. (doi:10.1142/9789812709752_0009)
44. Rosser N, Phillimore AB, Huertas B, Willmott KR, Mallet J. 2012 Testing historical explanations for gradients in species richness in heliconiine butterflies of tropical America. *Biol. J. Linn. Soc.* **105**, 479–497. (doi:10.1111/j.1095-8312.2011.01814.x)
45. Jiggins CD. 2017 *The ecology and evolution of Heliconius butterflies: a passion for diversity*. Oxford, UK: Oxford University Press.
46. Hart NS. 2001 The visual ecology of avian photoreceptors. *Prog. Retin. Eye Res.* **20**, 675–703. (doi:10.1016/S1350-9462(01)00009-X)
47. Hart NS, Hunt DM. 2007 Avian visual pigments: characteristics, spectral tuning, and evolution. *Am. Nat.* **169**, S7–S26. (doi:10.1086/510141)
48. Briscoe AD, Chittka L. 2001 The evolution of color vision in insects. *Annu. Rev. Entomol.* **46**, 471–510. (doi:10.1146/annurev.ento.46.1.471)
49. Kelber A. 2016 Colour in the eye of the beholder: receptor sensitivities and neural circuits underlying colour opponency and colour perception. *Curr. Opin. Neurobiol.* **41**, 106–112. (doi:10.1016/j.conb.2016.09.007)
50. Stavenga DG, Wilts BD, Leertouwer HL, Hariyama T. 2011 Polarized iridescence of the multilayered elytra of the Japanese jewel beetle, *Chrysochroa fulgidissima*. *Phil. Trans. R. Soc. B* **366**, 709–723. (doi:10.1098/rstb.2010.0197)
51. Vukusic P, Sambles JR, Lawrence CR. 2000 Structural colour: colour mixing in wing scales of a butterfly. *Nature* **404**, 457. (doi:10.1038/35006561)
52. Kelber A. 1999 Why 'false' colours are seen by butterflies. *Nature* **402**, 251. (doi:10.1038/46204)
53. Kinoshita M, Sato M, Arikawa K. 1997 Spectral receptors of Nymphalid butterflies. *Naturwissenschaften* **84**, 199–201. (doi:10.1007/s001140050377)
54. Dinwiddie A, Null R, Pizzano M, Chuong L, Leigh Krup A, Ee Tan H, Patel NH. 2014 Dynamics of F-actin prefigure the structure of butterfly wing scales. *Dev. Biol.* **392**, 404–418. (doi:10.1016/j.ydbio.2014.06.005)
55. Overton J. 1966 Microtubules and microfibrils in morphogenesis of the scale cells of *Ephestia kühniella*. *J. Cell Biol.* **29**, 293–305. (doi:10.1083/jcb.29.2.293)
56. Ghiradella H. 1974 Development of ultraviolet-reflecting butterfly scales: how to make an interference filter. *J. Morphol.* **142**, 395–409. (doi:10.1002/jmor.1051420404)
57. Ghiradella H. 1984 Structure of iridescent lepidopteran scales: variations on several themes. *Ann. Entomol. Soc. Am.* **77**, 637–645. (doi:10.1093/aesa/77.6.637)